



UNIVERSITÀ
DEGLI STUDI
FIRENZE

DOCTORAL PROGRAMME IN INDUSTRIAL ENGINEERING
DOTTORATO DI RICERCA IN INGEGNERIA INDUSTRIALE

XXX

**Safety systems for motorcycles:
Remote sensing from tilting vehicles**

ING/IND-14

Doctoral Candidate

Gustavo Damián Gil
Gargolani

Supervisors

Prof. Marco Pierini

Dr. Giovanni Savino

External Referees

Prof. Luigi Del Re

Dean of the Doctoral Programme

Prof. Maurizio De Lucia

Prof. Riender Happee

Years 2014/2017

© Università degli Studi di Firenze – Faculty of Engineering
Via di Santa Marta, 3, 50139 Firenze, Italy

Tutti i diritti riservati. Nessuna parte del testo può essere riprodotta o trasmessa in qualsiasi forma o con qualsiasi mezzo, elettronico o meccanico, incluso le fotocopie, la trasmissione fac simile, la registrazione, il riadattamento o l' uso di qualsiasi sistema di immagazzinamento e recupero di informazioni, senza il permesso scritto dell' editore.

All rights reserved. No part of the publication may be reproduced in any form by print, photoprint, microfilm, electronic or any other means without written permission from the publisher.

*A mi amorosa familia Silvia, José Luis y Rodrigo, que
a pesar de la distancia, siempre están conmigo.*

*To my beloved family Silvia, José Luis, and Rodrigo who,
despite the distance, they are always with me.*

*À ma chère famille Silvia, José Luis et Rodrigo, qui
malgré la distance, ils sont toujours avec moi.*

*Alla mia amorevole famiglia Silvia, José Luis e Rodrigo,
che nonostante la distanza, sono sempre con me.*

Summary

This research work is organized in two parts. The first one addresses how to analyze the interdisciplinary problem of motorcycle safety, in order to maximize the positive impact of future motorcycle safety systems through a new methodological tool, which it was developed in this work. The second part describes a remote sensor, developed in this work, aimed at avoiding or mitigating the motorcycle crashes, as these were found necessary in the first part. Therefore, this research focused on the requirements to accomplish a conceptual safety functionality, called Motorcycle Autonomous Emergency Braking (M-AEB). The reason for this is because this safety system does not exist for motorcycles. The specifications behind the M-AEB functionality were taken from the outcomes of a prior EU research project called ABRAM (Autonomous BRAKING for Motorcycles).

The first part of this research identifies the real needs to make motorcycling safer. A common practice consists of performing the analysis of motorcycle crash data aiming to get information about the main trends and characteristics of the road accidents, but usually the scarce number of cases analyzed does not allow generalization. In advantage, this research used big data (>1 million of cases) extracted from a record of motorcycle crashes occurred in Italy. Analysis of this data resulted in 26 representative motorcycle crash scenarios, and provided insights about the environmental conditions at the moment of the crashes (i.e. visibility, adherence of the surface). However, the analysis of vast amount of crash data cannot be sufficient to quantitatively estimate the impact of the usage of motorcycles safety systems.

In this regard, I proposed a systematic way to address this research problem that take advantage of the information of different types of data sources available, which are not harmonized. Therefore, the first Knowledge-Based System for Motorcycle Safety (termed KBMS) was developed and implemented. The KBMS method allows researchers to predict the effectiveness of possible safety functions based on crashes that happened in a country during the last two or three years.

The first outcomes of the analysis of Italian crash data using the KBMS showed that modern assistance systems existent in the automotive market (such as autonomous emergency braking and hazard warning systems), are very promising solutions also for motorcycle safety. Therefore, the goal of this thesis was clearly defined to enable Advanced Driver Assistance Systems (ADAS) existing in cars but not present in the motorcycle industry.

The second part of this research is framed in the safety application of artificial perception systems, composed of a sensing part and perception or inference part. This is similar to artificial perception systems that are used in the automotive industry as a part of ADAS. Thus, a detailed study of high-end automotive remote sensors (e.g. RADAR, LIDAR, and Machine Vision) and corresponding perception algorithms was conducted. This study revealed some important features of perceptual algorithms for the motorcycle safety application, such as obstacle detector and trajectory estimation. Regrettably, the study also revealed that none of the existent automotive remote sensors is able to operate properly in a motorcycle due to its tilting behavior.

Consequently, the second part of this research focused on the development of a new remote sensor for the application in advanced motorcycle safety systems, followed by an

assessment of its potential to be used in safety systems. The sensor was conceived to accomplish:

1. The technical requirements to perform 3D measurement of a real traffic scenario from a vehicle that presents tilting dynamics.
2. The utilization of algorithms for obstacle detection and trajectory prediction in road traffic scenarios.
3. The specifications for the triggering of the conceptual M-AEB safety system in different motorcycle accident scenarios.

During this part of the research, it was found that a camera-based sensor, in a particular configuration, can accomplish the 3D scanning requirements of safety systems for motorcycles. This remote sensor was conceived as a part of an integral perception system, it means, bearing in mind to enable the utilization of a perception framework called “stixel world”. The stixel framework was targeted because it has unique characteristics, such as performing obstacle detection and tracking of non-rigid obstacles without performing target classification, which is a computationally expensive task. Therefore, I found it feasible to transfer its characteristics, which allow a real-time application in embedded systems containing dedicated chips for specific tasks, into a preventive safety approach in the motorcycle safety context. In particular, its possibility for obstacle detection and trajectories’ prediction in real time from data acquired by a stereo camera sensor.

A progressive development approach, based in the study of proximal remote sensor technology and remote sensors, allowed us to obtain a technical solution based on stereo vision technology. The system was initially tested in static conditions and in controlled dynamical tests, in order to prepare it for the execution of a large field test campaign. The test campaign exposed the proposed sensor in a variety of realistic traffic scenarios. The tests included the emulation of motorcycle crashes that happened in the past for which the deployment of the conceptual safety system (M-AEB), which slows down the motorcycle, would have been beneficial.

To conclude, the results of this research have been published in 2 Journals (Traffic Injury Prevention, and Sensors) and 4 international technical Conferences papers (from the fields of Machine Vision and Vehicular Safety). The two main outcomes of this research are the following:

- a. The creation of the first Knowledge-Based System for Motorcycle Safety (KBMS), which is a methodological research tool that has the potential to bridge motorcycle accident research with industrial development of safety systems.
- b. The remote sensor developed is the first part for depth studies of the application in advanced safety systems of tilting dynamic vehicles, becoming an initial step towards the implementation of advanced safety systems with the potential to make motorcycling a safer means of personal transport.

Table of contents

- Summary 4**
- Table of contents 6**
- List of figures11**
- List of tables18**
- Acronyms List20**
- Preface23**
- Part I25**
- 1. Importance of motorcycle safety and its impact in the global society26**
- 2. Real needs in terms of safety for motorcycle users28**
 - 2.1. Types of road accident databases.....28
 - 2.1.1. Differences between the road accident databases.....29
 - 2.2. Type of information extracted from in-depth road accident databases for the application to motorcycle safety30
 - 2.2.1. Examples from In-SAFE road accident database32
 - 2.3. Data variables of ISTAT (National road accident database)37
 - 2.4. Analysis of motorcycle crashes from ISTAT data39
 - 2.5. Description of human factors.....42
 - 2.6. Conclusions46
- 3. How to predict the performance of the safety solutions?47**
 - 3.1. Context for the analysis of motorcycle safety systems47
 - 3.1.1. Overview of PISA Project50
 - 3.2. Fundamentals: Knowledge-Based system of Motorcycle Safety.....50
 - 3.2.1. Relationship between data, information and knowledge50
 - 3.2.2. Defining a Knowledge Base.....51

3.2.3. Defining a Knowledge-Based System.....	51
3.2.4. Core of the KBMS	51
3.2.5. KBMS Framework.....	52
3.2.6. The collecting stage	52
3.2.7. The processing stage	53
3.3. Method of the Knowledge-Based system of Motorcycle Safety	53
3.3.1. Operative Framework	53
3.3.1. The processing stage	55
3.3.2. Inference Engine	55
3.3.3. Collecting stage.....	58
3.3.3.1. Selection of experts for the assessment.....	59
3.3.3.2. Example of expert assessment	59
3.3.3.3. Increasing the KB (collective knowledge).....	60
3.3.3.4. Inferring with the KB.....	60
3.3.3.5. Application case: Reduced study	60
3.3.3.5.1. Results of the comparison (PISA vs. KBMS).....	63
3.4. Discussion about the KBMS	64
3.5. Conclusion of the KBMS	66
3.5.1. Future work	67
Part II	68
4. Preventive safety and artificial perception systems	69
4.1. Concept of preventive safety	70
4.2. Artificial perception systems in road vehicles.....	73
4.2.1. Perception systems after DARPA grand challenge of 2005.....	74
4.2.2. Automotive perception systems: The stixel world representation and 6D-Vision.....	78
4.3. Sensors for remote sensing.....	79
4.3.1. State-of-the-art of proximal sensing.....	79
4.3.2. Potential of Vision Processing Units (VPUs) for the motorcycle safety application.....	80
4.3.3. Background: structured light for proximal sensing.....	81
4.3.3.1. Gray code projection.....	81

4.3.3.2.	Datamatrix code projection	84
4.3.4.	Example of recent proximal sensors	84
4.3.4.1.	Real sense SR300	84
4.3.4.2.	Realsense R200 and R400	85
4.4.	State-of-the-art of high performance computers for perception systems in vehicles	86
4.4.1.	First automotive super computer: DRIVE PX	87
4.4.2.	First AI automotive super computer: DRIVE PX2	88
4.4.2.1.	Technical specifications of DRIVE PX2 and its future evolution	89
4.4.3.	Machine vision in autonomous vehicles	90
4.4.3.1.	Machine vision in the motorcycle field	90
4.4.3.2.	Development kits suitable for motorcycle safety	91
4.4.3.2.1.	NVIDIA Jetson	91
4.4.3.2.2.	Carrier boards for NVIDIA Jetson	92
4.4.3.2.3.	FPGA-based deep learning accelerator	93
4.4.3.2.4.	INTEL: case of Myriad chips	94
4.5.	Conclusions	95
5.	Is it possible to apply ARAS on motorcycles?	96
5.1.	Motivation of a 3D perception system for motorcycles	96
5.2.	Motorcycle safety needs	97
5.3.	Automotive remote sensing	98
5.3.1.	Automotive RADAR technology	99
5.3.2.	Feasibility of automotive RADAR sensors for motorcycle safety	102
5.3.3.	Automotive LIDAR technology	103
5.3.4.	Feasibility of automotive LIDAR sensors for motorcycle safety	104
5.3.5.	Automotive Machine Vision technology	105
5.3.6.	Feasibility of Automotive Machine Vision for motorcycle safety	106
6.	Can stereo vision be used as a remote sensing approach?	108
6.1.	Stereoscopic vision considerations for motorcycle safety applications	109
6.1.1.	Stereo vision fundamentals	109
6.1.2.	Concepts of Field of View and Depth of Field	110
6.1.3.	Characteristics of a stereo camera rig: Common FoV, Range Field and Horopter $d=10$	110

6.1.4. Depth triangulation error in stereo camera sensors: Case of long-range applications while moving	111
6.1.5. Sub-pixel accuracy and their relationship with depth accuracy: Case of car detection	112
6.1.6. Camera decalibration (calibration loss).....	113
6.1.7. Stereo confidence clues.....	113
6.2. Materials.....	114
6.2.1. Sensor architecture (multifocal stereo rig and processing)	114
6.2.2. Calibration of the multi-focal stereo camera sensors	116
6.2.2.1. Semi-automatic algorithms for camera calibration	117
6.2.2.2. Fully automatic algorithms for camera calibration	120
6.2.3. Determination of the Range Field (verification of desired depth accuracy)	121
6.2.4. Determination of the horizontal resolution of the stereo vision sensor	122
6.2.5. Determination of dynamic ground truth	123
6.2.5.1. Materials	124
6.2.5.2. Ground truth generation using the satellite marker	125
6.2.5.3. Measurement on a moving target vehicle	125
6.2.6. Online camera re-calibration.....	129
6.2.6.1. Online re-calibration of the cameras	130
6.3. Conclusions	134
7. Field tests	135
7.1. Prior experiences with the M-AEB UNIFI demonstrator	135
7.1. Current experience with the M-AEB UNIFI demonstrator	136
7.2. Small moving target from a moving motorcycle	137
7.3. Turning maneuver at an intersection	138
7.4. Pre-crash test (based on a real motorcycle crash).....	142
7.4.1. Real motorcycle crash and the results of the crash reconstruction analysis	143
7.4.2. Virtual simulation of the crash before to M-AEB deployment	144
7.4.3. Crash emulation: on road test or pre-crash test	147
7.5. The experience employing the camera-based remote sensor in a pedelec.....	149
7.6. Conclusions	152
8. Discussion	154

8.1. First part: the KBMS methodology	154
8.2. Second part: the remote sensor	156
Conclusions and Outlook	158
Appendix A.....	160
Appendix B.....	162
Appendix C.....	164
Appendix D.....	165
Appendix E.....	168
Appendix F	169
Appendix G	170
Appendix H	172
Acknowledgements	174
Bibliography.....	175

List of figures

Figure 1. GIDAS database: Detail of injury level for motorcyclists (Otte et al., 2013)	31
Figure 2. MAIDS Final report 2009: In-depth investigations of accidents involving powered two-wheelers	31
Figure 3. General description of In-SAFE database architecture and images of the information collected from the personal protective equipment of the motorcyclist and the crash deformation on the collided car	32
Figure 4. Topology of the motorcycles in the database	33
Figure 5. Injuries distribution (left side) and MAIS distribution (right side)	33
Figure 6. Example of injury causation for MAIS 3+	34
Figure 7. Head injuries and their impact point's location over the colliding car	35
Figure 8. Example of vehicle deformation by the use of 3D point cloud measurements	36
Figure 9. Example of a real motorcycle road accident scenario (In-SAFE: ID86)	36
Figure 10. Organization of the data variables of ISTAT road accident database and their arborescence. The circles at the end of the branches denote the continuation of the variable's arborescence (the same as the previous variable). Note: experience (*) is defined by Equation 1.	37
Figure 11. Detail of accident scenarios of ISTAT database and their arborescence. The circles at the end of the branches denote the continuation of the scenario's arborescence (the same as the previous variable).	38
Figure 12. Number of PTW road accidents by area: urban, rural, and motorway	39
Figure 13. Number of PTW road accidents by pavement conditions: dry asphalt, wet asphalt, slippery asphalt, frozen asphalt, and snowy asphalt	39
Figure 14. Number of PTW road accidents by weather conditions: clear, foggy, rainy, hailstorm, snow, and windy	40
Figure 15. Number of PTW by type of crash: Head-on, Angle, Sideswipe, Rear-end, Hit pedestrian, Hit stopped vehicle, Hit parked vehicle, Hit obstacle, Hit train, Run-of-the-road, Sudden braking, Falling from the PTW	40
Figure 16. Detail of total traffic accidents, PTW accidents, and its relationship during a period of 13 years (2000 to 2012). The upper graphs show a declining trend in the number of accidents, instead the bottom one that shows a stable ratio (around 35.4%) between the total vehicular crashes and the PTW ones	41
Figure 17. Detail of PTW crashes in four different street areas (normalized respect to the total PTW accidents of the year). The opposite slopes between intersection and roundabout could be explained by the fact that the roundabout is a particular case of intersection, and during the years some angular intersections layouts in Italy were replaced by roundabouts layouts	41

Figure 18. Detail of age of moped riders involved in a traffic accident.....	42
Figure 19. Detail of age of motorcycles riders involved in a traffic accident.....	42
Figure 20. Detail of age of motorcycles and moped riders involved in a traffic accident.	43
Figure 21. Detail of the years of experience of the moped riders at the accident moment. ...	43
Figure 22. Detail of the years of experience of the motorcycle riders at the accident moment.	44
Figure 23. Detail of the years of experience of the motorcycle and moped riders at the accident moment.....	44
Figure 24. PTW rider age of riders in a crash (2008)	45
Figure 25. PTW rider experience at the moment of the accident (2008).....	45
Figure 26. Explanation of the Safety Function concept by examples	49
Figure 27. Graphical abstract of the Knowledge-Based system of Motorcycle Safety.....	49
Figure 28. Scheme of the relationship between the data, information, knowledge and wisdom.	50
Figure 29. The components of the Knowledge-Based system of Motorcycle Safety are shown in grey. As an initial step the KBMS framework is formulated by defining the queries set, the selection of safety functions and accident scenarios. The queries extract the relevant information of the Road accident database, for the Inference Engine. Parallel in the workflow from the KBMS Framework to the Inference Engine, at the processing stage, the SF are assessed in several Road Accident Scenarios by experts, in order to obtain the contents of the knowledge base. This assessment is based on a list of Safety Functions which are evaluated for certain Road Accident Scenarios at the collecting stage (generating Input 2). Moreover, at the processing stage two tasks are performed: a) the validation of expertise coming from Input 2 in order to increase the Collective Knowledge of the KBMS; b) the combination of the Input 1 with the Collective Knowledge to define a prioritized list of Safety Solutions that corresponds to the country/region of the road accident data used.	52
Figure 30. Schematic process to build and apply a Knowledge-Based System as the KBMS.	53
Figure 31. Detail of data contained in the effectiveness matrix (Eki) and their arborescence. The circles at the end of the branches denote the continuation of the arborescence (the same as the previous variable).....	56
Figure 32. Example of an expert assessment of two Safety Functions (SFs) for parking-out maneuvers. The numbers in the table represent the outcome of the expert evaluation using the scoring scale defined in Table 4.....	60
Figure 33. Main variables of ISTAT road accident database. The circles at the end of the branches denote the continuation of the arborescence (the same as the previous variable).....	66
Figure 34. Proposed classification of safety systems.....	71
Figure 35. Safety performance expected for different safety systems.	72
Figure 36. Detail of instrumentation of Robotcar sensing platform (adapted from Oxford website)	73
Figure 37. Vehicle winner of 2005 DARPA challenge. (a) Remote sensing apparel in the top of the vehicle. (b) Scheme of the sensing and artificial perception strategy. (c) System architecture with detail of the perception strategy and its corresponding sensors.	74
Figure 38. Neural network vision model: (top) sketch of human brain in which areas associated with vision are shown in red, and (bottom) block diagram of human vision process. 75	
Figure 39. Visual sensing and perception of the off-road rover.....	76

Figure 40. Estimation of terrain traversability, in terms of both terrain slope and obstacles. .76	76
Figure 41. Example of an urban scene corresponding to the KITTI dataset: (top) the classified occupancy grid, (bottom) is the depth information.77	77
Figure 42. Two examples in which a perception system identify the depth, direction and speed of different obstacles. The arrows show the prediction of the location of the different parts of the obstacle sensed in the following half second. This technique for the perception of road scenes is known as “stixel world”78	78
Figure 43. Last ASIC for embedded artificial vision released in August 2017. Adapted from https://www.movidius.com/80	80
Figure 44. Detail of the neural computer featuring a VPU (Myriad 2) in a blue heat sink case connected to an embedded system - Released in July 201781	81
Figure 45. Scheme of 3D scanning with structured light.81	81
Figure 46. Aspect of the Asus Xtion Pro remote sensor (left lens belongs to the IR projector and the right lens corresponds to the IR camera)82	82
Figure 47. Graphical pattern corresponding to a Gray code of 10 bits (the pattern must be read in vertical scanning lines).....82	82
Figure 48. Calculation of depth by disparity measurement83	83
Figure 49. Infrared picture of the Grey pattern projected on a wall83	83
Figure 50. Infrared picture of the Kinect sensor scanning part of a room.84	84
Figure 51. Aspect of the SR300 proximal sensor camera based in structured light. Adapted from https://click.intel.com/realsense.html84	84
Figure 52. Scheme of main internal component of the SR300. (a) Detail of the position of the ASIC, IR camera, RGB camera and IR laser projector. (b) Scheme of the FoV of each component: IR & Projector (depth measurement), and RGB (color image)85	85
Figure 53. OEM proximal sensor of Intel Realsense portfolio. Adapted from https://click.intel.com/realsense.html86	86
Figure 54. Examples of DRIVE PX automotive super computers. On the left hand is the version of Bosch supplier and on the right side the implementation of ZF88	88
Figure 55. Render of prototype of DRIVE PX2 of NVIDIA. It includes the Pascal processor. Adapted from https://www.nvidia.com/en-us/self-driving-cars/drive-px/88	88
Figure 56. Roborace car with description of its perceptual sensors. Adapted from https://roborace.com/89	89
Figure 57. Actual and planned supercomputers for automotive applications. Adapted from https://www.nvidia.com/en-us/self-driving-cars/drive-px/90	90
Figure 58. Jetson TK1 developer kit. Note that the main chip need a heatsink with a fan for air cooling which are not present in the picture. Adapted from http://www.nvidia.it/object/jetson-tk1-embedded-dev-kit-it.html91	91
Figure 59. NVIDIA Jetson TX2. On the left hand there is the credit card size board with the main processor that can be installed in rugged hardware. On the right side there is the complete set of boards for development purposes. Adapted from http://www.nvidia.it/object/jetson-tx1-module-it.html91	91
Figure 60. Detail of connections of Astro Carrier of Connect Tech Inc.92	92
Figure 61. Detail of connections of Orbitty Carrier by Connect Tech Inc.92	92
Figure 62. Detail of connections of Auvidea carrier board.93	93
Figure 63. Aristotle architecture, which is designed for CNN acceleration. Adapted from link.94	94
Figure 64. Intel is supporting seven AI software frameworks95	95

- Figure 65. Circumstances of motorcycle crashes in Italy, more than 2 crashes every 15 minutes (percentages for the period 2000-2012). The left chart indicate where the crashes happened, totalizing more than 87% in urban areas. The center chart indicate the pavement conditions at the moment of the crashes, resulting in more than 88% over a dry street. The right cart present the weather at the moment of the crashes, indicating that more than 86% of the crashes occurred in clear visibility conditions..... 97
- Figure 66. Radar Cross-Section of a motorcycle. Adapted from (Köhler et al., 2013)..... 99
- Figure 67. Top view of the 3D scanning volume of a commercial automotive radar and relevant specifications corresponding to the short range. Adapted from the technical datasheet of the ARS 408-21 Continental radar 101
- Figure 68. Representations in scale of the size of the beam impacting on a generic car. The numbers in degrees correspond to the three azimuth beam width. In the left diagram the car is located 7 m away from the radar, while in the other diagrams the car is 14 m away 101
- Figure 69. Example of an ideal radar scanning 7 m ahead when the motorcycle is tilted only 10 degrees. The increment of the clutter (unwanted echoes) coupled with the reduction of the surface radiated by the car can lead to radar blind 102
- Figure 70. Aspect of the automotive LIDAR and its relevant specifications. Adapted from the technical datasheet of ibeo LUX. 103
- Figure 71. Representations in scale of the size of the beam impacting on a generic car. On the left picture, the numbers above of the laser footprints represent the distance to the laser scanner. For example, the rectangle below the number 43 have the size of the impacting laser footprint on a car 43 m away. On the right picture, the multi echo effect is depicted for a target car at 57 m from the laser scanner..... 104
- Figure 72. Example of an ideal LIDAR scanning 14 m ahead when the motorcycle is tilted only 10 degrees. Several condition in this case lead to the no visibility of sounding targets. On the right side part of the scanning plane will not intersect possible targets, while on the left side part of the scanning plane will impact on the floor 105
- Figure 73. Representation of the stereo camera and the different 3D plane projections of the traffic scene using the “U-V-Disparity” concept. On the right image is overlaid the identification of the street and other big surfaces. Adapted from Hu and Uchimura, 2005 105
- Figure 74. Left: conceptual representation of the stixel world. Center: the Disparity Map of the stereo vision system as interpretation of the depth of the traffic scene. Right: the stixel representation of the different obstacles. Adapted from Benenson 2011 and Badino 2009..... 106
- Figure 75. Top view of a conventional stereo vision system. Detail of the Range Field including the boundary of depth triangulation range adopted at the Horopter of 10 disparities. 111
- Figure 76. Overview of the imaging system. (a) Multi-focal stereo rigs installed in the frontal part of the vehicle and fixed to the scooter frame. (b) Top view of the 3D space to measure in front of the scooter (the outer stereo cameras are used for development purposes and future extension of the long range of measurement)..... 114
- Figure 77. Wiring detail for the synchronization of the six cameras. (a) Circuital scheme. (b) A disassembled camera showing the location of the electrical connections labeled “1” and “2”..... 115
- Figure 78. Characterization of the imaging system (monocular camera and fixed lens). (a) Shows the 3D location and pose (orientation) of the patterns used during the calibration

w.r.t. one camera. (b) 2D plot of the reprojection error for all the features. (c) Graph of lens distortion (aberration)	117
Figure 79. Example of one result of the projected points after an imprecise camera calibration	118
Figure 80. Scene to evaluate the remote sensor. The traffic cones of well-known dimensions are the landmarks used to generate ground truth. The targets were measured using a laser rangefinder.....	118
Figure 81. Example of the left image of the stereo pair processed. Image with big contrast and illumination changes	119
Figure 82. Disparity Map (DM) calculated from the stereo images. Dark areas represent objects that are farther away, while light areas represent nearby objects	119
Figure 83. 3D point cloud or 3D reconstruction of the scene imaged	119
Figure 84. Overview of the graphical user interface of the Matlab Application for the stereo camera calibration	120
Figure 85. Depth accuracy quantification of the calibrated stereo camera (long-range camera rig). (a) Rectified left picture acquired by the long range stereo camera sensor. (b) Disparity Map of the scene (range from 0 to 128d). (c) Three-dimensional reconstruction or 3D point cloud of the scene imaged. (d) Top view of the 3D point cloud highlighting the location of the traffic cones originally placed at 10m, 15m, and 20 m. This 3D point cloud can be download according to Appendix B for a better assessment of the reader	122
Figure 86. Analysis of small narrow objects in the farthest half of the Range Field (long-range camera sensor). 3D control points were located at similar places for each couple of cones for the analysis. (a) Detail of the 3D representation of the targets. (b) Frontal view of the targets (grid sized 10 cm). (c) Top view of the 3D point clouds (grid sized 50 cm). For the cones at 20 m the fattening effect becomes evident (depth artifact)	123
Figure 87. Overview of supporting structure and detailed measurements of the satellite marker and its alignment with respect to the target car. Only the lateral setup (satellite marker in one of the sides) was used in this experiment	124
Figure 88. Succession of 20 representative frames to describe the maneuvers for which the heading angle ground truth was obtained. The numbers represent the temporal order of the sequence during the maneuvers.....	126
Figure 90. Example of the 3D point cloud generated from the disparity map (all the units are in meters).....	127
Figure 89. 2D trajectory of the target car during the experiment. The measure indicates the relative position of the two yellow antennas installed in the vehicles. One antenna is positioned in the rear part of the PTW (coordinate origin) and the second antenna on the satellite marker frame	127
Figure 91. From left to right is illustrated in vectorial form the measurement performed (D-GPS) and the equivalent measure synthesized from three components of the ground truth (imaging system)	128
Figure 92. Comparison of the Ground Truth location generated with the satellite marker method and a more accurate reference provided for the D-GPS system	128
Figure 93. Illustration of the automatic camera extrinsic parameters re-calibration. (a) An initial rectification of the stereo frame according to the static calibration values. (b) SURF feature extraction in both images of the stereo pair (circle's diameter represents the scale of the feature – only 30 are shown for clarity). (c) The salient features matched	

	(correct pixel assignments indicated by yellow connections – the 1000 features are shown) are overlaid on a 3D anaglyph	129
Figure 94.	Chart showing the percentage of effective stereo frame used to calculate the Disparity Map (DM) during the first six neighboring frames (consecutive frames) of the 1 second pre-crash sequence. Below 45%, the number of reliable pixels is insufficient to compute the DM.....	133
Figure 95.	Concept of AEB for cars and M-AEB for motorcycles (UNIFI Demonstrator). 135	
Figure 96.	Investigating the feasibility of M-AEB from the perspective of the motorcyclist	136
Figure 97.	This is the left picture of the short-range sensor.....	137
Figure 98.	This is the disparity map containing 3D information of the scene	137
Figure 99.	3D point cloud showing that the scooter is located at 14 meters from the motorcycle demonstrator.....	138
Figure 100.	Analysis of a turning maneuver: measurement of the space in front of the scooter. Short-range and long-range measurements are depicted simultaneously for comparison. (a) Rectified left picture of the short range stereo camera sensor. (b) Rectified left picture of the long range stereo camera sensor. (c) Short-range Disparity Map (0 to 32d). (d) Long-range Disparity Map (0 to 128d). The 3D point cloud is available for download (see Section 6.2.2.1).....	139
Figure 101.	3D point clouds corresponding to the turning maneuver scene calculated from the information provided by the two stereo camera sensors. (a) Reconstruction for the short-range stereo camera (wide common Field of View). (b) Reconstruction for the long-range stereo camera (narrow common Field of View)	140
Figure 102.	Top view of the 3D point clouds corresponding to the turning maneuver. (a) Depth measurement delivered by the short range sensor (accurate depth measures are inside the Range Field). (b) Depth measures delivered by the long range sensor (Car 4 is not in the common Field of View of this stereo camera sensor).....	141
Figure 103.	Cleaned measurements of the corresponding to the turning maneuver. (a) The 3D point cloud inclined 13° to compensate the leaning of the scooter. (b) Top view of the measures	142
Figure 104.	Sketch of the motorcycle crash id90.....	143
Figure 105.	Visual results of the 3D crash reconstruction for two instants of time before the crash.	144
Figure 106.	Speed and acceleration evolutions before crashing (id90). Real case (top) in which the motorcyclist loss the control of the PTW during a hard braking. Simulated case (bottom) in which is supposed that the motorcyclist can handle the braking action due to ABS intervention.....	145
Figure 107.	Relative orientations and locations between the PTW and the Opposite Car (id90).	146
Figure 108.	Analysis of the pre-crash scene (id90 – InSAFE). (a) Rectified left picture of the long range stereo camera sensor. (b) The 3D anaglyph composed by the stereo frame. (c) Disparity Map (0 to 64d). (d) 3D reconstruction.....	147
Figure 109.	Detail of 3D reconstruction of the pre-crash scene (id90 – In-SAFE). (a) Cleaned 3D point cloud seen from the scooter point-of-view. (b) Cleaned top view representation of the pre-crash scene.....	148
Figure 110.	Roll angle fluctuations during 5 trials of the emulation of the motorcycle crash (id90 – In-SAFE).....	149

Figure 111. Pedelec with the stereo camera rig installed on the handle bar. (a) Complete vehicle view and detail of the frontal suspension. (b) Detail of the camera-based remote sensor (imaging system).....	150
Figure 112. Results of the remote sensor while taking a curve (pedelec tilted 22°). (a) Left image of the stereo camera pair. (b) Disparity Map calculation (0 to 128 disparities). (c) 3D measurement of the scene up to 14 m. (d) Top view of the 3D scene.....	150
Figure 113. Results of the remote sensor when traveling on a bicycle path (pedelec tilted 17°). In this case the 3D point cloud was mathematically rotated (straighten) to easy the depth inspection in the 3D reconstruction. All units are in meters.....	151
Figure 114. 3D sensing in a scene with strong changes of illumination. (a) Left image of the stereo camera pair. (b) Disparity Map calculation (0 to 128 disparities). (c) 3D measurement of the scene in meters.....	151
Figure 115. 3D sensing of a cyclist at an intersection of streets (cobblestone street – thick patterned surface).....	152
Figure 116. Descriptions of the Work Packages of MOTORIST project and the organizations involved. This research belongs to WP2 which is highlighted in light blue	160

List of tables

Table 1. List of publications done during the period of doctoral research showing the contribution of the Ph.D. Candidate to each publication and related thesis chapters.	24
Table 2. Characteristics of a National road accident database	28
Table 3. Characteristics of an In-depth road accident database	29
Table 4. Likert-type scoring scale defined to rank the benefit of the safety function in each accident scenario to analyze	55
Table 5. Expert legitimization table for KBMS assessment (it is filled as an example). In this way, it is possible to consider if the applicant could be accepted as a recognizable expert for the purpose of the KBMS or not, allowing recognizing both: academicals and industrial experts	59
Table 6. Information retrieved after the segmentation process applied to ISTAT road accident database. The information corresponds to the years 2010, 2011 and 2012	61
Table 7. List of Safety Functions (SFs) used in the application case. This subset contains a variety of SFs, going from a very specific target to broad ones	62
Table 8. Numerical values of the last two steps of the inference engine. They are the results that quantify the importance of each SF analyzed for Italy (in the reduced study). The left column indicate the number of the Safety Function (SF) evaluated. The three intermediate columns show the result of the inference engine until the penultimate step (this example is didactic because the assessment was performed only for three experts and with 10 SFs). The rightmost column is the output of the KBMS applied to ISTAT database, presenting as the most prominent the SF number 2, followed by the 61, 6, 34, 53,	62
Table 9. Prioritized safety solutions of KBMS-ISTAT and PISa studies. The left column is the prioritized list of Safety Functions in the KBMS method. The KBMS metric expresses the importance of each SF (larger numbers represents more importance). PISa columns represent the same information in a different manner (quartiles and absolute score), allowing comparison between the KBMS-ISTAT outcomes with those of PISa project (mark 36 means “less important”)	63
Table 10. SAE international’s J3016 provides a common taxonomy and definitions for automated driving in order to simplify communication and facilitate collaboration. .	70
Table 11. Overview of motorcycle crash scenarios in Italy (period 2010-2012).....	98
Table 12. Specification of the stereo rigs and constitutive cameras	115
Table 13. Range Field of the remote sensor calculated for the application on advanced safety systems	116
Table 14. Main values of the calibration of the stereo rigs for both measuring ranges	121

Table 15. The left column corresponds to the depth triangulation on the rectified images (Simple rectification) obtained from the static calibration (extrinsic + intrinsic parameters of the camera model). The central and right columns corresponds to the re-calibration (second step of the online re-calibration).131

Table 16. From the 4th and 5th frames of the static calibration cannot be measure the target due to the decalibration at these moments, while in the 6th frame the depth triangulation is reliable again (borderline)132

Table 17 Expert legitimization table for KBMS assessment (it is filled as an example)168

Acronyms List

ACC	Adaptive Cruise Control
ADAS	Advanced Driver Assistance Systems
AEB	Autonomous Emergency Braking
AI	Artificial Intelligence
AIS	Abbreviated Injury Scale
ALU	Arithmetic Logic Unit
API	Application Program Interface
ARAS	Advanced Rider Assistance Systems
ASIC	Application Specific Integrated Circuit
B	Bandwidth
BSD	Blind-Spot Detection
CV	Computer Vision
D-GPS	Differential Global Positioning System
DLT	Direct Linear Transformation
DM	Disparity Map
DNN	Deep Neural Networks
DRAM	Dynamic Random Access Memory
DSP	Digital Signal Processors
EC	European Commission
ECU	Electronic Control Unit
EIE	Efficient Inference Engine
ESC	Electronic Stability Control
EU	Europe Union
FMCW	Frequency Modulated Continuous Wave

FoV	Field of View
FPGA	Field Programmable Gate Array
FREAK	Fast REtinA Keypoint
GIDAS	German In-Depth Accident Study
GNSS	Global Navigation Satellite System
GPU	Graphics Processing Unit
ICS	Inevitable Collision State
ISS	Injury Severity Score
KB	Knowledge Base
KBMS	Knowledge-Based system of Motorcycle Safety
KBS	Knowledge-Based System
LCA	Lane-Change Assist
LIDAR	Light Detection and Ranging
M-AEB	Motorcycle Autonomous Emergency Braking
MAIDS	Motorcycle Accidents In-Depth Study
MEMS	Microelectromechanical Systems
MV	Machine Vision
NCS	Neural Computer Stick
NTTV	Narrow Track Tilting Vehicle
OD	Obstacle Detector
OEM	Original Equipment Manufacturer
OPA	Optical Phased Arrays
PC	Personal Computer
PTW	Powered-Two Wheeler
RADAR	RAdio Detection And Ranging
RANSAC	RANdom SAmples Consensus
RCS	Radar Cross-Section
RF SOI	Radio Frequency Silicon-On-Insulator
ROS	Robotic Operating System
RTK	Real Time Kinematic
RTL	Register-Transfer Level
SDK	Software Development Kit
SF	Safety Function
SfM	Structure-from-Motion

SiGe	Silicon Germanium
SLAM	Simultaneous Localization And Mapping
SoC	System on Chip
SRAM	Static Random Access Memory
SURF	Speeded-Up Robust Features
TEM	Transverse Electromagnetic Mode
TFLOPS	Tera Floating Point Operations
TOF	Time-Of-Flight
TTC	Time-To-Collision
UKF	Unscented Kalman Filter
UNIFI	University of Florence
V2V	Vehicle-to-Vehicle
VPU	Vision Processor Unit

Preface

The safety systems applied to transport are essential to support the development of our society because the growth of the population increases the complexity of means transport of goods and people. This has motivated the creation of an integral research framework, (Appendix A) from which emerges this research activity.

A number of reasons, like the expected increment of the worldwide population along all this century, are pushing towards the organization of designing new strategies and road legislations in order to fully automatize the transportation system. This goal promises to lead to a minimization of road accidents, with positive effect on the populations' life, and a decrement of expected medical costs due to rehabilitation of people involved in crashes.

However, the full automatization of the transportation network is something that possible will not happen. Other non-automated vehicles (for personal transportation) that have the desired characteristics, such as carbon neutral, simple to maintain and repair, will be adopted to travel daily in cities, and also, for recreation activities. In this context, tilting vehicles have a good potential to be these non-automated vehicles.

This work introduces the fundamentals behind tilting vehicles safety that may differ in certain aspects with respect to the automotive safety field. For example, the visibility conditions when crashes happen, or the dynamics of the vehicles prior crashing. The focus on the powered-two wheelers field is motivated due to the current usage of these vehicles, beside its promotion for the governments in the EU and around the world. Concerning the research activity presented in this document, the two-fold aim was:

1. Identifying Safety Functions (SFs) with the potential to produce a positive impact in motorcycle safety, by scoring the relevance of each SF in a qualitative manner.
2. Starting the development of one of the most promising safety solutions as a proof-of-concept and to evaluate it in representative and realistic motorcycle accident scenarios.

Chapters 1 and 2 describe the activity realized for the achievement of the first goal, for which the methodological solution consisted in a Knowledge-Based System. The methodology is unique in the field of motorcycle safety and it was well received for the road safety community. The method is already available to the research community through the following Journal publication [P1] (see Table 1).

Chapter 3 introduces the concept of Preventive Safety through a brief review of the state-of-the art of the advanced safety systems for cars. Additionally, selected novel

approaches (still under study) towards the concretization of the autonomous cars are presented. These approaches were selected based on their possible applicability for use in motorcycle safety. Finally, the Knowledge-Based System for Motorcycle Safety is developed.

The following chapters describe the activities towards the achievement of the second goal. Chapters 4 and 5 explain the proximal and remote sensing for the automotive application. These chapters describe the different sensing approaches and different perception algorithms. The operation of these sensing approaches allowed me to identify the technological gap that makes it difficult to implement advanced safety systems in tilting vehicles. This technological gap turns into a safety gap in the motorcycle application, which explains the lack of equivalent Advanced Driver Assistance Systems (ADAS) for motorcycles. These outcomes, together with the analysis of the different detection approaches, were accepted for publication in the international Transport Research Arena during the 2018 [P2].

Chapters 6 and 7 explain the development, evaluation and validation of the remote sensor conceived for the application in vehicles that lean over, such as motorcycles, pedeless and other L3 category vehicles (European category). Our remote sensing is the first in its type in the field of tilting vehicles safety; and the sensor was materialized as a demonstrator prototype. The outcomes of the research are already available to the research community through one additional Journal paper belonging to the Sensors field [P3], and four peer-reviewed conferences, of which two corresponding to the Machine Vision field [P4, P5] and two corresponding to vehicular safety systems [P2, P6].

This thesis finalizes discussing the limitations of all the experiments performed, suggesting further experiments with their motivations, mentioning improvements on the actual sensor design, and concluding about the potential of this sensor technology to enable preventive safety approaches in tilting vehicles.

Table 1. List of publications done during the period of doctoral research showing the contribution of the Ph.D. Candidate to each publication and related thesis chapters.

[P1]	Related with chapter 1, 2, 3	Are automatic systems the future of motorcycle safety? A novel methodology to prioritize potential safety solutions based on their projected Effectiveness; <i>Journal: Traffic Injury Prevention 2017</i> <u>Authors: Gustavo Gil , Giovanni Savino , Simone Piantini , Niccolò Baldanzini , Riender Happee , Marco Pierini</u>
[P2]	Related with chapter 4, 5	Is stereo vision a suitable remote sensing approach for motorcycle safety? An analysis of LIDAR, RADAR, and computer vision technologies subjected to the dynamics of a tilting vehicle; <i>Transport Research Arena 2018 (TRA 2018)</i> <i>Section: 10. Safe, Secure and Resilient Transport Systems</i> <u>Authors: Gustavo Gil, Giovanni Savino, Simone Piantini, Marco Pierini</u>
[P3]	Related with chapter 3, 6, 7	Motorcycle that see: multifocal stereo vision sensor for advanced safety systems in tilting vehicles; <i>Sensors for Transportation. A special issue of Sensors (ISSN 1424-8220) belonging to the section "Physical Sensors". 2017</i> <u>Authors: Gustavo Gil, Giovanni Savino, Simone Piantini, Marco Pierini</u>
[P4]	Related with chapter 6, 7	Satellite Markers: a simple method for ground truth car pose on stereo video; <i>10th International Conference on Machine Vision. SPIE Digital Library, 2017</i> <u>Authors: Gustavo Gil, Simone Piantini, Giovanni Savino, Marco Pierini</u>
[P5]	Related with chapter 6, 7	First stereo video dataset with ground truth for remote car pose estimation using satellite markers; <i>10th International Conference on Machine Vision. SPIE Digital Library, 2017</i> <u>Authors: Gustavo Gil, Giovanni Savino, Marco Pierini</u>
[P6]	Related with chapter 3, 6, 7	Obstacle detection tests in real-world traffic contexts for the purposes of motorcycle autonomous emergency braking (MAEB); <i>25th International Technical Conference on the Enhanced Safety of Vehicles (2017). Paper Number 17-0047</i> <u>Authors: Giovanni Savino, Simone Piantini, Gustavo Gil, Marco Pierini</u>

Part I

1. Importance of motorcycle safety and its impact in the global society

World population will continue growing this century by 33-70% (Gerland et al., 2014). In 2017, the United Nations reported a world population projection of 11.18 billion by 2100 compared to 7 billion in 2011 (UN, 2017). In this context, urban zones will experience an increase in its population, therefore an efficient administration of its resources and community services will be a need.

Consequently, cities will turn into smart cities and optimization of common public spaces and the control of pollutant gas emissions produced for the personal transportation needs of its citizens will become a must. In this regard, the common view is that personal electric mobility is the solution, but it is only a partial view of the whole urban mobility problem.

Motorcycles, pedelecs (electric bicycles), and powered vehicles which presenting a tilting motion, such as scooters, mopet, mofas, and three- or four-wheeled tilting vehicles denominated Narrow Track Tilting Vehicles (NTTVs) have shown to be advantageous in congested cities. For example, they require less parking space than passenger-cars, and they are used in successful shared mobility services in Europe. The advantages of these vehicles have also been highlighted by various authors, which stated their potentialities to enhance personal mobility (Festini et al., 2011).

Additionally, cost reasons (Will et al., 2011) and their potential for sustainability, especially in the case of electrification (Bishop et al., 2011; Weiss et al., 2015; Santucci et al., 2016; Sindha et al., 2017), favor the potential adoption of these vehicles. In the case of China, which is the largest country in terms of population, the government led the industry in this direction (Ruan et al., 2014; Simha, 2016) to face the air-pollution caused by the personal mobility of its citizens.

In the EU, hybrid electric-internal combustion powertrains for three-wheelers vehicles have been proposed in the market. Specific studies confirmed the favorable recyclability and recoverability of hybrid three-wheelers according to the most demanding regulation adopted for automotive products, which are not current requirements for this type of vehicles (Berzi et al., 2016).

On the other hand, countries with developed cycle path infrastructures shown societal healthy benefits (Oja et al., 2011; Schepers et al., 2015; Götschi et al., 2016). Health benefits of cycling can be extended to the elderly population by the adoption of pedelecs but the risk of crashes increases (Schepers et al., 2014) and significant number of accidents with less severe injuries may be not reported (Schepers et al., 2017). Research underlines that population health

benefits need to be supported by appropriate transport safety measures (de Hartog et al., 2010; Simha, 2016).

The injury severity level in case of crashes is the biggest barrier for the societal adoption of tilting vehicles. In the case of motorcycle crashes, these type of road users are generally subjected to serious consequences for life. Motorcyclist are the 23% of the deaths on the world's roads (World Health Organization, 2015), and they have 26-fold higher risk of death than those driving other types of vehicles (NHTSA USA, 2015).

In the context of an important increment of the population (about twice as much as today in the year 2100 – UN, 2017) and a more complex traffic environment, this research focuses on motorcycle safety. The achievement of safer motorcycles through technology is important due to the possibility of extending the safety solutions to all vehicles that have a tilt dynamic. In this sense, the final aim of this research is to make tilting vehicles safer, which contribute to a needed sustainable and effective urban mobility solution.

2. Real needs in terms of safety for motorcycle users

Chapter 2 describes the type of data collected on road accident databases or crash databases. An analysis of motorcycle crashes in Italy was developed using two different type of crash databases. The In-SAFE database (in-depth road accident database of the University of Florence) was used for the understanding of specific motorcycle crash scenarios, by employing detailed crash information of these crashes. The National database used has provided large data corresponding to 13 years of road accidents, including more than one million motorcycle crashes. The big data belongs to ISTAT database (Italian government database), and it was used to identify the features of the more frequent road accidents that involved motorcycles.

2.1. Types of road accident databases

To analyze the road accident problem, two types of databases contain the information of the accidents, the National databases and the in-depth accident databases. When the database is constituted for a standard set of data which is collected where the accident occurred, these are generally a national road accident databases (Table 2). These databases are commonly filled by the police force and the first-aid services. Thus, national databases contain the main aspects of the accidents including data about the vehicles and people involved, the traffic scenario, and the testimony of witnesses to the crash.

Table 2. Characteristics of a National road accident database

Advantages	Drawbacks
All countries have one	Accuracy of data
Big data (quantity)	Unknown values
Country coverage	
Yearly updated	
Main data variables (20)	

When the content of the database is more detailed than those of the National road accident database, it is common to refer to an In-depth road accident database (Table 3). The information of these type of databases are obtained as a results of different investigations. Depending of each particular case, the investigations can be carried out from the analysis of video footages that captured the road crash, medical and/or forensic analysis of the people involved, and the crash analysis reconstruction (virtual environment) that is a result of the investigation of the damages in the vehicles and skid marks in the road scene.

Table 3. Characteristics of an In-depth road accident database

Advantages	Drawbacks
High accuracy of data	Small dataset
Allowing crash analysis reconstruction	Not available in several countries
Data variables (200 – 1500)	Confidential info.
	Reduced coverage
	Expensive

2.1.1. Differences between the road accident databases

National road accident databases contain a reduced set of variables (about 20 variables), that helps to describe the circumstances of the accident. These variables help to provide a description of the type of vehicles involved in the crash, the people involved, and the type of crash scenario. The reduced set of variables are standardized by each country in order to provide a meaningful description of all road accidents of the country. The set of variables collected by each country is similar, and this can allow researchers for the comparison of the main crash trends among different countries.

The advantages of National road accident databases relies on the possibility to access to big amounts of data for statistical purposes, which is updated yearly. This databases involves a big region of study (e.g. a full country). The drawbacks of National road accident databases relies on inaccurate or coarse information which is often collected. This can be motivated because the police officers sometimes must rely on the statement of eyewitnesses of the accident, or as another example, the sketch describing the accident is not clear or incomplete. From the side of the first-aid services, inaccuracies can be produced during the medical report which is filled after the event, because different people are involved during the process. The examples, can led us to classify as “unknown” part data of the data collected and therefore marked as unknown in the statistics.

In-depth accident databases have a different way of data collection which is aimed to produce reliable and more accurate data. These databases contain information about the accident elaborated for specialists in road safety. They collect relevant measurements of the traffic scenario for the particular accident type, inspect the vehicles in order to measure vehicles’ deformation (damages). Other specialist review the type and level of injuries from

the people involved in the crash. Subsequently, all these kind of data is used to calculate the energy dissipated during the impact (road crash), and perform simulations describing the crash.

The advantage of In-depth databases is the high quality of data collected, allowing for different analysis. For example, the crash analysis reconstruction outcome a variety of information about the accident, this translate in a big set of variables that describes the accident, ranging from 200 to 1500 depending the complexity of the crash. However, the drawbacks of these databases relies on the difficulty to conduct these meticulous analysis.

In-depth road accident databases requires the availability of specialized people to investigate the road accident scenario shortly after the accident happens. This is vital to obtain skid marks and other traces that fade in less than 20/30 minutes. This makes that the In-depth databases are circumscribed to a small area (reduced coverage), and also that some cases cannot be treated for a complete in-depth analysis due to the lack of important evidence. Therefore, this databases contain significantly less cases with respect to National road accident databases.

The following sub-section presents an overview of information contained in in-depth road accident databases, aiming to point out how difficult can be to perform an inter-comparison between different databases. The description of the variables of National road accident databases will be explained later in the presentation of the results of the analysis of ISAT database.

2.2. Type of information extracted from in-depth road accident databases for the application to motorcycle safety

This section shows only results of motorcycles crashes as example of the information available in different in-depth databases. The examples were selected from GIDAS (German In-Depth Accident Study), MAIDS (Motorcycle Accidents In-Depth Study) and In-SAFE (an Italian In-depth accident investigation study) databases.

The quantification of the injuries of the people involved in a road accident is defined by doctors of medicine that treat the victims by employing standard scale. The Abbreviated Injury Scale (AIS) incorporates current medical terminology providing an internationally accepted tool for ranking injury severity. AIS is an anatomically based, consensus derived, global severity scoring system that classifies an individual injury by body region according to its relative severity on a 6 point scale (1 = minor and 6 = maximal). AIS is the basis for the Injury Severity Score (ISS) calculation of the multiply injured patient.

The usage of AIS provides standardized terminology to describe injuries and ranks injuries by severity, an example of usage can be found in Figure 1. In this way, AIS establishes a code for the injuries, based on defined rules and guidelines, which increases interrater reliability worldwide. Vehicle crash investigators used it to identify mechanism of injury and improve vehicle and road infrastructure design.

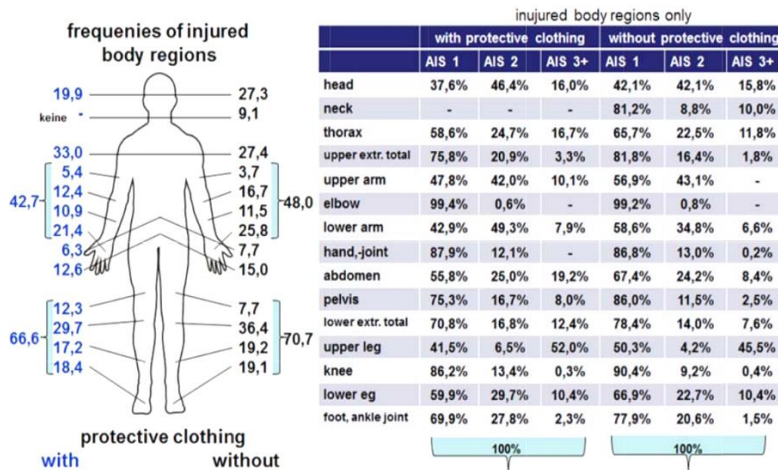


Figure 1. GIDAS database: Detail of injury level for motorcyclists (Otte et al., 2013)

A different representation of the injuries based in the Injury Severity Score (ISS) is depicted in Figure 2. The ISS is a score based on AIS to make focus in road crash investigation. The Injury Severity Score (ISS) is an established medical score to assess trauma severity. It correlates with mortality, morbidity and hospitalization time after trauma. It is used to define the term major trauma.

The results depicted in Figure 2 corresponds to the MAIDS (Motorcycle Accidents In-Depth Study) report. It is a large-scale, comprehensive study of Powered Two-Wheelers (PTWs, i.e., motorcycles, scooters and mopeds) accidents carried out across five European countries, using both accident and exposure or control cases. Starting in September of 1999, over 2000 variables were coded in 921 accidents. Control data (no crash took place) was collected on an additional 923 cases, collected at five locations in France, Germany, Netherlands, Spain and Italy.

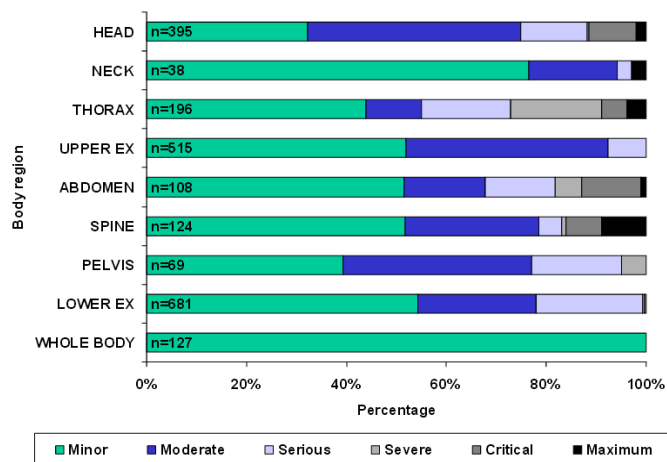


Figure 2. MAIDS Final report 2009: In-depth investigations of accidents involving powered two-wheelers

In Figure 2 is explicit the number of accidents that corresponds to each injury case, in which it can be seen that even with an extensive coverage of 5 European countries the number of accidents collected is very low (less than 1,000 motorcycle crashes) in comparison with the average yearly crashes of a single country as Italy (about 60,000-80,000 motorcycle crashes).

2.2.1. Examples from In-SAFE road accident database

Examples of the information used in this research belongs to In-SAFE database, which is illustrated in Figure 3. The database contains information from all type of road crashes but all the information used in this research belongs exclusively to motorcycle crashes, for which the vehicle's topology is shown in Figure 4. More detail of the database and its information can be found in the following publications (Piantini et al., 2012, 2013; Franci et al., 2015; Piantini et al., 2016).

Inclusion Criteria

1. Major trauma (ISS>15) for at least one person involved in a crash
2. Admittance to Intensive Care Unit

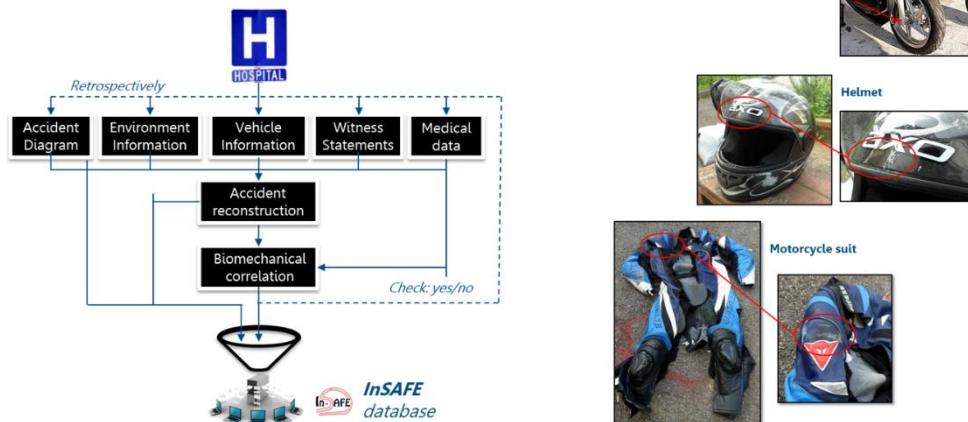


Figure 3. General description of In-SAFE database architecture and images of the information collected from the personal protective equipment of the motorcyclist and the crash deformation on the collided car

Generally, the analysis comprises the vehicles involved, personal protective equipment of the motorcyclist and the people. The injury level and distribution along the bodies are identified (Figure 5) and matched with the point of impacts of the motorcyclist against the opposite car (Figure 6 and Figure 7). These figures are the outcomes of several in-depth analysis performed for the road crash researchers, and this kind of information is present in this type of crash databases.

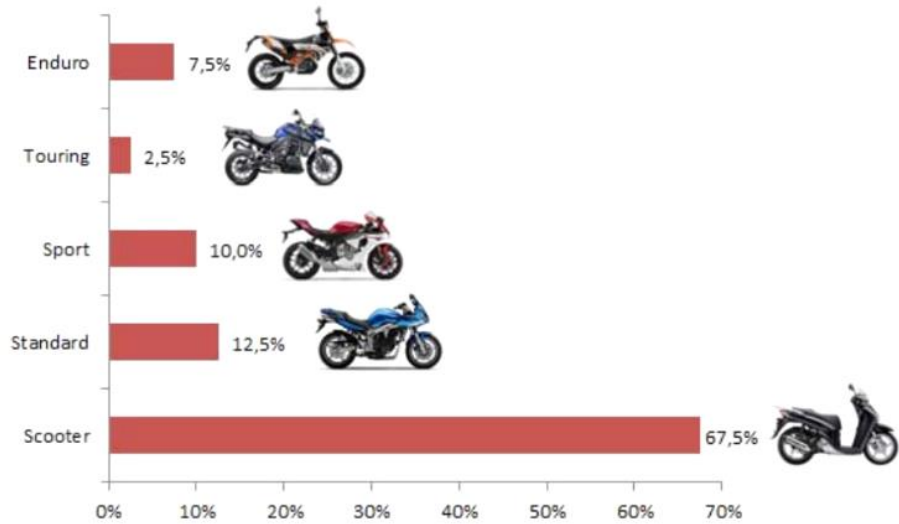


Figure 4. Topology of the motorcycles in the database

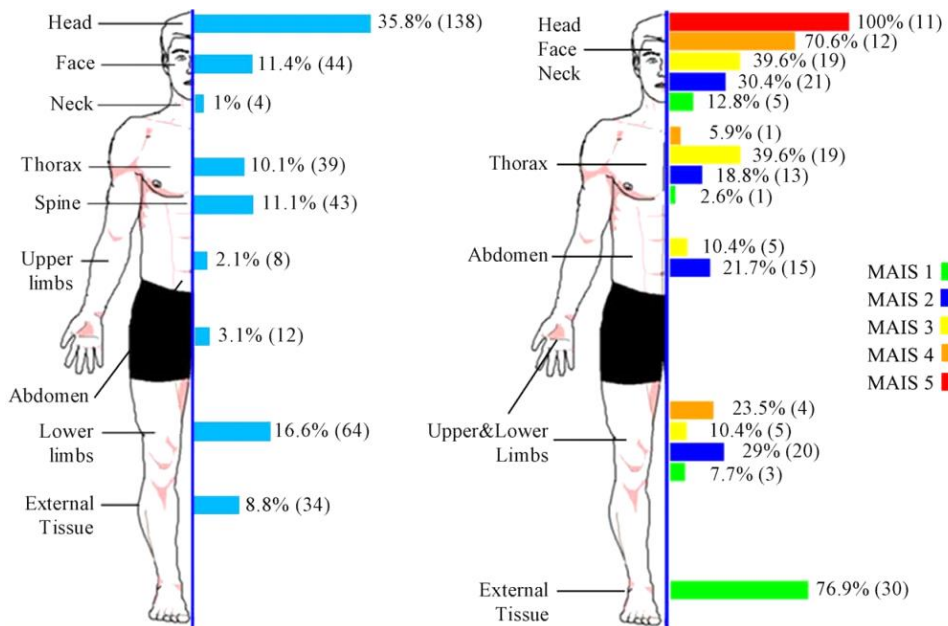


Figure 5. Injuries distribution (left side) and MAIS distribution (right side)

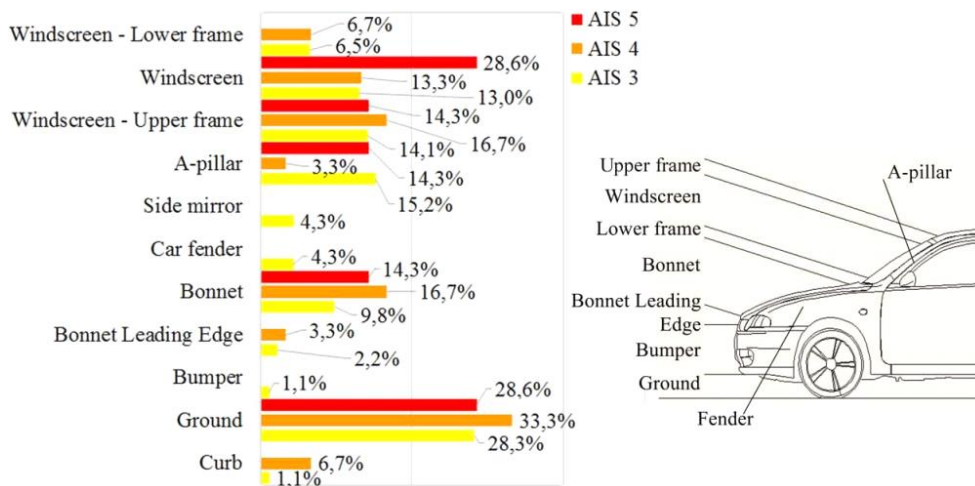


Figure 6. Example of injury causation for MAIS 3+

The information corresponding to the kinematic of the vehicles under the circumstances of the motorcycle crashes are obtained from the analysis of the movement of the vehicles and its interactions with the road. To do this a retrospective 3D reconstruction simulation is matched with the analysis performed by using the information of the energy dissipated during the impact (see examples of this measurements shown for the van of Figure 8).

The matching process between the 3D simulation and the evidences collected from the crash scenario is an iterative process that involves several considerations. When the simulated road accident matches with all the results of the analysis performed from the physical evidence collected about the crash accident scene (traffic or road accident scenario), the simulation is able to provide detailed information about the crash.

The detailed information simulated turns into several variables of the in-depth databases which describe in detail what happened during the vehicular crash. This explains the large amount of data variables, about 1500-2000 ones, present in an in-depth road accident database.

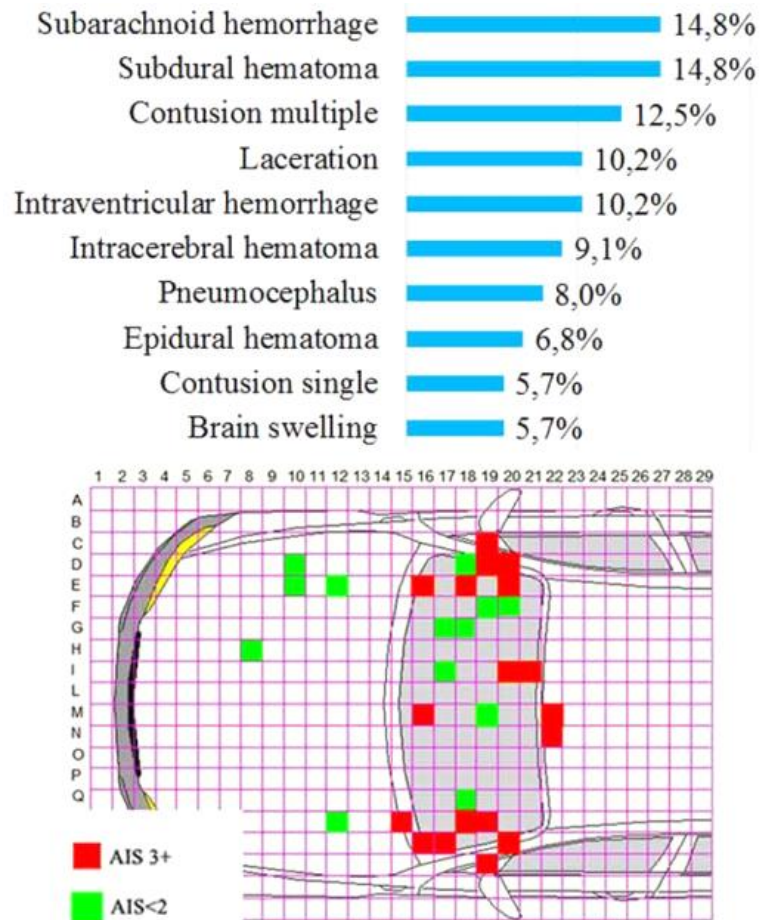


Figure 7. Head injuries and their impact point's location over the colliding car

Next, in Figure 8 is presented an accurate way to measuring the permanent deformations on the vehicle as a consequence of the crash. The measures are the result of scanning the vehicle with laser technology, by moving the laser scanner around the vehicle. Other valid approaches consist in the generation of the 3D measurement with the use of photo cameras (Morales et al., 2015). This method consist in the acquisition of several high quality pictures of the vehicles crashed to generate the 3D measurements by specific post processing techniques.

Using the calculated energy dissipated during the collision (vehicle deformations) and the final position of the vehicles (position of rest), it is possible to propose the feasible trajectories and speeds ranges to perform a simulation of the crash in a virtual environment. Mainly, dedicated software's such as Pam-Crash and Madymo are used to match the information collected from the road scene (an example depicted in Figure 9) with the reconstruction of the case study.

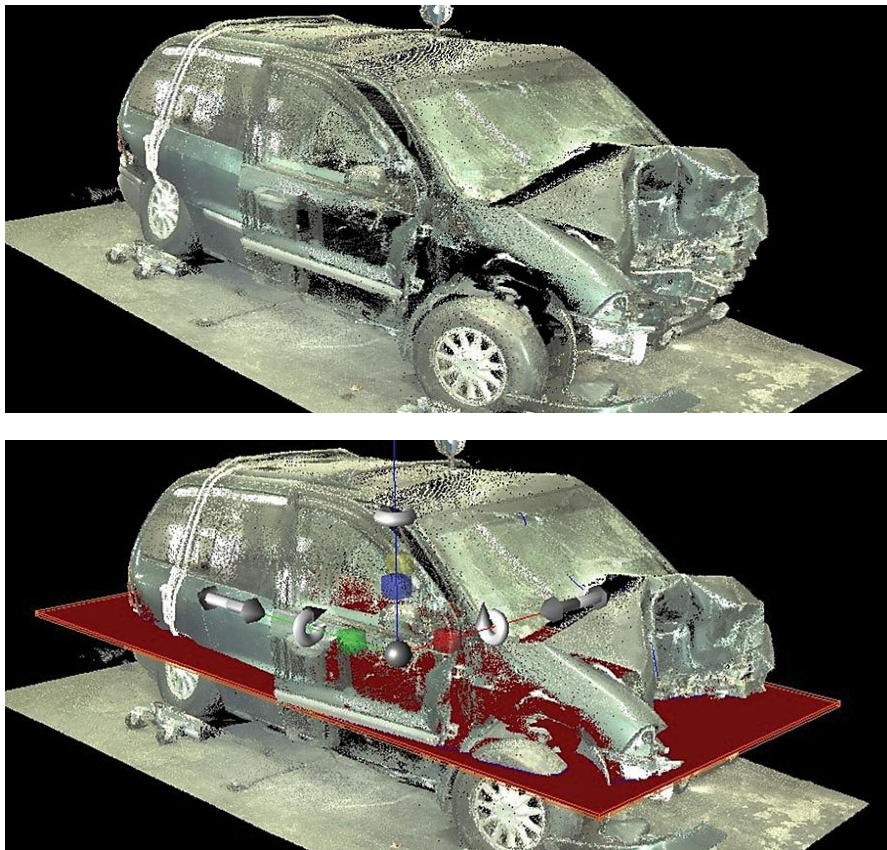


Figure 8. Example of vehicle deformation by the use of 3D point cloud measurements



Figure 9. Example of a real motorcycle road accident scenario (In-SAFE: ID86)

2.3. Data variables of ISTAT (National road accident database)

As the present research focus on motorcycle or Powered Two-Wheelers (PTWs) safety, only the meaningful variables to describe the motorcycle crashes were selected to segment the crash data (ISTAT database). These variables are depicted in Figure 10.

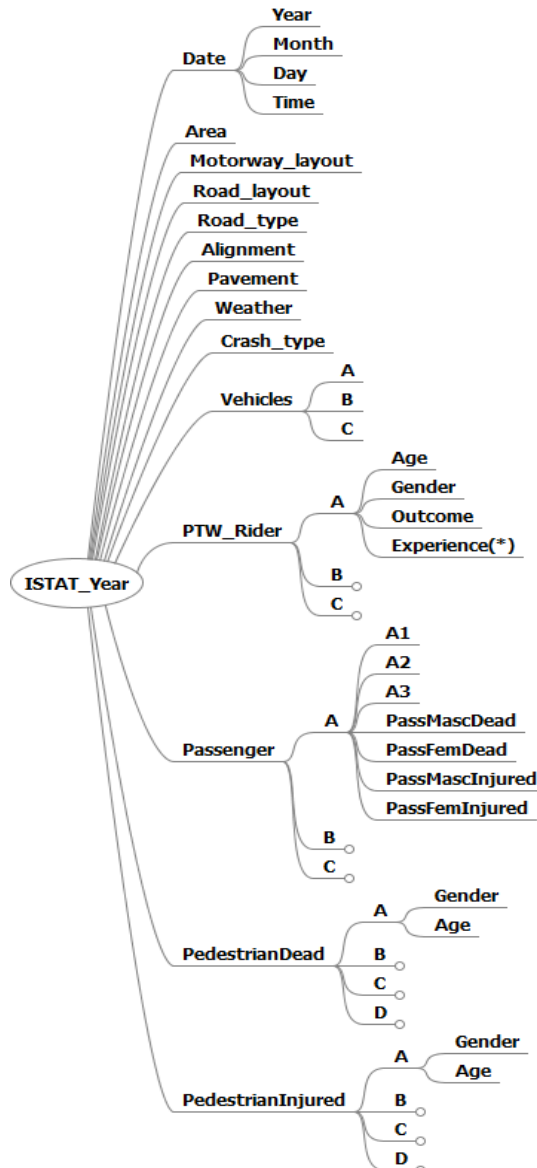


Figure 10. Organization of the data variables of ISTAT road accident database and their arborescence. The circles at the end of the branches denote the continuation of the variable's arborescence (the same as the previous variable). Note: experience (*) is defined by Equation 1.

Several variables contain child variables noted as A, B, C... the reason of that is due to the complexity of the road accident to describe. For example, in Figure 10 are defined the variables “Vehicles.A”, “Vehicles.B”, and “Vehicles.C” which are used to represent up to three vehicles different to the motorcycle involved in the crash.

The diagram of Figure 10 also shows a variable called “PTW_Rider.X.experience”, which is not present in ISTAT database. However, only for the purposes of our investigation, this is computed from real data during the data importation process. This fictitious variable is explained later and it is used only to get insights about human factors of the motorcyclist population.

The Figure 11 described the variety of motorcycle road crash scenarios which are described in ISTAT road accident database. The crash scenarios are stratified in three different levels which are identified from left to right and using the colors: blue, violet and black. For all motorcycle crashes which cannot be described in with the variables presented in Figure 10 and Figure 11 (unlikely situation), the accident is identified as unknown.

Additionally, some variables that describes the crash in practice are filled as unknown due exceptional reasons. For example, the type of motorcycle can be registered for the police agent as an unknown due to an almost total destruction of the motorcycle during the crash or if it catches fire.

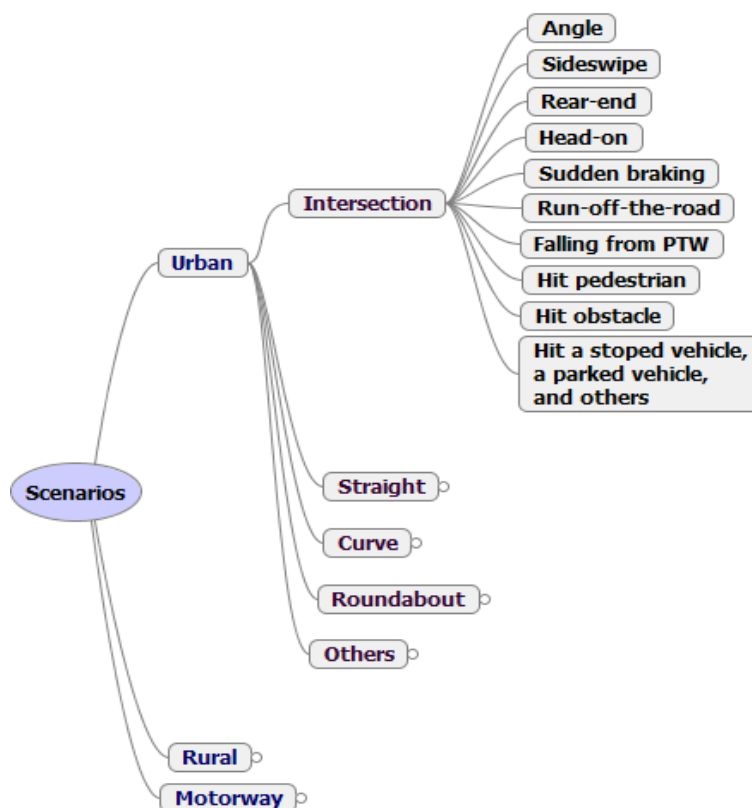


Figure 11. Detail of accident scenarios of ISTAT database and their arborescence. The circles at the end of the branches denote the continuation of the scenario's arborescence (the same as the previous variable).

2.4. Analysis of motorcycle crashes from ISTAT data

The following analysis, based on descriptive statistics, allowed me to quantitatively summarize the main features of the big data available in the ISTAT (Italian National road accident database). The following graphs are accounting for more than 1 million of motorcycle crashes in the period 2000-2012. The analysis included less than 10% of unknown data which was removed from the charts.

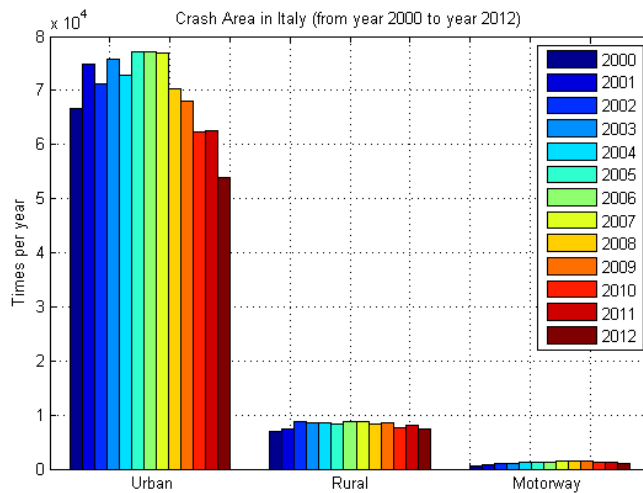


Figure 12. Number of PTW road accidents by area: urban, rural, and motorway

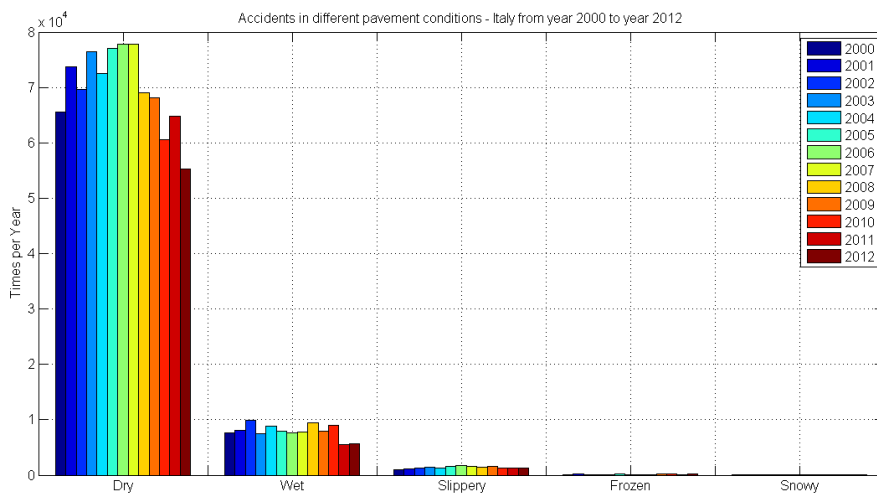


Figure 13. Number of PTW road accidents by pavement conditions: dry asphalt, wet asphalt, slippery asphalt, frozen asphalt, and snowy asphalt

In Figure 12 it can be seen that more of the 87% of PTW crashes happen in urban scenario. In Figure 13 is shown that more than 88% of PTW crashes happen in dry asphalt. The Figure 14 depicts that more than 86% of PTW crashes happen in clear visibility conditions. Figure 15 shows a stratification of the crashes according to the type of collision.

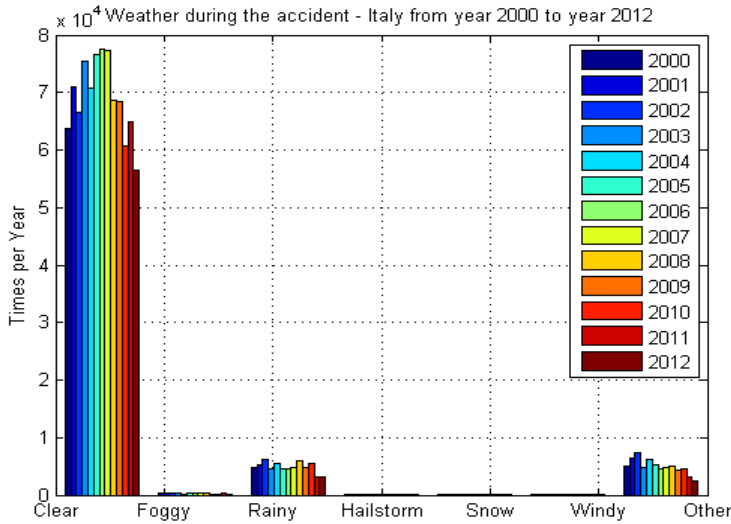


Figure 14. Number of PTW road accidents by weather conditions: clear, foggy, rainy, hailstorm, snow, and windy

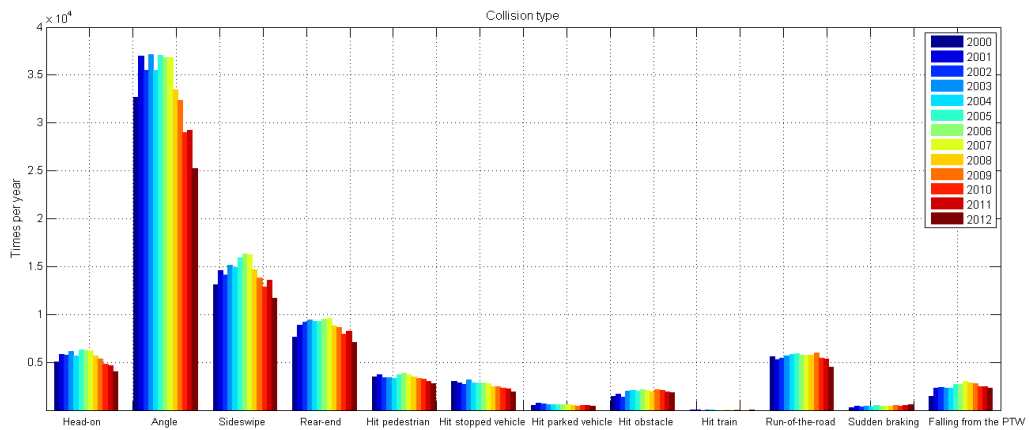


Figure 15. Number of PTW by type of crash: Head-on, Angle, Sideswipe, Rear-end, Hit pedestrian, Hit stopped vehicle, Hit parked vehicle, Hit obstacle, Hit train, Run-of-the-road, Sudden braking, Falling from the PTW

The trend for PTW crashes (Figure 16 and Figure 17) slowly decreased over the years in all cases except for the roundabout scenario, which increased in the same period. However, the increasing trend in the number of crashes in roundabouts could be due to the process of replacing standard intersections with roundabouts. Italy performed the replacements during the years analyzed and the safety performance of the roundabouts is under study (Giuffrè et al., 2015; Montella, 2011; Pecchini et al., 2014; Sacchi et al., 2011)

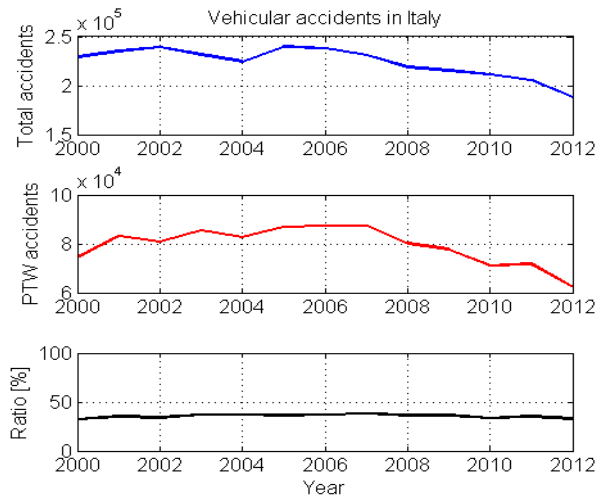


Figure 16. Detail of total traffic accidents, PTW accidents, and its relationship during a period of 13 years (2000 to 2012). The upper graphs show a declining trend in the number of accidents, instead the bottom one that shows a stable ratio (around 35.4%) between the total vehicular crashes and the PTW ones

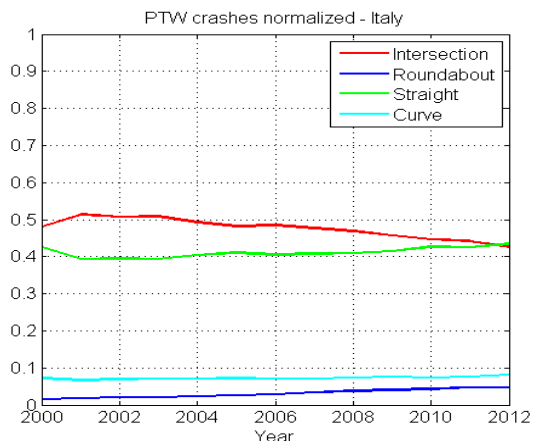


Figure 17. Detail of PTW crashes in four different street areas (normalized respect to the total PTW accidents of the year). The opposite slopes between intersection and roundabout could be explained by the fact that the roundabout is a particular case of intersection, and during the years some angular intersections layouts in Italy were replaced by roundabouts layouts

2.5. Description of human factors

The present study addresses two relevant human factors involved in the traffic accident, the age of the rider, and his "experience" at the moment of the accident. The information is presented in six of color contour maps: Rider Age (Figure 18, Figure 19, Figure 20), and Rider Experience at the moment of the accident (Figure 21, Figure 22, Figure 23).

The color scale represents the quantity of accidents in each point of the map. The same color scale is used for allow an easy comparison between them. The ordinates axe displays in a linear scale the years analyzed for the maps. Finally, the abscise axe displays in a logarithmic scale the years (Age or Experience). Note: the reason for not using a linear scale on the abscise axe is due to a better graphical representation because the most significant events happens in a few consecutive years.

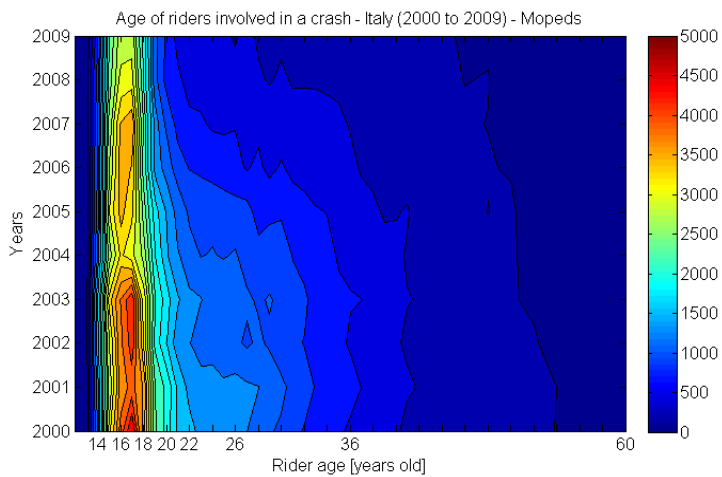


Figure 18. Detail of age of moped riders involved in a traffic accident.

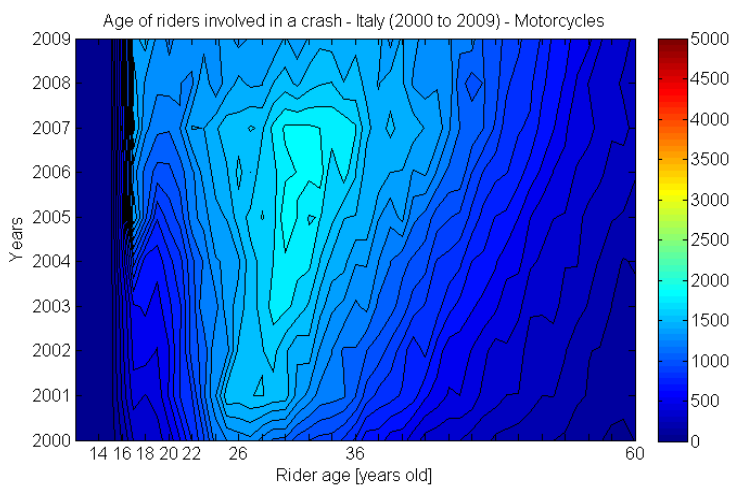


Figure 19. Detail of age of motorcycles riders involved in a traffic accident.

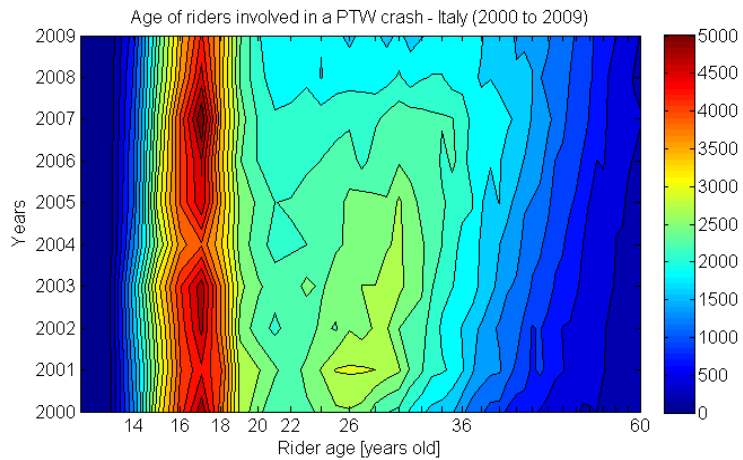


Figure 20. Detail of age of motorcycles and moped riders involved in a traffic accident.

Because it is not known the age of the rider population (age of riders without accidents) it is not possible to generalize the results of these color maps. However, it is possible to compute the “experience of the rider” by Equation 2.1. This is a fictitious variable represented in our variable selection of ISTAT database.

$$\text{Rider Experience} = \text{Year of the accident} - \text{Year of matriculation} \quad (2.1)$$

The simplicity of the metric do not captures all the possible cases of the reality but due to the analysis conducted, I consider that it captures the main behavior in a practical level; allowing me to get insights. In addition, this fictitious variable is easy to be implemented in national databases.

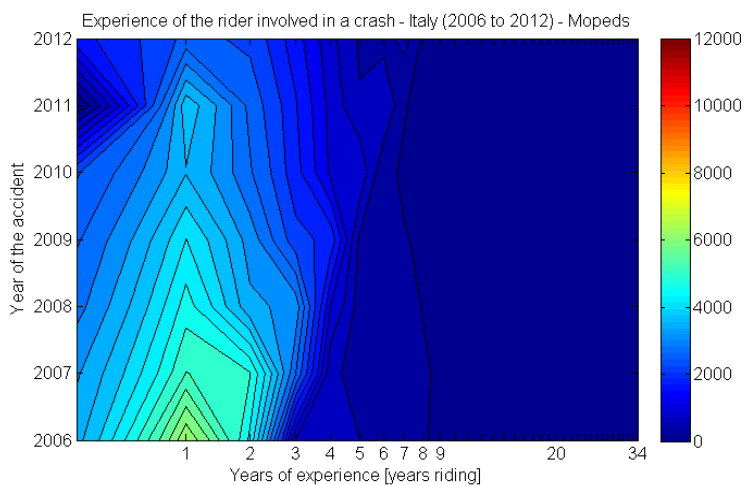


Figure 21. Detail of the years of experience of the moped riders at the accident moment.

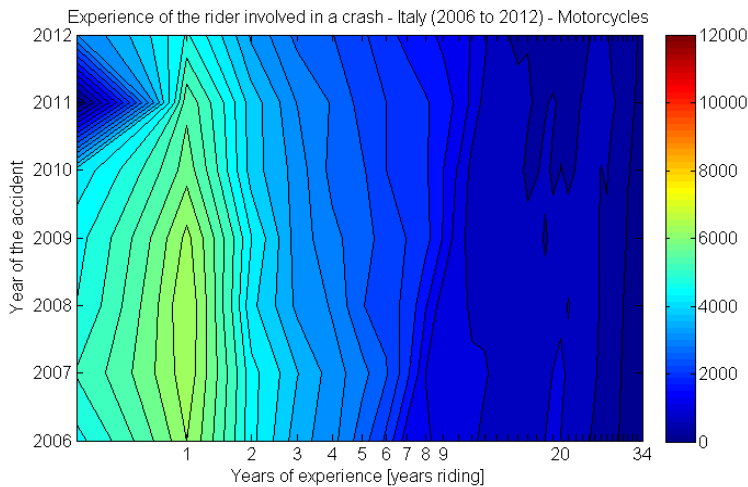


Figure 22. Detail of the years of experience of the motorcycle riders at the accident moment.

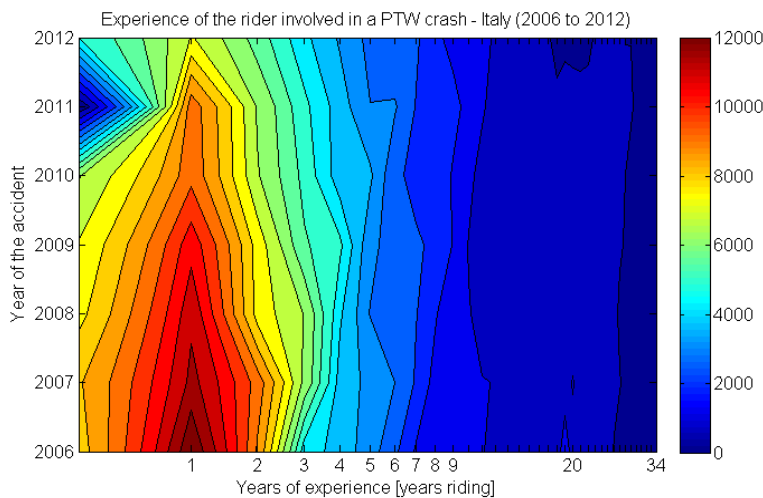


Figure 23. Detail of the years of experience of the motorcycle and moped riders at the accident moment

From the maps can be interpreted that newbie PTW riders have much higher accident than 3 or more years of experience ones. As a remark, it has commonly been assumed that is due to an insufficient training, resulting in a lack of safety. In the maps, the latest years display less quantity of accident due to global decrease of accidents (maps not normalized), however the accident peak of newbie PTW riders continues stable and well defined along all the lapse of years.

After these results, it stands to reason that age and experience are contributory factors in PTW accidents. These also can be seen in single trends of one year, as are presented in

Figure 24 and Figure 25. However, to properly quantify “rider experience” is far from been possible due to its subjectivity and maybe a limitation of this kind of analysis. Possibly, the fictitious variable simply defined in Equation 2.1 required to be called in a different way.

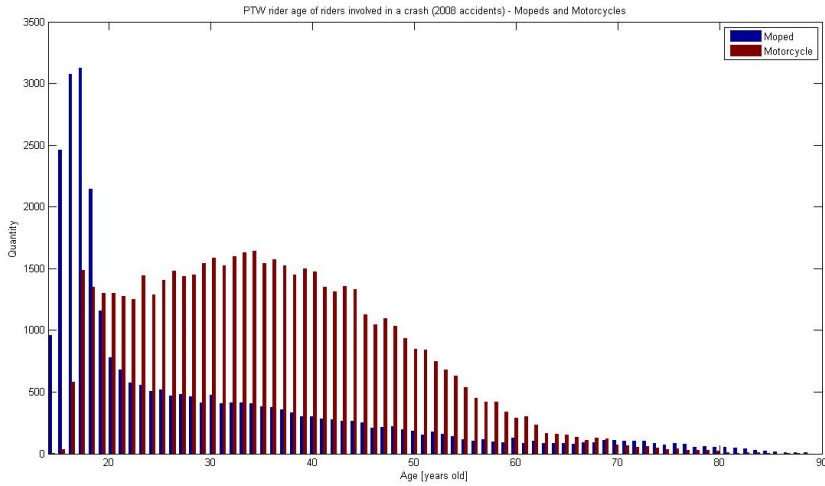


Figure 24. PTW rider age of riders in a crash (2008)

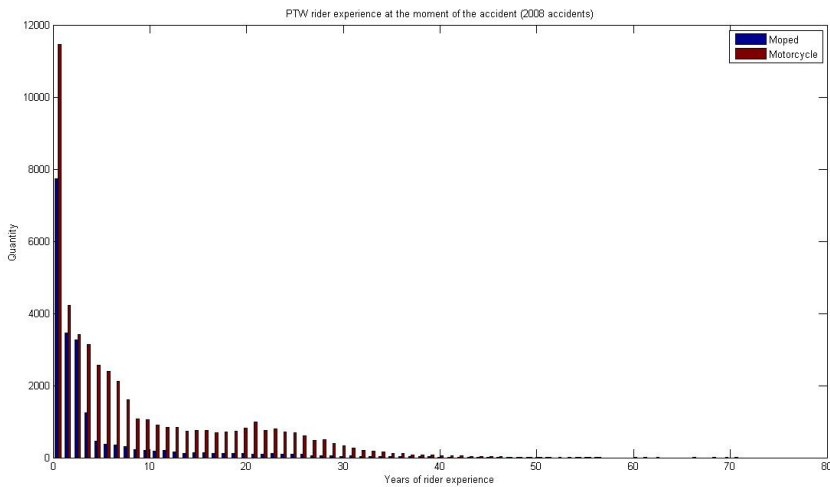


Figure 25. PTW rider experience at the moment of the accident (2008)

2.6. Conclusions

National databases provide large number of PTW crash data. Consequently, the frequency of the crashes among the variety of road accident scenarios point out the most urgent needs in terms of safety in the region of study. However, the coarse definition of the crash scenarios in the National databases implies a variety of the PTW crash kinematics that fit in the crash scenario description. These reasons help to identify a range of circumstances needed to address but do not contribute to find a solution to avoid or mitigate the crash.

In-depth databases proportion detailed information about the PTW crash kinematic and details about the reasons that caused specific crashes. The crash simulations realized for in-depth investigations can be used to assess the applicability of fictitious PTW safety solutions. Regrettably, this databases contains few PTW crashes and its representatively in terms of crash type cannot be extrapolate to propose safety solutions because the crashes analyzed in these regions correspond to local characteristics of the crash scenarios.

Finally, the PTW safety needs of a country can be established from the crash data available but it is not enough to proportion a possible solution to the problem. Detailed information that can be used to predict the safety the performance of safety solutions is delocalized and of difficult access for researchers and industrial stakeholders interested in develop PTW safety systems. These difficulties motivated the solution proposed in Chapter 3.

3. How to predict the performance of the safety solutions?

In the motorcycle industry, a seldom-acknowledged and uncomfortable tension exists between the desire to provide effective rider safety and keeping the vehicle cost affordable. The problem derives from the multifaceted aspects of motorcycle safety (e.g. conspicuity problem, exposure of the rider's body in case of accident, controllability of the motorcycle during the execution of a hard braking), and the small size of an industry that cannot divide its limited resources to explore the large number of solutions.

To guide the usage of these resources, in this dissertation is proposed a simple and systematic approach intended to support the tough human decision-making process for the development of adequate safety solutions, which is implemented by an *ad hoc* software tool (spreadsheets). The method was inspired by artificial intelligence techniques, and uses road accident data and categorical variables to fill the lacking information. The categorical variables (e.g. road layout, visibility, kind of injuries) come from the expertise of researchers in the safety field, and the methodology proposed captures and encodes this expertise in a Knowledge Base (KB).

Knowledge-Based Systems (KBS) are constructive tools which have been used with success in other fields for decision-making. Big Data (ISTAT: 205.272 motorcycle road accidents from 2010 to 2012, and more than one million since year 2000) were used during the definition and implementation of the KB for the new KBS. Consequently, the use of this specialized KBS called Knowledge-Based system of Motorcycle Safety (KBMS), can help to the industry to confidently target their efforts and allocate resources to significantly improve motorcycle safety. The potential of the KBMS methodology is shown by comparing preliminary results with a prior study that attempted a systematic prioritization of safety systems/technologies for motorcycles called PISA project.

3.1. Context for the analysis of motorcycle safety systems

Motorcycle safety research aims to contribute to the understanding of motorcycle accidents and their causes in order to make motorcycling safer. Its societal relevance is increasing due to the proliferation of Powered-Two-Wheelers or PTWs (Sekine, 2014; Haworth, 2012; Jamson and Chorlton, 2009; Rogers, 2008). In crowded cities, PTWs offer several advantages to riders, mainly time saving when travelling in congested roads, and more parking areas with respect to car drivers (Wigan, 2000). Additionally, due to the air-pollution problem (Shuhaili et al., 2013; Colvile et al., 2001) more cities are promoting electric

Two/Three-Wheelers sharing programs for commuting (Barcelona/Grenoble) and there are some current/future initiatives of road space rationing (commonly in several Latin American cities) and car-free cities (Brussels, Dublin, Madrid, Milan, Paris, and Oslo) do not apply to PTWs.

However, the protection of motorcyclists is a pending issue. The societal cost of PTW accidents is high, and while passenger car safety improved dramatically in the past decades (Glassbrenner, 2012; Orsi et al., 2012), PTW safety improved marginally (NHTSA, 2014; Sekine, 2014; Broughton et al., 2013; Nicol et al., 2012; Deutermann, 2004). This might be explained due to about the multidisciplinary complexity of PTW safety (motorcycle dynamics, rider/driver behavior, etc.), which is a broad subject to be addressed only for a small PTW industry (11.9 million of cars yearly registered in EU versus 1.0 million of PTWs (ACEA 2013, ACEM 2014)). Therefore, the arising question is: how to channel the constrained economical resources of this industry to the research into the most promising solutions in motorcycle safety? Next, I present a method for prioritizing different safety systems or technologies that would drive the efforts in R&D to a set of key targets. However it is hardly possible due to the nature of certain safety technologies (e.g. diverse settings in a Traction Control System can modify the vehicle dynamics in different emergency situations). Thus, our study introduces the Safety Function (SF) concept, which is a broader w.r.t. safety system because it describes a final desired outcome, allowing for a simpler evaluation and prioritization process for the safety solutions.

For example, three motorcycle safety systems and other three SFs are presented in Figure 26. Note that one SF can be achieved by a combination of safety systems operating together and that the same safety system can accomplish several SFs.

Regarding the prioritization of different SFs, they can be attempted using retrospective crash data from several databases. Unfortunately, the motorcycle crash databases are not harmonized (IMMA 2014), and their combined use can be demanding. Alternatively, the prioritization can be conducted based on expert opinions, but these assessments can only be performed considering particular accident scenarios. The truth is that the field of vehicular safety is characterized by a plethora of expert knowledge among a variety of specializations (e.g. crash analysis reconstruction, crash test analysis, energy absorbers design, traction & braking control, traffic control, forensic, driver/rider training, injuries treatment, etc.) that are not linked. Thus, there is a need to exploit this distributed knowledge and to combine it with crash statistical data in a systematic and constructive manner.

The aforementioned reasons motivated this methodology for PTW safety that aims to manage quantitative, imperfect, and not harmonized information, enabling to store, analyze, and reuse “collective expert knowledge” for a wise decision-making. The methodology developed is a Knowledge-Based System entitled Knowledge-Based system of Motorcycle Safety (KBMS) and it is illustrated in Figure 27.

The chapter is structured as follows: an overview of the only reference study (PISA project) that attempted a prioritization method; then, the methodology for prioritization based on a KB (Knowledge Base), for which a comprehensive definition of KB and KBS (Knowledge-Based System) are provided in order to support the view of the KBMS (Knowledge-Based system of Motorcycle Safety); thirdly, the methodology is explained and illustrated by a case study; fourthly, a comparison is performed with PISA study outcomes; and finally the discussion and recommendations sections are presented.

Safety Systems



- ABS for Motorcycles
- Motorcycle Traction Control
- Anti-stoppie



Safety Functions

VS.

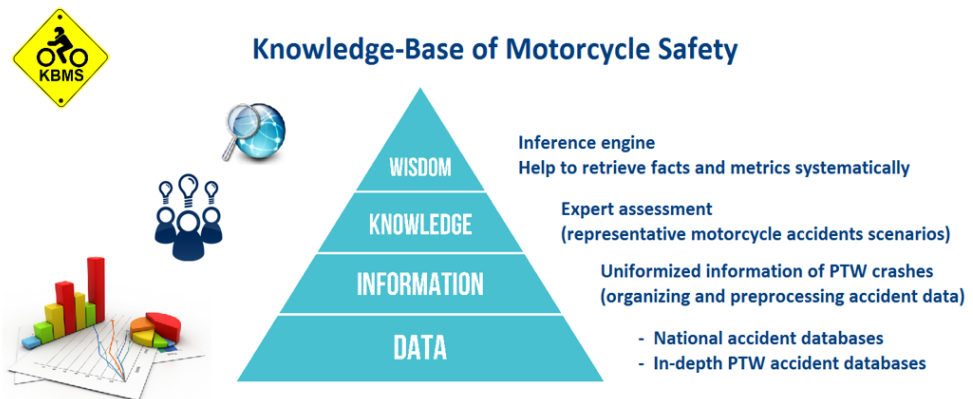
#1 Assist the rider to perform a hard braking without falling from the PTW

#2 Avoidance of the rear wheel lifting off the ground

#3 Distribute more properly the braking action on the two wheels even if one brake is actioned



Figure 26. Explanation of the Safety Function concept by examples



Knowledge-Based System approach is used for:

- The **harmonization** of traffic accident information
- Systematic accumulation of **experts judgements**
- **Ranking of possible solutions**

Figure 27. Graphical abstract of the Knowledge-Based system of Motorcycle Safety

3.1.1. Overview of PISA Project

The PISA study (2007-2010), a database of 60 in-depth motorcycle accident cases was gathered, sampling from On-The-Spot study and two LMU databases: Forensic and COST 327. These crashes were classified in a set of relevant motorcycle accident scenarios defined in the APROSYS project (APROSYS, 2009). The study identified 43 safety functions/systems to be assessed. An international team of experts in traffic accident analysis and prevention used the information of each crash case to establish how effective each safety functionality/system could have been had if it been present in each case.

Finally, the safety functions/systems were prioritized for each accident scenario presenting different rankings. The PISA priority list was used to perform a comparison with the results of the new methodology that will be introduced in the following section.

3.2. Fundamentals: Knowledge-Based system of Motorcycle Safety

3.2.1. Relationship between data, information and knowledge

The concept of a Knowledge Base requires a clear distinction between the concepts of data, information and knowledge, because they will be used along the chapter. Figure 28 shows a graphical representation of how from the analysis of sparse data collected, it may evolve in meaning towards information through the establishment of new weak relationships in the data collected. Next, the reinforcement of data relationships and the establishment of new weak relationships to prior well establish information in the field of study become in the so called “knowledge in the field”.

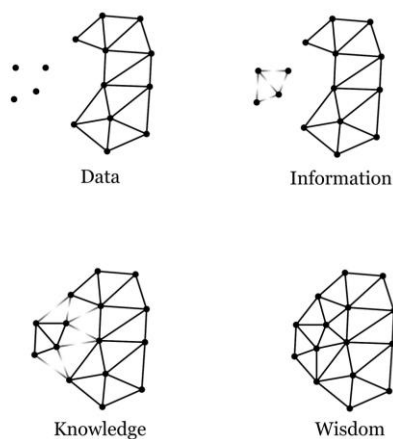


Figure 28. Scheme of the relationship between the data, information, knowledge and wisdom.

Finally, more strengthen relationships between varieties of fields of knowledge shape a more general “wisdom”.

3.2.2. Defining a Knowledge Base

Definition 1: A Knowledge-Base (or KB) is an organized repository of facts and expert understandings about a particular aspect of reality that are systematically classified and adapted to be computed by a machine.

The information collected includes objective variables and subjective or categorical ones. They are stored in a codified manner. This allows for the combination of newly perceived information with the knowledge previously acquired, making it possible to perform computation.

This current definition is aligned with the first broad concepts and particular definitions of KBs developed in the field of artificial intelligence in the 70's. At that time, the topic was called expert system (Minsky, 1974; Waterman, 1976; Waterman and Jenkins, 1976; Buchanan and Feigenbaum, 1978; Waterman, 1978; Hayes-Roth, 1985; Waterman, 1986; Chapman and Pinfold, 1999).

3.2.3. Defining a Knowledge-Based System

Definition 2. A Knowledge-Based System (or KBS) is a tool that by computing on the KB allows reasoning with the content of the KB, presenting the characteristics of the case analyzed to the user, whom will be able for well-grounded decision-making process.

The utilization of a KBS in a specific field is intended to emulate some aspects of human cognition (such as memory, reasoning and decision-making), but it differs in the fact that memories and reasoning come from the interpretation of experimental data and the contributions of many persons with expertise in this field.

Current successful applications of KBS as tools for decision-making can be found in the following fields: Medicine (Shortliffe, 1976; Warner, 1968; Gennari et al., 2003; Pavlovic-Veselinovic et al., 2016), Pharmacogenomics (Thorn et al., 2013), Engineering Design Applications (Shaw and Gaines, 1987; Blount et al., 1995; Sainter et al., 2000; Verhagen et al., 2012; Quintana-Amate et al., 2015), Environmental science (Orgiazzi et al., 2016), Research operations (Negre et al., 2015; Radivojevic and Milbredt, 2016), Corporative Management (Grant, 1996; Meso and Smith, 2000; Soliman and Spooner, 2000), Energy production (Law et al., 2016), Automotive (Craig B. Chapman, 2000), and Aeronautics (Xu et al., 2012; Zhu et al., 2012).

In conclusion, the KBS approach can be very useful in multidisciplinary fields that have to deal with imperfect information (subjective or categorical variables). Accordingly, I applied it in motorcycle safety.

3.2.4. Core of the KBMS

The Knowledge-Base system of Motorcycle Safety (KBMS) is a KBS which intends to capitalize on the scattered knowledge about vehicular safety with emphasis on motorcycles or Powered-two Wheelers (PTWs). The KBMS allow us for the creation of a hierarchical list of motorcycle safety solutions based on traffic accident information and expert judgements about possible accident countermeasures. The process consists of two separate stages (collecting and processing), which allow for the delocalization of actors involved. These stages are strictly defined for an operational framework.

3.2.5. KBMS Framework

The default framework of the KBMS (Figure 29) was designed to be applied which several traffic accident databases without modifications. It defines:

- a) A set of queries to conduct in the road accident database.
- b) The SFs (Safety Functions) list to assess.
- c) The PTW road accident scenarios to analyze.

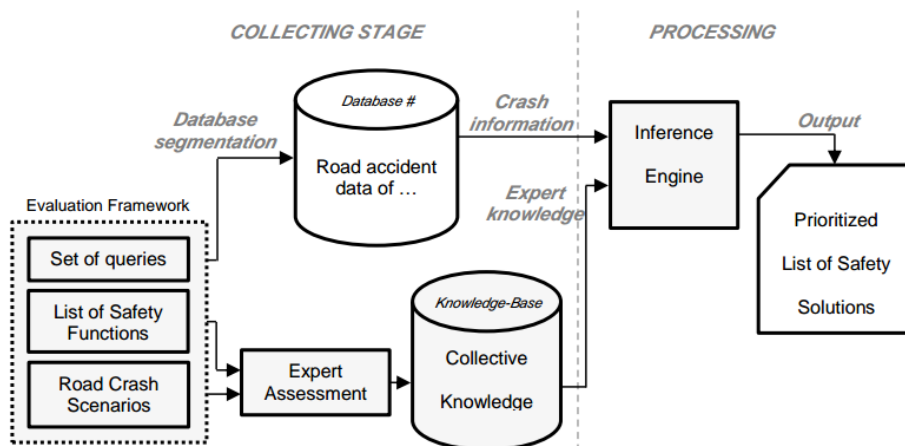


Figure 29. The components of the Knowledge-Based system of Motorcycle Safety are shown in grey. As an initial step the KBMS framework is formulated by defining the queries set, the selection of safety functions and accident scenarios. The queries extract the relevant information of the Road accident database, for the Inference Engine. Parallel in the workflow from the KBMS Framework to the Inference Engine, at the processing stage, the SF are assessed in several Road Accident Scenarios by experts, in order to obtain the contents of the knowledge base. This assessment is based on a list of Safety Functions which are evaluated for certain Road Accident Scenarios at the collecting stage (generating Input 2). Moreover, at the processing stage two tasks are performed: a) the validation of expertise coming from Input 2 in order to increase the Collective Knowledge of the KBMS; b) the combination of the Input 1 with the Collective Knowledge to define a prioritized list of Safety Solutions that corresponds to the country/region of the road accident data used.

3.2.6. The collecting stage

The collecting stage consists of two independent parts where information is harmonized for the following stage. In part one (upper branch), a segmentation of statistical road accident data is conducted in a road accident database by a set of queries (Figure 29). The road accident data must be representative of the type and quantity of accidents in the analyzed region for this period of time. In part two (lower branch), the level of effectiveness of SFs is estimated and encoded for given accident scenarios. These estimations come from the analysis of people with expertise in the vehicular safety field and can be stored so as to be used in several analyses. The accumulation of expert assessments in the KB of the KBMS will be referred to as “collective knowledge” (Figure 29).

3.2.7. The processing stage

The processing stage combines harmonized accident information with collective knowledge to compute a list of SFs prioritized according to relevance and effectiveness. As a result, a list of SFs is obtained that applies to the region and period in which the accident information was collected.

3.3. Method of the Knowledge-Based system of Motorcycle Safety

Here is explained how to build each block of the KBMS previously defined and how I used the method (Figure 30). Each part of the methodology is complemented with a short practical example to illustrate the concepts.

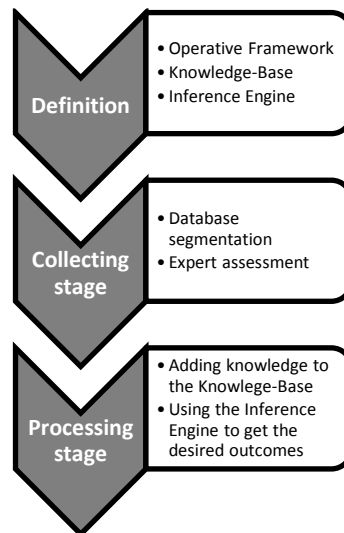


Figure 30. Schematic process to build and apply a Knowledge-Based System as the KBMS.

3.3.1. Operative Framework

The framework defines the type of data to be used during the analysis, and how to use it in order to obtain useful information. For the application in motorcycle safety, I defined four pillars based on: I) definition of the road accident scenario; II) database segmentation by a set of queries; III) definition of safety functions to be evaluated; and IV) definition of how to perform the evaluation.

I) Road Accident Scenarios

The road accident scenarios are a way to represent the circumstances in a crash (e.g. type of road; trajectory of the vehicles; and type of collision). Generally, all the information is

summarized in a pictographic system and each road accident database contain their own representation. Therefore, in order to be able to employ the methodology with different accident databases is necessary to create a subset of relevant accident scenarios able to include these cases in a harmonic way. Finally, these accident scenarios will be used for the experts in safety at the collecting stage.

Example: in the KBMS default Framework I defined 26 representative accident scenarios for motorcycle accidents by a comparison between the following five in-depth road accident databases: VALT, DaCoTA, Vic roads, GDV, and CADaS. The pictograms are provided as a downloadable and editable resource (see Appendix B).

II) Queries set

The criteria to select the accident cases for the analysis are used by the investigator to define a set of queries. Queries should be in a form that a database manager can use to extract accident information (database segmentation) at the collecting stage. The database manager will provide the outcome of the queries in a predefined form.

Example: in our framework are defined nine queries (Appendix C) to cluster the 26 accident scenarios in 9 general ones, labeled from “A” to “I” (Appendix B). The use of accident scenarios fused is a tradeoff between the level of detail of the traffic accident scenario (resolution), and the data present in the traffic accident database employed (data availability).

III) List of Safety Functions

Each Safety Function (SF) defines the expected outcome for a motorcycle safety solution. Several SFs will be used during the expert assessment at the collecting stage and a set of them will represent the most promissory solutions to develop, for this reason each SF must be expressed in a univocal manner. Many SFs could match with the expected outcome of an existing safety system/technology; in these cases it is necessary to take the safety systems/technologies and turn them in SFs, because the SF concept is easier to evaluate with few information than a safety system/technology. Additionally, the formulation of nonexistent SFs is an innovation enabler.

Example: the available safety systems/technologies was evaluated to elaborate a list containing 64 SFs for the PTW application (Appendix D). The review have included the automotive market, specialized literature in vehicular safety (Bayly et al., 2006; Anderson et al., 2011; Savino et al., 2012b; Van Elslande et al., 2012; Savino et al., 2014), sensing (Corke et al., 2007) and safety technologies (Montanari et al., 2011; Garcia et al., 2013; Corno et al., 2015; Mukhtar et al., 2015). In addition, some conceptual SFs were proposed.

IV) The expert assessment

To define the procedure for perform the expert assessment is necessary to consider:

- 1) What are the conditions for the evaluation? (e.g. type of accident scenarios)
- 2) What things are going to be evaluated? (e.g. SFs)
- 3) What is the purpose of the evaluation? (e.g. estimate the capability of a SF to avoidance/mitigation the crash)
- 4) How to express the evaluation in a standardized way? (e.g. using a ranking scale).

The first three considerations were previously exemplified. Now is presented the ranking scale criteria adopted in the KBMS which aims to quantify the valuation judgements. Therefore, a scoring scale (from 0 to 4) is used (Table 4). Likert proposed this kind of scoring system in his doctorate (Likert, 1932).

This scale is conceived as a bipolar scaling method: measuring either negative (0, 1, 2) or positive (3, 4) responses to a statement. The score scale pertaining to the ratio scale classification (Heise, 2001) in the field of statistics and quantitative research methodology.

Score Value	The assessed function would ... in accident avoidance / mitigation for this scenario
0	... <u>not have</u> an effect ...
1	... have a <u>very little</u> contribution ...
2	... have a <u>little</u> contribution ...
3	... have an <u>important</u> contribution ...
4	... have a <u>very important</u> contribution ...

Table 4. Likert-type scoring scale defined to rank the benefit of the safety function in each accident scenario to analyze

3.3.1. The processing stage

The Knowledge-Base (KB) capitalizes on the human expertise in the field that is not present in road accident databases by storing the judgements of the expert assessment. The judgements are encoded in a manner that allows comparing the assessment between different experts, and performing calculations.

KB example: a multidimensional matrix that contains numerical values was defined; each cell corresponds to a SF ranked for a human expert (presented in Table 4). Each numerical value is indexed for five characteristics:

- 1) Road accident scenario (26 types)
- 2) SF (64 types of Safety Functions)
- 3) Objective (avoidance or mitigation)
- 4) Expert category (e.g. Biomechanics, Passive Safety, Active Safety)
- 5) Individual expert (anonymized information).

3.3.2. Inference Engine

The inference engine is designed to apply logical rules, or math calculations, to the collective knowledge stored in the KB and the statistical info of the country/region analyzed to deduce new insights.

In this research a set of algebraic equations were defined in order to achieve our objective of prioritize SFs for different road accident scenarios depicted in Figure 31. The complete example of the math calculations used in the KBMS is also presented.

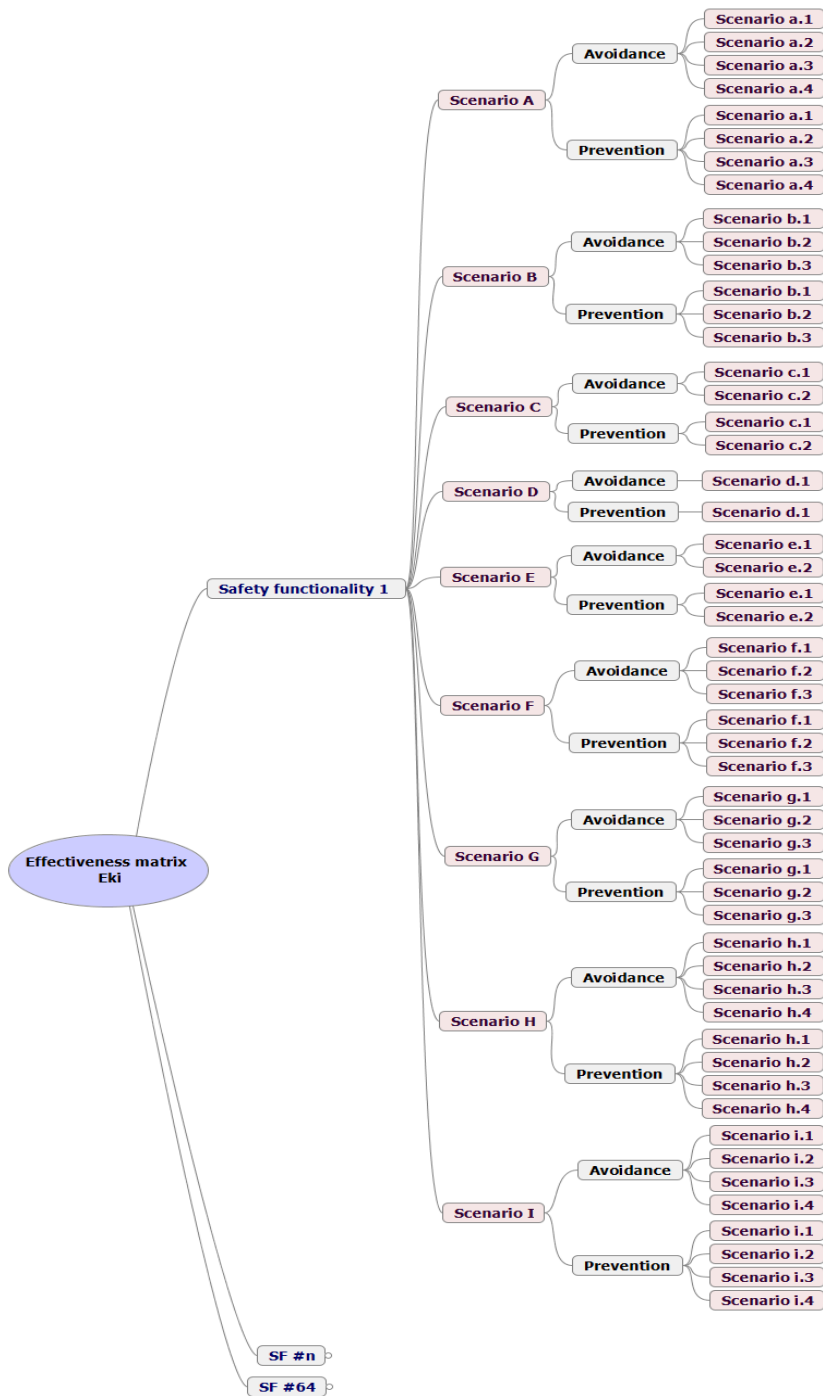


Figure 31. Detail of data contained in the effectiveness matrix (Eki) and their arborescence. The circles at the end of the branches denote the continuation of the arborescence (the same as the previous variable)

A set of equations generate numerical values representing the effectivity of each SF in each accident scenario. More precisely, the effectiveness matrix output [Eki] contains the collective intelligence until this analysis (Figure 29 – upper branch), and the importance matrix output [Iki] contains the collective knowledge but regarding to the specific country/region where statistical accident information belongs (Figure 29 – lower branch).

In the application case, the inference calculation used three years of ISTAT database (205.272 PTW accidents from 2010 to 2012) as are stated below:

a) *Coverage metric > 90% - 1 metric by year*

The default framework has nine general road accident scenarios. These are a simplification to perform the global traffic accident analysis. Consequently, not all the possible PTW crashes are included in these cases. Therefore, a minimal floor of 90% of accidents coverage was adopted in order to neglect less than 10% of the total PTW accidents, ensuring the possible generalization of the conclusions inferred from the analysis.

The coverage metric computes the sum of the nine general accident scenarios types (defined Appendix B), and compares it to the total yearly PTW accidents to determine PTW accidents coverage level [%].

b) *Accident reduction by scenario (compared to the previous year) [%] – 18 metrics (9 metrics by precedent year)*

For example, using the information of the last three years is possible to compute the trend of PTW accidents happened in each accident scenario type two times. This information provides a ratio of change of accident occurrence among the time for each scenario.

Note: these metrics are computed using the previous year as a percentage reference.

c) *Crash quantity coefficients – 27 coefficients (9 by year)*

$$Q_{i_n|_y} = \frac{Q_{i|_y}}{Q_y} \quad (3.1)$$

Notation: i means the crash scenario number; y means year of statistical crash data; $Q_{i|_y}$ is the quantity of PTW accidents in the scenario i during the year y normalized to the Total PTW crashes of the year; Q_y is the number of PTW accidents during the year y ; $Q_{i_n|_y}$ is the Q_y normalized to the total PTW crashes of the year.

d) *Relevance coefficients – 9 coefficients (1 for each accident scenario type)*

To obtain the relevance level of each accident scenario type, compute the weighted mean for the last years of each accident scenario. The weights defined by the default framework are included in a vector of three elements called “kernel”. Different kernels shall compute annual, biannual, and triennial information.

$$Kernel_j = \{K_{j|_y-2}; K_{j|_y-1}; K_{j|_y}\} \quad (3.2)$$

$$R_i = \frac{K_{j|_y-2} * Q_{i|_y-2} + K_{j|_y-1} * Q_{i|_y-1} + K_{j|_y} * Q_{i|_y}}{\sum Kernel_j} \quad (3.3)$$

Notation: R_i means relevance of accidents in the scenario i and j is the kernel number.

e) *Effectiveness matrix coefficient – Matrix size = 64x18*

The effectiveness matrix contains 1152 coefficients that are computed from the rankings produced for the expert's assessment (64 safety functionalities by 9 avoidance general assessments and 9 mitigation general assessments).

Below is detailed how to build the effectiveness matrix.

$$\text{Assessment type}_r|k, i = \frac{1}{\sum i|pss} * \sum_m \frac{V_{k,i}|pss}{m_{k,i}|pss} \quad (3.4)$$

$$E_k|i = [\text{Assessment type}_1|k, i, \dots, \text{Assessment type}_r|k, i] \quad (3.5)$$

Notation: k means safety function number; $Type\ r$ refers to the kind of analysis performed (e.g. Avoidance or Mitigation); pss means a particular sub-scenario; $i|pss$ refer to the particular sub-scenario of the i th crash scenario; $V_{k,i}|pss$ indicates the numerical value of the assumed effectiveness of the safety function k and also in scenario $i|pss$; and $E_r|k, i$ is the effectiveness matrix that represents the effectiveness of the function k under scenario i with regard to the type of goal r .

f) *Importance matrix coefficient – Matrix size = 64x18*

It acts as a proxy, highlighting only the important cases of the effectiveness matrix. The content of this matrix is originated combining the statistical data of a particular country or region and the knowledge (expert's assessment).

$$I_r|k, i = R_i * E_r|k, i \quad (3.6)$$

Notation: $I_r|k, i$ is the importance of the safety function k for the accident scenarios i with regard to the safety goal r .

g) *Output list*

The output list consist of the addition of all the importance one-dimensional arrays by each SF. Then, ordering the new one-dimensional array from the biggest numerical value to the lowest one.

3.3.3. Collecting stage

The operational framework defined two manners to collect information from two separated sources (different kind of information's are collected). The first task involves the segmentation of a road accident database with the set of queries, in order to statistically quantify accident scenarios. The second task corresponds to the expert assessment.

The first task is an analysis that must be defined in a set of queries employing common variables sectioning the database accidents (e.g. by road location, road layout, type of collision). The aim is to identify the quantity of accidents in different accident scenarios (e.g. PTW accidents that happened in "intersection of streets" AND "sideswipe collision type").

The second task requires an appropriate criteria's for the selection of the experts involved in the analysis. Next is presented the criteria adopted in the KBMS within a short example of how to collect the information in the expert assessment.

3.3.3.1. Selection of experts for the assessment

The expert is a person with a recognized knowledge on the topic of interest. For the KBMS the experts could come from a variety of disciplines (e.g. crash analysis reconstruction, crash test analysis, energy absorbers design, traction & braking control, traffic control, driver/rider training, injuries assessment, etc.), then aiming to manage the degree of heterogeneity of the sources of knowledge involved a categorization of the technical background of the experts involved in the KBMS was defined (e.g. Biomechanics, Mechanical Engineers, etc.).

The application as an expert for the KBMS research can be summarized by fulfilling the requirements (Table 5). Thus, a peer-review process will enable the participation. More details about the selection of the experts can be found in Appendix E.

Table 5. Expert legitimization table for KBMS assessment (it is filled as an example). In this way, it is possible to consider if the applicant could be accepted as a recognizable expert for the purpose of the KBMS or not, allowing recognizing both: academicals and industrial experts

Main activity	Research in Vehicle Safety
Years of experience	5
Background	Mechanical Engineer
Name of best three publications on the topic	Paper #, Tech. Report, Book chapter...
Patents related with the topic	Patent ...
Participation in projects	Project 1 (tasks performed), ...

3.3.3.2. Example of expert assessment

The experts are provided with guidelines (Appendix F), to conduct the assessment, and a homogenous terminology to facilitate the exchange and participation with different experts. Additionally, they count with a scoring table (Table 4) to assess the possible effectivity of a set of SFs (Appendix D) in a set of road accident scenarios (Appendix B).

For a best reference of the modality of the assessment, an example of expert assessment is depicted (Figure 32). The example corresponds to the analysis of level of traffic accident avoidance/mitigation of two SFs in the set of accident scenarios "h".

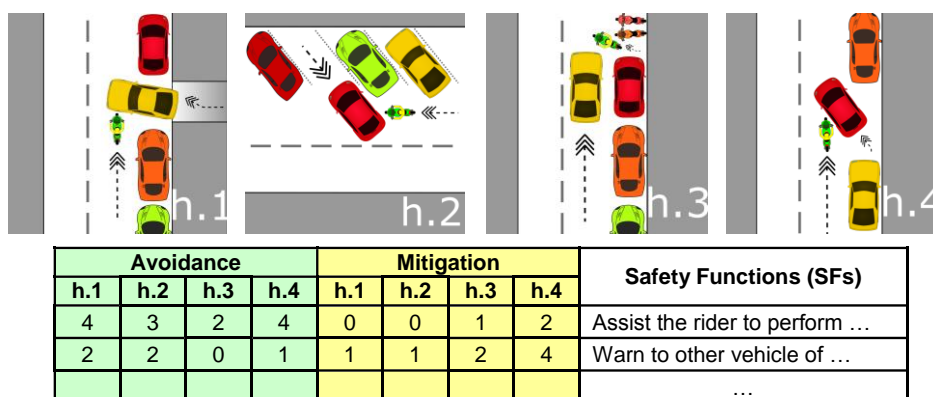


Figure 32. Example of an expert assessment of two Safety Functions (SFs) for parking-out maneuvers. The numbers in the table represent the outcome of the expert evaluation using the scoring scale defined in Table 4

3.3.3.3. Increasing the KB (collective knowledge)

Prior to accept the ranked list assessed for an expert, is necessary to verify somehow if the numbers presented follow a criteria or if it were random selected, in order to avoid introducing erroneous assessments in the KB. Therefore, a coherence verification test works as a filter on the information coming from the expert assessment. To this end, a Fleiss's kappa calculation (extension of Cohen's kappa measure) is performed against the preexistent values of the KB to identify possible random responses in the assessment. The aforementioned coefficient measures the inter-rater agreement for qualitative items (Carletta, 1996; Gwet, 2008) and this calculation can be performed in spreadsheets (Zaiontz, 2015).

Once the information encoded by the experts is verified as not random, this is incorporate to the collective knowledge to be used in the following and in further analysis.

3.3.3.4. Inferring with the KB

The inference engine uses the rules or equations defined in the operative Framework to generate different results easier to interpret for the researcher that is manipulating all these information and allows to him/her to take well-funded decisions.

In the case of the KBMS, the results consist in a set of arrays organized numerically. These arrays represent quantitatively the relevance of each SF along the different road accident scenarios for the particular region/country analyzed.

3.3.3.5. Application case: Reduced study

In order to implement and evaluate the complete workflow of the KBMS, I present the results of KBMS-ISTAT (reduced expert assessment employing the crash data of ISTAT database). The preliminary results are compared with the previous work done on PISA project.

In the KBS method developed, the upper branch of the collecting stage (Figure 29) is used to extract road accident data of ISTAT database, corresponding to the years 2010-12, with the nine queries of Appendix C. For reference, the information is presented in Table 6.

The nine general scenarios of PTW accidents were defined by the queries performed in the ISTAT road accident database. For this reason, the Appendix B is organized with nine rows of pictograms. Each row corresponds to one general accident scenario, they are labeled with the capital letters: A, B, C..., and H. In addition, the general road accident scenarios are a combination of all the scenarios contained in the row (e.g. in the scenario "H" depicted in Figure 32, the scenarios to combine are: h.1, h.2, h.3, and h.4). Consequently, in the processing stage (Figure 29), the statistical information presented in Table 6 is used in the Inference Engine (IE – Section 3.3.2) to compute the steps a, b, c, and d.

Coming back to the collecting stage (Figure 29), through the lower branch of the method is conducted the expert assessment. Here is analyzed the impact of each SF (described in Appendix D) among the accident scenarios depicted in Appendix B. In this reduced study a subset of 10 SFs presented in Table 7 were assessed for three experts, enabling the feeding of the KB and consequently, computing the remaining steps of processing stage (IE – steps: e, f, and g).

To conclude the analysis, the results obtained in the inference engine provides a prioritized SF list. The results of the processing stage (output in Figure 29) are presented as numerical values in Table 8 (Iki_Sum column).

Year	2010	2011	2012
Total vehicular accidents	211404	205638	188228
Total PTW accidents	71108	71790	62374

PTW accidents in a collision scenario type:			
A	18262	18188	15145
B	5424	5641	4663
C	6001	6376	5583
D	5479	5396	4489
E	4811	4693	4004
F	7932	8226	7089
G	5320	4981	4614
H	8317	8553	7742
I	3090	3385	2893

Table 6. Information retrieved after the segmentation process applied to ISTAT road accident database. The information corresponds to the years 2010, 2011 and 2012

SF#	SF description
2	Assist the rider to perform a hard braking without falling from the PTW
6	PTW send a signal to Slow/Stop other vehicle
18	Energy dissipation element placed in the PTW to dissipate rider kinetic energy during a crash. Case: frontal collision of the PTW
34	PTW - Alert to the rider of an oncoming vehicle
44	Improvement of PTW conspicuously (help to the PTW to be seen for others)
48	Driver state detection (guarantees a minimum level of alert)
50	Other vehicle alcohol interlock
53	PTW restricts its maximum speed to street top speed
59	PTW Lane keeping
61	PTW autonomous-braking

Table 7. List of Safety Functions (SFs) used in the application case. This subset contains a variety of SFs, going from a very specific target to broad ones

SF #	Iki_1	Iki_2	Iki_3	Iki_Sum
2	1.17	1.32	1.38	3.87
6	0.72	0.78	1.02	2.52
18	0.52	0.55	0.44	1.51
34	0.73	0.74	0.88	2.35
44	0.53	0	0.89	1.42
48	0.51	0.12	0.69	1.32
50	0.04	0	0.7	0.74
53	0.76	1.32	0.08	2.16
59	0.1	0	0.04	0.14
61	0.82	1.3	0.86	2.98

Table 8. Numerical values of the last two steps of the inference engine. They are the results that quantify the importance of each SF analyzed for Italy (in the reduced study). The left column indicate the number of the Safety Function (SF) evaluated. The three intermediate columns show the result of the inference engine until the penultimate step (this example is didactic because the assessment was performed only for three experts and with 10 SFs). The rightmost column is the output of the KBMS applied to ISTAT database, presenting as the most prominent the SF number 2, followed by the 61, 6, 34, 53, ...

3.3.3.5.1. Results of the comparison (PISA vs. KBMS)

The main outcomes of PISA study are presented in (Appendix H). The case study (KBMS-ISTAT) used 205,272 PTW crashes occurred in Italy in the period 2010-2012 (data correspond to the last years of the data presented in Chapter 2 – Sections 2.3 and 2.4).

The ISTAT crashes involved at least one PTW (moped powered less than 50cc, scooter or motorcycle), and resulted in at least one injured or killed person. With the crashes' classification of the KBMS default Evaluation Framework, I observed the following percentages regarding the total PTW crashes: a) 51% were represented by only four types of crash scenarios (namely A, H, F, and C); b) 25% occurred at intersections (scenarios A and B) with a clear predominance of angular collisions; c) 12% occurred in angle collisions in straight road segments (scenario H); and d) 11% were rear-end collisions (scenario F).

Safety Function description	KBMS	PISa ranking	
	Metrics	Quartile	Absolute position
Assist the rider to perform a hard braking without falling from the PTW	3.87	1	7, 8, 9
PTW autonomous-braking	2.98	1	4
PTW send a signal to Slow/Stop other vehicle	2.52	1	1
PTW Alert to the rider of an oncoming vehicle	2.35	3	21
PTW restricts its maximum speed to street top speed	2.16	2	14
Energy dissipation element placed in the PTW to dissipate rider kinetic energy during crash. Case: frontal collision of the PTW	1.51	2 & 3	17, 18, 24
Improvement of PTW conspicuity (help to be seen for others)	1.42	1 & 4	6, 35
Driver state detection (guarantees a minimum level of alert)	1.32	4	36
Other vehicle alcohol interlock	0.74	4	36
PTW Lane keeping	0.14	4	36

Table 9. Prioritized safety solutions of KBMS-ISTAT and PISa studies. The left column is the prioritized list of Safety Functions in the KBMS method. The KBMS metric expresses the importance of each SF (larger numbers represents more importance). PISa columns represent the same information in a different manner (quartiles and absolute score), allowing comparison between the KBMS-ISTAT outcomes with those of PISa project (mark 36 means “less important”)

A prioritized list of Safety Functions (SFs) is obtained by applying the KBMS approach in our case study (Table 9). The SFs with higher priority are those with potential to avoid and mitigate the greatest possible number of motorcycle crashes in Italy. The top three SFs were: “Assist the rider to perform a hard braking without falling from the PTW”, “PTW autonomous-braking”, and “PTW send a signal to slow/stop other vehicle”. At the bottom of the prioritized list we found: “Driver state detection”, “Other vehicle alcohol interlock”, and “PTW Lane keeping”. Concerning the reasons for the lowest scored SF (PTW lane keeping) the rating reflects the fact that this function is obviously inadequate for urban motorcyclists. This finding becomes explicit by comparison of the numerical metric of this SF (0.14) with regard to the precedent ones (scored 0.74 and greater than 1.32). As a supporting fact of this result, we can

highlight the practice of lane-splitting commonly observed in dense traffic (Aupetit et al., 2015).

Table 9 shows a comparison of our outcomes (analysis KBMS-ISTAT) against the findings of the PISA study. The comparison is complex because the methods have different SFs list, therefore some cases I have to add the contribution of two or three SFs of the PISA to match one corresponding of the KBMS method. These comparison reflects good correspondence in the top three and bottom three SFs of the prioritized lists, notwithstanding the different approaches, expert subjects and crash material. A more detailed comparison would be possible, however it would also be quite complicated due to a number of factors including also periods and places of the crash data, but also methodological factors.

Finally, by using the KBMS method was identified that 35-50% of PTW crashes in Italy could have been positively influenced by mitigating and avoidance SFs. The top scores of automatic systems to assist the rider during the crash precipitation event suggest an important role for these SFs. In practical terms, for the first two SFs in the ranking, equivalent safety systems in cars are currently available, namely Anti-lock Braking System + Electronic Stability Program (ABS+ESP) and Autonomous Emergency Braking (AEB). The effectiveness for passenger cars of ABS+ESP and AEB was demonstrated in real cases (Lie et al., 2004; Burton et al., 2004; Fildes et al., 2015). However, the solutions for motorcycles still need to be clearly defined and the KBMS method can contribute to this end.

3.4. Discussion about the KBMS

In spite of the undeniable valuable findings of the European projects – shared though public deliverables and other dissemination activities like conferences and congresses – some members of the scientific community do not have access to the confidential documents and, therefore, they do not have sufficient information to validate or question their findings. In this respect, the new program launched by the European Commission known as Horizon 2020 seems to be an improvement due to the promotion of more open access to scientific publications. Time will tell if that is the case.

During the analysis of the large documentation of the PISA project, I found a mix of concepts concerning the safety solutions list to assess. This issue motivates me to explicit the concept of safety function (SF) in the KBMS method. The problem in PISA consisted in the lack of distinction between SF and safety system/technology. Consequently during the expert assessment the researchers assessed a functionality or a technology respectively without distinction. Clearly, to assess how may behave a technology in a circumstance, requires much more and accurate information than assessing a functionality (desired behavior). Anyway, PISA project was a very good first attempt of prioritization of safety solutions for PTWs, and for this reason I compared the KBMS with it.

Another issue worth mentioning regarding other EU research project, is the case of the road accident scenarios defined in the APROSYS project. This multi-objective and integrated safety investigation defined a reduced set of PTW accident scenarios that were used as starting point in other contemporary safety research investigations (e.g. PReVENT, AIDE, EASIS, GST). In fact, the resolution of those PTW accident scenarios is lower w.r.t. the nine “general” accident scenarios presented in the KBMS-ISTAT case study. In addition, the KBMS framework offer the possibility to increment the resolution of the general accident scenarios when is used a road accident database with more variables that the employed in this research.

Regarding more specific projects related to PTW safety, some activities (i.e. statistical traffic accident analysis and in-depth accident analysis) must be carried out each time during the early stage of the projects. Then, different complex studies are conducted several times (requiring current statistical analysis, review of technologies, and considering the new road politics that influence the circumstances regarding past years). However, the main constraint is the subjectivity of certain analysis given the nature of the information and the judgments being made, as well as the methodology adopted. In order to overcome all the aforementioned difficulties, the authors suggest the KBMS (Knowledge-Based system of Motorcycle Safety) as a clear, flexible (e.g. reorganization of accident scenarios, modification of the inference engine), and scalable methodology (e.g. addition of new accident scenarios, new SFs, new objectives as: injurie criteria, medical fares, convalescence days, etc.), that could be used and updated in the coming years, regardless of confidentiality issues.

The framework of the KBMS method overcomes common limitations as: heterogeneous road accident data collection between different countries/regions; and restricted access to the databases due to sensible information about the victims involved. In particular, the segmentation of a road accident database by using queries list can be easily replicated in several databases locally, enabling database managers to disseminate the harmonized numerical information.

This drastic simplification of the contents of the database may summarize one year of road accident data in a few variables – a dozen for example – that contain the quantity of accidents in a given accident scenario. Therefore, in order to explicitly define how many variables are needed to be representative of reality, the “accident coverage” metric is defined. Although each traffic accident is unique, they share some characteristics that allow us to cluster the accident in different accident scenarios. However, certain accidents cannot be grouped into the most typical cases and might be neglected. Thus, the coverage metric helps to ensure a threshold of neglected accidents by performing the addition of PTW accidents in each accident scenario analyzed and comparing it with the total amount of PTW accidents registered for the region analyzed in the current year.

Regarding our experience in the execution of the expert assessment, unattended problematics comes-up forcing us to find a solution and remade the expert assessment of some SFs. The problem appears with preventive safety solutions that may acts in a broad or in all type of accident scenarios. For example, an assessment of an alcohol interlock function. Obviously, riders or drivers under effects of alcohol are not a desired in any case, as a consequence, this may force to the expert to assess this function with a top score when in the mostly cases the SF is not required. To solve these issues some assumptions and guidelines to conduct the assessment backed for statistics data were proposed.

About the two weakness of the actual research, they are also its further improvements aspects. The limitations are:

- 1) The quantity of experts assessing the SF list in the study (3 persons).
- 2) The resolution of the accident scenarios.

The first limitation is possible to overcome with the collaboration of more experts in the analysis, because all the collaborations are “additive contributions”, then constructive in this way. The second one, it is a particular limitation in the ISTAT database that may be not present in others road accident databases.

In particular, the limitation consist in the level of detail of descriptive variables used during the description of the accident depicted in Figure 33. It forced me to perform only nine

queries, therefore in our study is not present the information of which vehicle collides to the other one. Thus, the four sub-scenarios (a.1, a.2, a.3, and a.4) were assigned a 0.25% of occurrence to each one that surely is not true. It is worth saying that even with this low resolution in the general scenario due to the limitation imposed for the ISAT data; it was shown the good potential and consistent approach of the KBMS methodology.

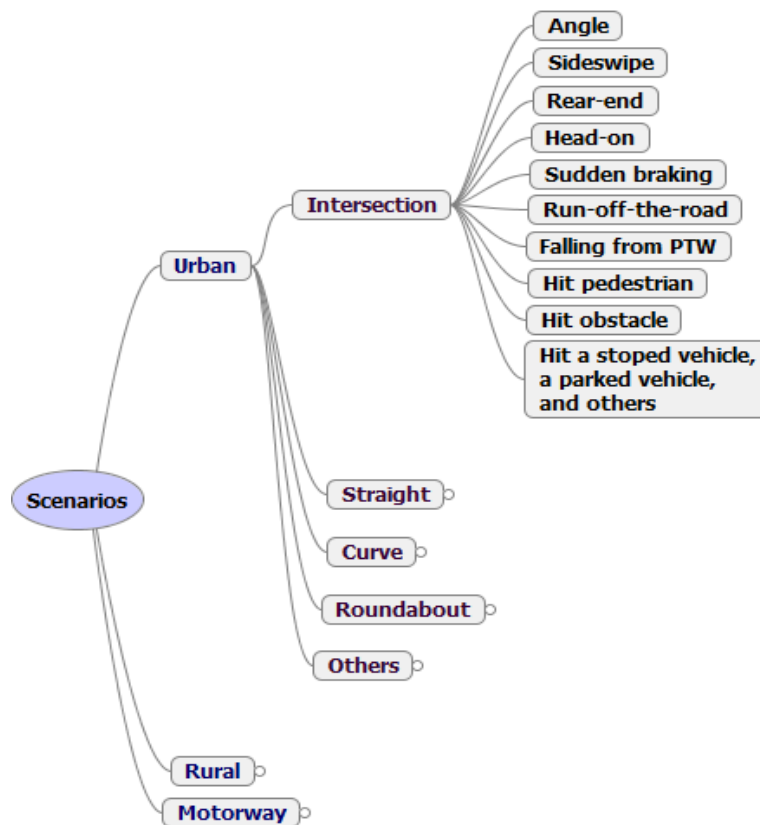


Figure 33. Main variables of ISTAT road accident database. The circles at the end of the branches denote the continuation of the arborescence (the same as the previous variable)

3.5. Conclusion of the KBMS

The KBMS (Knowledge-Based system of Motorcycle Safety) is a contribution as a new way to cross the gap between road crash data and knowledge. A tool of road accident research and decision making that enables the collaboration between researchers and data sharing, while keeping critical/confidential population data in the source. The significant outcomes of this kind of collaboration are the simple and concrete goals to transmit to scientist, engineers, developers and industrial stakeholders interested in vehicular safety.

The key points learned during our preliminary attempt to collecting and storing expertise in the KB of the KBMS were:

- a) Defining a common vocabulary to perform workshops and facilitate the exchange between experts of different specializations.
- b) In the expert assessment is hardly recommendable to use a binary Liker type scale in order to avoid ambiguous assessments (e.g. it SF may contribute sometimes).
- c) Defining a set of guidelines based in facts of in-depth accident databases to reduce the degree of variability of the assessment in the accident scenarios.
- d) A very comprehensive list of SFs for the expert assessment, present the drawback to convert the evaluation of each accident scenario in a big time consuming task, and it may go against to the quantity of collaborators.

For these reasons, more research is needed in the definition of a shorter SFs list to assess. The reduction of the SF list is a trade-off between the quality of expertise collected and the time required to encode it, in order to be stored in the KB of the KBMS.

Currently, the KBMS method is being implemented between a recognized motorcycle manufacturer and the University of Florence. This joint research is somehow a proof that the method can provide interesting outcomes for the industry, and it is my hope that new stakeholders will join the methodology in the future to contributing to make motorcycling a safer mean of transport.

3.5.1. Future work

A validation of the effectivity of the methodology need to be conducted against real crash data including the cases of intervention of real motorcycle safety systems. As most of them are not present in the market today, the validation will need to be conducted in the future, for this reason a comparison of the results versus the results of PISA project was conducted.

Part II

4. Preventive safety and artificial perception systems

I will briefly develop the concept of preventive safety as a new aspect of vehicular safety, which currently is separated in two aspects called passive and active safety. After that, it is introduced by examples a preventive safety approach used in cars which are suitable for artificial perception in the motorcycle safety case. Consequently, this motivated the research of a suitable sensing approach to cope with the requirements of the preventive safety solutions envisaged.

Hereinafter, a brief overview the technology behind selected artificial perception sensors (considered important for the application in advanced safety systems in motorcycles) is presented. Recent proximal sensors (it is possible to define a proximal sensor as a remote sensor designed for measurements in a range below to 3 or 4 meters) are analyzed. The operation principles of proximal sensors can provide good insights about the potential and limitations of these sensing technologies. Clearly, proximal sensors cannot be directly applied to a real application with motorcycles, however the signal processing circuits are similar to remote automotive sensor but scaled in terms of range, power, and performance. From the algorithms side, the algorithmic core behind proximal sensors and remote sensors used in industrial and aerospace applications is very similar.

The usage of some inexpensive proximal sensors allowed me to experiment with them. The practical utilization of the sensors allowed me to capitalize on my prior background in electronics engineering and firmware development by conducting reverse engineering of them, and learning details about their sensing limitations which are not properly specified. The learning on these sensors was then applied to the study of technical specifications and scientific publications of automotive sensors. This allowed me to assess current automotive sensors for application on tilting vehicles in Chapter 6.

This chapter concludes with the introduction of the target hardware required for the embedded processing required for an artificial perception system in motorcycles. Also mentioning the related software platforms for its development. This is important for the motorcycle safety application because not information is available in literature concerning motorcycle safety. In addition, I mention the differences between them and explain their election among other alternatives. The considerations mentioned in this study helped to restrict the plethora of algorithms that can be used for safety systems implementations, and guided the development of the remote sensor described in Chapter 7.

4.1. Concept of preventive safety

In vehicular safety, it is currently accepted the classifications of active and passive safety. The term active safety (or primary safety) refers to safety systems that are active prior to an accident. This has traditionally referred to non-complex systems such as good visibility from the vehicle and low interior noise levels. Nowadays, this classification contains complex systems such as anti-lock braking system, and electronic stability control. Passive safety (or secondary safety) refers to safety systems which act during an accident with a mitigation scope. For example, helmets, protective garments and air-bag jackets belong to passive safety.

Advances in passive safety systems have progressed enormously in recent years, in contrast, in the active safety domain there are still several unexplored solutions. Most of these unexplored solutions refer to certain intend to the automation of the driving task, as it was established by the SAE J3016 international standard (Table 10). These definitions are commonly associated to self-driving cars but involve all kind of road vehicles.

SAE level	Name	Narrative Definition	Execution of Steering and Acceleration/Deceleration	Monitoring of Driving Environment	Fallback Performance of Dynamic Driving Task	System Capability (Driving Modes)
Human driver monitors the driving environment						
0	No Automation	the full-time performance by the <i>human driver</i> of all aspects of the <i>dynamic driving task</i> , even when enhanced by warning or intervention systems	Human driver	Human driver	Human driver	n/a
1	Driver Assistance	the <i>driving mode</i> -specific execution by a driver assistance system of either steering or acceleration/deceleration using information about the driving environment and with the expectation that the <i>human driver</i> perform all remaining aspects of the <i>dynamic driving task</i>	Human driver and system	Human driver	Human driver	Some driving modes
2	Partial Automation	the <i>driving mode</i> -specific execution by one or more driver assistance systems of both steering and acceleration/deceleration using information about the driving environment and with the expectation that the <i>human driver</i> perform all remaining aspects of the <i>dynamic driving task</i>	System	Human driver	Human driver	Some driving modes
Automated driving system ("system") monitors the driving environment						
3	Conditional Automation	the <i>driving mode</i> -specific performance by an <i>automated driving system</i> of all aspects of the <i>dynamic driving task</i> with the expectation that the <i>human driver</i> will respond appropriately to a <i>request to intervene</i>	System	System	Human driver	Some driving modes
4	High Automation	the <i>driving mode</i> -specific performance by an automated driving system of all aspects of the <i>dynamic driving task</i> , even if a <i>human driver</i> does not respond appropriately to a <i>request to intervene</i>	System	System	System	Some driving modes
5	Full Automation	the full-time performance by an <i>automated driving system</i> of all aspects of the <i>dynamic driving task</i> under all roadway and environmental conditions that can be managed by a <i>human driver</i>	System	System	System	All driving modes

Table 10. SAE international's J3016 provides a common taxonomy and definitions for automated driving in order to simplify communication and facilitate collaboration.

Latest researches (up to 2017) in vehicle safety focus mainly on collision avoidance (with other vehicles, pedestrians and wild animals), like collision warning/avoidance and through automatic braking/steering (intervention systems) corresponding to SAE Level 0.

In the pursuit of the development of collision avoidance safety systems, I classified these type of research as preventive safety (Figure 34). The motivation to classify the preventive safety systems outside of the current classification of active safety is because of two reasons:

1. Preventive safety predicts potential crashes, as long as certain conditions are met, which differs from active safety. The SAE J3016 taxonomy, described in Table 10, expresses that the capability of “monitoring the driving environment” requires an artificial perception system foreseen only in SAE Level ≥ 3 .
2. Active safety systems enhance driver/rider actions to perform a hard braking and/or help to stabilize the vehicle under difficult scenarios (intervention systems corresponding to SAE Level 0). However, the preventive safety system can take over the control of the vehicle, based in the idea that the safety system (which includes an artificial perception system) identified properly the traffic scenario under certain conditions of operation.



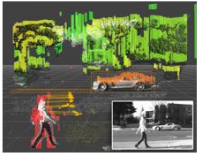
Type of Safety	Accident Mitigation	Accident Avoidance	Accident Forecasting
Passive 	★★★★★	☆☆☆☆☆	☆☆☆☆☆
Active 	★★★☆☆	★★★★★	☆☆☆☆☆
Preventive 	?	?	★★★★★

Figure 34. Proposed classification of safety systems.

Consequently, preventive safety systems may help drivers and riders to avoid or mitigate an accident through the use of in-vehicle systems which senses the nature and significance of the danger. Depending on the significance and timing of the threat, the preventive safety systems will:

- Inform the driver/rider of a critical situation (potential crash) as early as possible.
- Assist actively the vehicle or ultimately intervene (the system have more hierarchy level than the human driver/rider) in order to help prevent any collision or mitigate its consequences.

In my opinion, a substantial difference exist between preventive safety and other active safety systems. Preventive safety allows for taking the control of the vehicle under the inaction of the human driver/rider, I decided to separate the preventive safety systems from the category of active safety systems.

Summarizing, preventive safety applications can help drivers/riders to:

- Keep a safe distance to precedent vehicle.
- Avoid overtaking in critical situations.
- Avoid crashes with other Vulnerable Road Users (VRUs).
- If the crash occurs, they may reduce the crash severity by reducing the speed of the collision (crash mitigation).

Finally, the preventive safety will make use of automotive remote sensors to perceive the traffic environment (massive data), communications between vehicles and/or infrastructure, geo-localization solutions, and artificial intelligence for improving road safety. The fusion and coordination of all these technologies make these systems more complex than active safety systems, such as Anti-lock Braking System (ABS), and Electronic Stability Control (ESC), as is illustrated in Figure 35.

Performances (Passive Safety & Active Safety)



New active safety technologies (perception + communication)



Figure 35. Safety performance expected for different safety systems.

Remark: some remote sensors are introduced in the pictures for a best reference, however more detailed information about the automotive remote sensors are opportunely explained in Chapter 4 (Section 4.3) and Chapter 5 (Section 5.3).

4.2. Artificial perception systems in road vehicles

Artificial perception is a technology that provides the ability to understand, to some degree, the surrounding environment of an intelligent system embodied in a robot. In the case of road vehicles that attempts to understand the road environment, they are usually referred as robot cars, or driverless cars, or autonomous cars. Datasets are collected from moving sensing platforms, like the depicted in Figure 36, which store considerable amounts of data in order to provide support for the development of perception algorithms.

As example, I selected three references which contains automotive datasets: The Ford Campus (Pandey et al., 2011), the KITTI (Fritsch et al., 2013; Geiger et al., 2012a, 2013; Menze and Geiger, 2015), and the Oxford Robotcar (Maddern et al., 2017). The links below present the datasets organized by year in which they released the data to the scientific community:

- Year 2011: Vision and Lidar Ford Campus dataset
<http://robots.engin.umich.edu/SoftwareData/Ford>
- Year 2012-15: KITTI Vision Benchmark Suite
<http://www.cvlibs.net/datasets/kitti/>
- Year 2017: Oxford Robotcar
<http://robotcar-dataset.robots.ox.ac.uk/>
<http://ori.ox.ac.uk/the-oxford-robotcar-dataset/>



Figure 36. Detail of instrumentation of Robotcar sensing platform (adapted from Oxford website)

4.2.1. Perception systems after DARPA grand challenge of 2005

The initial DARPA Grand Challenge was created to stimulate the development of technologies needed to create the first fully autonomous vehicles capable of completing a substantial off-road course within a limited time. This competition was an important milestone in the field of artificial perception systems, and current systems are based in the most performant competitors' strategies.

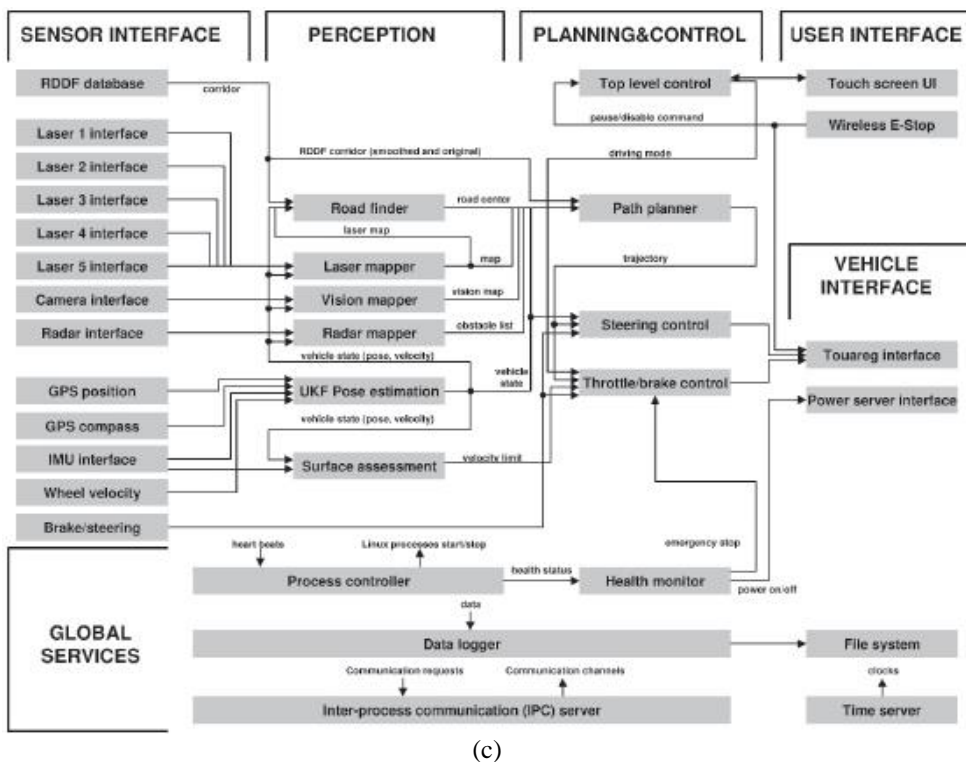


Figure 37. Vehicle winner of 2005 DARPA challenge. (a) Remote sensing apparel in the top of the vehicle. (b) Scheme of the sensing and artificial perception strategy. (c) System architecture with detail of the perception strategy and its corresponding sensors.

The winner of DARPA competition was a vehicle called “Stanley” (Figure 37). The perception strategy was based in the information provided by a single color camera, supported by a set of off-the-shelf industrial LIDARs (detail in Figure 37a) and a GNSS (Global Navigation Satellite System) to follow the waypoints of the competition. Figure 37b is a scheme of the sensing and artificial perception strategy used, for which its four main components (red labeled in the scheme) are explained below:

- 1) GPS antenna: it receives data that has actually traveled twice into space, once to receive an initial position that is accurate up to a meter, and a second time to make corrections. The final reading is accurate up to 1 meter.
- 2) Laser Range Finder (LIDAR): it scans the terrain 22 meters ahead and to either side of the grill five times a second. The data is used to build a map of the road.
- 3) Video camera: it points on the road beyond the LIDAR range and pipes the data back to the computer. If the lasers have identified drivable ground, software looks for the same characteristics in the video data, extending car’s vision to 70 meters and permitting safe acceleration.
- 4) Odometry: a photo sensor in the wheel well monitors a pattern imprinted on car’s wheels. The data is used to determine how far the car has moved since the blackout of GPS location.

From the system architecture diagram (Figure 37c) the perception system implemented has three objectives: a) The road perception and obstacle detection, mainly performed by the video camera and LIDARs; b) Localization managed with a non-linear estimator, the Unscented Kalman Filter (UKF); and c) Surface assessment (roughness of the off-road terrain). More detailed information about the perception system of the winner vehicle is available in (Thrun et al., 2006).

The evolution of these perception systems has turned into the use of visual information sensors because they provide huge amounts and significant information. In fact, most mammal animals have not equivalent sensor capabilities like a RADAR or LIDAR. These animals perform mostly of the sensing and interpretation from visual information gathered from the eyes. This is also the case of humans, for with a significant part of the brain is dedicated to visual interpretation (Harvey et al., 1991), as it is shown in Figure 38.

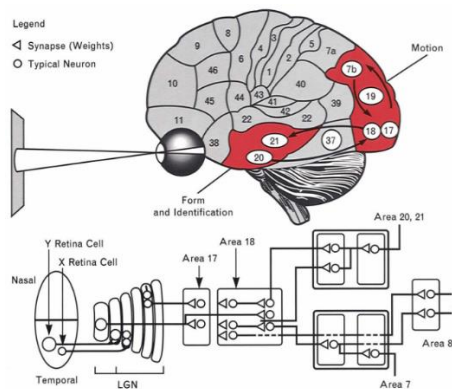


Figure 38. Neural network vision model: (top) sketch of human brain in which areas associated with vision are shown in red, and (bottom) block diagram of human vision process.

Posteriorly, special interest was given to the interpretation of binocular vision or stereo vision due to its capability of providing depth estimation from the visual information. In (Rankin et al., 2009) more than 10 years of research of the Jet Propulsion Lab (JPL-NASA) were implemented in a single off-road rover which performs the perception of the environment from stereo vision sensors. Figure 39 shows from left to right the visual information of one camera of the stereo vision system, the depth information computed of the scene, and the interpretation of the scene by a voxel representation (regular grid in three-dimensional space).

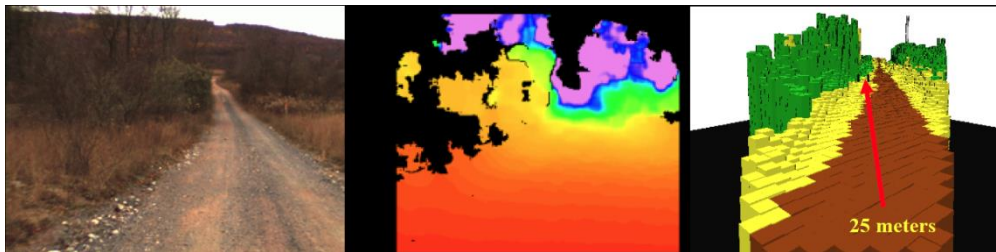


Figure 39. Visual sensing and perception of the off-road rover.

Targeting a rural traffic environment, other interpretation of the terrain and its obstacles is presented by (Broggi et al., 2013a). The artificial perception was also based on stereo video. Figure 40 shows the interpretation of terrain irregularities or obstacles growing from a green grid that represents a free road space. Details of this perception system are available in (Broggi et al., 2013b).

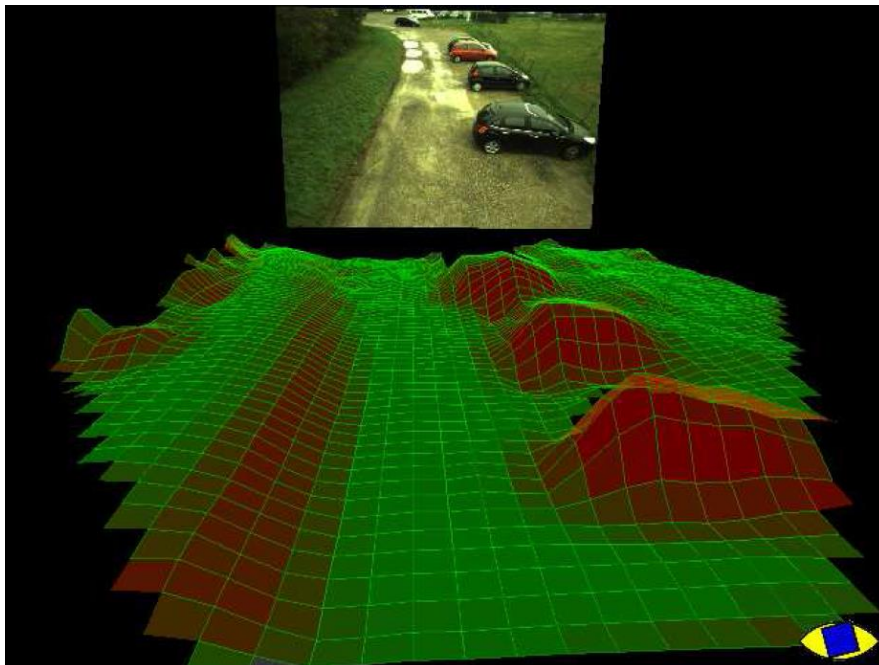


Figure 40. Estimation of terrain traversability, in terms of both terrain slope and obstacles.

Sub-pixel interpolation on stereo vision systems (Haller and Nedeveschi, 2012) is another technique that provides a more accurate depth calculation. This feature is important because it enhances the perception capability of the camera-based sensor to distinguish small irregularities in an urban scene. For example, the curbs in the side of the streets (Figure 41).

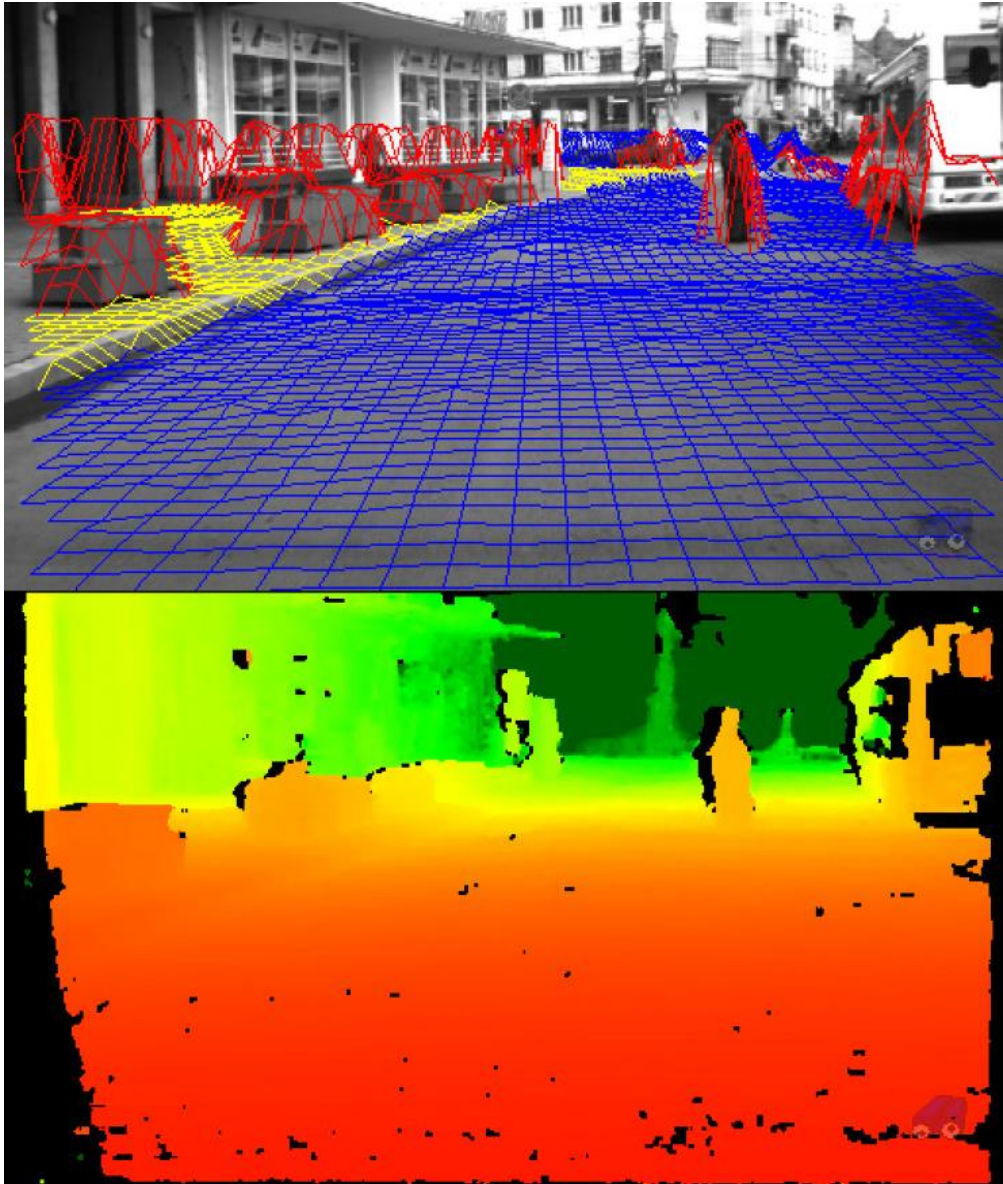


Figure 41. Example of an urban scene corresponding to the KITTI dataset: (top) the classified occupancy grid, (bottom) is the depth information.

4.2.2. Automotive perception systems: The stixel world representation and 6D-Vision

This perception system is based on stereo vision and radar technology as main remote sensors. Modern stereo matching algorithms deliver a depth estimate for nearly every pixel of the image (Hirschmuller, 2005) established a matching scheme called Semi-Global Matching (SGM) that was made available on FPGA (Field Programmable Gate Array) hardware by (Gehrig et al., 2009). This low-power solution for matching stereo image pairs delivers dense disparity images in real-time.

However, the dense disparity images plus the original images represent huge amounts of data to process. The effort spent to extract task-relevant information grows significantly with the variety of independent vision tasks. To avoid this, a generic pre-processing step has been designed to manage the huge amount of data in video sequences and its pixel attributes (the “Stixel World” representation).

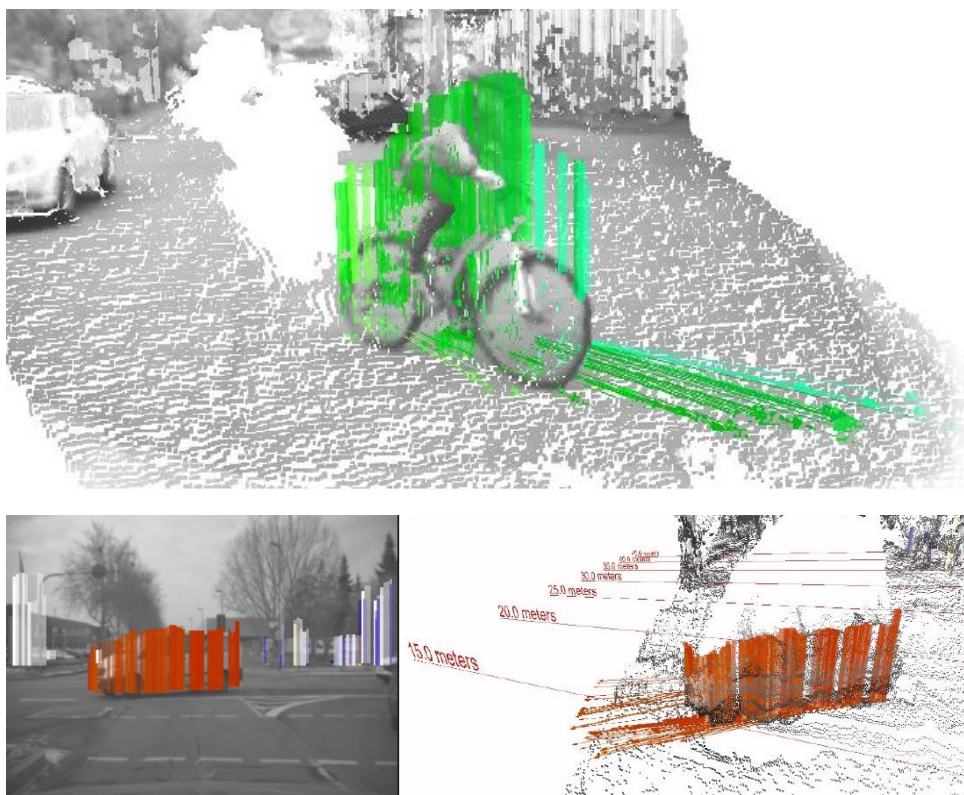


Figure 42. Two examples in which a perception system identify the depth, direction and speed of different obstacles. The arrows show the prediction of the location of the different parts of the obstacle sensed in the following half second. This technique for the perception of road scenes is known as “stixel world”.

The stixel world is a medium level representation for three-dimensional objects. These are approximated by a set of rectangles called stixels, all sharing the same width within the

image (e.g. 5 pixels). Each stixel describes the distance and height of an object in a certain image column. The space up to the base point of each stixel is considered as free.

Furthermore, the stixel world representation comes along with significant compression rates of the input data. For example, for a given width of 5 pixels for the stixels, the relevant content of a 1024 x 440 pixels disparity image can be described by 205 stixels only. In total is possible to achieve a reduction of the data volume of 99.9%: more than 450,000 disparity measurements reduced to 410 values.

The stixel world is well suited as a medium level representation to decouple low-level data from high-level algorithms. It corresponds to a figure-ground segmentation that offers a precise contour approximation. By varying the width of the stixels, it can be selected the compactness and the detail of the medium level representation.

By introducing a tracking scheme similar to the principle of 6D-Vision (Franke et al., 2005), which consist in 3D-position and 3D-motion, and the stixel representation is extended into the time domain (Pfeiffer and Franke, 2010). As a result, velocity information for each stixel independently is obtained. An example is shown in Figure 42, in which the vertical lines are the stixels and the arrows indicate its future location. More details of this approach can be found in (Pfeiffer and Franke, 2011).

4.3. Sensors for remote sensing

This section explains the clever adaptations done for the automotive and entertainment applications of the main remote sensing technologies, which initially were developed for sophisticated applications such as military and space exploration. Inevitably, the process of cost-reduction of the adaptation of these technologies occasioned the degradation of sensing performance (several aspects), but complying with the needs of 2D or 3D measurement of the road scene.

4.3.1. State-of-the-art of proximal sensing

Sensors for proximal sensing are relatively new technologies for 3D sensing which are relevant for artificial perception systems. These solutions were developed mainly for the entertainment industry, however proximal sensing technologies are based on principles of the remote sensing technology developed for earth exploration from satellites.

Proximal sensing is oriented to short range measurements within controlled environmental conditions, also they are economically constrained (10 to 20€). These 3D sensors developed for the entertainment industry have been seen with a particular interest from the robotic community, which started to use these devices for radically different applications. After a decade of developments of proximal 3D sensors, multiple strategies and principles were used to enhance measurement performance in different situations, such as texture less surfaces and low light conditions.

The world's top semiconductor companies (e.g. Intel, Qualcomm, IBM, etc.) are promoting advanced proximal sensors, in which their data can be processed by specific purpose chips called ASIC (Application Specific Integrated Circuit). This makes possible to define embedded low power systems able to use the information provided for smart sensor, because the sensor heavily pre-process the data on the source. Recently (year 2016), Intel started to sell these smart sensors under the name Intel RealSense™ cameras, which also includes a Vision Processing Unit (VPU) on chip.

4.3.2. Potential of Vision Processing Units (VPUs) for the motorcycle safety application

The important potential of VPUs for the motorcycle safety application relies on the possibility to build embedded artificial perception systems. VPUs can run algorithms needed for 3D triangulation on the camera itself. In this way, the camera can transmit the results of the calculations together with the image acquired. These type of calculations are pixel-wise, such as dense disparity map, optical flow, and SURF image features extraction (as explained in Chapter 6).

Myriad X (Figure 43) is a modern ASIC oriented to VPUs calculations. This chip is able to compute 3 stereo video frames (6 cameras) with a resolution of 1280x720 at 60 fps, and power consumption of 1.2W. This low power consumption is feasible for embedded applications in motorcycle safety systems. On the contrary, GPUs technology that can accomplish with the same functionalities consumes up to five to ten times more energy due to its more general architecture and in particular by the memory management required (e.g. total NVIDIA Jetson TK1 power 4.7W running a memory-intensive task).

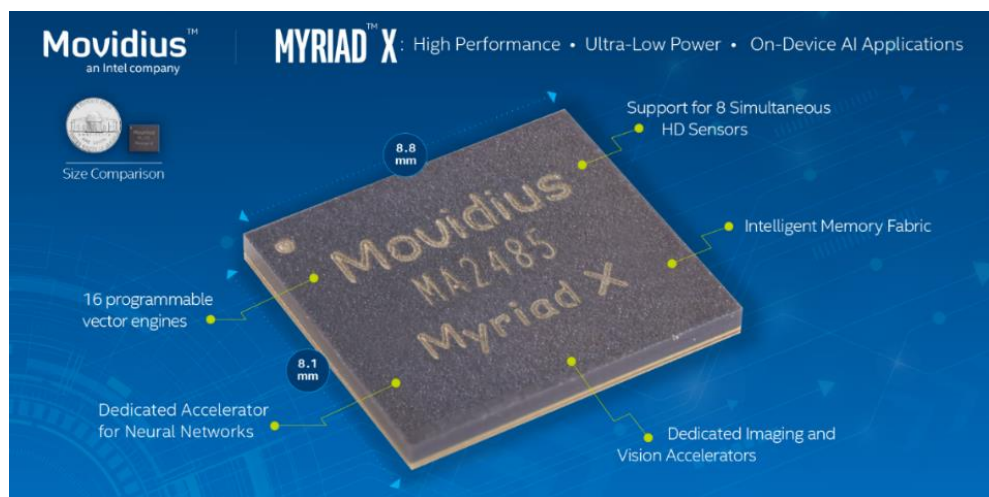


Figure 43. Last ASIC for embedded artificial vision released in August 2017. Adapted from <https://www.movidius.com/>

As the technology is new, there are not agreement between manufacturers to denominate these ASICs that acts as Artificial Intelligence (AI) hardware accelerators, to which VPUs belong. The terminologies used are: neuromorphic processor, neural processing unit, tensor processing unit and neural compute engine.

Recently, Intel released an USB-stick (based on Myriad 2) for embedded artificial intelligent applications. This device integrates a USB port for modular connection with embedded boards, and integrates a powerful chip for algorithm calculations (Figure 44).

Therefore, the usage of these VPUs on remote sensors for motorcycle safety is a very interesting possibility that did not exist before. In the following sections, I present representative examples of recent proximal sensors that have used this ASIC chips to perform 3D sensing in near range.

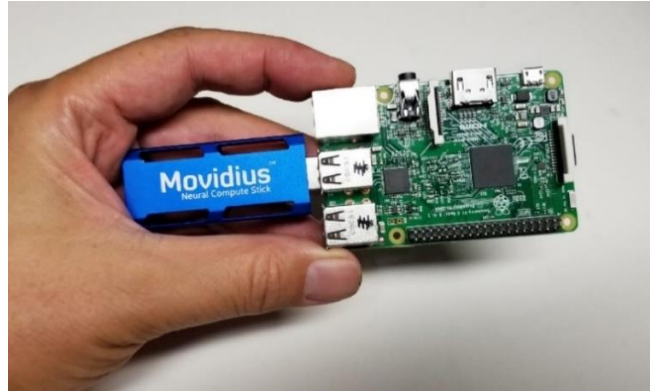


Figure 44. Detail of the neural computer featuring a VPU (Myriad 2) in a blue heat sink case connected to an embedded system - Released in July 2017

4.3.3. Background: structured light for proximal sensing

Following, the physical principle of proximal sensor is explained. These concepts include examples of recent sensors and its real-world applications.

4.3.3.1. Gray code projection

Structured light is a technique used to measure the depth and surface of a beamed object. This technique is based on projecting a light pattern, which contains horizontal and vertical bars, onto a scene where an object interferes. The width and surface of the object can be extracted by the deformation of the bars beamed on the object (Proesmans et al., 1996). A visual representation of the measuring principle is presented in Figure 45.

Recently, the method was extended for the application under sunlight (Gupta et al., 2013), at expenses of increasing the time of acquisition. A complete tutorial paper about this technology (Geng, 2011) is explaining the 3D sensing technique.

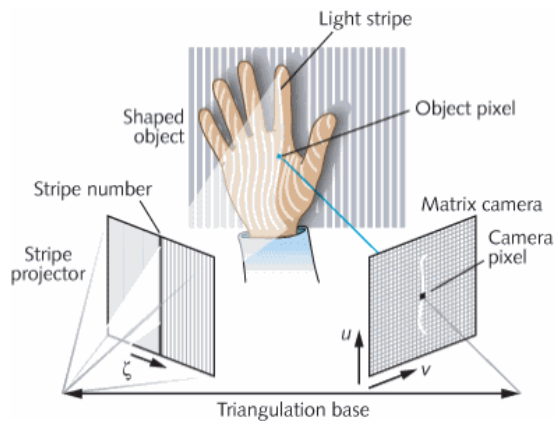


Figure 45. Scheme of 3D scanning with structured light.

Adapted from <https://www.esat.kuleuven.be/psi/research/structured-light>

The proximal sensors generate structured light by using a set of temporally encoded patterns that are sequentially projected onto the scene and acquired by a camera. The depth provided by the technique results in high resolution depth maps of relatively static scenes. An example of this type of sensor can be seen in Figure 46.



Figure 46. Aspect of the Asus Xtion Pro remote sensor (left lens belongs to the IR projector and the right lens corresponds to the IR camera)

The projected encoded pattern uses a binary Gray code shown in Figure 47. This code has the property that only single bit changes at a time, therefore it is used to reduce errors to ± 1 bit (Low Significant Bit) while decoding the captured structured light images acquired by the camera.

Once every pixel is decoded, it is possible to calculate depth of the scene. For example, the column number for each captured pixel (0 = first pixel on left and 480 = last pixel on the right) and the decoded projector column. The depth is calculated by geometrical triangulation. The technique is called depth from disparity.

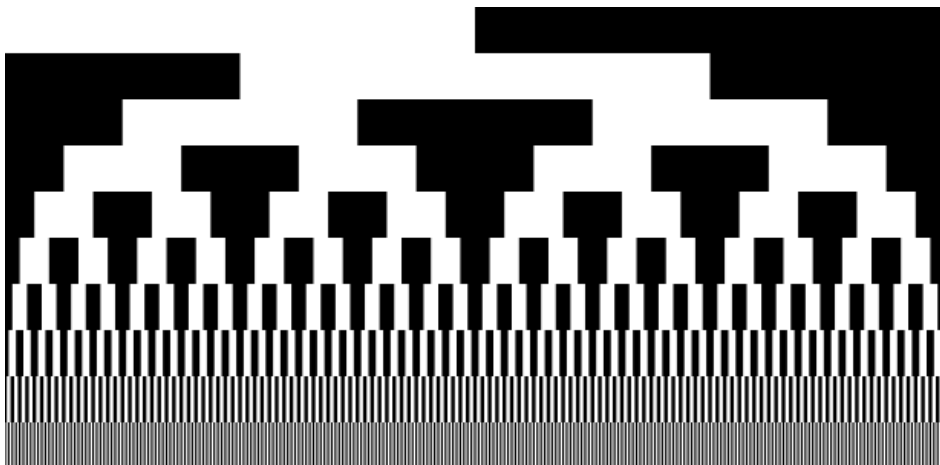


Figure 47. Graphical pattern corresponding to a Gray code of 10 bits (the pattern must be read in vertical scanning lines)

In Figure 48, the box on the left represents the projected set of structured light images and the box on the right represents the captured image. The line running through the middle of the boxes is called a scan line. As the surface moves closer, the reflected light will be captured by pixel further to the left on the imager sensor. The calculation of the disparity (the difference between the two) is performed by subtracting the decoded projector pixel from the corresponding camera pixel. As a consequence, the depth is calculated as inversely proportional to disparity.

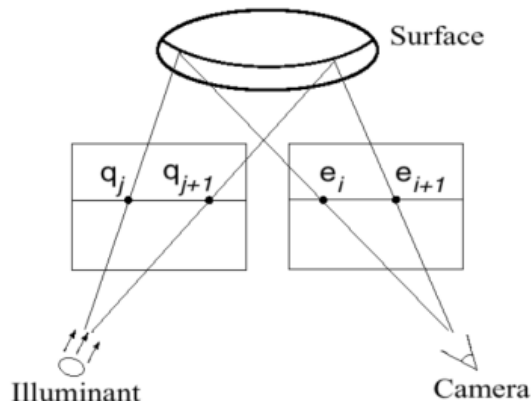


Figure 48. Calculation of depth by disparity measurement

In Figure 49 is depicted how this proximal sensor is scanning the 3D space by projecting a set of Gray binary codes that can be captured for an IR camera.



Figure 49. Infrared picture of the Grey pattern projected on a wall

4.3.3.2. Datamatrix code projection

The technique used by the Kinect sensor (similar sensor to Asus Xtion Pro) is a static spatially encoded pattern projected onto the scene. The pattern belongs to the family of datamatrix (or two-dimensional barcode) codes. The projected code consists of IR light squares arranged in a rectangular grid. The camera reads it and processes the code using Reed–Solomon error correction.

The example of Figure 50 illustrates the set of dots scattered on the scene. The pattern is deformed as it falls onto the objects. The camera then captures an image of the scene and decodes the result. This method calculates a single depth reading to a group of projected pixels (it takes multiple spatially encoded pixels to map back to unique camera pixels). As a result, there is a loss of depth resolution but depth can be calculated with only one capture in all the image, therefore the sensor can handle dynamic scenes (desired characteristic).



Figure 50. Infrared picture of the Kinect sensor scanning part of a room.

4.3.4. Example of recent proximal sensors

4.3.4.1. Real sense SR300

This sensor (Figure 51) uses structured light technology to perform the 3D measurement. These sensors have a MEMS laser projector that creates a coded IR pattern (an 8-bit code for every point in space), and a high speed IR camera that captures the reflected pattern. Based on the displacement of the pattern due to objects in the scene, it can be calculated the distance of the objects from the camera.



Figure 51. Aspect of the SR300 proximal sensor camera based in structured light. Adapted from <https://click.intel.com/realsense.html>

In addition, this sensor contains an additional camera that captures the scene in color (common RGB camera) to fusion depth and visual information (details in Figure 52). Then, the sensor laser-generated 2D spatial patterns, the IR camera is taking pictures of them, and the sensor is calculating the coordinates of the 3D point cloud while doing the matching of the color image and the corresponding depth.

Consequently, the ASIC processes in real-time the depth for each corresponding pixel of the color video streamed. The advantage of this sensor is that it creates an overall texture map in IR, so the sensor can measure texture-less objects.

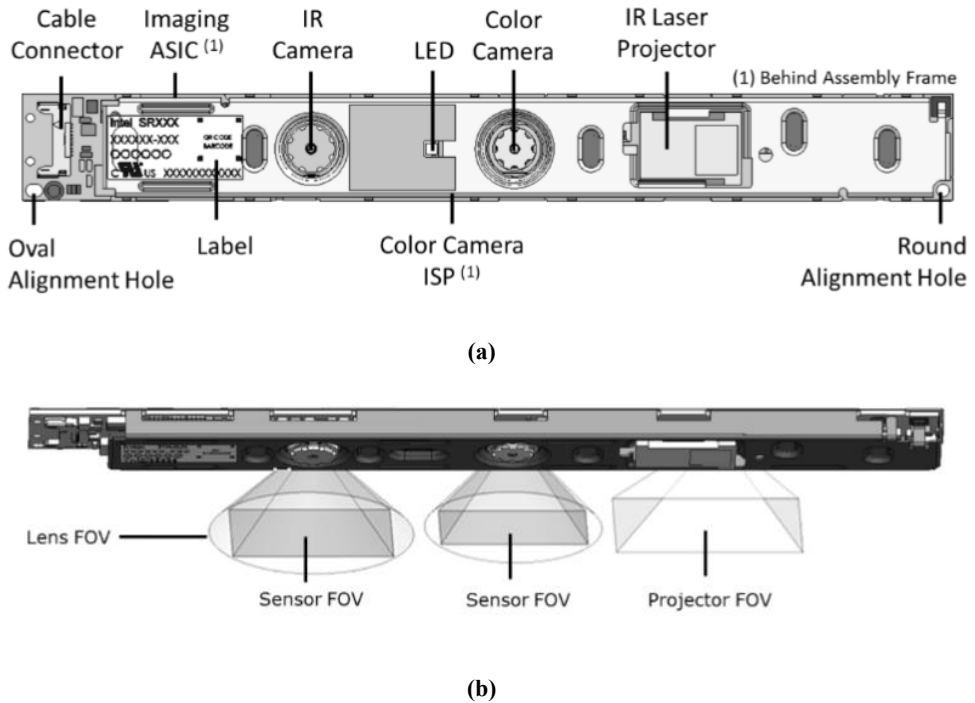


Figure 52. Scheme of main internal component of the SR300. (a) Detail of the position of the ASIC, IR camera, RGB camera and IR laser projector. (b) Scheme of the FoV of each component: IR & Projector (depth measurement), and RGB (color image)

4.3.4.2. Realsense R200 and R400

Another versions of a RealSense camera, shown in Figure 53, differ from the SR300 sensor because they have an additional IR camera for stereo vision. This extends the depth range to outdoors applications.

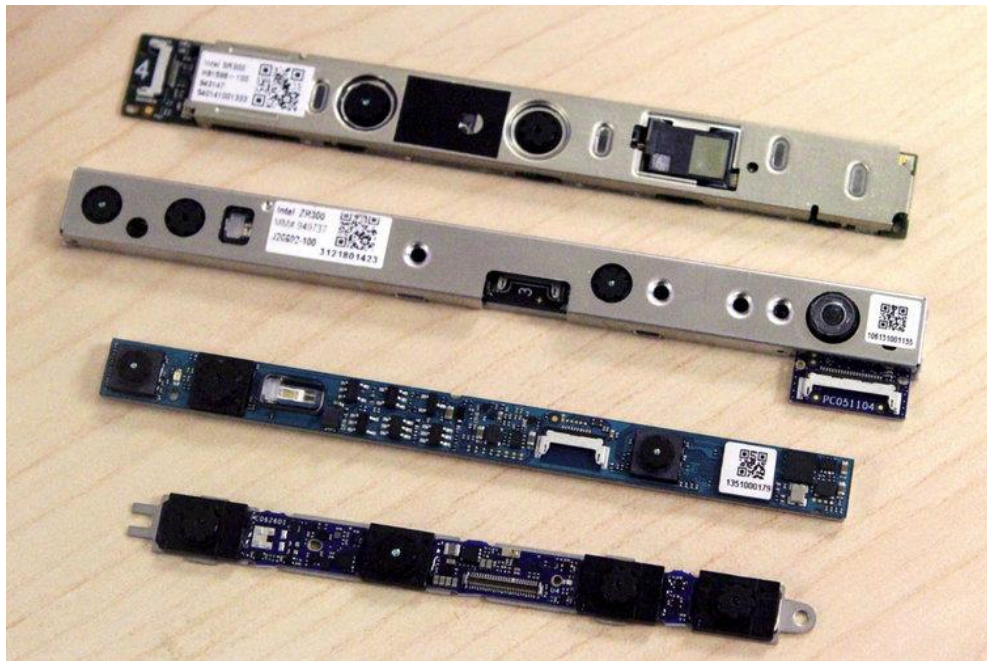


Figure 53. OEM proximal sensor of Intel Realsense portfolio. Adapted from <https://click.intel.com/realsense.html>

4.4. State-of-the-art of high performance computers for perception systems in vehicles

This section is strongly related with the evolution of electronics and consequently the computation capabilities of the chips, providing an indication of the computing capabilities that perception systems can use. The reference of this subject can be expressed by mentioning Moore's law, which predicted more than half century ago a doubling every year in the number of components per integrated circuit looking forward to the next decade. Surprisingly, Moore's prediction proved accurate for several decades in spite of the technological arrival to the limitation in number of transistors of unit of surface due to the increment of the speed of the transistors.

Moore's law is an observation or projection and not a physical or natural law. Although the rate held steady from 1975 until around 2012, and nowadays the technological barriers of size and speed achieved are being tackled due to the implementation of parallel architectures, mainly multiple cores and parallel processors called GPUs (Graphics Processing Unit).

The embedded processors also benefited from this evolution. Nowadays are economically accessible powerful microcontrollers that contain co-processors integrated FPU's (Floating Point Units) which were unthought ten years ago, and nowadays are allowing very intensive real time applications. Other actual view of the embedded processor is the degree of integration between dedicated processors. For example, nowadays it is possible to count which a variety of SoCs (System-on-a-Chip) that concentrates in the same chip reconfigurable analog

and digital processing capabilities, others mix dedicated DSPs (Digital Signal Processors) or powerful FPGAs (Field Programmable Gate Array) with microcontrollers.

The new era in embedded computation is the adoption of software functionalities implemented in hardware. These chips are denominated ASICs (Application Specific Integrated Circuit). The ASICs are meant to perform repetitive tasks that will require intense computation if they were implemented in a software fashion. These kind of chips proliferating with the concept of smart sensor and some big ones were developed for the development of proximal sensing sensors.

Nowadays, there is an intense development of ASICs mainly in two directions. One towards smart cameras (see the section “State-of-the-art of proximal sensors”), for which the integration of some algorithmic capabilities for visual understanding of the scene captured are being incorporated into the camera sensor chip. The second is towards AI (Artificial Intelligence), in which the ASICs are aimed to host certain types of neuronal network layers that can be configured to present certain levels of AI for specific and well defined applications.

The advantage is the low power and small form factor of the embedded device. One of the most recent examples is the ASIC Myriad of Intel that can be obtained also as an USB-stick (neural computer).

4.4.1. First automotive super computer: DRIVE PX

The term super computer is a simplistic way to express that the capacity of perform operations of this particular computer exceeds in more than one or two orders of magnitude a conventional PC (Personal Computer). In the case of the first automotive super computer, it will be as powerful as 150x Macbook Pro’s.

The design comes from an agreement between two big technological manufactures, one belonging to the informatics industry and the other to the automotive industry. NVIDIA and the automotive supplier Bosch. Other automotive suppliers, as ZF, are making agreements with NVIDIA due to their know-how in scientific computation with applications to Artificial Intelligence (AI).

The automotive suppliers as Bosch are also Tier 1 of the motorcycle industry. Independently of the name of the company, a Tier 1 company is the most important member of a supply chain. It is supplying components directly to the OEM (Original Equipment Manufacturer) that set up the chain.

In a typical supply chain, Tier 2 companies supply companies in Tier 1; Tier 3 supplies to Tier 2, and so on. Tiered supply chains are common in industries such as aerospace or automotive manufacturing where the final product consists of many complex components and sub-assemblies that must comply with stringent quality, manufacturing and business standards.

Tier 1 companies are generally the largest or the most technically-capable companies in the supply chain. They have the skills and resources to supply the critical components that OEMs need and they have established processes for managing suppliers in the tiers below them. In motorcycle industry, Tier 1 companies provide a manufacturing service for the OEM, leaving the OEM to concentrate on final assembly or marketing.

From the side of NVIDIA, the informatics company was innovating in parallel computation for more than 20 years and during the last decade built a framework for scientific computation. From this scientific framework the company derivate one for target autonomous driving and it is called NVIDIA DriveWorks. This software framework is only available to

select Automakers, Tier 1 Suppliers, and Research Institutions working on developing systems that enable cars to drive themselves.

The first generation of an automotive super computer is the DRIVE PX. It can achieve until automation level 2 (see Table 10), and two cases are depicted in Figure 54. Is it expected that more Tier 1 companies start to produce the devices and the cost of the technology will start to drop off.

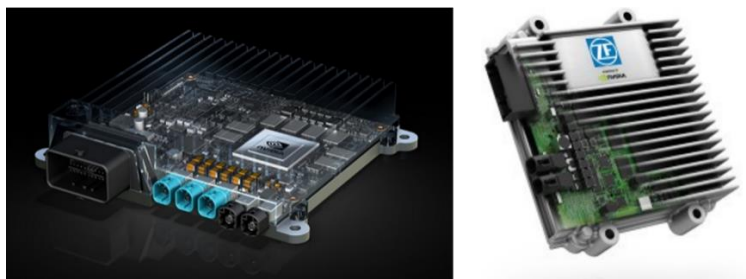


Figure 54. Examples of DRIVE PX automotive super computers. On the left hand is the version of Bosch supplier and on the right side the implementation of ZF

4.4.2. First AI automotive super computer: DRIVE PX2

A computer designed for AI applications is a computer that have a co-processor, which is a specialized processor that acts as a companion of the main processor. The co-processor performs specific tasks and deliver its results to the main processor, acting as an assistant of the main processor. In this way, the main processor can perform other operations until it receive the outcome of specific tasks realized by the co-processor. In the case of NVIDIA hardware solutions the co-processor are GPUs (Graphics Processing Units).

A couple of years ago started the ongoing development of the first AI automotive super, the DRIVE PX2 (Figure 55) of NVIDIA, it will be based on the chip Pascal and will be the first single-chip processor to achieve Level 4 autonomous driving (see Table 10). The DRIVE PX2 is going to be used by cars manufacturers which believe that the solution to self-driving cars will be mostly based in Computer Vision (CV), Depth Neural Networks (DNN), accurate road map datasets, and high level software agents.

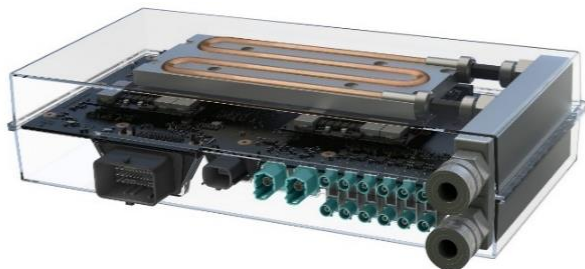


Figure 55. Render of prototype of DRIVE PX2 of NVIDIA. It includes the Pascal processor. Adapted from <https://www.nvidia.com/en-us/self-driving-cars/drive-px/>

To experiment and assess their own technologies, NVIDIA get associated with automakers to build autonomous racecars. The racecars used a demonstrator of DRIVE PX2. This hardware have become the brain of the Roborace cars, which consist of an instrumented race car as is shown in Figure 56.

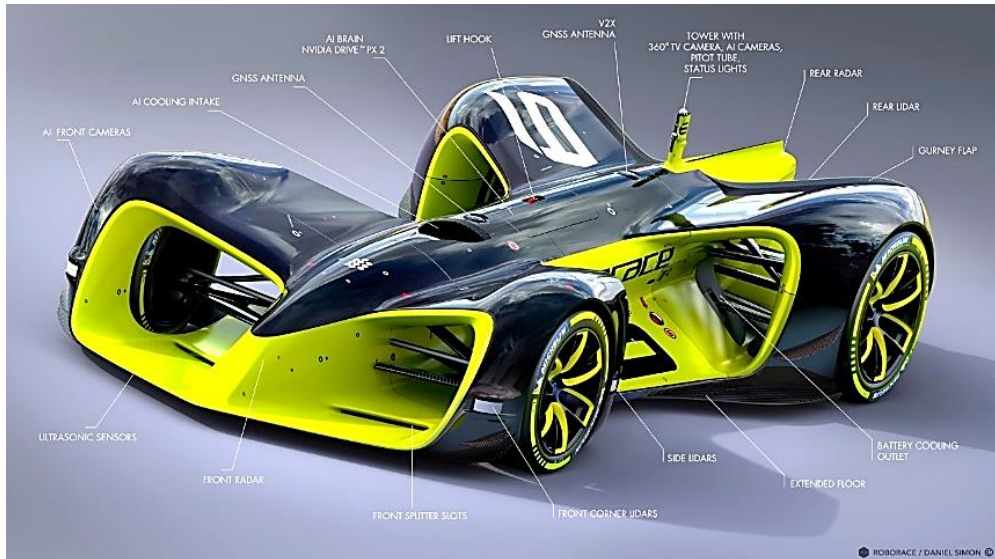


Figure 56. Roborace car with description of its perceptual sensors. Adapted from <https://roborace.com/>

Roborace is meant to be a motorsport championship with autonomously driving, electrically powered vehicles. The series used the same tracks the FIA Formula E Championship uses, and it is the first global championship for driverless cars. All the teams will have the same hardware in the race cars and the only think that the will be able to change is its software.

4.4.2.1. Technical specifications of DRIVE PX2 and its future evolution

The technical specifications of DRIVE PX2 (AutoCruise) are: 12 CPUs, 1 Pascal GPU, 8TFLOPS, 24 DL TOPS, 250 Watts liquid cooled). TFLOPS and DL TOPS are somewhat meaningless terms because they represent theoretical peak performance. NVIDIA provides a separate measurement of performance using AlexNet, an image classification approach using deep convolutional neural networks. They quotes performance of 450 images per second with a Titan X compared to 2,800 images per second on DRIVE PX2. So in this case, NVIDIA shows a single supercomputer DRIVE PX2 delivering more than six times the performance of a single high-end processor (Titan X).

In Figure 57 are shown the three super computers for the automotive industry. The smallest (AutoCruise) is the one in process of industrialization with the Tier 1 companies aforementioned. The board in the middle (AutoChauffeur) is the current platform for

autonomous cars development and only partner companies can have access to it. On the left side, the board (Full Autonomy) is in ongoing development as a more powerful supercomputer.

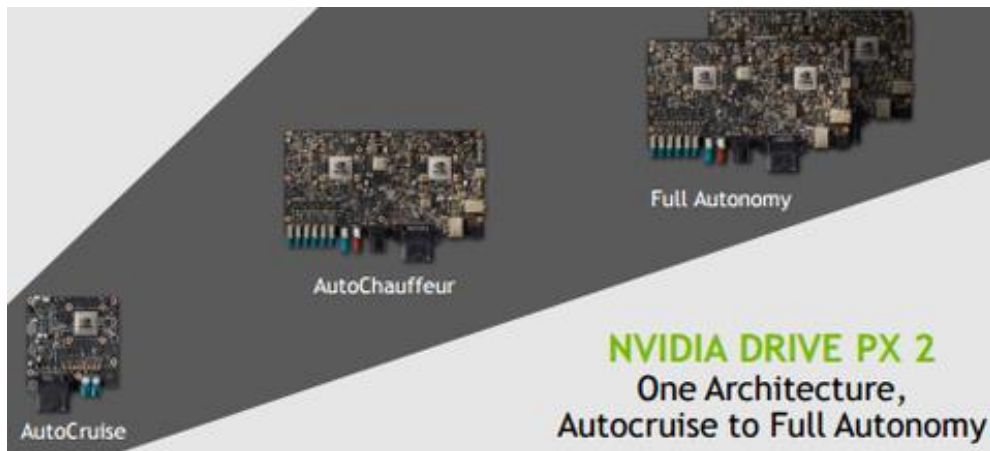


Figure 57. Actual and planned supercomputers for automotive applications. Adapted from <https://www.nvidia.com/en-us/self-driving-cars/drive-px/>

The next generation of supercomputer (left image of Figure 57) will be designed to handle the massive amount of computation required for self-driving tasks, such as running deep neural nets to sense surroundings, understanding the 3-D environment, localizing on a HD map, predicting behavior and positioning of other objects, as well as computing car dynamics and a safe path forward.

4.4.3. Machine vision in autonomous vehicles

This section is a brief explanation of a broad state-of-the-art in artificial perception systems which application to vehicular field. The research is mainly driven with the objective to achieve autonomous cars, so the examples will correspond to this topic.

Linking with the previous sections, the next video provides a full picture of the possibilities of MV (Machine Vision) and CV (Computer Vision).

Three minutes video: <https://www.youtube.com/watch?v=84M3ghUKILk>

4.4.3.1. Machine vision in the motorcycle field

Nowadays there is a lack in machine vision systems and remote sensors in the motorcycle industry. However, the perception technologies in development towards the accomplishment of automation level 3 (see SAE J3016 in Table 10) in autonomous cars, have the potential to be adapted for motorcycle safety.

The level 4 of automation is expected to be achieved commercially in 2020 (agreement between NVIDIA and Audi), but it may happens later. Anyway, it is not necessary to wait until the end of the car automation process to transfer the technology from an industry to the other.

Therefore, today is feasible start to develop safety systems for motorcycles that employ these kind of technologies, and the UNIFI demonstrator that I created is a proof of this.

4.4.3.2. Development kits suitable for motorcycle safety

4.4.3.2.1. NVIDIA Jetson

The NVIDIA Jetson TK1 developer kit (Figure 58) is the starting point to use GPU for embedded systems applications. It is built around the Tegra K1 SoC and uses the NVIDIA Kepler framework for software development. This is a general purpose framework for the development of compute-intensive systems for computer vision, robotics, medicine, and possibly motorcycle safety.



Figure 58. Jetson TK1 developer kit. Note that the main chip need a heatsink with a fan for air cooling which are not present in the picture. Adapted from <http://www.nvidia.it/object/jetson-tk1-embedded-dev-kit-it.html>

Similar development kits that contains the main processor chips in a small credit card format (an AI module) are the NVIDIA Jetson TX1 and TX2 (Figure 59). The key advantage of this development board is that it is relatively simple to install the module in a rugged carrier board and testing applications in harsh environments, such as a motorcycle. The main limitation is the power consumption and the need of a heatsink with fan for air cooling.



Figure 59. NVIDIA Jetson TX2. On the left hand there is the credit card size board with the main processor that can be installed in a rugged hardware. On the right side there is the complete set of boards for development purposes. Adapted from <http://www.nvidia.it/object/jetson-tx1-module-it.html>

4.4.3.2.2. Carrier boards for NVIDIA Jetson

The carrier boards are needed to simplify the process of integration of the AI module in a prototype or short series of final applications. The need of this carrier boards is based in the fact that the signals that need to travel for the circuit are of very high frequency (in the orders of GHz), so the design specification of the PCBs (Printed Circuit Boards) is challenging.

When it comes to PCB layout and routing, high speed application is a multidisciplinary task. High speed PCB layout required to ensure the integrity of signals, which starts to be affected by the physical characteristics of the circuit board, like the layout, packaging, interconnections (bias), etc. Some common problems in high speed PCB layouts are: delays, attenuation, crosstalk, reflections, or electromagnetic emissions. Therefore, to avoid all these tedious problems, the design of the final PCB can be done in a posterior stage of the development.

Next, I explain three of them because they are suitable for the constraints of motorcycle safety application from an electronic point-of-view. In Figure 60 is shown the Astro Carrier. One of the main features is that it has 8 coax video inputs. This may be useful for projects that want to work with several stereo vision systems.



Figure 60. Detail of connections of Astro Carrier of Connect Tech Inc.

In Figure 61 is shown the Orbitty Carrier. This is the cheapest carrier board available of our comparison, but it still has most of the main interfaces like Ethernet, USB 3.0, HDMI, etc. What it is lacking in this board are the CSI (Composite Serial Interface) video inputs, but for the using USB 3.0 cameras that should be no problem.

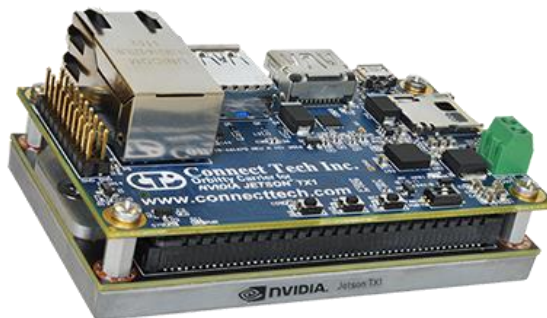


Figure 61. Detail of connections of Orbitty Carrier by Connect Tech Inc.

The most advisable board to start the development in motorcycle application is shown in Figure 62. I recommend this board for its main features, such as four CSI (Composite Serial Interface) video inputs, and two USB 3.0 ports, which allows to connect a lot of digital camera sensors. Most interfaces including USB are routed to custom connectors that require special cables.



Figure 62. Detail of connections of Auvideo carrier board.

4.4.3.2.3. FPGA-based deep learning accelerator

The company DeePhi has produced two separate FPGA (Field Programmable Gate Array) based deep learning accelerator architectures. The first is Aristotle, which is aimed at Convolutional Neural Network (CNN) acceleration. The second is called Descartes, which is directed at sparse LSTM (Long Short Term Memory) deep learning acceleration. These are matched against work that has been done on model compression and “activation quantization” wherein the team found that getting the precision of 8 bits is perfectly reasonable on this architecture.

The problem with existing processing is in the access to DRAM (Dynamic Random Access Memory – capacitance based). Fetching the weights from DRAM can be as much as two orders of magnitude more expensive than an ALU (Arithmetic Logic Unit) operation, and dominates power consumption. A possible solution can be the use of an Efficient Inference Engine (EIE), that maximizes the role of SRAM (Static Random Access Memory – not refresh required) in processing the inference side of neural networks, while on the backend, a new technique (made up of old EIE techniques) called deep compression, packs the nets down to manageable sizes for ultra-rapid and efficient processing (Han et al., 2016).

Using the deep compression techniques, the neural network problem can be fit into on-chip SRAM. EIE then executes the inference across the compressed set with some rather stunning results. For example, a benchmark using nine different deep neural network benchmarking suites, EIE performed inference operations anywhere (depending on the benchmark) between 13x and 189x faster over regular CPU and also GPU implementations, although this is without any compression. As the benchmarks show, the energy efficiency is better by between 3,000X on a GPU and 24,000X on CPU (Han et al., 2015).

The DeePhi hardware (Figure 63) is a first demonstration that there is a more efficient route to real-time inference in a dramatically lower power envelope. The company’s own custom built compiler and architecture is used instead of OpenCL. The algorithm designer doesn’t need to know anything about the underlying hardware. The compilers generates RTL (Register-Transfer Level) code. Deep compression maybe useful in real-world neural networks and can save a great deal in terms of the number of computations and the bandwidth demands.

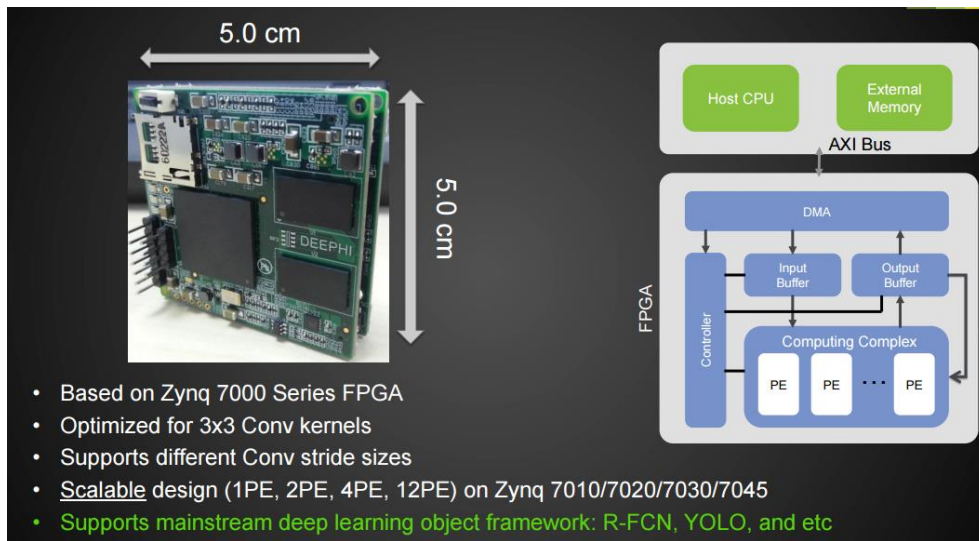


Figure 63. Aristotle architecture, which is designed for CNN acceleration. Adapted from [link](#).

4.4.3.2.4. INTEL: case of Myriad chips

In previous sub-sections I introduced the chips Myriad 2 and Myriad X. In particular, the Intel Movidius Myriad 2 VPU includes 4 Gbit of LPDDR3 DRAM, and its architecture includes specific imaging and vision accelerators and an array of 12 VLIW vector media processors called SHAVE processors. These processors are used to accelerate neural networks by running parts of the neural networks in parallel for achieving the highest performance.

The Intel Movidius NCS (Neural Computer Stick - Figure 44) is connected to an Application Processor (AP), such as a Raspberry Pi, using the USB interface on the Intel Movidius Myriad 2 VPU. The USB3 interface can be used both in USB 3.0 (5 Gbps) or USB2.0 (480 Mbps) modes.

The CPU in the Intel Movidius Myriad 2 VPU is a SPARC microprocessor core that runs custom firmware. When the Intel Movidius Neural Compute Stick is first plugged in, there is no firmware loaded onto it. The Intel Movidius Myriad 2 VPU boots from the internal ROM and connects to the host computer (application processor) as a USB 2.0 device.

Applications executing on the host computer (AP) communicate to the Intel Movidius Myriad VPU SOC using the Neural Compute API (Application Program Interface). When the API initializes and opens a device, the firmware from the Neural Compute SDK (Software Development Kit) is loaded onto the Intel Movidius Neural Compute Stick. At this time, the Intel Movidius NCS resets and now shows up to the host computer as a USB 2.0 or USB 3.0 device depending on the host type. It is now ready to accept the neural network graph files and commands to execute inferences on the graph files.

4.5. Conclusions

Preventive safety systems for motorcycles need to be based on artificial perception systems but these vehicles have serious constraints in terms of power budget. Embedded solution will required specific ASICs to be able of processing big amounts of environmental data in real-time. Different chip solutions were described in this chapter but my recommendation for the PTW application is towards the Intel processor Myraid 2 and Myraid X. The reasons are related to the low power consumption (less than 1.2W), the VPUs (Vision Processing Unit) that acts as co-processors for video processing in real-time and their capability to manage up to three streams of stereo video data simultaneously. This is suitable for the multi focal stereo sensor developed in Chapter 6.

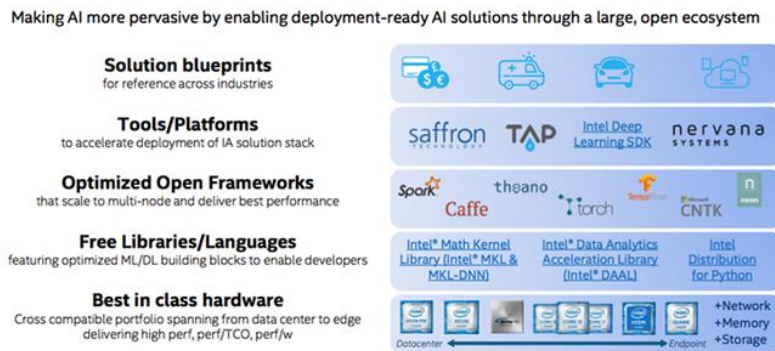


Figure 64. Intel is supporting seven AI software frameworks

From the software development side, Artificial Intelligence applications can be implemented with a lot of development frameworks. The current frameworks to develop Artificial Intelligence applications are 7 (Figure 64). However, for the utilization of Myraid processors only 2 frameworks are supported by the chip manufacturer. The frameworks accepted are: Tensor Flow, and Caffe 2. Therefore these two are the only suggested for the implementation of preventive safety systems for motorcycles.

5. Is it possible to apply ARAS on motorcycles?

This chapter is dedicated to analyze the difficulties encountered for the automotive perception systems when they are subjected to motorcycle dynamics. The reason is simple, these systems stay out of specifications when they are applied to a two-wheeler dynamics. The fact that they were designed bearing in mind a different ego dynamics, which makes the systems fails in physical and algorithmic terms. An analysis of the three main technologies (RADAR, LIDAR, and Machine Vision) highlight the main limitations encountered for these sensors. After that, a possible ways to deal with the limitations is explained.

5.1. Motivation of a 3D perception system for motorcycles

Smart vehicles need to be able to interpret and predict the immediate future location of other vehicles and road users in the context of advanced safety systems and autonomous driving. The remote estimation of car pose and in particular its heading angle is key to predict its future location. This chapter explains why automotive remote sensors are not currently used in vehicles that present a tilting dynamics behavior. The technical reasons of the safety gap, which motivates the absence of rider assistance technologies in tilting vehicles, are overcome by a proposed remote sensor camera-based solution.

Stereo vision systems allows to get the 3D information of a scene from a couple of 2D sensed projections of the same scene. The ground truth in this specific context is associated with referential information about the depth, shape and orientation of the objects present in the traffic scene. The creation of a 3D ground truth to validate the 3D information obtained from the stereo vision sensor is a complex measurement and data fusion task. The ground truth of a road scene in real traffic is generally obtained by the combination of different remote sensors. Conveniently, camera-based sensors can use a satellite marker to generate ground truth car pose in a post processing stage. This technique enable the quantitative evaluation of machine vision solutions.

5.2. Motorcycle safety needs

In motorcycle several terms and acronyms are commonly used to identify sets of vehicles with given legal requirement or features associated with their dynamics behavior. For example, single-track vehicle, Powered Two-Wheeler (PTW), and Narrow Track Tilting Vehicle (NTTV) among others. This section use two expressions: motorcycles and tilting vehicles. The term “motorcycle” will refer to pedelecs (electric bicycles), mofas, moped, scooters and motorcycles, while “tilting vehicle” will add to “motorcycle” three- and four-wheeler vehicles characterized by tilting dynamics behavior. Another preliminary consideration deals with the expression “advanced safety systems”. In the car industry these are called Advanced Driver Assistance Systems (ADAS), whereas the motorcycle industry they are called Advanced Rider Assistance Systems (ARAS).

In the first part of this dissertation was analyzed a large traffic accident dataset (ISTAT, National crash database in Italy, period 2000-2012, >1,000,000 motorcycle crashes) to developing the KBMS methodology, which estimate the effectiveness of safety systems for motorcycles. Part of the crash data is summarized in Figure 65. One outcome of the data analysis is the fact that most of the motorcycle crashes occurred in clear visibility conditions. Therefore, ARAS can contribute to protect motorcycle riders without the need to operate in difficult visibility conditions, such us rainy, foggy, and snowy conditions.

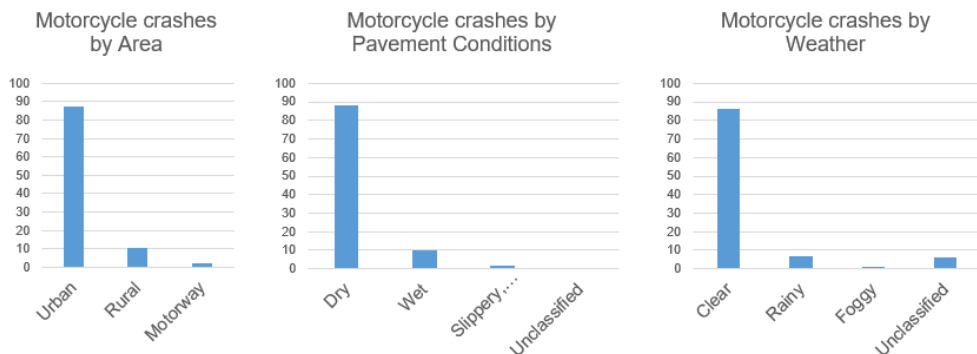


Figure 65. Circumstances of motorcycle crashes in Italy, more than 2 crashes every 15 minutes (percentages for the period 2000-2012). The left chart indicate where the crashes happened, totalizing more than 87% in urban areas. The center chart indicate the pavement conditions at the moment of the crashes, resulting in more than 88% over a dry street. The right cart present the weather at the moment of the crashes, indicating that more than 86% of the crashes occurred in clear visibility conditions

For a more up-to-date insight, it was necessary to focus in the last three years of data (2010-2012), which comprise more than 200,000 motorcycle crashes. I used these information and the classification of crash scenarios of the Knowledge-Based system of Motorcycle Safety (Appendix B) to create Table 11. This table make explicit that more than 70% of motorcycle crashes in Italy took place from ahead of the motorcycles. Therefore, installing in the frontal part of motorcycles an artificial perception system for ARAS, presents a great potential.

This finding justified our analysis of automotive remote sensing technologies employed for ADAS, in the perspective of possible applications to motorcycles and tilting vehicles. However, ADAS sensors would fail on tilting vehicles due to the large roll angles reached by the motorcycle, even in normal riding conditions, thus motivating the new approach “stixel world” based on stereo vision (introduced in Chapter 4).

Scenario	Description	Crashes	Crash from ahead of the motorcycle
A	Intersection and angle collision	24.80%	Yes
H	Straight street and angle collision	12.16%	Yes
F	Rear-end collision	11.41%	Yes
C	Straight street and sideswipe collision	8.91%	Yes
B	Intersection and sideswipe collision	7.66%	Sometimes
D	Single-vehicle accident	7.35%	Sometimes
G	Hit obstacle + hit pedestrian	7.16%	Yes
E	Head-on collision	6.47%	Yes
I	Roundabout	4.67%	Sometimes
Z	Unclassified	9.41%	Unknown

Table 11. Overview of motorcycle crash scenarios in Italy (period 2010-2012)

5.3. Automotive remote sensing

Remote sensing sensors provide the inputs for artificial perception systems. Typically, camera sensors are reliable to identify objects or targets to look at, RADAR sensors provide targets velocities, and LIDAR sensors measures distance to targets. Nowadays, cutting edge RADAR and LIDAR measurement techniques can provide estimations of the other target information’s (target identification, velocity and distance) with a single sensor device. On the other hand, machine vision has allowed it from more than a decade ago but with limitations of robustness and accuracy.

These automotive technologies provide smart vehicles with information about their surroundings, e.g. to monitor safety gaps between vehicles or to detect imminent collisions and react consequently. Examples are in the form of warnings, to early alert the car driver about an action to be executed, or performing automatic actions even without human intervention, such as maintaining the vehicle position in the lane or executing an emergency stop.

Automotive remote sensing is based on powerful remote sensing technologies employed in earth observation from satellites, aeronautics and military applications. However, the high cost of these technologies do not allow for a massive adoption in vehicles to accomplish the safety tasks. This economic constraint originates a de facto standard of the automotive industry, in which safety devices must cost less than 100\$ mass-produced to be considered for adoption. Manufacturers were forced to tailor remote sensing technologies to accomplish the minimal needs of the automotive application. The microelectronics industry benefited for being the only known way to manufacture such sophisticated sensor systems in an economical way. Different directions for development, such as MEMS (Microelectromechanical Systems), photonic and radio integrated circuits, have recently gained importance. Thus, novel technologies, such as MEMS mirrors, OPA (Optical Phased

Arrays), SiGe (Silicon Germanium), RF SOI (Radio Frequency Silicon-On-Insulator), and dielectric lens antennas, became affordable for automotive safety application.

Nowadays, the tailored remote sensors for the automotive industry have achieved a great maturity level, thanks to the progress in microelectronics and creative remote sensor design. As expected, the high degree of tailoring of a sensor to fit in a specific application makes the sensor less flexible to be used in a different application. Therefore, the following analysis aims to assess whether these tailored sensors can operate properly under a vehicle dynamic (tilting dynamics) they were not specifically designed for.

5.3.1. Automotive RADAR technology

RADAR (RADio Detection And Ranging) is an object-detection system that uses radio waves to determine the distance (range) and the velocity of objects. For automotive applications in ADAS, two types of RADAR are available: Short-Range RADAR (SRR) and Long-Range RADAR (LRR). These are tailored to perform specific tasks. For example, SRRs handle the requirements of Blind-Spot Detection (BSD), Lane-Change Assist (LCA) and front/rear cross-traffic alert, whereas LRRs are responsible for Adaptive Cruise Control (ACC) and Autonomous Emergency Braking (AEB).

Advanced safety functions demand for accurate 3D object discrimination in short and long range, that in RADAR terms translates in large Bandwidth (B). The European Union has defined the spectrum band of 79GHz (77-81GHz = 4GHz) as the most suitable for long term and permanent deployment of high resolution automotive radars (Verheugen, 2005). The 79GHz band offers significant benefits in terms of low power consumption, leading to a lower risk of mutual interference because of the smaller emission power required (Schneider, 2005), and lower the electromagnetics pollution in contexts of market saturation.

Experiments are quite common in the radar field because the variety of the reflections provided by real targets in uncontrolled environments is very challenging to predict. The energy that is reflected back from the targets to the radar can be influenced for several factors, such as the material of the target, its size, or the incident angle among others. The radar metrics of detectability of an object is denominated Radar Cross-Section (RCS). In general terms, a large RCS indicates that this target is easily detectable from the radar and it allows to look for radar signatures associated to specific types of targets.

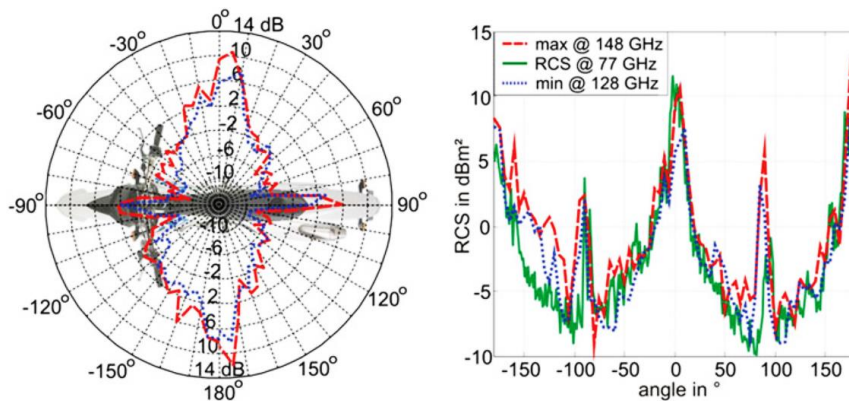


Figure 66. Radar Cross-Section of a motorcycle. Adapted from (Köhler et al., 2013)

Europe has carried out an extended measurement campaign to identify the RCS of pedestrians (Fortuny-Guasch et al., 2013) aiming to ensure that pedestrians can be seen by automotive radars, for the purposes of improved safety for vulnerable road users. Figure 66 shows an example of the RCS of a motorcycle (Köhler et al., 2013). The radar signal for the band of 79GHz (77-81GHz) is depicted in green, being the weakest of the three bands analyzed. These measurements show that the motorcycle returns a strong echo to the radar when it is placed with perfectly perpendicular alignment (0° and 180°). On the contrary, for different alignments the strength decrease considerably. For example, at 15° the signal is 10 times weaker with respect to the maximum signal received from the motorcycle, and it falls down to 40 times weaker for other orientations. Concerning the radar conspicuity problem, it can be seen the poor visibility of the target in the measures realized to the front (between -50° and -130°) and rear (between 50° and 130°) side of the motorcycle.

Valuable insights about the possibilities in terms of 3D discrimination by automotive radars in the 79GHz band were obtained experimentally. Experiments conducted from a static radar setup to static cars located 10m away (Andres et al., 2012), helped to define the maximum capabilities of the system in terms of discrimination from direct measurements. Recent experiments also realized from a static setup (Kellner et al., 2016) achieved the tracking of a single moving car target turning 20 m away by combining the information measured with a math model which described the movement of a vehicle with Ackermann kinematics on a planar surface. This possibility to couple mathematical models with the sensor received data, which is a common practice in automotive 3D machine vision (Barth et al., 2009; Barth and Franke, 2008), have a great potential to enhance radar data interpretation.

Other way to interpret the data received from a radar sensor for dynamic scenarios can come from the use of a cognitive processing approach. The early stage of this discipline called cognitive radar (Haykin, 2006) is growing in the research community and its practical applications are being discussed (Ender and Brüggewirth, 2015; Haykin, 2014).

Regarding the physical aspects of the automotive radar sensors, in order to attain an adequate 3D discrimination for vehicular safety while maintaining low production costs, each part of the system must attain certain technical considerations. Up-to-date examples for the main constitutive elements of the radar are:

- The radio frequency front end and the antenna feeders (Hasch et al., 2011, 2012; Ku et al., 2014)
- The types of folded reflectarray antennas (Bildik et al., 2015; Dieter et al., 2011; Menzel and Kessler, 2009)
- The appropriate packaging technology and dielectric lenses (Baur et al., 2011; Mayer et al., 2009)

As a result of the aforementioned developments, nowadays automotive radars are able to measure independent the distance (range) and velocity (Doppler's principle) to objects in one measuring cycle thanks to FMCW (Frequency Modulated Continuous Wave). The different brands of automotive radars offer products with very similar specifications because they are tailored for the same specific application. In Figure 67, part of the specifications of a high-end commercial automotive radar (ARS 408-21 of Continental) are presented.

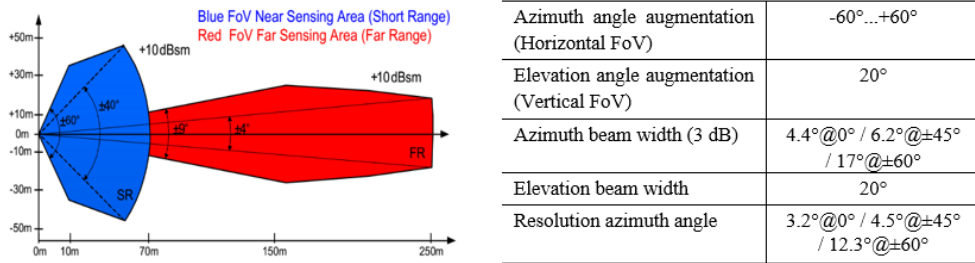


Figure 67. Top view of the 3D scanning volume of a commercial automotive radar and relevant specifications corresponding to the short range. Adapted from the technical datasheet of the ARS 408-21 Continental radar

The information provide corresponds to the short range (blue section of the diagram). I focus on this part of the specification because the near field (up to 70 m) is the most relevant to sense in urban scenarios. In addition, the short range present a wider FoV allowing to cover more volume ahead of the vehicle with a single sensor. In the azimuth beam width specification are defined three different sizes for beam a 0°, ±45°, and ±60°. This is an expected consequence of the electronically steering beam technique, in fact, the radiation lobe of the antenna is constantly changing its 3D shape when it is moving. Therefore, the resolution and discrimination capability of the radar is variable according to the orientation of the measure. As it can be seen from the top view diagram (Figure 67) and the specification corresponding to resolution azimuth angle, the possibilities to sense targets about ±60° from the central radar reference is poor, about half range in terms of depth (less than 35 m). Additionally, as the beam size changed the resolution in this orientation is almost 4 times less that a 0° (resolution azimuth angle 12.3°).

The scale drawings of Figure 68 intends to express visually the consequences of the prior statements. In the figures are depicted how the beam footprint (the transversal area of the beam impacting on the target) change for the three different angles specified in the technical datasheet (±45°, 0°, and ±60°). The left figure is representing a car located 7 m away from the radar and how the beam footprint change with respect to the orientation of the scanning. In the central and right pictures the same car is located a 14 m. In them almost half part of the beam energy is passing over the car (energy not used for the detection). In them also is noticeable the coarse horizontal resolution of the 3D space at only 14 m of distance.

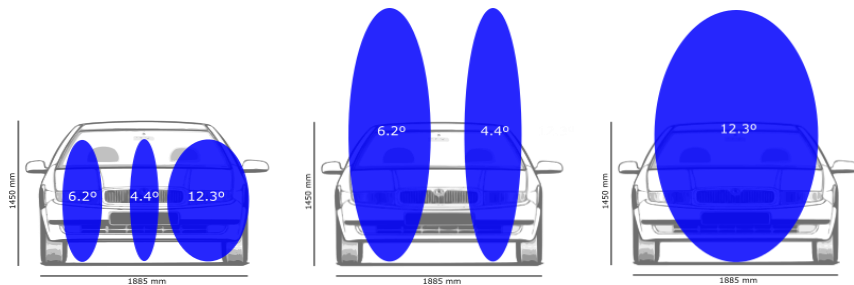


Figure 68. Representations in scale of the size of the beam impacting on a generic car. The numbers in degrees correspond to the three azimuth beam width. In the left diagram the car is located 7 m away from the radar, while in the other diagrams the car is 14 m away

5.3.2. Feasibility of automotive RADAR sensors for motorcycle safety

In the RCS depicted in Figure 66, it was highlighted the difficulty for radars in the band of 79GHz to identify objects as motorcycles. The motorcycle geometry and main constitutive materials scatter the energy of the radar in multiple directions causing a weak returning echo. This can be seen in the radar measurements for the angles different to 0° and 180°. Therefore, vehicles cannot rely on radar information for the identification of motorcyclist.

The use of automotive radars for the implementation of advanced safety systems for motorcycles (denominated ARAS) does not seem to be a viable choice. From the interpretation of the technical specification of high-end commercial radars for the car industry (Figure 67), it was highlighted that the size of the scanning beam become considerably wider at 14 m. Therefore, in order to be able to scan ahead of the motorcycle with enough discrimination in a wide FoV (close to 180°) is necessary the use of at least two radars. In terms of mass and dimension of the sensor the installation of two or three sensors in the front of the motorcycle will not compromise this dynamics. However, this will increase the cost of the sensing strategy and duplicate or triplicate the power consumption (being 13.2 W or 19.8 W respectively). The power budget of a motorcycle is considerable lower with respect to a car.

Nevertheless, the major impediment for the use of an automotive radar in a motorcycle is the non-compliance with the upright assumption (Figure 69). Automotive radars are tailored considering that the reference coordinate system of the sensor have a fix alignment with the vertical gravity component. This consideration define the 3D space to scan, and consequently all the hardware and the software to accomplish the measurement of this 3D space. In a tilting vehicle, simple change lanes and traffic filtering requires roll angles up to ±10°. To taking curves this vehicles may achieve up to ±26° of roll angle in urban environment. As illustrated in Figure 69, the directivity of the radar beam was designed to provide horizontal discrimination (resolution) that in a non-upright position of the host motorcycle is seriously affected.

On the right side of Figure 69 it can be seen how the radar measures away of the road plane. This reduce the net energy which will impact on the possible targets and produce weaker echoes. On the left side the situation is even worse because two unwanted effects occurs leading to a possible radar blindness. One, the reduction of the net energy that hits the possible targets. Second, the drastic increment of the radar clutter which are unwanted echoes measured due to the strong reflections occasioned from the street. The intensity of this echoes will generally occlude the real echoes leading to the condition of radar blinded.

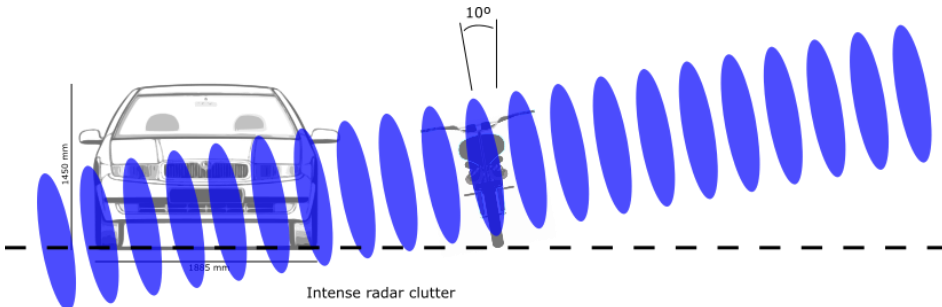


Figure 69. Example of an ideal radar scanning 7 m ahead when the motorcycle is tilted only 10 degrees. The increment of the clutter (unwanted echoes) coupled with the reduction of the surface radiated by the car can lead to radar blind

5.3.3. Automotive LIDAR technology

A LIDAR (Light Detection and Ranging) system is based on the time-of-flight (TOF) method. Our analysis focus on the ibeo LUX automotive laser scanner (Figure 70) due to its broad use in the automotive industry and its possible incorporation to motorcycles. Nowadays, research in photonics and microelectronics towards the Optical Phased Arrays (Abediai and Hashemi, 2015; Heck, 2017; Kwong et al., 2014; Weihua Guo et al., 2013) technology, is enabling new capabilities for LIDAR sensors, but at this moment it is a technology in development.

The technical manual of the ibeo LUX sensor explain the principle of measurement, which consist in slicing the 3D volume in front of the sensor in a set of stacked horizontal planes (4 or 8 planes depending of the model). In this way the depth of the environment sensed is represented by simple two-dimensional representations and the remaining tridimensional space which is not traversed by the planes is ignored.

When the sensor is working in nominal conditions, it is expected similar (redundant) measures in all planes for short distances up to 14 m because these horizontal planes are almost parallel between them. A slight inclination between the planes allow to compensate changes in the coordinate reference system of the sensor when the vehicle is braking (the front of the car tilt downwards). Thus, the sudden change in the pitch angle of the car is compensated by the wise selection of a superior scanning plane, avoiding LIDAR blindness (to sense the floor). For simplicity, our analysis considered a single beam corresponding to a single plane.



Multi echo	Up to 3 distance measurements by laser pulse
Horizontal FoV	110° whit overlapping planes
Angular resolution & Scanning frequency	0.125°@12.5Hz / 0.25°@12.5Hz / 0.25°@25Hz / 0.5°@50Hz
Depth resolution	40 mm ± 100 mm (1 sigma)
Horizontal & vertical beam divergence	0.08° & 0.8°

Figure 70. Aspect of the automotive LIDAR and its relevant specifications. Adapted from the technical datasheet of ibeo LUX.

In Figure 70 is presented part of the specification of a high-end automotive laser scanner of ibeo. Concerning to the laser beam that produce scanning planes, from the horizontal (0.08°) and vertical (0.8°) beam divergence it can be intuited that the laser is operating in a high transverse electromagnetic (TEM) mode. As a result, the laser footprint (the transversal area of the beam impacting on the target) cannot be described as circular dot. The laser footprint is better described as a thin rectangle or line because it was engineered to provide high horizontal discrimination. The horizontal discrimination can be interpreted by the specification of the angular resolution (0.125°, 0.25°, and 0.5°) which change according different scanning speeds. In other words, the laser beam was tailored for the automotive application.

The scale drawings of Figure 71 intends to express visually the prior statements, showing the rectangular footprints of the LIDAR for the automotive industry. The numbers over the laser footprints represent the distance between the target car and the LIDAR (from 7 m to 57 m) and consequently, the laser footprint grows due to the beam divergence. The dashed lines sounding the laser footprints represent the movement of the laser over the car surface when the sensor is under a hypothetical vibration that causes angular deviations about $\pm 0.05^\circ$.

The right part of the picture show the car from the side. When the car 57 m away from the sensor a single laser pulse is able to sense different parts of the car, denominated in the example from P1 to P5.

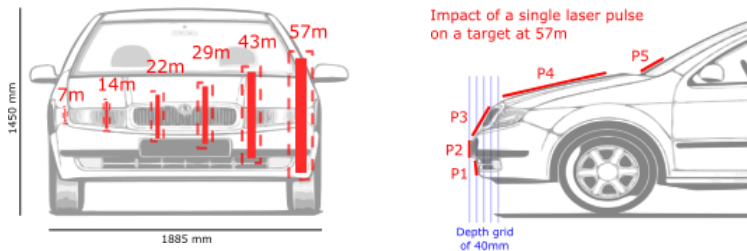


Figure 71. Representations in scale of the size of the beam impacting on a generic car. On the left picture, the numbers above of the laser footprints represent the distance to the laser scanner. For example, the rectangle below the number 43 have the size of the impacting laser footprint on a car 43 m away. On the right picture, the multi echo effect is depicted for a target car at 57 m from the laser scanner

5.3.4. Feasibility of automotive LIDAR sensors for motorcycle safety

In the technical specification there is indicate the number of bounces back allowed for a single laser pulse by the term multi echo. This feature is related with the TOF measurement principle, therefore the sensor will not be able to measure if the target impacted generates more than 3 bounces for the same laser pulse. In the cases of more than 3 bounces the LIDAR get blind.

Brief analysis of the case depicted in Figure 71: the car is 57 m away from the laser scanner and due to the beam divergence the laser footprint impact in several parts of the frontal part of the car. The impacts are described in 5 parts corresponding to the same laser pulse. As the depth resolution of the laser is $40\text{ mm} \pm 10\text{ mm}$, the impact in different parts of the car present different depths for the same pulse. The parts P1 and P2 presents one bounce each, while the part P3 present two or three bounces and the parts P4 and P5 also present different pulses. Therefore, the car is invisible for the automotive LIDAR at this 57 m of distance even if the laser beams have a maximum range specified at 200 m. This undesired effect that shorten the range of detection was reported in a previous experiment that involved 140 tests (Savino et al., 2012a). The automotive laser scanner installed in a scooter, which traveled in an upright position towards the target (three foam boxes, each one with a hole on it), started to detect the obstacle from distances about 58.3 m (sd. 14.5 m).

Nevertheless, the major impediment for the use of an automotive LIDAR in a motorcycle is the non-compliance with the upright assumption (Figure 72). Automotive LIDARs are tailored considering that the reference coordinate system of the sensor have a fix alignment with the vertical gravity component. This consideration define the 3D space to scan, and consequently all the hardware and the software to accomplish the measurement. In a tilting vehicle, simple change lanes and traffic filtering requires roll angles up to $\pm 10^\circ$. To taking curves this vehicles regularly achieve up to $\pm 26^\circ$ of roll angle in urban environment.

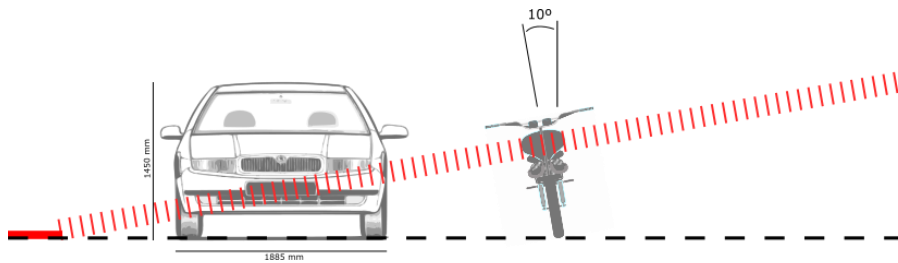


Figure 72. Example of an ideal LIDAR scanning 14 m ahead when the motorcycle is tilted only 10 degrees. Several condition in this case lead to the no visibility of sounding targets. On the right side part of the scanning plane will not intersect possible targets, while on the left side part of the scanning plane will impact on the floor

5.3.5. Automotive Machine Vision technology

Machine Vision (MV) is the ability of a computer to see. It can employ one or more video cameras that can be of different types. MV involves a large number of technologies, software and hardware elements to perform the processing, and involves the Computer Vision (CV) discipline. In particular, CV deals with algorithms for gaining high-level understanding from digital images or videos. Some of these algorithms seeking to automate tasks that the human visual system can do in terms of 3D perception and understanding.

Automotive Machine Vision concerns to the real-time application of MV in road vehicles, which is currently booming due to the development of autonomous cars. For the M-AEB (Motorcycle Autonomous Emergency Braking) application, it is interesting in to identify possible automotive MV systems that can be used as a remote sensor for the development of ARAS. Our focus is CV algorithms for 3D perception and road traffic understanding that only use of camera sensor information. In this way, the strength of stereo vision techniques relies on that heavy dense calculation of the disparity map is a pixelwise operation that can be achieved by hardware in real-time (Gehrig et al., 2009). Thus, the visual and depth information can be given to a high performance embedded system to implement an Obstacle Detector (OD) system.

Most of OD algorithms needs certain assumptions about the ground in the image, such the ground is parallel to the orientation of the camera (Hu and Uchimura, 2005; Kubota et al., 2007; Xia et al., 2014), or planar ahead of the vehicle (Suganuma et al., 2008; Suganuma and Fujiwara, 2007a; Zhang et al., 1997). An example is presented in Figure 73.

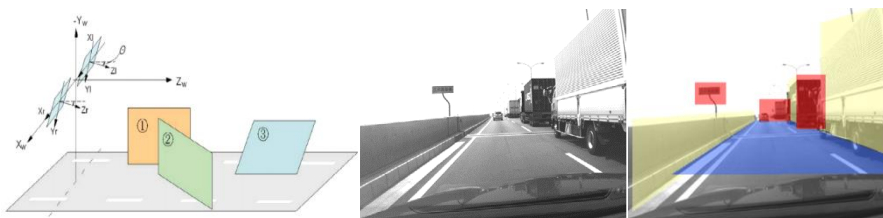


Figure 73. Representation of the stereo camera and the different 3D plane projections of the traffic scene using the “U-V-Disparity” concept. On the right image is overlaid the identification of the street and other big surfaces. Adapted from Hu and Uchimura, 2005

Strategies for non-planar roads (Suganuma et al., 2008) relies on the importance of the physical camera setup and calibrate the system in order to use less software transformations to rectify the images (Broggi et al., 2006; Sergiu Nedevschi et al., 2004; S. Nedevschi et al., 2004), saving computation. Other approaches, instead to localize the road attempt for approximate free space in the 3D volume. The free space is expected to be over the road (Badino et al., 2007; Broggi et al., 2013a; Oniga and Nedevschi, 2010).

A recent review of the most evolved OD approaches for the car application, (Bernini et al., 2014) analyzed and categorized the approaches in four categories:

- a) Probabilistic occupancy grids
- b) Digital elevation map
- c) Scene flow segmentation
- d) Geometry-based cluster

Most of these approaches proved to be: deterministic (important for real-time), possible to implement high performance embedded computers, and robust in a variety of clear visibility conditions at very different hours of the day. The “stixel” concept (Benenson et al., 2011) is presented in Figure 74, next to the “stixel” world (Badino et al., 2006, 2009) as example of mature OD system.



Figure 74. Left: conceptual representation of the stixel world. Center: the Disparity Map of the stereo vision system as interpretation of the depth of the traffic scene. Right: the stixel representation of the different obstacles. Adapted from Benenson 2011 and Badino 2009

Low light and nighttime situations requires totally different algorithms, because the performance of ordinary CV algorithms is seriously affected. Vehicle front and rear lights are often the only characteristics used to detect vehicles at nighttime, but they suffer from distraction of shops lights and other bright regions.

5.3.6. Feasibility of Automotive Machine Vision for motorcycle safety

Cameras, differ from RADAR and LIDAR sensors in cost, size, power consumption, and FoV (Field of View). The imaging sensor can have wide horizontal and vertical FoV, providing enough information of the environment even with large roll angles ($\pm 30^\circ$). Camera-based driver assistance was intensively developed in the 1990s and nowadays are standard ADAS in several vehicles. Thanks the advances in algorithm developments, today is possible to combine the depth information of the stereo vision system and visual data allowing distance and velocity estimation at pixel level.

Nevertheless, most of these approaches contain algorithms that requires certain alignment between the camera sensors and the 3D space to sense, due to the upright assumption inherited from ADAS. Therefore, to cope with the tilting dynamics is necessary adapting existing algorithms or develop new ones that accomplish the same thing.

In our informed view, with nowadays automotive remote sensor technologies, camera-based sensors is the only feasible solution for tilting vehicles. The reasons are mainly:

- a) The tilting dynamics
- b) The constrained space and power budget available in this vehicles to install sensors and safety systems
- c) The cost of the entire safety solution that may not impact drastically in the final price of affordable tilting vehicles

This chapter mentioned several promising state-of-the-art solutions that are include machine-learning techniques. These technics requires an intensive computational power that consumes significant amounts of energy that will not be available in a tilting vehicles. Fortunately, recent embedded neural computers designed in a single chip (ASIC: Application-Specific Integrated Circuit), provide the capability to deploy certain Deep Neural Networks (DNNs) which a power consumption inferior to 1.2 watts.

Other relevant aspect is that these ASICs have a Vision Processing Unit (VPU) to process camera data in real-time. This is important because all the algorithms used in this chapter can be implemented in VPUs. These new chips and the upcoming improvements in camera sensors are promising technologies to make remote sensors camera-based, such as the one developed in this research for motorcycle safety application.

6. Can stereo vision be used as a remote sensing approach?

This chapter presents the development of the camera-based remote sensor that is aimed to solve the technological safety gap that produces the lack of ADAS for motorcycles or ARAS (Advanced Rider Assistance Systems). It also includes the considerations for the design of this type of sensors, its calibration and algorithms.

Automotive remote sensors are the cornerstone of current ADAS. As explained in Chapter 5, the roll angle fluctuations characterizing the dynamics of motorcycles and tilting vehicles (even when vehicles travelling straight) prevents the correct operation of the sensors. For this reason, my design is based on cameras that present a large FoV (Field of View) and important spatial resolution in all different directions.

A multifocal stereo vision was conceived to cover different regions of interest simultaneously, and to guarantee adequate depth accuracy, as a requirement to be part of future ADAS for motorcycles. The importance of this approach is to allow the use of artificial vision methods developed for ADAS in motorcycle safety. Consequently, this is a way to capitalize on relevant cutting-edge algorithms created for ADAS during the last 20 years and speed-up the development of needed motorcycle safety systems (ARAS) to make motorcycles and mopeds a safer means of transport.

In particular, these stereo vision algorithms for vehicular application are successful in the following tasks: separating objects and surface structures by fast features extraction (Franke and Kutzbach, 1996); estimating the ground plane and perform a partial 3D reconstruction above it (Zhang et al., 1997); estimating the vertical road profile from the lateral projection of the 3D point cloud and model it as a clothoid (Sergiu Nedeveschi et al., 2004); classify surfaces on the road scene by the U-V Disparity concept (Hu and Uchimura, 2005); performing obstacle detection in unstructured environment (Broggi et al., 2005, 2006); fusing stereo and optical flow to improve depth estimation accuracy, enabling fast detection of moving targets without classification processing (Franke et al., 2005); modeling the scene by a polar occupancy grid (Badino et al., 2007); generating a disparity map without perspective, simpler to analyze (Suganuma et al., 2008; Suganuma and Fujiwara, 2007b); matching the motion of a rigid point cloud with the kinematic model of a car with a tracker filter, allowing to predict its immediate future location (Barth and Franke, 2008); defining a 3D perception primitive called “stixel” to capitalize on the depth information of almost all pixels of the image (Badino et al., 2009); using dense disparity maps to create digital elevation maps useful to detect important hazards for motorcyclist like traffic isles and small curbs (Oniga and Nedeveschi, 2010); triggering an autonomous emergency braking (Wedel and Franke, 2007;

Xia et al., 2014); and employing different obstacle detection strategies in real-time (Bernini et al., 2014).

However, the algorithms indicated in Section 5.3.5 assume that the stereo vision sensor is rigid (nearly not deformable) and operates parallel to the road surface, different from motorcycle functioning. The chapter address these aspects and explain the problems that imaging systems based on stereo vision technology need to overcome to be used as a part of a motorcycle safety system. Section 6.1 introduce concepts of stereo vision together with the technical vocabulary used in the following sections. Section 6.2 presents the design of our custom build camera-based remote sensors. In this section is also explained the key operational consideration required for motorcycle operation (the online re-calibration to counteract the deformations of the sensor) and how they were achieved.

6.1. Stereoscopic vision considerations for motorcycle safety applications

A proper operation of stereo camera-based sensors requires the use of two synchronized cameras as a whole, which is achieved through the jointly characterization of them (the stereo camera calibration). An invariant calibration of the 3D sensor would assume constant parameters of the imaging system, such as relative distance and orientation between the two cameras, which are physically determined by the location of the cameras in the stereo rig.

Regrettably, the assumption is not valid for the motorcycle application due to the deformation (micro-bending) of the stereo rig. A motorcycle, as a lightweight vehicle, has less potential than a car to damp the vibrations generated from road irregularities. In fact, in normal riding conditions the vehicle frame is subjected to intense shocks, which passes to the stereo camera rig, producing dynamical changes in the instantaneous distance and orientation between the cameras. These very small changes, that may be imperceptible to the naked eye, can make the stereo vision system unable to operate (unable to compute the Disparity Map and obtaining the depth of the scene imaged). As a consequence, an invariant stereo calibration is not suitable for a moving motorcycle setup. In addition, the optical zoom of the long range cameras makes common mechanical anti-vibration solutions ineffective. However, one possible software solution is the online stereo re-calibration.

6.1.1. Stereo vision fundamentals

Concepts of stereo vision considered relevant for the design and implementation of our multifocal stereo camera sensor are recapitulated hereafter. More details on stereo vision and 3D geometrical modeling principles can be found in (Hartley and Zisserman, 2004) and (Bradski and Kaehler, 2011).

Estimating depth from stereo imaging is a triangulation task. In the human vision, to solve this task visual information derived from two eyes is used to estimate depth from the so called binocular disparities (Qian, 1997). The disparity is the parallax observed between corresponding world-points (in 3D space), and it is inversely proportional to the distance from the sensor viewpoint (Z , see Equation 6.1).

If we consider the stereo triangulation in epipolar geometry, the correspondence of points between two images is obtained by means of imaginary scan lines. The distances in

pixels along scan lines are the disparities between couples of correspondent points. Epipolar geometry defines epipoles and epipolar lines. For each camera and each point in space, the epipole is defined as the intersection of the camera imager and the line passing from that given point and the focal point of the camera. The line in the space connecting two corresponding epipoles of the two cameras is the epipolar line. Finally, epipoles and epipolar lines have a representation in a rectified space computed using the fundamental matrix (Hartley, 1997; Luong and Faugeras, 1996), thus generating rectified images (after lens distortion correction).

Epipolar lines in rectified images are horizontally aligned. This characteristic simplifies the search for matching correspondent features to a simple search within image rows between the pair of rectified images (Baker and Bolles, 1989). For real time computation, a suitable stereo correspondence method is the Semi-Global Matching algorithm (Hirschmuller, 2005).

In our setup, both cameras are assumed to have the same focal length f expressed pixels unit. The distance between the cameras is their baseline b in distance unit. The difference of the relative projection of a world-point is the disparity d , generally expressed in terms of pixel units. Resulting depth can be computed using Equation 6.1, which shows that the disparity is inversely proportional to the distance Z (expressed in distance units) of the object.

$$Z = \frac{f \cdot b}{d} \quad (6.1)$$

6.1.2. Concepts of Field of View and Depth of Field

The Field of View (FoV) of a single camera is a solid angle through which the imaging sensor is sensitive to the light. Therefore, the FoV defines the periphery of the 3D volume of the inspection captured on the camera imager sensor. The FoV depends of a combination between the size of the imager and the camera lens. Therefore, the focal length defines the FoV (Equation 6.2), which is related to the focal length f (in distance units) and the horizontal size of the imager h (in distance units).

$$FoV[^\circ] = 2 \cdot \tan^{-1} \left(\frac{h}{2f} \right) \quad (6.2)$$

Lenses with a fixed focal length are designed to be focused for different distances but at expenses of less quantity of light from the scene imaged (brightness). Therefore, in the case of a multifocal strategy is recommended to use fixed lenses that select a limited Depth of Field (selective focus along the depth axis) in the desired depth range of measurement, in order to maximize the light sensed from this part of the scene.

6.1.3. Characteristics of a stereo camera rig: Common FoV, Range Field and Horopter $d=10$

Rectangular imager sensors modifies the concept of circular FoV, as a consequence, it is specified as Diagonal FoV, Vertical FoV and Horizontal FoV. Additionally, in this chapter is defined common FoV as the overlap between the FoVs of the pair of cameras on a stereo rig. The common FoV between the left and right cameras define the lateral boundaries (vertical and horizontal) of the Range Field (Figure 75). Employing fixed lenses ($b \cdot f = \text{constant}$) the

possible depth range to perform triangulation is defined for the range of disparities (d_{min} and d_{max}), which determines the rear and frontal boundaries of the Range Field.

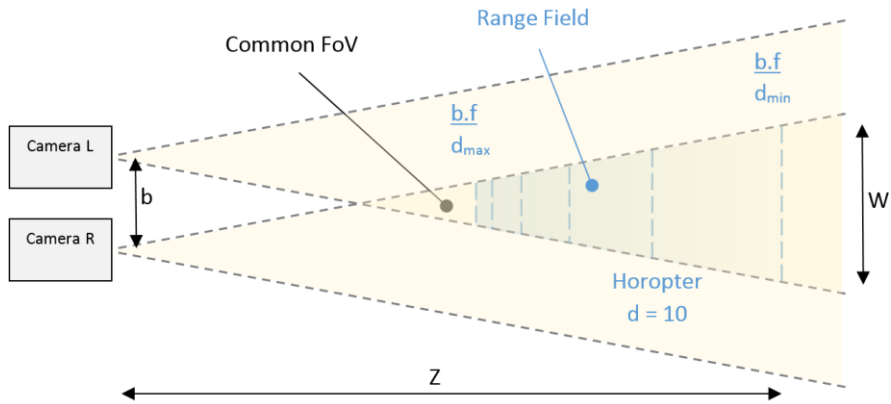


Figure 75. Top view of a conventional stereo vision system. Detail of the Range Field including the boundary of depth triangulation range adopted at the Horopter of 10 disparities.

The previous top view representation of the Range Field (Figure 75) is a simplification of a 3D volume termed frustum, which defines the Range Field. Thus, it is possible to determine the depth information for all objects inside this frustum. The Range Field was shortened by the transversal surface defined as Horopter of 10 disparities, in order to neglect the bias error of depth and satisfy the real-time constraints of our application.

6.1.4. Depth triangulation error in stereo camera sensors: Case of long-range applications while moving

The triangulation error (ΔZ) in a stereo system is defined according to Equation 6.3, for which Z is the depth in world coordinate frame and ΔZ is the depth error in distance units. The value Δd (disparity step) is directly related to the depth error and this component of the error depends on the capabilities of the stereo matching algorithm for achieve sub-pixel refinement.

$$\Delta Z = \frac{Z^2}{f \cdot b} * \Delta d \quad (6.3)$$

In stationary stereo measurements, the triangulation error follows a normal distribution (Clark F. Olson et al., 2001; Jung and Lacroix, 2005; Langer et al., 1994; Matthies and Shafer, 1987). However range bias error is induced for the camera position (Chowdhury and Chellappa, 2003; G.S. Young and R. Chellappa, n.d.; Kostas Daniilidis and Minas E. Spetsakis, n.d.) and depending the application researchers neglected it or no. Thus, the range bias error in moving systems need to be considered different from the Gaussian distribution. For this reason, in Simultaneous Localization and Mapping (SLAM) applications in order to ensure robustness, the maximum depth triangulation is defined a priori until a maximum distance 40 times the baseline (Mur-Artal and Tardos, 2017). This limit adopted for SLAM (mapping needs) is very conservative for long-range stereo, for example our long-range

baseline is duplicating this relationship (depth range 80 times the baseline) while keeping the maximum depth error below to 3% (more details in Section 6.2.4).

Research of long-range stereo applications have quantified the nature of depth stereo error. In their research, an experimental setup was conceived in order to tracking distant features with sub-pixel accuracy. They showed that the probability density distribution of the depth measurement error is non-Gaussian (Sibley et al., 2007). In fact, the distribution is skewed and present a long tail (Sibley et al., 2007). This produce an effect of over estimation of the triangulated position that increase with the distance. Other research point out the possibility of correct the bias error of depth in the lower values of disparity, for integer disparities calculations (Freundlich et al., 2015).

6.1.5. Sub-pixel accuracy and their relationship with depth accuracy: Case of car detection

Digital images are limited to pixel resolution because the objects in an image are spatially quantized at the resolution of the imager. However, the edges of the real object cannot necessarily be sensed for the entire pixel of the imager. In this cases, a more accurate object location must be defined in fraction of pixels. This situation is referred as sub-pixel resolution, which is common to encounter for far objects imaged (Keren et al., 1988).

From Equation 3, it is clear that a disparity value (Δd) inferior to one will decrease the triangulation error, or for the same error the triangulation Range Field can be extended. On the other hand, a fractional value of disparity can be seen as virtual expansion of the baseline (b). In this second regard of fractional Δd , for example, a portable stereo sensor designed to assist the visually impaired has achieved 1/8 sub-pixel resolution in an embedded system, compensating for the short baseline allowed for the wearable application (Di Stefano and Mattocchia, 2002).

In the automotive field, the first application of this concept to car detection reported an empirical limit in 1/4 of sub-pixel accuracy by employing a quadratic interpolation (Williamson, 1998), which is a simple constant-time operation suitable for real-time implementations. Beyond this empirical limit of sub-pixel accuracy, the car depth triangulation is not robust due to the pixel-locking effect (Shimizu and Okutomi, 2002; Szeliski and Scharstein, 2004). Subsequent experiments, endorsed the 1/3 or 1/4 as a robust sub-accuracy measurement on road traffic scenarios (Gehrig and Franke, 2007; S. Nedeveschi et al., 2004), but they extended the measurement case to texture-less regions (Gehrig and Franke, 2007), which is a big challenge for stereo matching algorithms.

A recent publication (Haller and Nedeveschi, 2012) reports the achievement of 1/5 of sub-pixel accuracy highlighting the importance of the census transform (Zabih and Woodfill, 1994; Hirschmuller and Scharstein, 2009; Spangenberg et al., 2013; Lee et al., 2016) to provide a robust stereo matching. The robust matching function “census” was also pointed in a previous analysis of sub-pixel decalibration error (Hirschmuller and Gehrig, 2009). Nowadays, the census transform is recognized as a noise robust stereo matching. It is used to provide proper disparity maps during the training of machine learning algorithms in applications of 3D understanding (Poggi et al., 2017).

For our remote sensor, I considered HD imagers (resolution 1280x720) to set an equivalent value of 1/2 of sub-pixel accuracy with respect to the imagers in the literature aforementioned. This conservative decision limits the full range of the measurement at expenses of a gain in robustness against sub-pixel camera decalibration (calibration loss).

6.1.6. Camera decalibration (calibration loss)

Depth triangulation in stereo camera systems depend critically on accurate calibration of each camera pair and in a vibration-free set up. The calibration is constituted by intrinsic and extrinsic parameters, for which the latest refers to the relative camera pose (3D orientation) between the two cameras. The extrinsic calibration depends on the physical fixation of the pair of cameras along the time. In this regard, a motorcycle is a harsh environment where vibrations coming from the engine (which is rigidly fixed to the motorcycle frame), the vehicle-road interaction, and aerodynamic drag forces can slightly modify the instantaneous pose between the camera pair along time (that cannot be seen with the naked eye).

Depending on the application, a variety of techniques are used to solve this issue. Examples: a) In visual odometry is usual to perform continuous stereo extrinsic re-calibration (5 Degrees of Freedom) operating on sparse stereo correspondences on stereo frame basis (Hansen et al., 2012); b) In mapping applications the re-calibration is 6 DoF between the cameras in the way of visual odometry but with the addition of GPS information (Kelly et al., 2011); c) In low altitude aerial imagery (< 30 m), the modal deflection of the drone wingspan is monitored which accelerometers in the tip of the wings where the cameras are located, using this information to compensate the relative angle of the stereo pair (Prather Lanier et al., 2011); d) In satellite imagery the undamped micro-vibrations on the satellite are software-compensated by the measures realized over known flat points in the earth (Roques et al., 2004); e) In areal imagery, a tailored bundle adjustment technique is used to refine camera parameters achieved altitude operations up to 120 m employing a wide baseline (Warren et al., 2013); f) Automated driving have also bundle adjustment implementations in which they estimate online both extrinsic and intrinsic camera parameters with a pre-definition of the scale (Rehder et al., 2017); g) A recent approach for robotic applications computes 5 DoF of extrinsic by a marker-less nonlinear optimization method (Ling and Shen, 2016); and h) In “motion stereo” or Structure-from-Motion (SfM) applications a relaxation of the epipolar constraint is performed. In these cases, the stereo frame is generated for a monocular moving camera, which moves over a rigid scene. The main assumption of this technique is a small vertical displacement, and consequently the matching strategy is relaxed by exploring a corridor around the epipolar line (Unger et al., 2011).

For our remote sensor (Section 6.2.1), I considered for a two-step calculation (Section 6.2.6). First, I perform the pre-rectification of the images based in an accurate static calibration, obtaining a similar effect to the strategy developed (Rehder et al., 2017). Second, I use the a visual odometry method (Hansen et al., 2012) but employing different feature descriptors .

6.1.7. Stereo confidence clues

The results corresponding to the Disparity Map (DM) calculation may have associate a level of confidence meaning that, for each pixel of the DM can be associate a probability that express how real is the triangulation calculated. Non-real triangulations due to lighting reflections or circumstances of bad visibility, like rainy weather, can lead to wrong detections. Several metrics were developed as a way of quantify the stereo confidence, a first framework for stereo confidence clue evaluation define a taxonomy (Scharstein and Szeliski, 2002) that was adopted for the research community to this end.

The stereo confidences is a valid measure that can be used in absence of ground truth data (Banks and Corke, 2001). This is important because rendering artificial scenarios which contains realistic outdoor adverse situations, and realistic erroneous sensor data, it is a huge

challenge (Scharstein and Szeliski, 2002; Kondermann et al., 2012). Therefore, even the advantage of the ground truth of syntactic imagery, it is not a practical approach to use for this case. The practical approach consist in to use real imagery acquired in adverse situations and human annotations or labeling of the DM based in the visual information (Pfeiffer et al., 2013). The tedious approach of binary labeling the confidence zones, allows to implement a Bayesian inference that is better for assess confidence metrics because it does not use only the annotations in the images.

The variety of stereo confidence metrics perform differently in varying outdoor conditions, thus the wise fusion of them implies more robustness against stereo matching errors. Machine-learning approaches allow to use a set of metrics to improve the accuracy of the stereo confidences (Haeusler et al., 2013; Saygili et al., 2014, 2015; Mostegel et al., 2016). Recently, machine-learning approaches to big stereo data collected in adverse weather allowed for a self-supervised strategy that automatically label confidence zones effectively (Tosi et al., 2017).

6.2. Materials

This section provide a detailed explanation of the design considerations of our camera-based remote sensors and consequently, how the system was evaluated for the application in motorcycle safety. For the evaluation, a new marker-based technique denominated satellite marker was developed. This marker-based technique is explained in Sections 6.2.1.1, 6.2.1.2 and 6.2.1.3 while presenting measurements realized with our remote sensor.

6.2.1. Sensor architecture (multifocal stereo rig and processing)

The multi-focal stereo rig is shown in Figure 76a. It is composed by 8 low-cost cameras with fixed focal lenses conforming 4 stereo camera pairs. All cameras have a rolling shutter imager sensor with HD resolution (1280x720).

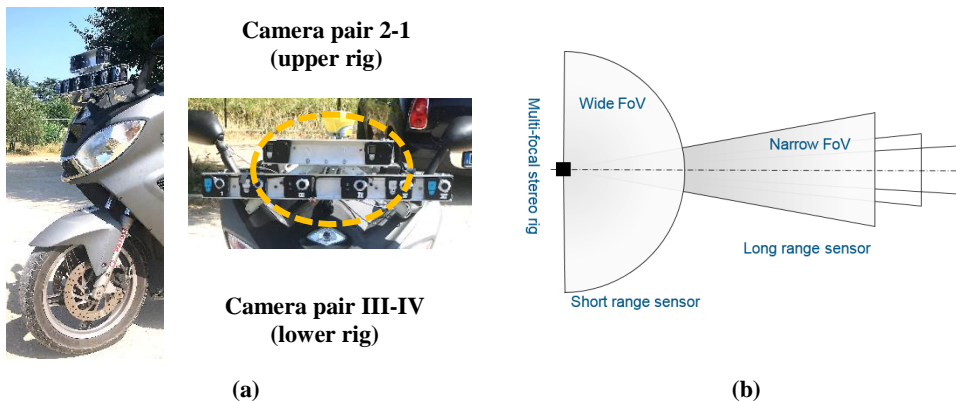


Figure 76. Overview of the imaging system. (a) Multi-focal stereo rigs installed in the frontal part of the vehicle and fixed to the scooter frame. (b) Top view of the 3D space to measure in front of the scooter (the outer stereo cameras are used for development purposes and future extension of the long range of measurement)

The synchronization between the six cameras (Camkong) of the lower rig was performed by hardware (Figure 77), while the two cameras (GoPro Hero Black) of the upper rig used wireless parring. In this publication are used only the central cameras corresponding to the camera pair III-IV (short-range sensor < 8 meters) and the camera pair 2-1 (long-range sensor < 22 meters) as indicated in Figure 76a. The other cameras are installed for development process.

The design of the remote sensor initially requires to define the spatial zones at the front of the scooter which are necessary to scan, as it is shown in Figure 76b. The depth range of these zones need to be defined according to the highest traveling speed allowed for the scooter and the possible colliding car. The application focusing on the urban scenario were top speed is restricted to 50 km/h.

Applications in advanced safety systems like the conceptual Motorcycle Autonomous Emergency Braking (M-AEB), requires a precise triggering to avoid false positives. In particular, for M-AEB safety system, the depth resolution required for the proper identification of the inevitable collision state was defined in a spatial grid of 20 cm (Savino et al., 2016). Thus, our remote sensor target this specification.

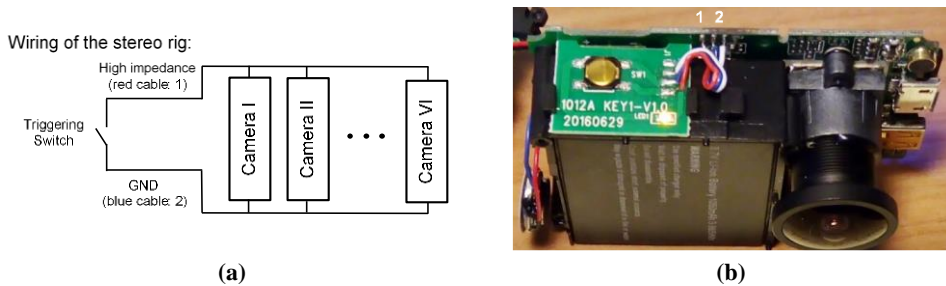


Figure 77. Wiring detail for the synchronization of the six cameras. (a) Circuitual scheme. (b) A disassembled camera showing the location of the electrical connections labeled “1” and “2”

The short-range stereo pair have fisheye lenses to scan a wide 3D space ahead of the vehicle. The light arrives to the imager from multiple directions, these motivated to define a short Range Field for the stereo triangulation. The case of the long-range cameras differ, because the narrow Field of View (FoV) of the lenses focalize the scanning volume in a narrow frustum.

Consequently, the lenses were selected through their FoVs. Next, the baselines for the two pair of cameras that allow us having a common Depth of Field (DoF) enclosing the desired frustum, as shown in Figure 76b. Additionally, to ensure capturing sharp images in the range of the sensor (e.g. short- or long-range) with the aim of performing the stereo triangulation, a trade-off between the FoV and the focal length was chosen (Table 12).

Short-range: Camera pair III-IV			Long-range: Camera pair 2-1		
Baseline [cm]	15.0		Baseline [cm]	26.5	
Diag. FoV [°]	170		Diag. FoV [°]	90	
Depth Field [m]	1	8	Depth Field [m]	8	22
Resolution	1280	720	Resolution	1280	720
fps	30		fps	30	

Table 12. Specification of the stereo rigs and constitutive cameras

After that, the 3D space measured is confined in a frustum, which is defined by the common FoV and the disparity range determining the Range Field of the stereo sensor (Figure 75). Regarding the Range Field of our sensors, they have to be included on the Depth of Field of each camera. In our application the Range Field was shortened as a manner to warranty repetitively at the full range of the measured space in a robust manner.

For the initial definition of the Range Field, the adoption of a Horopter of 10 disparities for the farthest measure was motivated to neglect the bias error of depth. At disparities on the order of 10 pixels or less, the effect of the non-Gaussian error in depth cannot be negligible for the triangulation calculation (Sibley et al., 2007). The Table 13 shown the values calculated using the Equation 6.1 for our specific application.

The depth discretization is not linearly distributed inside the frustum, as illustrated in Figure 75 by the parallel lines (top view of parallel planes). Thus, the largest and the shortest depth discretization are defined by the last and first two Horopters (depth planes) of the Range Field.

Considering the requirements for motorcycle safety systems, a depth grid of 20 cm is required by the conceptual M-AEB. The Table 13 shows the potential of the designed sensor. For example, when the long-range sensor (Camera pair 2-1) is measuring 18.93 meters ahead the sensor, the depth discretization using $\frac{1}{4}$ of sub-pixel accuracy is 19 cm. When the obstacle is approaching, the depth discretization become even smaller offering more depth accuracy.

	Camera pair III-IV		Camera pair 2-1	
	Far	Near	Far	Near
Disparity [pix]	17	118	24	57
Depth [m]	8.382	1.207	18.936	7.973
Depth discretization [m] & Sub-pixel = 1	0.465	0.010	0.757	0.137
Depth discretization [m] & Sub-pixel = 1/4	0.121	0.002	0.195	0.034

Table 13. Range Field of the remote sensor calculated for the application on advanced safety systems

Remark: in some Disparity Maps showed in this section, the reader may find different range of disparities of that required for M-AEB (Table 13), this is only for better visualization in the printed thesis.

6.2.2. Calibration of the multi-focal stereo camera sensors

The procedure allowed the calibration of all the cameras of the stereo rigs, it means obtaining all the intrinsic and extrinsic parameters that are used to model the camera and its pose in the space. In (Zhang, 2000a) is presented and explained the first method that allowed to calibrate a 3D imaging sensor with an inexpensive planar calibration pattern. The intrinsic and extrinsic parameters of the camera mathematical model are also described in this important paper.

Different planar calibration patterns exist but one of the most used is the checkerboard pattern. The reason of the election of this kind of pattern is that it presents visual features (corners) that are easy to identify for a variety of algorithm strategies. The identification of the features enable the semi-automatization or full automatization of the calibration process. This is very desirable because a correct camera characterization is a demanding process.

6.2.2.1. Semi-automatic algorithms for camera calibration

In this section is used the camera calibration toolbox of Jean-Yves Bouguet (Caltech Vision: www.vision.caltech.edu/bouguetj/), which is a standard the facto for camera calibration. Nowadays, many vision systems utilizes the procedure established in this toolbox to perform the camera calibration. The toolbox evolved in terms of automatization and algorithms until the year 2015 (more than 15 years). The semi-automatic fashion of the tool allowed me to experiment in the different stages of the calibration process.

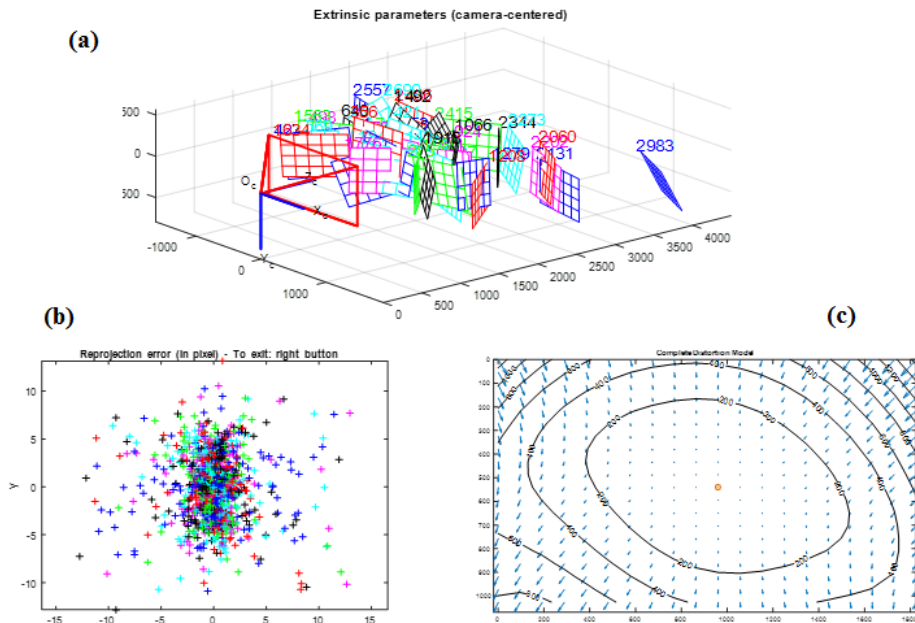


Figure 78. Characterization of the imaging system (monocular camera and fixed lens). (a) Shows the 3D location and pose (orientation) of the patterns used during the calibration w.r.t. one camera. (b) 2D plot of the reprojection error for all the features. (c) Graph of lens distortion (aberration)

Initially, I want to use each camera of the imaging system as a measurement device. Therefore, it is necessary to characterize how the light reflected in a 3D space or environment in front of the camera arrives to the imager (CMOS sensor) thought the camera lens. As a brief example, Figure 78 shown the results of the characterization of only one camera of the stereo rig. The physical volume and the pattern used in the characterization is shown in Figure 79. In addition, the characterization comprises the quantification of the effects produced for the physical location of the imager (CMOS sensor) and the plastic lens of the camera, which is not expected to be perfectly aligned.

Figure 78a shows in a 3D Cartesian space the volume used in the calibration process, in which it is defined the location and pose of the pattern detected in the space. Each measurement on the pattern is labeled (e.g. 2983) to associate it to a specific video frame. The location and pose is relative to the camera view (pyramid O_c), and the resulted mathematical model that is used to convert the camera in a remote measuring device. Figure 78b displays a geometric error corresponding to the image distance between a projected point and a measured one, the so-called reprojection error. The distribution of the reprojection error indicates how

well fit the mathematical model adopted to the reality. For example, because errors until 14 pixels were obtained, the mathematical model used in the example is not appropriate to long range stereo vision. The level curves chart of Figure 78c shows how the image is altered by the optics in the zones away of the center of image.

In Figure 79 is overlaid over one frame of the calibration images set, the reprojected points of the detected features (corners of the pattern), which are based in the mathematical model of the camera. The corresponding calibration parameters of the model where obtained from a nonlinear optimization fitment on the full set of images. Therefore, effects of an imprecise camera calibration can be seen because the cyan circles have not a concentrically matching against the red “+” marks (detected features for this frame). An additional problem on this calibration relies on the fact that corner features located in the boundaries of the pattern are not accurately identified (symmetrical features for all corners solve the problem).

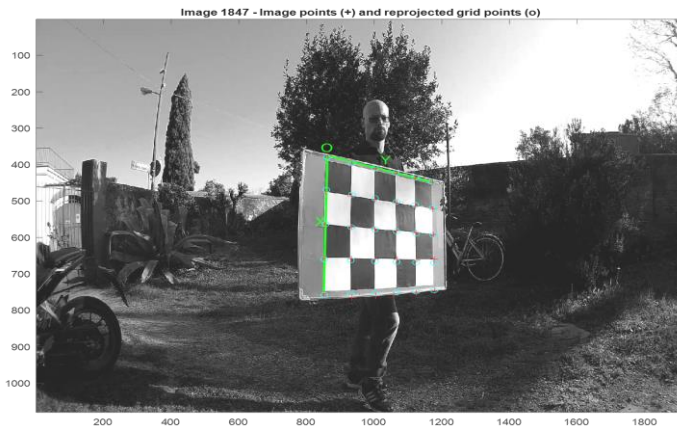


Figure 79. Example of one result of the reprojected points after an imprecise camera calibration

Next, Figure 80 shown a static outdoors scene with landmarks (traffic cones) in order to verify the measuring capabilities of the custom built camera-based remote sensor based in stereo vision. The scene corresponded to the garden of my office, at the University of Florence (UNIFI), which allowed me to conduct experiments in a variety of different lighting conditions.

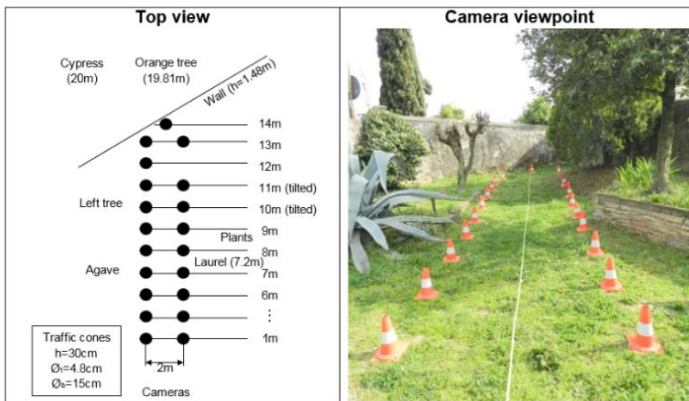


Figure 80. Scene to evaluate the remote sensor. The traffic cones of well-known dimensions are the landmarks used to generate ground truth. The targets were measured using a laser rangefinder



Figure 81. Example of the left image of the stereo pair processed. Image with big contrast and illumination changes



Figure 82. Disparity Map (DM) calculated from the stereo images. Dark areas represent objects that are farther away, while light areas represent nearby objects

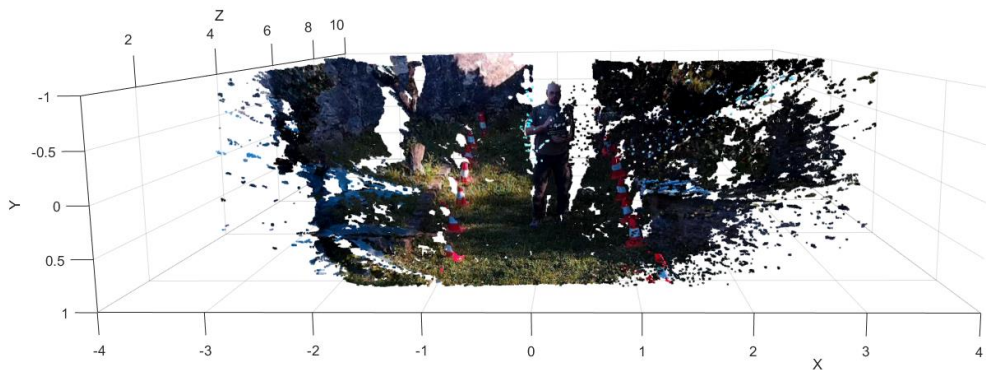


Figure 83. 3D point cloud or 3D reconstruction of the scene imaged

Figure 81 shows the output of the camera-based sensor when there is different contrast (challenging lighting conditions). Figure 82 shows the results of the Disparity Map (DM) calculation in gray scale, in which it can be seen the detection of the people in the center of the image, regardless the shadows and colors on it. Finally, Figure 83 shows the 3D depth measurement performed by the sensor in the form of 3D point cloud.

For a more comprehensive analysis and tests of our custom build sensor, which includes traffic scenes with different vehicles, such as scooters, motorcycles, cars, vans, and buses, can be found in (Savino et al., 2017).

6.2.2.2. Fully automatic algorithms for camera calibration

In this fully automatic process was used the Matlab stereo calibration application. The calibration algorithm (Bouquet, n.d.) uses the pinhole camera model (Zhang, 2000b) and the lens distortion calculation (Heikkila and Silven, 1997).

During the procedure of calibration, two people moved an asymmetric checkerboard pattern throughout the common Field of View (FoV) of all stereo pairs, while all cameras were recording video concurrently. Consequently, the analysis of the footages of each camera allowed to picking up the suitable stereo frames (these that contain a complete view of the checkerboard in the couple of images that conform the stereo frame) to perform the stereo calibration for each pair of cameras.

Next, corner detection algorithms are in charge of searching for symmetrical corner features in the images in order to find the checkerboard. State-of-the-art subpixel accuracy algorithms (Geiger et al., 2012b) contributed to obtain a proper calibration of our remote sensor. During the calibration process, I selected the frames for which the reprojection error was below to a low threshold empirically selected. To conclude, the two-step nonlinear optimization needed (Heikkila and Silven, 1997) was conducted to get the camera calibration parameters.

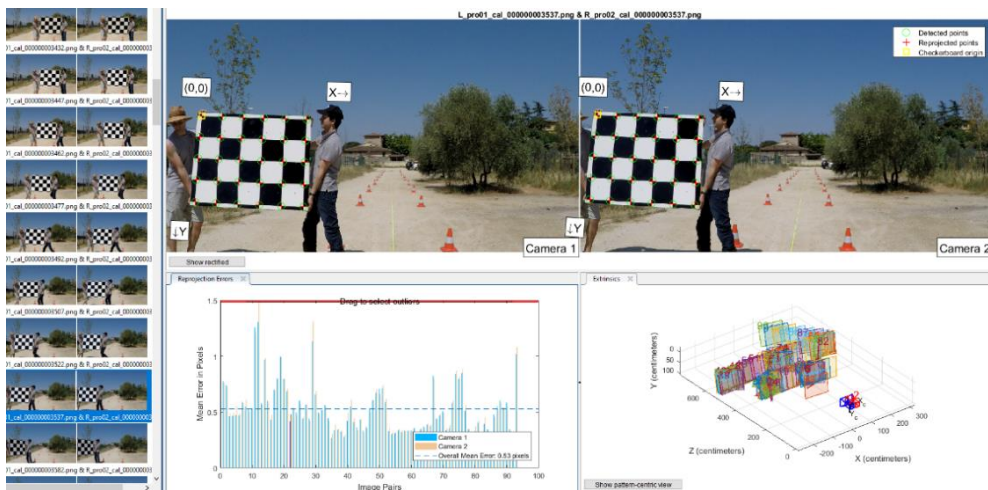


Figure 84. Overview of the graphical user interface of the Matlab Application for the stereo camera calibration

In Figure 84, the calibration procedure illustrated by an example that corresponds to the long-range stereo camera sensor. The procedure is the same for each stereo camera pair. The thumbnails on the left shows a set of stereo frames employed for the calibration. On the top, the pictures labeled “Camera 1” and “Camera 2” have overlaid the corners detected on the checkerboard in the stereo frame. The bar plot (reprojection flap) depict the calibration accuracy for each stereo frame, the reprojection error of the corners detected are due to the set of camera parameters obtained, which tends to satisfice the calibration of all the set of images simultaneously. The 3D diagram show the pose of the checkerboard in the space for each stereo frame (extrinsics flap).

The main camera parameters obtained as a result of the static camera calibration performed for both stereo sensors are shown in Table 14.

Short-range: Camera pair III-IV				Long-range: Camera pair 2-1			
Baseline [cm]		14.9157		Baseline [cm]		26.4867	
Right Focal length Vector [pix]		Left Focal length Vector [pix]		Right Focal length Vector [pix]		Left Focal length Vector [pix]	
897.2688	897.6886	1027.5	1040.7	1715.3	1719.6	1712.6	1717.8

Table 14. Main values of the calibration of the stereo rigs for both measuring ranges

6.2.3. Determination of the Range Field (verification of desired depth accuracy)

The design considerations of the imagining system developed, mainly in terms of focal lenses, common FoVs, baselines, resolution of the imagers, proportioned a baseline with the ideal measurement capabilities of the stereo vision sensors. However, several practical factors can affect the measurement range of a stereo camera system and this experiment was designed to quantify the Range Field of all the stereo camera rigs.

The test was conducted in an open and flat surface after having delimited a rectilinear corridor by traffic cones (Figure 85a). The corridor had 2 m of wide and 45 m of length, and it was defined by cones of 30 cm height placed in couples spaced 5 m. The nearest couple of cones are located a 5 m of our sensor. The same stereo videos recorded during the camera calibration process were re-used, for this reason two people appear holding a checkerboard. In the Disparity Map (DM) of Figure 85b, the planar surface of the checkerboard was used to assess the homogeneity of the disparities calculated in function of the depth.

The 3D reconstruction of the scene imaged (Figure 85c) shows the capability of the remote sensing approach to measure the 3D space. The 3D point cloud was calculated for a three-dimensional space starting from 5 m to 30 m of depth for development purposes and the definition of the Range Field.

The point cloud calculations are not supposed for a real time application, it is only used for helping to assess the quality of the 3D information measured. For the top view of the scene (Figure 85d) the point cloud was calculated from 10 m to 22 m which corresponds with the Range Field of the long-range sensor. The location of the 2nd, 3th and 4th couple of cones corresponding to the depth distance of 10 m, 15 m, and 20 m was highlighted.

The bias error of depth grows for longer distances as is expected for Equation 6.2, this is being negligible for the first two pairs of cones and a tolerable 1.68% and 2.25% systematic errors (more details in Figure 86). It is adequate to consider our systematic depth errors as a tolerable because they are inferior to 3% (even without the proper error cancelation). The 3%

of error was found as a requirement for reliable driving assistance functions in cars (Pantilie and Nedeveschi, 2012).

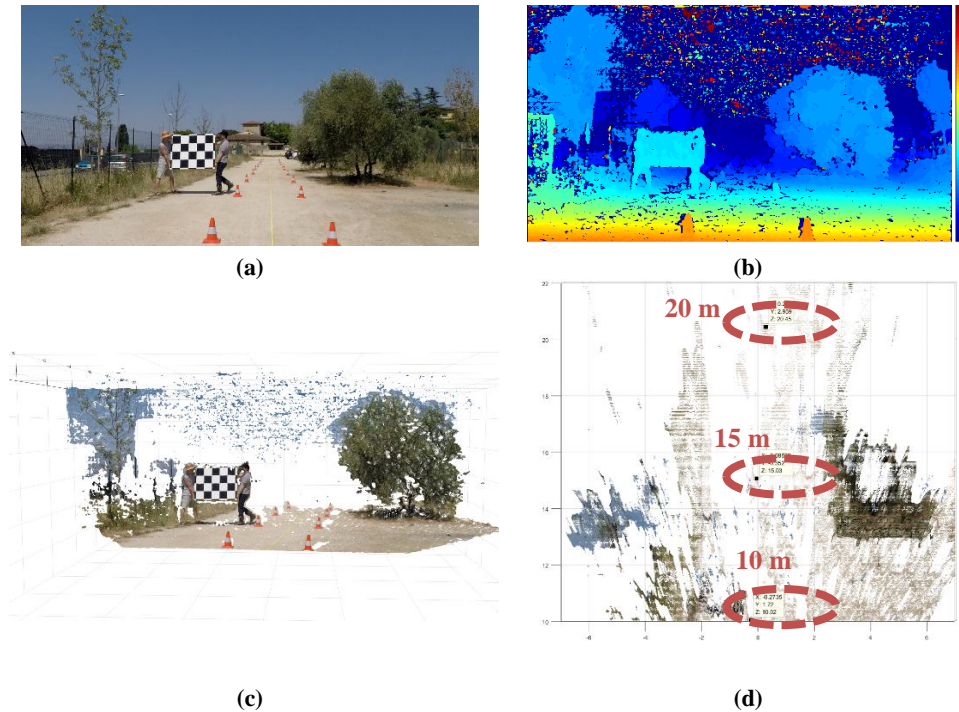


Figure 85. Depth accuracy quantification of the calibrated stereo camera (long-range camera rig). (a) Rectified left picture acquired by the long range stereo camera sensor. (b) Disparity Map of the scene (range from 0 to 128d). (c) Three-dimensional reconstruction or 3D point cloud of the scene imaged. (d) Top view of the 3D point cloud highlighting the location of the traffic cones originally placed at 10m, 15m, and 20 m. This 3D point cloud can be download according to Appendix B for a better assessment of the reader

6.2.4. Determination of the horizontal resolution of the stereo vision sensor

In order to quantify the horizontal resolution of the stereo vision system the objects of known dimensions were carefully located, like traffic cones of 30 cm of height separated 2 m inside the Range Field of the stereo camera sensor. In Figure 86 are depicted three different views of the measurement corresponding to the couple of cones located a 15 m and 20 m. From the measured values it can be seen that the horizontal measurement of the targets present a systematic error about 7% to 8% from the two measures.

Therefore, the 20 cm of horizontal resolution required for the Motorcycle Autonomous Emergency Braking (M-AEB) application (Savino et al., 2016) can be achieved for our stereo camera sensor. Additionally, this the horizontal resolution have the potential to be used in for the detection of small road hazards strategies (Ramos et al., 2017).

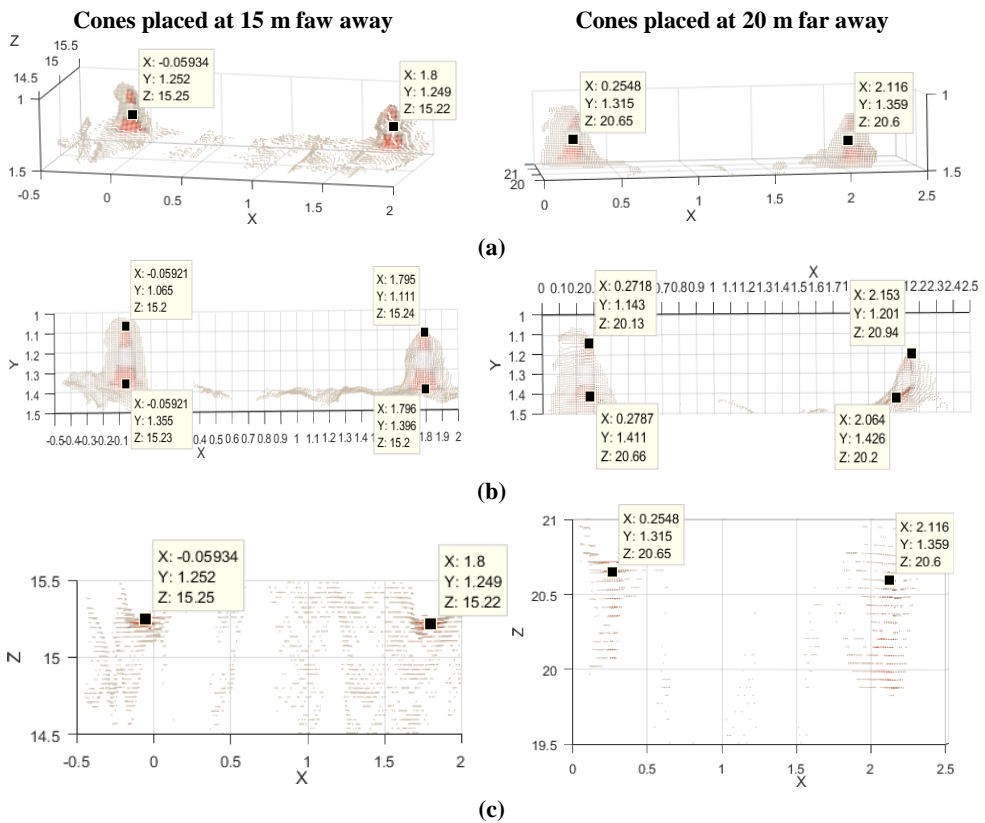


Figure 86. Analysis of small narrow objects in the farthest half of the Range Field (long-range camera sensor). 3D control points were located at similar places for each couple of cones for the analysis. (a) Detail of the 3D representation of the targets. (b) Frontal view of the targets (grid sized 10 cm). (c) Top view of the 3D point clouds (grid sized 50 cm). For the cones at 20 m the fattening effect becomes evident (depth artifact)

6.2.5. Determination of dynamic ground truth

Dynamic ground truth in this specific context is associated with referential information about the depth, shape and orientation of the objects present in the traffic scene. Creating 3D ground truth is a measurement and data fusion task associated with the combination of different kinds of sensors. However, employing the technique of the satellite marker (Section 6.2.1.1) is possible to obtain accurate car heading angle estimation of a moving car under realistic imagery.

This is important because the method provides accurate car pose at frame level, and the instantaneous spatial orientation for each camera, also at frame level. This can be used for the generation stereo video of datasets with ground truth, which can be used to assess the online camera re-calibration algorithms of Section 6.2.2.

6.2.5.1. Materials

The marker chosen was an asymmetric checkerboard pattern. This type of pattern allowed to estimate the intrinsic and extrinsic parameters of cameras with common a camera calibration tool. The satellite marker was built from a planar wood panel of 95x120x1 cm. Black and white squares with sides of 22 cm painted on the board constituted a checkerboard pattern of 4 by 5 full squares (Figure 84). The checkerboard pattern was extended to the edges of the wood panel (detail in Figure 87) to define symmetric corner features for all the corners belonging to the 4 by 5 full squares pattern. In this way, cutting edge algorithms for automatic corner localization which provides sub-pixel accuracy (Geiger et al., 2012b) could be used during the ground truth generation.

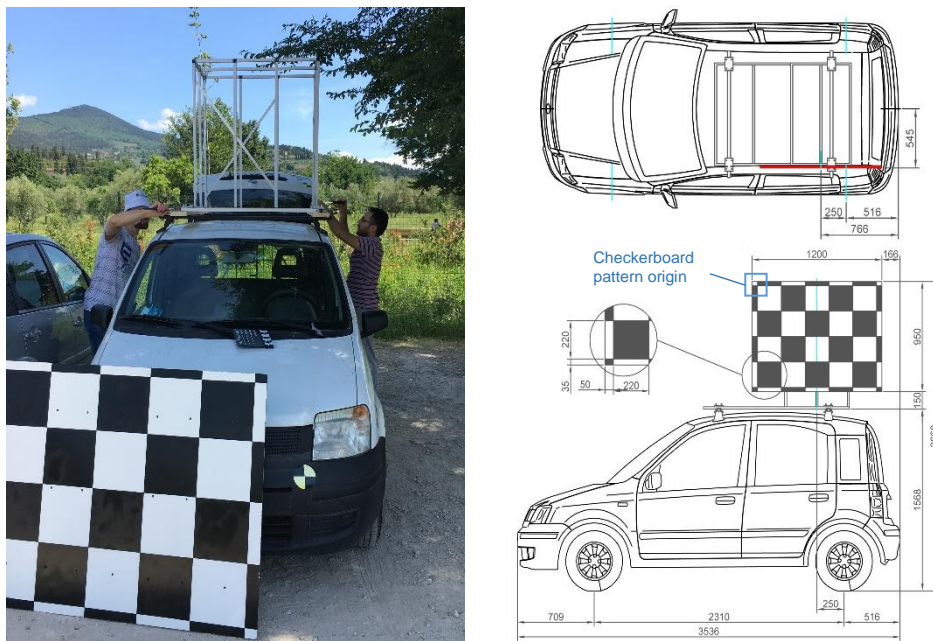


Figure 87. Overview of supporting structure and detailed measurements of the satellite marker and its alignment with respect to the target car. Only the lateral setup (satellite marker in one of the sides) was used in this experiment

For the validation of the dynamic measures acquired, a highly accurate Real Time Kinematic (RTK) satellite navigation system was employed to validate the ground truth generated from the stereo video with the satellite marker method. The D-GPS units (GeoMax Zenith 20) provided the locations of the PTW and the moving target at 20Hz and an accuracy of ± 2 cm over the ground plane. Note: According to the user manual several factors of the can affect it, I assumed ± 2 cm which 1-sigma accuracy (68.27%).

6.2.5.2. Ground truth generation using the satellite marker

Our proposed strategy is to measure the pose of the target car via measuring the pose of a satellite marker rigidly connected to the target itself. In our application case, the marker was placed on top of the target (Figure 87) in order not to occlude or change in any way the aspect of the target vehicle.

The calculation of the ground truth heading from the stereo videos was post-processed analyzing only the pose of the marker in the tridimensional space for left and right frames independently. All the information contained in the stereo video corresponding to the moving target was neglected. The algorithm is a double-step method that first uses the results of the Direct Linear Transformation (DLT) based on the pinhole camera model (Zhang, 2000b) to initialize the Levenberg-Marquardt non-linear optimization (Heikkila and Silven, 1997).

In order to obtain the desired ground truth with the satellite marker method, first is necessary to create an “etalon” for the camera system. An etalon for our imaging system as set of stereo frames acquired in static conditions (the camera rig is not moving therefore not dynamic decalibration can occurs), which contains enough stereo features along all the FoV to direct the optimization process to converge to very similar intrinsic camera parameters, even if other stereo pairs containing different stereo features are added in the calibration process. Therefore calibrating the stereo camera system. Regarding the accuracy, the measurements obtained were controlled maintaining the maximum reprojection error of the etalon set below 0.75 pixel (3/4 sub-pixel accuracy). This ensures the conservative 1/2 sub-pixel accuracy adopted for our measurements in dynamic situations.

Once the etalon was defined, it was set as input of the stereo camera calibration tool together with the stereo frames of the video sequence to be analyzed. For example, our application case consisted of 60 stereo frames for which the first 23 pairs belonging to the etalon.

To obtain the ground truth, it is necessary to remove the extrinsic data corresponding to the etalon set from the obtained results. As a consequence, ground truth files complementing the video containing the pose of the target to measure for each video frame can be created. The information obtained as a ground truth consists in three rotational and three translational values of the satellite marker for each camera. The convention used for the 6DoF measurement are referred to the optical center of the left camera of the stereo pair.

Regarding to the heading angle reference, the rotational value around Y-axis correspond to the heading angle of the target car. Therefore, once the satellite marker position is defined, obtaining the ground truth heading is straight forward from the stereo camera calibration tool.

6.2.5.3. Measurement on a moving target vehicle

Our case study is a single moving vehicle that perform a set of three manoeuvres in front of our imaging system. The experiments were performed in an outdoor car parking in daylight conditions. This setup allowed us to obtain realistic imagery while performing a series of simple and complex maneuvers in a controlled environment.

The stereo system, in the frontal part of the PTW sensing platform, remained static and in upright position during the tests. The manoeuvres performed by the test car are illustrated in Figure 88.

First, the target car was approaching the PTW from opposite direction and turned in front of the PTW's path. Second, the car stopped and reversed passing again in front of the PTW. Finally, after stopping again, the car moved forward merging in front of the PTW's longitudinal axis.

The experiment was conducted at noon with the sun high in the sky, and the satellite marker was placed in the lateral position to guarantee a correct sight of view during the execution of the maneuvers. The car driver was instructed to perform the maneuvers with both slow and quick dynamics (not exceeding 45 km/h).



Figure 88. Succession of 20 representative frames to describe the maneuvers for which the heading angle ground truth was obtained. The numbers represent the temporal order of the sequence during the maneuvers

As a result of the stereo video sequences acquired, the disparity maps were computed thus generating a 3D reconstruction of the scene (Figure 90). This step allowed us to verify the integrity of the images acquired.

A representation of the accurate geo-localization of the moving car during our experiment is shown in Figure 89. The dashed trajectory corresponds to the movements of the vehicle where the satellite marker was not visible from the imaging system due to its lateral placement. The solid line represents the vehicle trajectory while the marker was in the line of sight of the stereo camera. Ground truth was generated in all these locations.

The ground truth obtained from the stereo video employing the method of the satellite marker provided 6DoF information (pose of the marker) with respect to each single camera of

the stereo rig. 3DoF corresponds to the translation of the marker in the space, and 3DoF corresponds to the rotation. Our interest corresponds only to the Y-axis rotational component, however the D-GPS system do not provides heading to compare. The D-GPS antennas provides Cartesian coordinates over the ground plane with an error of ± 2 cm 1-sigma.

Consequently, other two components of the ground truth were used (generated from the imaging system) to obtain a fair comparison metric which is depicted in Figure 91.

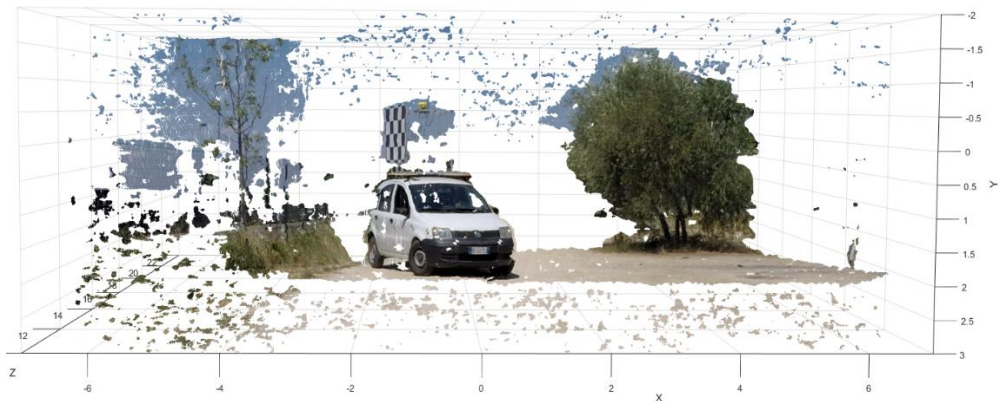


Figure 90. Example of the 3D point cloud generated from the disparity map (all the units are in meters)

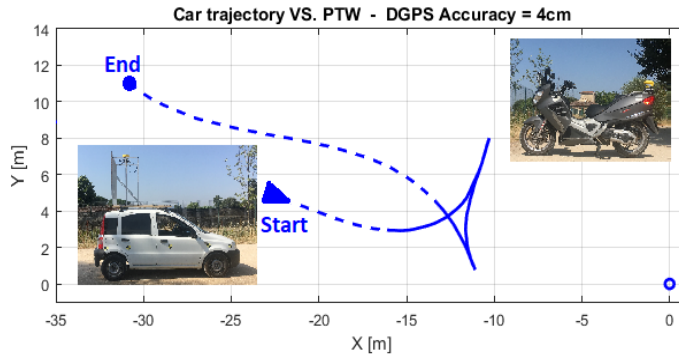


Figure 89. 2D trajectory of the target car during the experiment. The measure indicates the relative position of the two yellow antennas installed in the vehicles. One antenna is positioned in the rear part of the PTW (coordinate origin) and the second antenna on the satellite marker frame

Bearing these considerations in mind, I overlaid on the X-Z plane (delivered for the D-GPS) the locations calculated from the ground truth in order to assess it (Figure 92). The information to the location present a deviation up to 18 cm in the section analyzed. The biggest errors appear when the marker have big heading angles (62° and -50°) with respect the stereo camera in the PTW.

During the analysis of the stereo triangulation, was noticed that these pair of cameras of our imaging system tend to overestimate in 3.75% the depth range close to the Full Scale

Output (FSO) of the stereo sensor. For example, traffic cones of 30.0 cm of height aligned with the center of the stereo rig and located at 20.0 m away from it indicated a depth distance of 21.75 m in the 3D point cloud obtained from the calculation of the disparity map. Nevertheless, this does not contribute to the error of the satellite marker method because it does not use the stereo triangulation to measure.

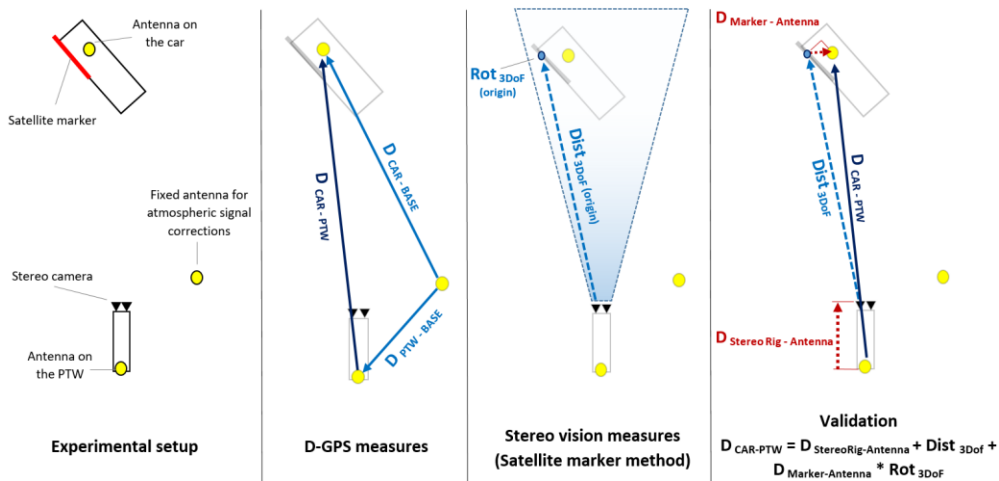


Figure 91. From left to right is illustrated in vectorial form the measurement performed (D-GPS) and the equivalent measure synthesized from three components of the ground truth (imaging system)

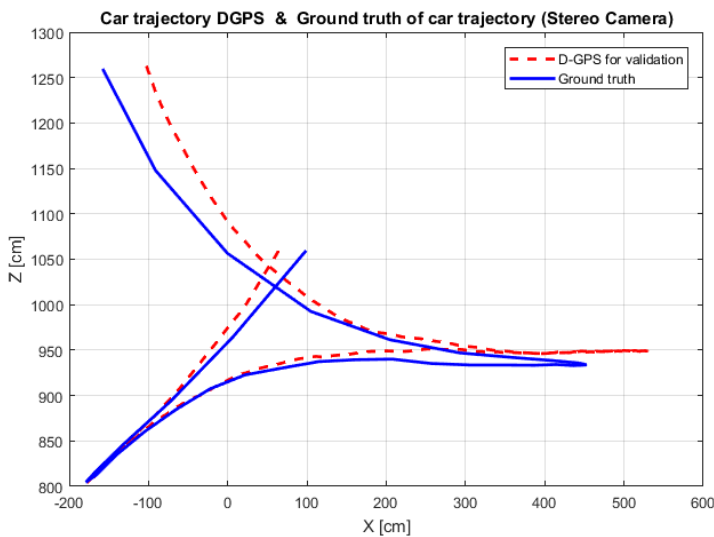


Figure 92. Comparison of the Ground Truth location generated with the satellite marker method and a more accurate reference provided for the D-GPS system

6.2.6. Online camera re-calibration

The vibrations in the scooter temporally misalign the cameras of the calibrated stereo camera sensor (decalibration). Therefore, an online re-calibration is needed to perform triangulation. The re-calibration implemented is based on a two-step rectification under two assumptions:

- Invariance of intrinsic parameters of each camera.
- The extrinsic parameters of each camera pair varies within a small range.

In this way, the images are rectified two times to avoid problems of scaling (scale-drift). The first time uses the camera parameters obtained in the static calibration, and a second time uses the sparse pixel image correspondences (rectification tuning).

Nevertheless, as multiple correspondence measures are available and matching methods can lead to significant differences in matching results, there is a trade-off between execution time and descriptor quality to be evaluated empirically (Rublee et al., 2011; Leutenegger et al., 2011; Miksik and Mikolajczyk, 2012; Alahi et al., 2012; Schaeffer, 2013; Panchal et al., 2013; Gupta and Cecil, 2014) for each application case.

As starting step, a qualitative comparison was performed by employing two different kind of keypoint descriptors, a histogram-based descriptor and a binary descriptor. It is worth saying that the two feature descriptors chosen have shown good performance in real-time implementations (comparison in Section 6.2.5.1). The correlation methods were excluded of our comparison due to its high computational complexity (Mikolajczyk and Schmid, 2005).

The election of SURF (Speeded-Up Robust Features) method (Bay et al., 2006, 2008) as image feature descriptor and extractor was because it is a robust (Schaeffer, 2013) and quick

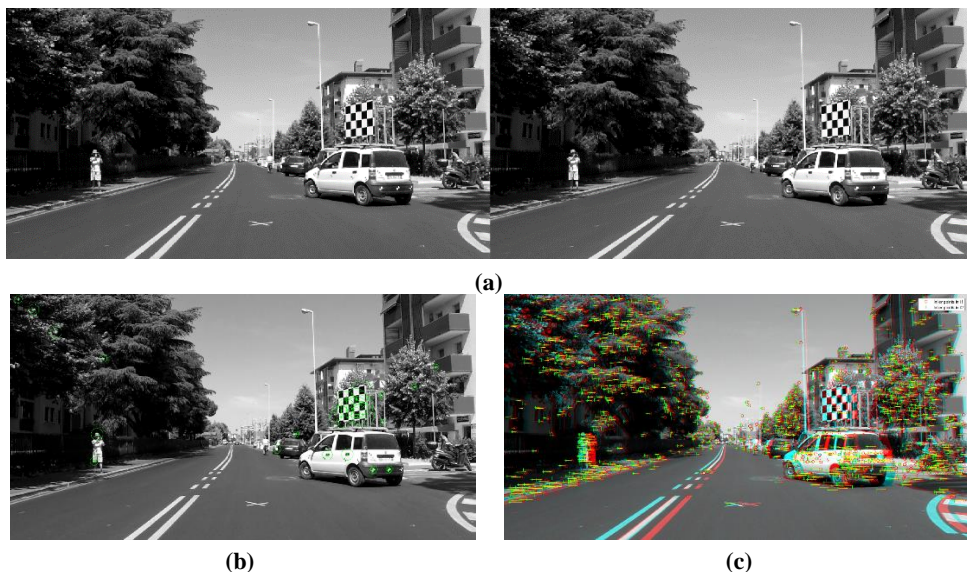


Figure 93. Illustration of the automatic camera extrinsic parameters re-calibration. (a) An initial rectification of the stereo frame according to the static calibration values. (b) SURF feature extraction in both images of the stereo pair (circle's diameter represents the scale of the feature – only 30 are shown for clarity). (c) The salient features matched (correct pixel assignments indicated by yellow connections – the 1000 features are shown) are overlaid on a 3D anaglyph

(Rublee et al., 2011) keypoint descriptor (Gupta and Cecil, 2014). These characteristics make it suitable for the self-calibration of wide baseline stereo camera systems.

In Figure 93 is illustrated the procedure for the second step of the re-calibration implemented. First, calculate sparse point correspondences between the images rectified to identify 3D salient points of the scene (Figure 93b). Compute salient points per image with the point descriptor SURF. Next, putatively match the correspondent features between the images (Figure 93c) in order to estimate the “fundamental matrix” (Bradski and Kaehler, 2011; Hartley and Zisserman, 2004) thanks to the RANSAC (RANdom SAmple Consensus) method. Thus rectifying the images, it means, aligning the images such that corresponding points will appear on the same rows in both new images to perform triangulation.

Up to now, it is implemented the online camera re-calibration employing SURF features and SURF feature descriptors. However, binary descriptors are more suitable for real-time applications because they requires significantly less memory than histogram-based descriptors like SURF. This motivated our second re-calibration test employing SURF features and FREAK (Fast RETinA Keypoint) descriptors. FREAK is based in human retina behavior (Alahi et al., 2012).

A real example of dynamic decalibration acquired from our stereo camera rig is presented in Section 6.2.5.1 next to the results of the two re-calibrations implemented. In addition, an image dataset with ground truth corresponding to a trial of the pre-crash experiment is provided. The dataset is provided through an online repository and the ground truth can be obtained from the satellite marker on the colliding car.

6.2.6.1. Online re-calibration of the cameras

Table 15 and Table 16 present in the form of Disparity Maps (DMs) the inability of the stereo camera system to perform the depth triangulation due to the fitment of the sensor on a motorcycle (first column). The reason of it is the invalid assumption of having rigid stereo camera rig, which maintains stable the baseline and orientation of each camera.

The second and third column depicts the DM computed with the proposed two-step online recalibration technique. The results point out the need of a continuous recalibration of the system for the motorcycle safety application, because the decalibration (calibration lost) of the stereo rig generates the corruption of the Disparity Map (DM).

In our system, it was empirically noticed that it is not possible to calculate a proper 3D point cloud from the DM data when it contain less than 45% of matched pixels of each camera (belonging to the shortened frustum at the Horopter 10d). Therefore, Figure 94 shows a comparison of the percentage of pixels properly employed to compute the Disparity Map and obtain the depth of the scene. The comparison is by normalizing the number of pixels on the Disparity Map computed and the number of pixels of an input imagen. The chart present in three different colors the results of the Simple rectification (static stereo calibration parameters), and the two strategies used for the re-calibration based in SURF and FREAK.

The continuous and dashed lines of the chart distinguish between the totality of the pixels used to compute the DM and the most relevant set of disparities calculated, which are above of the Horopter 10d. For the two online re-calibration cases, the percentage of pixels used to calculate the DM appear to be stable around 70% to 74%, which is convenient. Also, in these cases the number of disparities below the Horopter 10d are negligible and consequently, the continuous and dashed lines in the chart are almost overlapping.

	Static calibration	Re-calibration (SURF-SURF)	Re-calibration (SURF-FREAK)
1st frame			
2nd frame			
3th frame			

Table 15. The left column corresponds to the depth triangulation on the rectified images (Simple rectification) obtained from the static calibration (extrinsic + intrinsic parameters of the camera model). The central and right columns corresponds to the re-calibration (second step of the online re-calibration). **Remark:** in the 2nd frame corresponding to the static calibration it can be seen that the DM is corrupted, so it is not reliable to perform depth triangulation

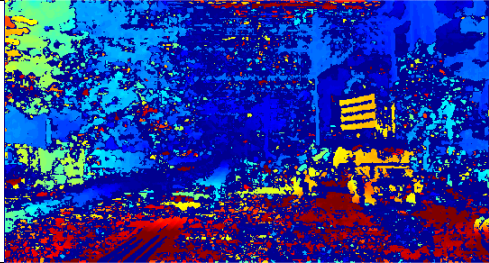
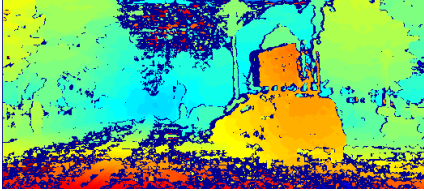
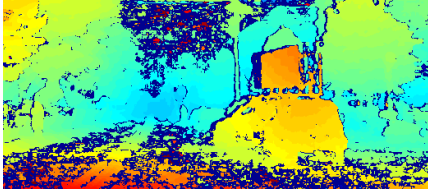
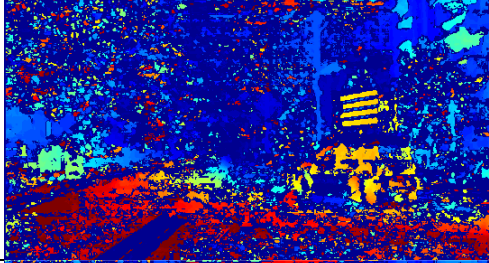
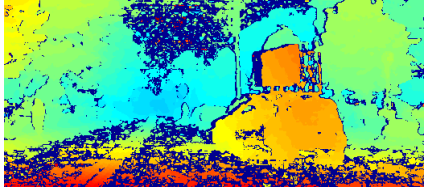
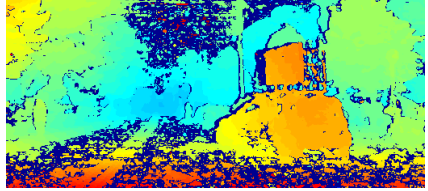
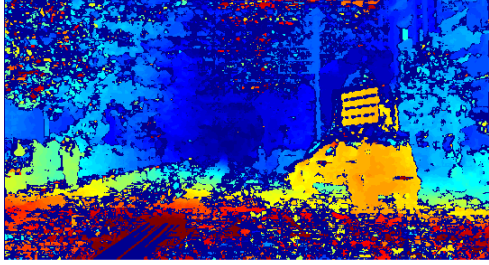
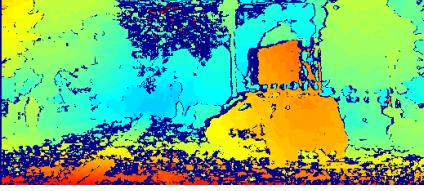
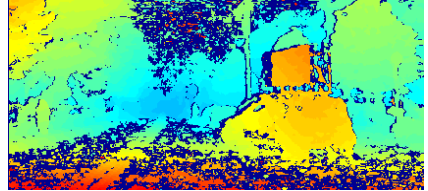
	Static calibration	Re-calibration (SURF-SURF)	Re-calibration (SURF-FREAK)
4th frame			
5th frame			
6th frame			

Table 16. From the 4th and 5th frames of the static calibration cannot be measure the target due to the decalibration at these moments, while in the 6th frame the depth triangulation is reliable again (borderline)

This short sequence of 6 consecutive frames (Table 15 y Table 16) make explicit the consequences of the dynamic stereo decalibration in the motorcycle application. In the two columns corresponding to the online re-calibration, it can be seen that both strategies present satisfactory results. Note that the color disparity scale between the online re-calibrated DMs is different to the scale of the fixed calibration to facilitate the visual comparison.

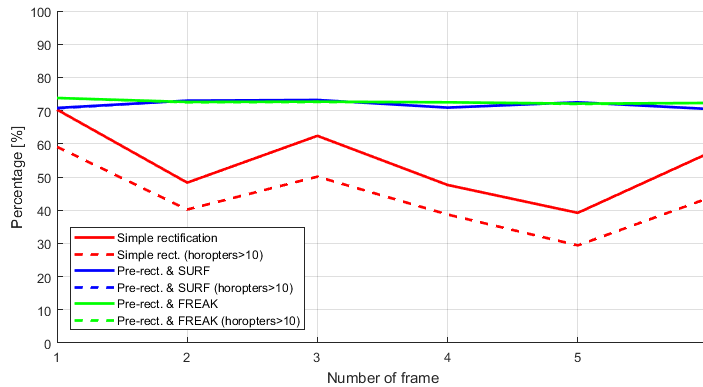


Figure 94. Chart showing the percentage of effective stereo frame used to calculate the Disparity Map (DM) during the first six neighboring frames (consecutive frames) of the 1 second pre-crash sequence. Below 45%, the number of reliable pixels is insufficient to compute the DM

The data is available in the following repository:

https://github.com/GusRep/StereoDecalibrationProblem_and_PointClouds

The Wiki page associate to the repository is:

https://github.com/GusRep/StereoDecalibrationProblem_and_PointClouds/wiki

The provided data can be used for visualization and experimentation purposes:

- 3D reconstructed scenes: (*.pcd) files corresponding to the 3D point clouds acquired for the system which are shown in the publication. Files named "testFirenze*.pcd".
- Decalibration dataset: (*.png files):
 - A set of 30 color stereo pairs (raw data) corresponding to the pre-crash test sequence. Six files named "Original_crash_*.zip.*".
 - A set of 30 rectified stereo pairs (pre-rectification according to the static camera calibration) corresponding to the pre-crash test sequence. Four files named "PreRect_crash_*.zip.*".

The satellite marker method can be used in the stereo frames to retrieve the ground truth heading angle of the vehicle and the instantaneous orientation of each camera.

6.3. Conclusions

The possibility to use only stereo vision as a remote sensor is feasible. The results of static and dynamic measurements performed by the remote sensor installed in the UNIFI demonstrator were satisfactory within the design condition of good visibility. The static cases correspond to controlled environments which presented ground truth conditions in challenging outdoor lighting conditions. The dynamic cases presented, added the complexity of moving targets and ego motion with ground truth provided by the D-GPS and the satellite marker technique.

The performance of the developed sensor, employing low-cost action cameras, was satisfactory in a static setup and the sensor showed good potential for the application in advanced motorcycle safety systems. The sensor was able to measure small targets sized 30 cm height (traffic cones) from distance up to 21 meters and some curbs of street islands during the test in the traffic scenarios. The bias error of depth in this measure of the cones was +2.25% which is inferior to the 3% of error used as a requirement for reliable driving assistance systems in cars (Pantilie and Nedevschi, 2012).

The analysis of the point clouds, which are available in the online repository, showed the possible discrimination of targets using a grid of 20 cm up to 16 meters of depth. This grid size was a target requirement to avoid false positives in the conceptual Motorcycle Autonomous Emergency Braking (M-AEB). The sensing capabilities of our sensor are very promising for motorcycle safety application in urban scenarios, because the intervention of M-AEB is expected to be in the range of 8 to 10 meters from the colliding vehicle. Thus the developed sensor more than meets the M-AEB requirements.

Additionally, it is important to remark that depth measurement by a moving stereo vision setup relies on the combined movement of the camera set (static camera calibration), therefore it is seriously affected by relative movement between the cameras. However, the satellite marker technique used for the ground truth generation is a monocular depth measurement technique, therefore it is not affected by the bending of the stereo rig that causes a relative displacement between the cameras set.

The obtained results, with the two online recalibrations implemented, were very satisfactory for avoiding the problem of calibration loss. In the dynamic tests of id90, without online recalibration 66% of the measurements were missing, while with online recalibration 100% the measurements were obtained. The example of Table 15 and Table 16 depicted several frames of these test in which the depth stream computed with a static calibration is corrupted (classical stereo vision approach), due to the deformations of the sensor. However, the proposed online recalibration overcomes this problem.

As a final remark, the algorithms employed can be implemented in embedded hardware such as, the Vision Processing Units (VPUs) described in Chapter 4. In particular, the low-power consumption (less than 1.2 Watts) of Myriad 2 processor is very convenient for an industrial implementation of this technique in real-time.

7. Field tests

This chapter contains the results of the remote sensor engineered for the motorcycle safety application. The sensor is targeting a perception system for a conceptual safety system for motorcycles, such as the M-AEB (Motorcycle Autonomous Emergency Braking). The UNIFI (University of Florence) started the development of M-AEB in a previous EU project.

The camera-based remote sensor developed in this research is used to investigate the feasibility of this remote sensing technology to trigger the M-AEB under real traffic and in cornering conditions. In particular, the evaluation use the information of the in-depth accident database In-SAFE to select real PTW crashes that happened. Therefore, a part of the experiments conducted involve similar situations to those that lead to a collision. The assessment of the sensor in these realistic pre-crash conditions have an added value.

7.1. Prior experiences with the M-AEB UNIFI demonstrator

AEB have the potential to assist the user to avoid the collision. In cars, AEB is a well-accepted solution and nowadays commercially available. Years ago UNIFI used an automotive laser-scanner in an instrumented scooter, making it able to brake by itself (Figure 95).



Figure 95. Concept of AEB for cars and M-AEB for motorcycles (UNIFI Demonstrator)

Contrary to cars, the dynamic of PTWs (Powered-Two Wheelers) cannot guarantee that a motorcyclist is able to control the bike against an unexpected deceleration.

The main two reasons are:

- 1) A two-wheeled vehicle is intrinsically (or inherently) unstable.
- 2) The rider is not retained to the vehicle.

These topics were addressed in the EU research project ABRAM, which is summarized in Figure 96. In this EU project, the Monash University of Australia collaborate with UNIFI in the definition of safe thresholds of unexpected deceleration that motorcyclist can manage without loose the control of the vehicle. This human factor is key to identify the real applicability and potential of the M-AEB as a safety solution.



Rider monitoring at unexpected braking of the motorcycle

Figure 96. Investigating the feasibility of M-AEB from the perspective of the motorcyclist

7.1. Current experience with the M-AEB UNIFI demonstrator

To address when to trigger M-AEB in a real traffic scenario, a perception system that can deal with the PTW dynamics is needed. In our motorcycle demonstrator, an automotive laser-scanner to detect obstacles until 60 m, and the camera-based remote sensor explained in Chapter 6 was used. Next, some representative measurements are presented.

7.2. Small moving target from a moving motorcycle

In the next example, illustrated through Figure 97, Figure 98, and Figure 99, it can be seen the results of the measurement of a small obstacle (other scooter).

The camera-based remote sensor measures the scooter at 14 m from the host motorcycle (UNIFI Demonstrator). This was validated with the automotive laser scanner of our motorcycle demonstrator. As a remark, the tailored automotive LIDAR of our motorcycle was able to measure the target distance because the host motorcycle was upright.



Figure 97. This is the left picture of the short-range sensor

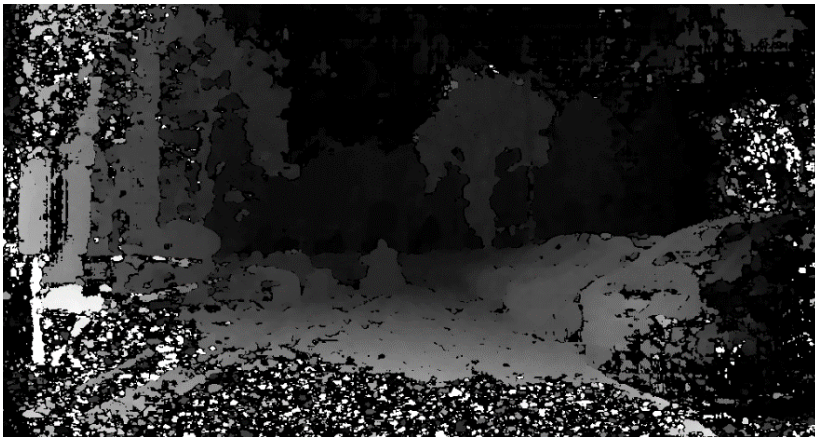


Figure 98. This is the disparity map containing 3D information of the scene

From the information of the remote sensor is possible to compute a tridimensional reconstruction of the scene in which appeared the obstacle. The scooter is located at 14 m from the UNIFI motorcycle demonstrator. This distance was validated with the information provided for the automotive laser-scanner of our demonstrator which was able to operate properly in this particular condition.

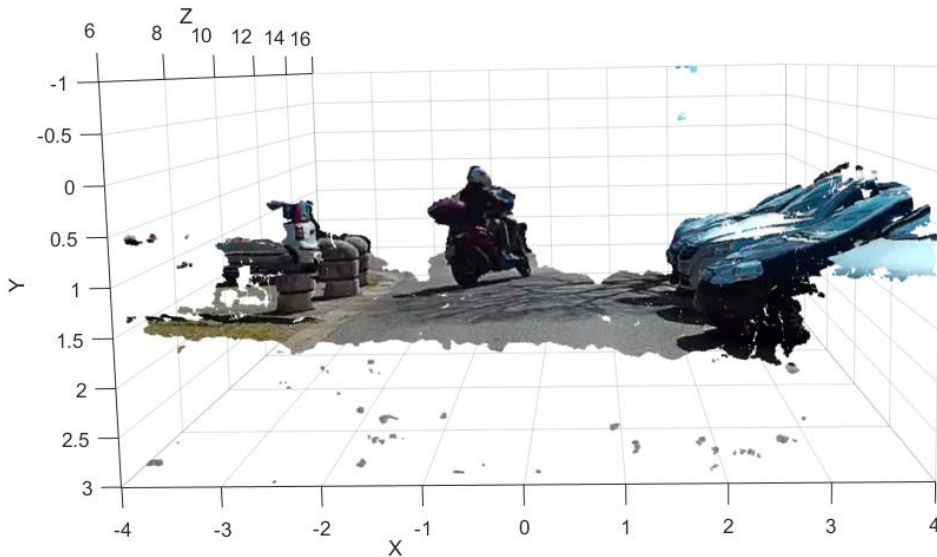


Figure 99. 3D point cloud showing that the scooter is located at 14 meters from the motorcycle demonstrator

7.3. Turning maneuver at an intersection

The following results correspond to the case in which the UNIFI demonstrator is executing a turning maneuver at an intersection. In this situation the scooter is tilted more than 13 degrees, excluding the successful use of traditional automotive remote sensing sensors (details in Chapter 5 – Sections 5.3.2 and 5.3.4).

Figure 100 shows the traffic scene sensed by the short- and long-range sensor and the associated DMs. With regards to the parked cars visible in the scene, which did not move throughout the experiment, the measurements in repeated trials presented similar information. This condition allowed us to compute similar depth measurements of the static scene.

Both DMs depicted in the figure show the accurate measurement of the ground surface. This can be interpreted with an elevation map technique (e.g. the 2.5D boxel approach to simplify the 3D point cloud data density) employed in off-road vehicles. This approach has been used to define the ground plane ahead of the vehicle (Rankin et al., 2009; Broggi et al., 2013a) and from that, the Region of Interest (RoI) for the subsequent analysis. Other approaches used in autonomous cars (Oniga and Nedeveschi, 2010; Harms et al., 2015) cannot be applied to tilting vehicles because the assumption of a road plane almost parallel to the stereo sensor.

In the short-range sensor (the shorter baseline of the stereo camera rig), the fisheye lenses used embraced the light coming from a wide volume of the 3D space into the imaging sensors. Consequently, the maximum value of the disparity becomes big. In Figure 100c DMs were represented using a color scale of 32d instead of 128d to highlight the presence of a car (car 4) that was not visible in the long range view. In addition, the different range values

contained in the DMs are consistent with the type of lenses and baselines employed for the short- and long-range sensing, respectively.

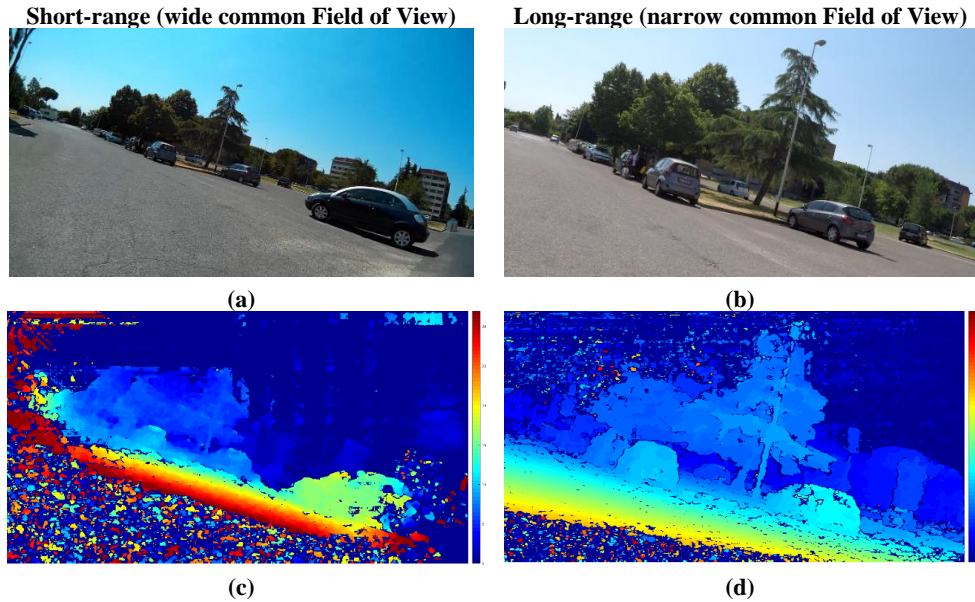


Figure 100. Analysis of a turning maneuver: measurement of the space in front of the scooter. Short-range and long-range measurements are depicted simultaneously for comparison. (a) Rectified left picture of the short range stereo camera sensor. (b) Rectified left picture of the long range stereo camera sensor. (c) Short-range Disparity Map (0 to 32d). (d) Long-range Disparity Map (0 to 128d). The 3D point cloud is available for download (see Section 6.2.2.1)

In the long-range sensor, the more directional type of lenses (narrow FoV) and longer baseline of the stereo camera rig produced a smaller range of values of the disparities. This is a consequence of measuring a smaller part of the 3D space with an imager of the same size, thus providing more depth discrimination of the 3D space.

Figure 101a shows the 3D point cloud of the 4 target cars measured by the short-range sensor (manually labelled). In Figure 101b shows the long-range sensor measures of the same scene. Only 3 of the previous target cars are visible, because of the narrower FoV of this sensor. In addition to this, it is worth noticing the tail of an additional car visible behind the trees at the boundary of the Range Field (Figure 100, Figure 101, and Figure 102).

In Figure 101 the depth measurement performed for the imaging system (short- and long-range) are presented in more detail. In both measurements cars 1, 2, and 3 can be identified. However, only the depth measure delivered by the long-range sensor (Figure 101b) is reliable. In fact, these cars were visible in both sensors, but they were located inside the Range Field of the long-range sensor only. As mentioned before, the condition that the targets are inside the boundaries for the triangulation (horopter of 10 disparities) ensures the possibility to neglect the influence of the non-Gaussian error in the DM. Otherwise, such error should be taken into account for proper depth triangulation (Sibley et al., 2007).

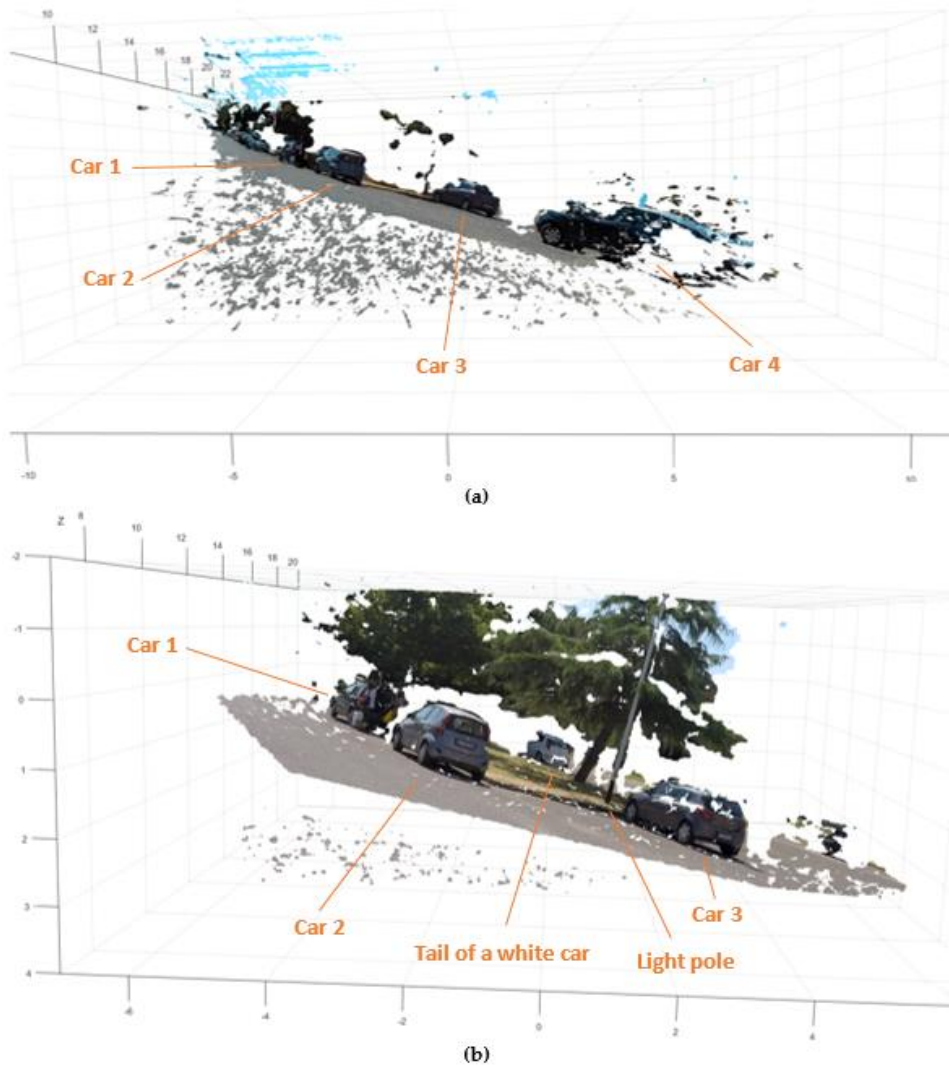


Figure 101. 3D point clouds corresponding to the turning maneuver scene calculated from the information provided by the two stereo camera sensors. (a) Reconstruction for the short-range stereo camera (wide common Field of View). (b) Reconstruction for the long-range stereo camera (narrow common Field of View)

Considering Figure 102a, car 4 is properly sensed due to the wide common FoV of the short-range sensor. Additionally, in the same figure artifacts are present outside the Field Range, in the low values of disparities. At very low disparity values, the erroneous matchings of the SGM (Semi-Global Matching algorithm) (Hirschmuller, 2005) generates fattening, which is a matching error amplified by the depth discretization for the pixel accuracy resolution (including subpixel accuracy). Fattening are common artifacts in outdoor stereo

vision, and post-processing approaches that remove them in 3D mapping applications are not a real-time task.

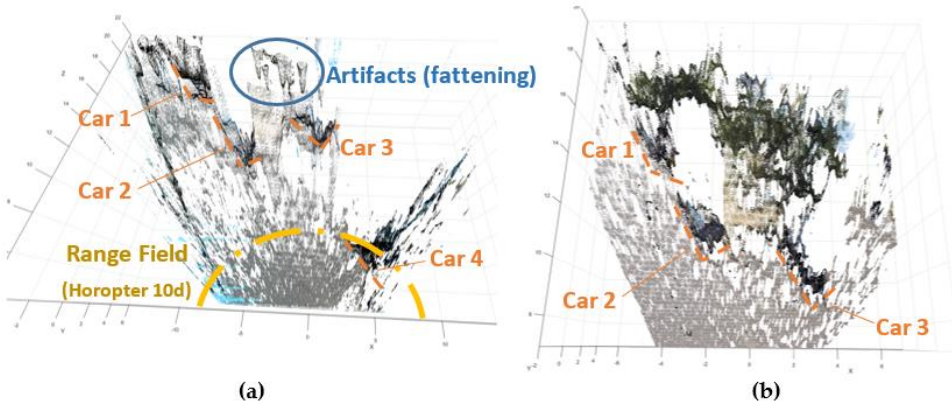


Figure 102. Top view of the 3D point clouds corresponding to the turning maneuver. (a) Depth measurement delivered by the short range sensor (accurate depth measures are inside the Range Field). (b) Depth measures delivered by the long range sensor (Car 4 is not in the common Field of View of this stereo camera sensor)

Note: the 3D point clouds presented until now contain all the raw data measurements retrieved from the stereo cameras. However, certain details are difficult to assess the 3D measurements. Therefore, in order to simplify the assessment of the quality of the measures corresponding to the long-range sensor, I “cleaned up” the 3D point cloud. The cleaning process consisted in two steps:

- To post process the three-dimensional representation by removing the 13 degrees of inclination of the scene without altering the quality of the 3D reconstruction.
- To extract the points that lies outside of a Region of Interest (RoI).

In this manner, I extracted and inspected a RoI above the ground plane as it can be seen in Figure 103a, where the detection of a narrow object (light pole) is highlighted.

In Figure 103b the top view of the clean imaged scene is presented, with the reference to the vehicles and the light pole location.

The results presented in Figure 103 illustrate the measurement capability of the sensor to measure the sides of the parked vehicles, even under large inclination of the sensor (13 degrees), where other automotive remote sensor technologies cannot deal with it, as was stated in Chapter 5. This capability of the proposed remote sensing approach enables the utilization of the obstacle detection, tracking, and depth perception during the normal operation of a tilting vehicle.

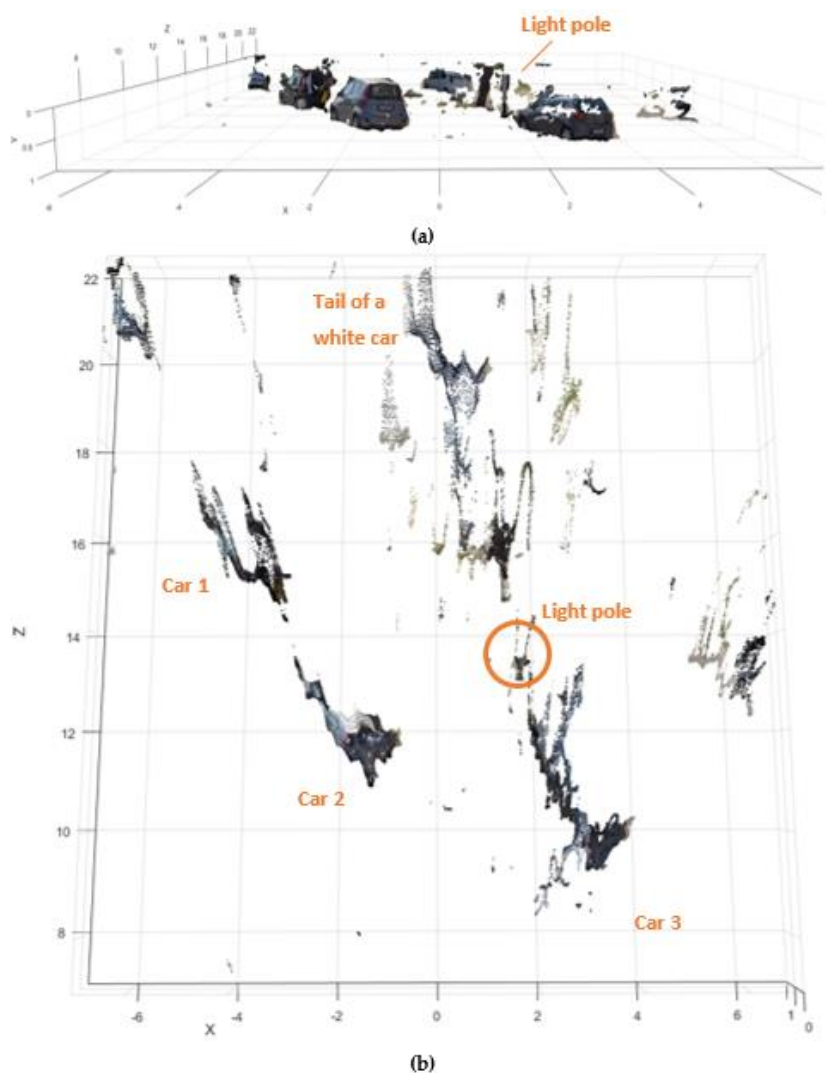


Figure 103. Cleaned measurements of the corresponding to the turning maneuver. (a) The 3D point cloud inclined 13° to compensate the leaning of the scooter. (b) Top view of the measures

7.4. Pre-crash test (based on a real motorcycle crash)

This section describes the performance of the camera-based sensor in a real crash scenario. The description is organized in three sub-sections: 1) the analysis of a real crash event; 2) the virtual simulation of this crash when the M-AEB is activated, and before (pre-crash scenario); and 3) the results of the camera-based sensor during the emulation of the motorcycle crash id90.

7.4.1. Real motorcycle crash and the results of the crash reconstruction analysis

An accident that occurred under conditions of good visibility (daylight), and dry and flat asphalt surface has been considered in this study. In the accident, a stopped car made a U-turn from the right lane, crossing the path of an oncoming motorcycle. The motorcyclist activated the brakes hardy, but he/she lost the control of the motorcycle. At this moment, the motorcycle and its rider fall and slide on the pavement until they hit the car.

Figure 104 shows a top view of the accident scenario indicating different landmarks of the scene and the point of rest of the car (after the collision). The motorcycle landmarks “+” of our interest are represented for the labels 6 to 11. References +6 and +7 defines the segment of the road in which skid marks shown a hard braking performed by the motorcyclist before he/she lose the control and consequently fall down from the motorcycle. The range from +8 to +11 defines two segments that corresponds to scratches on the road caused by the sliding of the motorcycle up to the collision with the car (in the red box area).

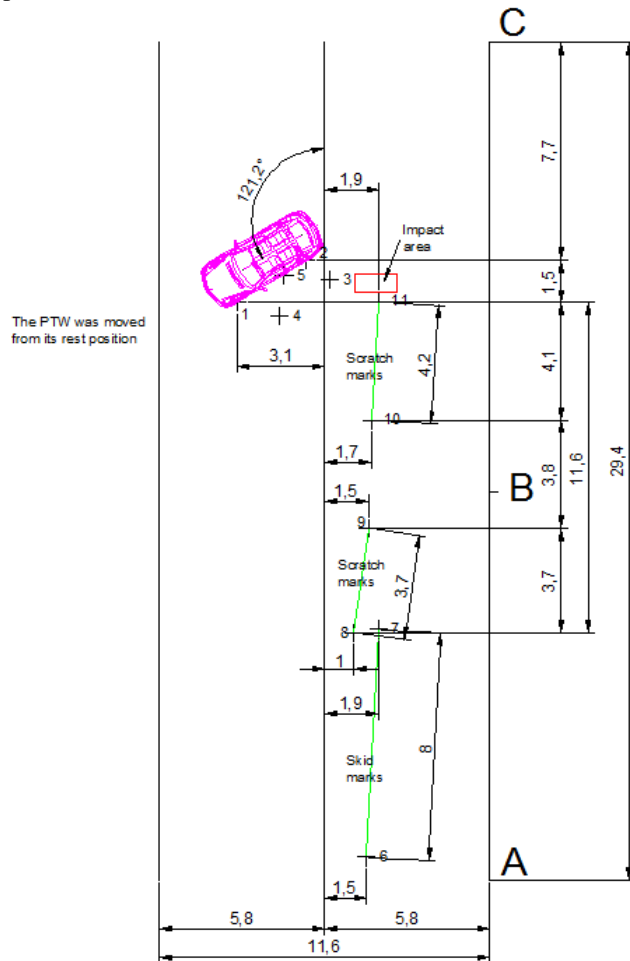


Figure 104. Sketch of the motorcycle crash id90.

Figure 105 shows the critical moments of the pre-crash phase, which was modeled (using Virtual Crash software) as the other crashes of the in-depth database described in (Piantini et al., 2012; Franci et al., 2015). These events occurred in a Time-To-Collision (TTC) of 1.50 s and 1.00 s. At TTC=1.50 s the motorcyclist still continues travelling without braking, and half second later (at TTC=1.00 s) the motorcyclist braked hard and lost the control of the vehicle due to the locking up of the front wheel.

Note: an Anti-lock Braking System (ABS) in the motorcycle could have helped to avoid this PTW crash.

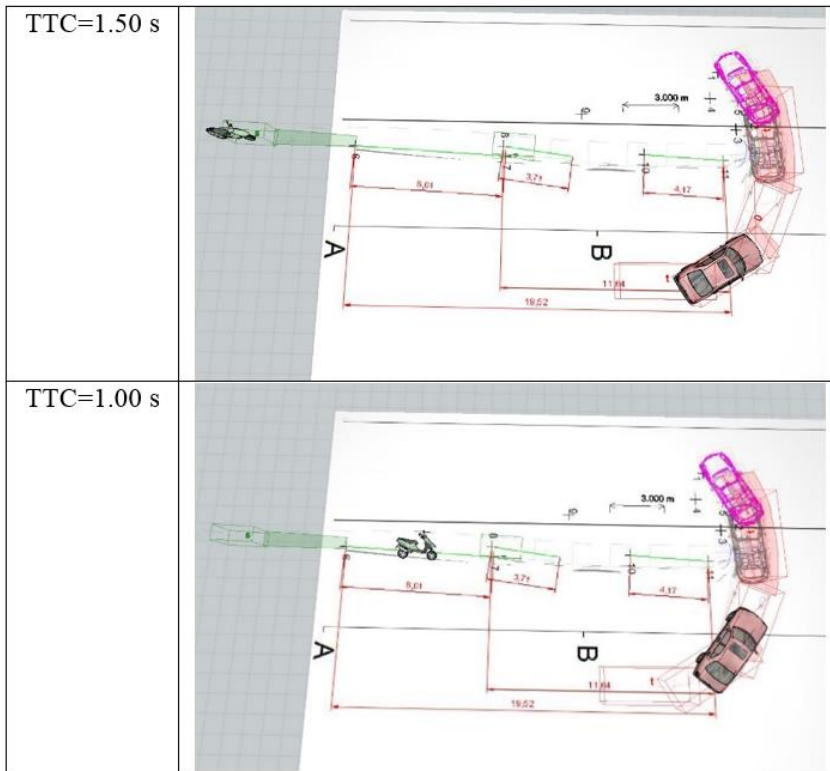


Figure 105. Visual results of the 3D crash reconstruction for two instants of time before the crash.

7.4.2. Virtual simulation of the crash before to M-AEB deployment

Based on the in-depth information provided by the crash reconstruction, a simplified kinematic of the crash scenario is performed under the assumption of ABS (Matlab/Simulink software). Then, a co-simulation (BikeSim software) calculate the dynamics of the motorcycle or Powered-Two-Wheeler (PTW) while simulate the action of the M-AEB (remark: M-AEB requires the use of ABS). The same approach served to quantify the effectiveness of M-AEB using real crash circumstances as in (Savino et al., 2012b, 2013, 2014) .

The crash simulation up to the instant of Inevitable Collision State (ICS defined in Savino et al., 2016), in which the remote sensor must trigger the M-AEB, is presented. In addition, the information of the instants previous to ICS were collected and analyzed, to

establish if our sensing system can be used to activate other faster safety systems (that require an earlier deployment than M-AEB) such as, airbag jackets, or the AEB in the opposite car through Vehicle-to-Vehicle (V2V) communication.

Figure 106 shows the curves of the real and simulated cases for the instantaneous speed and acceleration of the motorcycle or PTW and passenger car, as a function of time. In the curve of real case, the motorcycle braking was activated at the time of 2 seconds, and the sliding phase occurred at the time of 2.5 seconds. In the curve of simulated case, the hard braking was maintained for more than 1.5 seconds, until ICS. This assumption is based in the intervention of the ABS (acceleration -6.622 m/s^2), which assists to the motorcyclist to keep the control of the motorcycle to brake in straight line. The assumption reduces the speed of the motorcycle at the ICS, which occurs beyond 3.5 seconds.

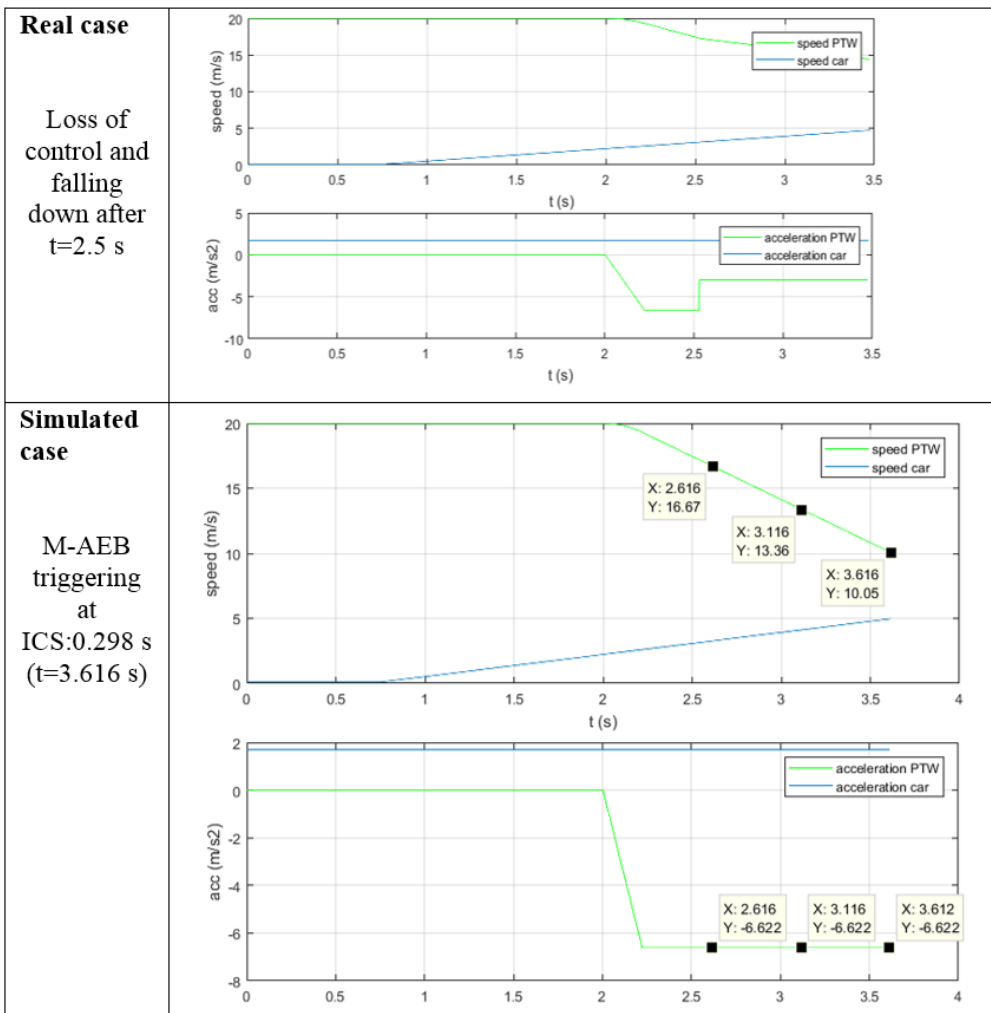


Figure 106. Speed and acceleration evolutions before crashing (id90). Real case (top) in which the motorcyclist loss the control of the PTW during a hard braking. Simulated case (bottom) in which is supposed that the motorcyclist can handle the braking action due to ABS intervention.

The deceleration caused by the hard braking (assumed in -6.622 m/s^2) is coherent with the average deceleration reported for motorcycle ABS, with a maximum value of -7.5 m/s^2 only obtained by professional riders (Vavryn and Winkelbauer, 2004).

The Figure 107 shows the relative orientations and locations of the vehicles during the pre-crash phase. As it was indicated in the below charts of Figure 106, the times corresponds to 1.0 and 0.5 seconds before the ICS and the ICS itself. In the kinematic simulation both vehicles are referred to their centers. Therefore, a compensation is needed to compare $d(t)$ distance against the measurement from the remote sensor in the PTW (installed in the front of it) to the sides of the car.

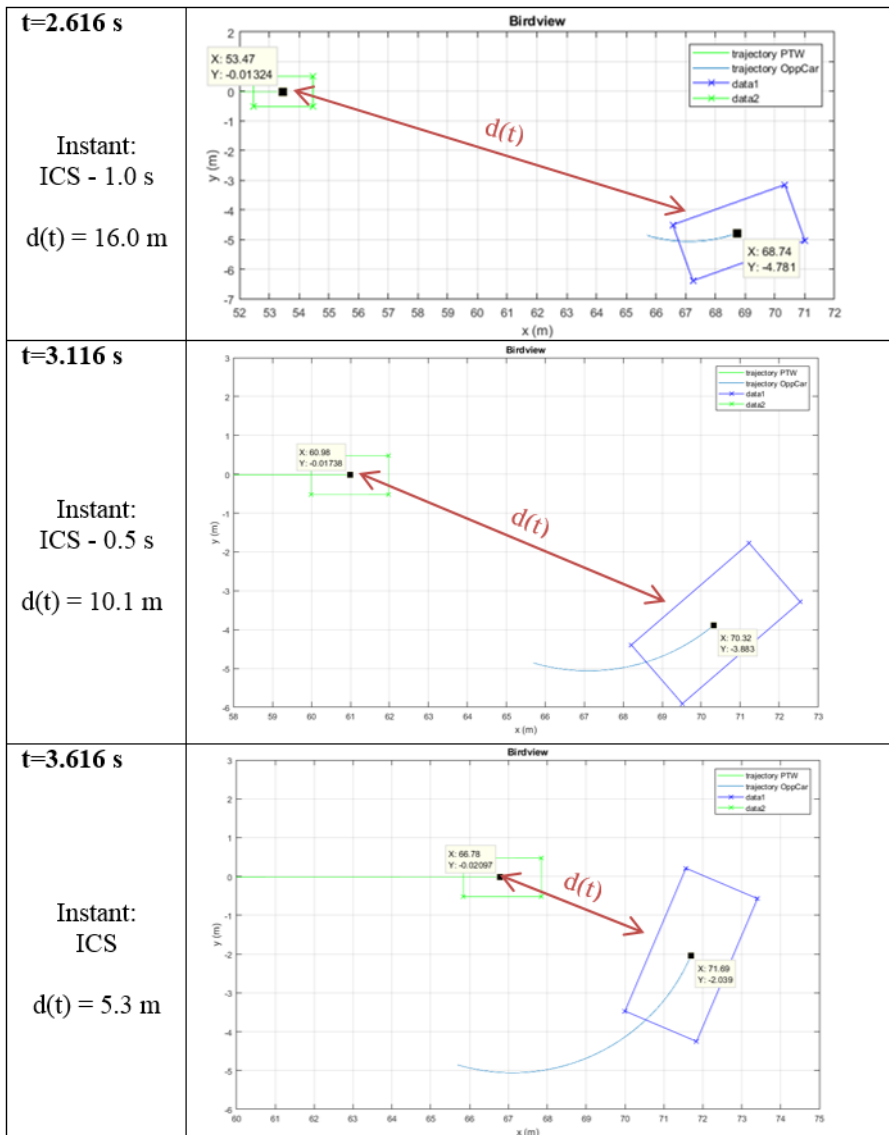


Figure 107. Relative orientations and locations between the PTW and the Opposite Car (id90).

7.4.3. Crash emulation: on road test or pre-crash test

For the study of pre-crash condition, I adopted the methodology of (Savino et al., 2017) for computing accurate triggering for Advanced Rider Assistance System (ARAS). This methodology involves a series of tests in real traffic, which was approved by the ethical committee of UNIFI (University of Florence).

This test emulated one particular real-world motorcycle crash (id90) and assess the capabilities of our camera-based remote sensor to sense the conditions of the traffic scene in the neighborhood of the point where the collision became inevitable. In particular, the experiment consisted in remotely measuring the distance and orientation of the opponent vehicle (a passenger car) from the sensors in the scooter. As shown in Figure 108a, the reference point of the deployment M-AEB was marked as X-white on the road, for visual helping. This point corresponds to the location of the scooter at the ICS (Figure 107). The test was designed and executed so that, when the scooter was located at this point the opponent car was located and oriented as it was in the real crash (when the collision became inevitable).

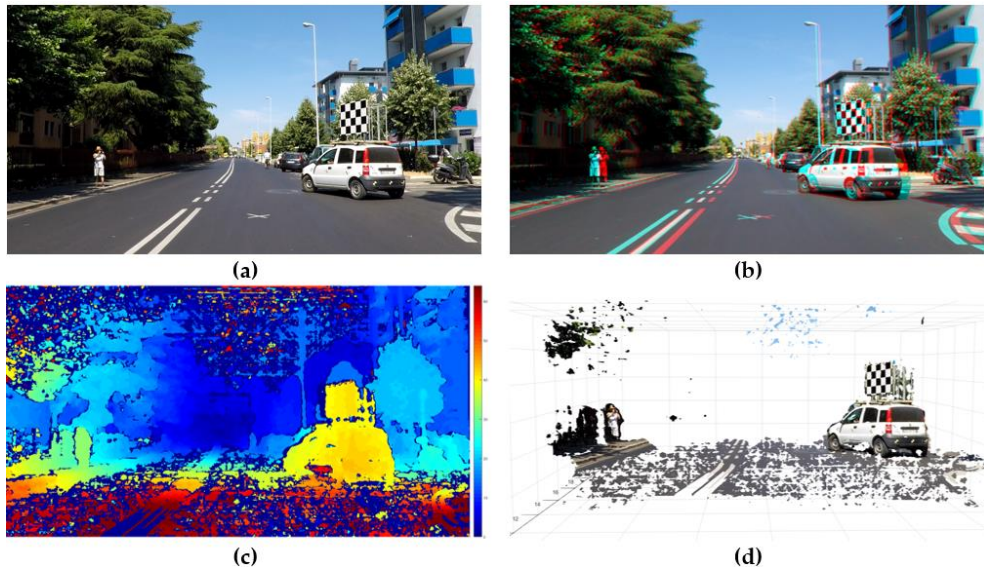


Figure 108. Analysis of the pre-crash scene (id90 – InSAFE). (a) Rectified left picture of the long range stereo camera sensor. (b) The 3D anaglyph composed by the stereo frame. (c) Disparity Map (0 to 64d). (d) 3D reconstruction

To reproduce the crash properly, the test of was repeated several times. Five test results were chosen, which are coherent with the D-GPS data.

During the experiments of the pre-crash test (id90 - Figure 108), the capability of the camera-based remote sensor for 3D measurement of the traffic scene was analyzed. The assessment of the capability of sensing the traffic scene started from 1 second before the ICS.

This 1 second before ICS was considered by:

- The information of the crash reconstruction and the corresponding simulation results, shown in Figure 107.
- The depth resolution required for M-AEB to avoid false positive deployments, which is of 20 cm. The sensor achieved this until 16 meters (see Chapter 6 - Section 6.2.4).

In the 3D anaglyph of Figure 108b, the remote sensor is slightly tilted with respect to the road plane, as it can be seen from the small vertical shifting of the features in the scene. For example, the vertical pixel misalignment in the stereo frame is noticeable in the “x” marking on the road, or in the corners of the asphalt marks located at the bottom right corner of the picture.

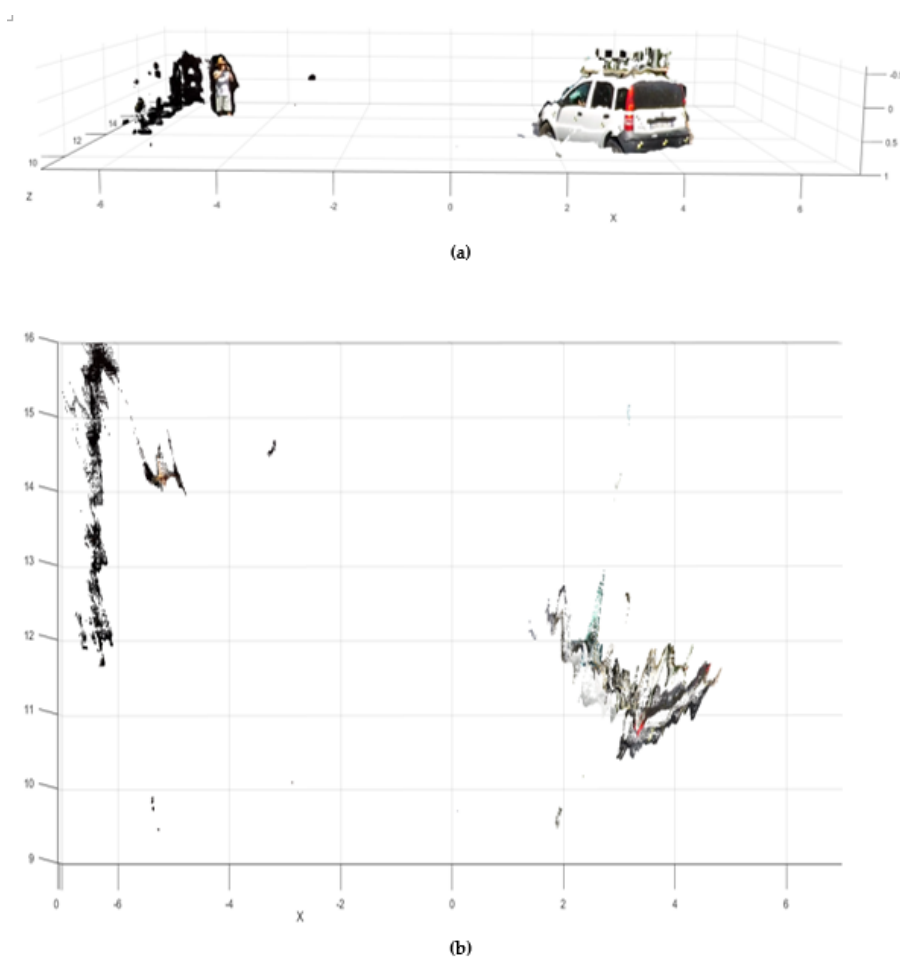


Figure 109. Detail of 3D reconstruction of the pre-crash scene (id90 – In-SAFE). (a) Cleaned 3D point cloud seen from the scooter point-of-view. (b) Cleaned top view representation of the pre-crash scene

The results shown (Figure 108c, Figure 108d) indicated that the stereo camera sensor was able to accurately sense the condition of the traffic scene 1 second before the ICS. In addition, the sensing approach is able to detect narrow obstacles including Vulnerable Road Users (VRUs), which is a challenging task for other automotive remote sensors. In this case, a pedestrian was measured along the left sidewalk.

A clean 3D point cloud (extracting only the information from above the street up to several centimeters above the roof of the target cars) is shown in Figure 109. It can be seen that part of the supporting frame of the satellite marker appears in the reconstruction. These results showed that the remote sensing strategy is able to measure the car pose and narrow obstacles in real conditions even in the presence of roll angle fluctuations (Figure 110), that also can affect the operation of other automotive sensors as the LIDAR.

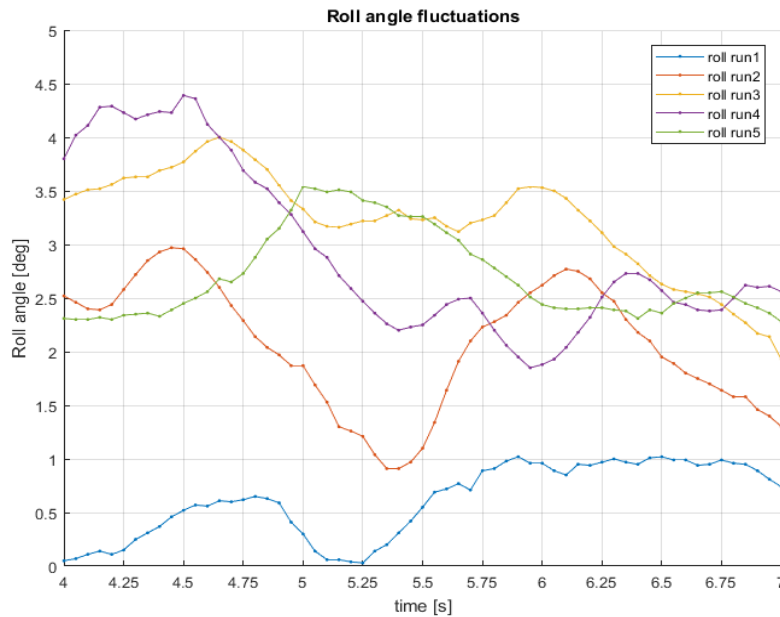


Figure 110. Roll angle fluctuations during 5 trials of the emulation of the motorcycle crash (id90 – In-SAFE)

The temporal chart (Figure 110) illustrates the roll angle fluctuations due to the dynamics of a tilting vehicle when traveling straight (note that the traveling surface is a flat asphalt).

7.5. The experience employing the camera-based remote sensor in a pedelec

As a proof-of-concept, a simplified version (shown in Figure 111) of the camera-based remote sensor was installed in a pedelec (electric bicycle). The objective of these test was to assess the sensor in a different vehicle and in cycling traffic.

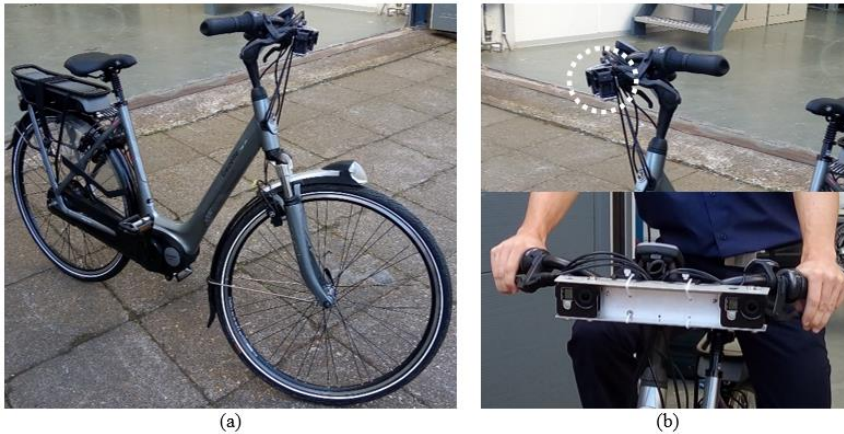


Figure 111. Pedelec with the stereo camera rig installed on the handle bar. (a) Complete vehicle view and detail of the frontal suspension. (b) Detail of the camera-based remote sensor (imaging system)

The results presented in Figure 112 and Figure 113 correspond to traffic situations in which the tilting vehicle (pedelec) presents a roll angle about 22° and 17° respectively. Figure 112a shows one of the images of the stereo frame which are used to calculate the Disparity Map (Figure 112b). The maximum value of the disparity range allows to start to perform triangulation from 4 meters, for this stereo rig setup.

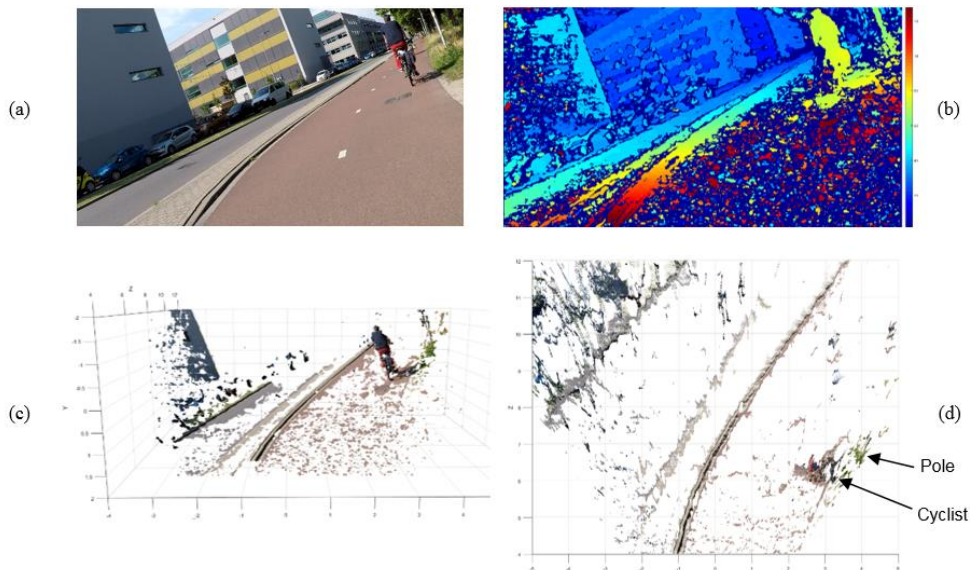


Figure 112. Results of the remote sensor while taking a curve (pedelec tilted 22°). (a) Left image of the stereo camera pair. (b) Disparity Map calculation (0 to 128 disparities). (c) 3D measurement of the scene up to 14 m. (d) Top view of the 3D scene

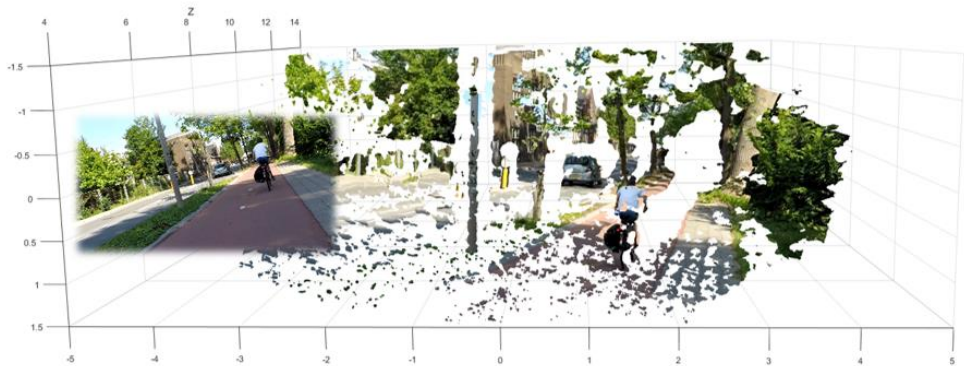


Figure 113. Results of the remote sensor when traveling on a bicycle path (pedelec tilted 17°). In this case the 3D point cloud was mathematically rotated (straighten) to easy the depth inspection in the 3D reconstruction. All units are in meters

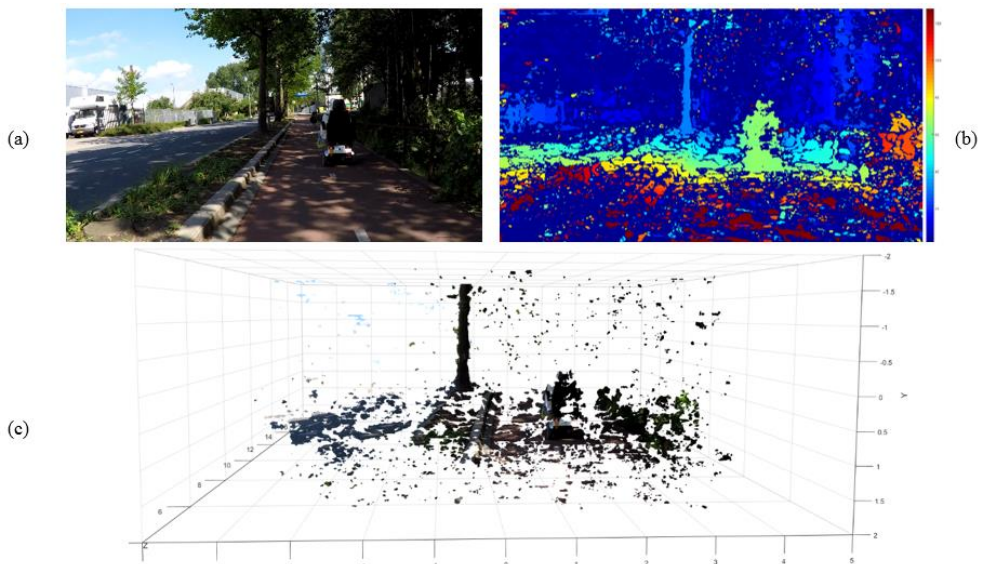


Figure 114. 3D sensing in a scene with strong changes of illumination. (a) Left image of the stereo camera pair. (b) Disparity Map calculation (0 to 128 disparities). (c) 3D measurement of the scene in meters

The Figure 112d shows the top view of the 3D reconstruction, which makes explicit the capability of the sensor to obtain the depth of the scene.

Figure 114 shows a traffic scene with strong changes in the illumination. This type of situations have not proven to be a problem for the Semi-Global Matching (SGM) algorithm adopted (Hirschmuller, 2005; Hirschmuller and Gehrig, 2009). The test were realized against

a prior histogram equalization of the same stereo frames that presents abrupt illumination changes and not improvement in the Disparity Map (DM) was found.

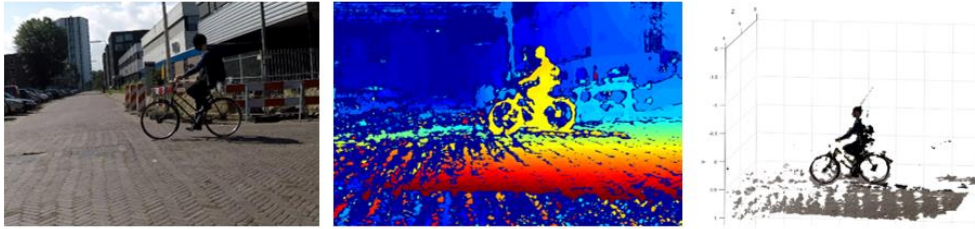


Figure 115. 3D sensing of a cyclist at an intersection of streets (cobblestone street – thick patterned surface)

Finally, the results presented in Figure 115 were acquired when the vehicle traveled by a cobblestone street. This is the most challenging situation for the remote sensor because the sensor accuracy is compromised under important deformations on the stereo rig.

7.6. Conclusions

The camera-based remote sensor was used to determine the feasibility of triggering a conceptual motorcycle safety system (M-AEB) under real traffic and in cornering conditions. Special attention was given to the operation of the sensor under fluctuations of the roll angle because these fluctuations are present in the PTW dynamics, even when the vehicle is traveling straight and over a flat asphalt. This roll angle fluctuations translated into inexistent lateral accelerations of detected obstacles in other sensors, such as automotive LIDARs and RADARs, which negatively affects their measurement accuracy and object tracking capabilities.

The field test extends the results of Chapter 6, assessing the remote sensor in real traffic scenarios similar to PTW crashes that happened (In-SAFE crash id90). The sensor was able to measure the distance to the opposite car within the grid of 20 cm required by M-AEB during the pre-crash phase (one second before arriving to the instant of inevitable collision avoidance). The raw data obtained from the sensor and the processed results are available as a part of an online dataset (Section 6.2.6.1). In the future, this dataset will include more PTW crash scenarios based on the emulation of real crashes, which are needed for a better understanding of the limitations that the sensor can present as a part of a safety system for motorcycles.

Additionally, the operation of the remote sensor was analyzed in two different tilting vehicles when cornering. The sensor operates properly under roll angles of 13 degrees in the UNIFI demonstrator. A simplified version of the same sensor was installed in a pedelec, and it was able to measure the 3D environment up to 22 degrees of roll angle. The operation of the developed sensor overpassed the 10 degrees of roll angle achieved for other remote sensors for motorcycles (Savino et al., 2009, 2013), this is important because the sensor presents a good potential for the application in tilting vehicles.

In comparison, the experiments using the pedelec were not exhaustive as the ones carried out with the scooter (UNIFI demonstrator), because the stereo rig was not designed for this vehicle. The objective was to achieve bigger roll angles than in the scooter, in a safe manner. The precision accuracy seems to be similar to the scooter setup but in a shorter range, however a more extended test campaign with it would be needed to verify this statement. On the other hand, we can report that the level of vibrations in the stereo rig is considerably more intense in the pedelec setup. Mainly for the front fork assembly and the tire size difference between the vehicles. This is an important aspect to consider for commercial applications. Extensive multibody simulations and/or road tests on pedelecs can be needed to understand the limitations or requirements for the online calibration on these type of vehicles.

8. Discussion

This chapter discusses the limitations of the different core studies realized during the doctoral research, possible improvements and future actions. The future actions concerns tasks to be done after the period of time corresponding to this doctoral research.

The future actions are related to a bigger research scope concerning the development of the advanced safety system called Motorcycle Autonomous Emergency Braking (M-AEB). This safety system is one of the possible applications that can benefit from the research presented in this dissertation.

8.1. First part: the KBMS methodology

The use of Powered Two-Wheelers (PTWs) is high in Italy compared to the rest of Europe (Ordonez, 2016; Schaller and Perlot, 2016). PTW rider fatalities are high as well, 34% on the total road deaths in 2008 versus 19% of the mean in Europe (IRTAD 2010). However, in motorcycle safety the main constraint is the subjectivity of certain analysis due to the variability in the dynamics of the PTWs, the nature of the information and the judgments being made, as well as the methodology adopted. In order to overcome the difficulties, I propose the KBMS (Knowledge-Based system of Motorcycle Safety) as a constructive, flexible, and scalable methodology.

- Why constructive? Additional experts' contributions for the assessment of crash scenarios will lead to more accurate predictions about the solution's performance.
- Why flexible? The Evaluation Framework allows the reorganization of crash scenarios and the modification of the inference engine according to the crash data available.
- Why scalable? The Evaluation Framework also allows the addition of new crash scenarios, new Safety Functions, and new objectives as: injury criteria, medical fares, convalescence days, etc.

The KBMS was conceived to be updated (using fresh crash statistical data) and reused in the course of time. Another advantage of this method is the step of information extraction

from crash databases, which allows for confidentiality of the original crash data, and the collaborative sharing of data will be made easier.

To the best of my knowledge, the safety system prioritization performed in the PISa project was the most comprehensive in terms of safety systems evaluated focused on motorcycle technologies. Thoroughly analyzing the documentation of the PISa project, I found no distinction between Safety Function (SF) and safety system/technology. Consequently, during the assessment phase experts were requested to evaluate the functionality of a safety solution or the performance of a specific technology without any distinctions between the potential benefits of a theoretical function and those of a practical system. Assessing how a technology may behave in a given circumstance requires more accurate information than the evaluation of a specific functionality (a specific Safety Function in our case), because functionalities just define desired behaviors. For this reason, in our study I made the concept of Safety Function (SF) explicit in the KBMS method. However, the PISa rating process was a valuable step in the prioritization of safety solutions for PTWs and a good material to design a new methodology that overcome its weak points.

Concerning the road crash scenarios, previous EU research projects have used the 7 PTW crash scenarios defined in the APROSYS project as starting point (e.g. PReVENT, AIDE, EASIS, GST). However, 3 of the 7 crash scenarios concentrate less than 10% of total of motorcycle crashes in the EU. This implies that more than 90% of PTW crashes (a wide variety of crash configurations) were grouped together in only 4 general crash scenarios. To address this limitation, the definition of the PTWs crashes scenarios of the KBMS Evaluation Framework contains 26 cases (Appendix B) that can be grouped in function of the level of detail of the crash database used.

The KBMS introduces the concept of coverage metric. This helps to ensure a minimum of 90% of total motorcycle crashes included in the crash scenarios defined, monitoring the remaining percentage of road crashes that contains incomplete/unknown data.

An advantage of the KBMS method is the direct interpretation of the metric obtained. For example, the PISa priority list made clear which SF is more important, but it did not clarify the absolute importance of a function in quantitative terms. In the KBMS, the insight of how important a SF is with respect to the others is made explicit by its numerical value. For example in our case study, by simple numerical inspection of the metrics of the prioritized list (Table 8), was obtained that the SF “PTW autonomous-braking (2.98)” is considered twice as important as the SF “Improvement of PTW conspicuity (1.42)” in Italian roads. It shall be noted that low income countries with poor infrastructure, outdated vehicles, and limited safety awareness will see different priorities. The new method can be applied to such other countries when crash data is provided.

Summarizing the benefits of the KBMS Evaluation Framework, it overcomes common limitations as: heterogeneous road crash data collection between different countries/regions; and restricted access to the databases due to sensible information about the victims involved. In particular, the segmentation of a road crash database by using queries list can be easily replicated locally to several databases, enabling database managers to disseminate harmonized numerical information for the KBMS method.

The key points learned during our preliminary attempt to collecting and storing expertise in the KB of the KBMS were:

1. Define a common vocabulary simplifying the exchange between experts of different specializations.

2. In the expert assessment it is hardly recommendable to use a binary Likert type scale in order to avoid the accumulation of neutral responses in the KB.
3. Define a set of guidelines based on facts of in-depth crash databases to reduce the degree of variability of the assessment in the crash scenarios.
4. A very comprehensive list of SFs for the expert assessment, present the drawback to convert the evaluation of each crash scenario in a big time consuming task, and it may go against to the number of collaborators.

For this reason, more research is needed in the definition of a shorter SFs list to assess. The reduction of the SF list is a trade-off between the quality of expertise collected and the time required to encode it in order to be stored in the KB of the KBMS.

8.2. Second part: the remote sensor

The goal of the second part of the research activity was to contribute to making motorcycling safer by fostering the implementation of assistance technology. However, technological limitation on automotive remote sensors was identified and stated in Chapter 5, for which these sensors cannot operate on a tilting vehicle. To overcome this technological barrier I proposed an approach that utilizes camera-based sensors. These sensors resulted suitable for the task thanks to their wide diagonal FoV (Field of View) and additional desirable features, such as resolution, lightweight, passive (does not increase electromagnetic pollution), low consumption and affordable cost.

In this manner, I targeted the development of a novel multi-focal stereo camera sensor to provide a remote sensing sensor able to operate under the constraints imposed by the motorcycle dynamics. In motorcycles, simple change lane and traffic filtering tasks requires a counter steering maneuver and roll angles up to ± 10 degrees. This vehicle dynamics is completely inexistent in four-wheeled vehicles. In addition, when a motorcyclist negotiates a curve the circumstances, such as layout of the road, current traveling speed, other vehicles in the street, and rider skills among others, may require that the motorcycle exceed the ± 10 degrees of roll angle mentioned before.

The importance of the technological sensing solution proposed relies on the potential to bridge the technological gap that causes the existing lack of rider assistance technologies for tilting vehicles. An example of application of sensing technologies for improved safety of motorcycles was provided with the emulation of a real motorcycle crash, as described here and in (Savino et al., 2017). These tests conducted in real traffic conditions are part of the assessment of our remote sensor for the possible application in future ARAS (Advanced Rider Assistance Systems), for example a motorcycle application of Autonomous Emergency Braking (the so-called M-AEB).

In a camera-based perception system, the quality of the camera sensor is essential. The proliferation of mobile phones with camera sensors during the last decade, reinvent the way in which camera sensors work, as well as their performances. A proof of that is the ongoing standardization of the camera sensors for the automotive industry (Standard for Automotive System Image Quality - IEEE Project 2020), which started to work over the advanced draft of the current IEEE P1858 Standard for Camera Phone Image Quality. For related information, an overview of the image quality test for phone cameras is presented in (Jin et al., 2017).

Another important consideration is that the image sensor manufacturing technology is well below its limits. Image sensors use CMOS technologies that are at least 2 generations behind those of solid-state memories or digital integrated circuits. Thus, in the next few years several innovations in camera sensors are likely to take place. In particular, HDR imagers (High Dynamic Range camera sensors) are showing impressive capabilities using inexpensive technology (Kobayashi et al., 2017). Recent low-cost imagers feature a combination of RGB+IR (color and infrared) with controllable IR sensitivity (Machida et al., 2017). This will make night vision cameras ubiquitous.

On the stereo algorithms side, the algorithms can calculate disparities in regions where there are no specularities or occlusions. In regions with low contrast or with high sensor noise, most implementations have difficulties. However, specific implementations allow 3D perception also in adverse weather like rain (Gehrig et al., 2013; Pfeiffer et al., 2013; Scharwächter, 2013). This result can be achieved by exploiting stereo confidence clues based in a probabilistic implementation (a Bayesian manner) of scene and temporal priors (prior knowledge of scene instants before) for the improvement of the stereo matching.

In addition, stereo cameras allow the discrimination of water on the road (possible slippery surfaces) by polarization light filters installed in each camera and machine-learning methods (Iqbal et al., 2009; Kim et al., 2016). Another application for the detection of small road hazards was recently implemented by combining geometrical modeling and deep learning in autonomous cars context (Ramos et al., 2017). For further improvement, machine-learning researchers are also combining the visual information with the Disparity Map of stereo vision systems for an alternative three-dimensional understanding (Zbontar and LeCun, 2015; Poggi et al., 2017).

In our experiments, the performance of the sensor developed employing low-cost action cameras was satisfactory in a static setup. The sensor showed good potential for the application in advanced motorcycle safety systems as it was able to measure small targets sized 30 cm of height (traffic cones) from a distance up to 21 meters and road curbs during the test in the traffic scenarios. This sensing capabilities are promising for motorcycle safety application, for which unexpected small obstacles in the travelling path or occasional slippery surfaces can cause serious consequences to the motorcyclist (destabilization, crashing and falling).

In this section several promising state-of-the-art solutions that include machine-learning techniques are mentioned. These technics requires an intensive computational power that consumes significant amounts of energy that will not be available in tilting vehicles. Fortunately, recent embedded neural computers designed in a single chip (ASIC: Application-Specific Integrated Circuit), provide the capability to deploy certain Deep Neural Networks (DNNs) with a power consumption inferior to 1.2 watts.

Other relevant aspect is that these ASICs have a Vision Processing Unit (VPU) to process camera data in real-time. This is important because all the algorithms used in the on-line re-calibration can be implemented in VPUs. These new chips and the upcoming improvements in camera sensors are promising technologies to make remote sensors camera-based, such as the one developed in this research for motorcycle safety application.

Conclusions and Outlook

In the context of a continuous growth of the world population in the 21st century, smart tilting vehicles have a great potential as the future non-autonomous personal means of transport in congested urban areas. As tilting vehicles are, low price, small-size (optimized use of public spaces for parking), and have potential for fuel economy, recyclability and electrification, they are very recommendable for vehicle owners or vehicle sharing services.

Regrettably, the injury severity level in case of crashes is the biggest barrier for the societal adoption of tilting vehicles. To change it, this dissertation focused on the development of a safety system to anticipate possible crashes from a tilting vehicle. Research in the automotive industry is supporting the feasibility of the development of preventive safety systems. For example, the case studies concerning Autonomous Emergency Braking (AEB) systems in cars provides a solid foundation to preventive safety in tilting vehicles. Consequently, aiming to achieve safer mobility in tilting vehicles, effective preventive safety approaches need to be identified and cost-effective technologies must allow the development of corresponding safety systems.

The recapitulation of the main contributions of this dissertation are:

1. The creation of the first Knowledge-Based System for Motorcycle Safety (KBMS), which is a quantitative methodological research tool to identify effective safety approaches. The method synergistically combines crash data and human expertise in the motorcycle safety field. The relevance of the KBMS relies on its potential to bridge motorcycle accident research with industrial development of safety systems. For this reason, a motorcycle manufacturer is currently employing the KBMS together with researchers of the University of Florence, looking to maximize the positive impact of future motorcycle safety systems. Furthermore, a future widely accepted and open access KBMS would be advantageous to promote in the whole of Europe, becoming a tool to assist policy makers in taking well-funded decisions on safety regulations in order to make PTWs a safer means of transport.
2. The realization of the proof-of-concept of a camera-based remote sensor for road environment perception in tilting vehicles. The sensor design is a cost-effective remote sensor for application to advanced safety systems for vehicles with tilting dynamics. The proposed sensor can operate beyond the threshold limit up to 10

degrees of roll angle stated in the state-of-the-art. The approach developed has proven suitable and the following milestones were achieved during the tests:

- a. Improved stereo sensing performance during non-rigid registration (deformable stereo camera rig) by means of a novel two-step dynamic stereo camera recalibration technique proposed.
- b. Satisfactory measurement of the opponent car location in the motorcycle crash emulations (id86 and id90), which were made for the feasibility assessment of the remote camera-based sensor in Advanced Rider Assistance Systems (ARAS) applications.
- c. Success in the environmental depth sensing under roll angle conditions of 13° (scooter) and 22° (pedelec) with respect to a vertical line.

The second part of this research is an integral approach to develop a remote sensor capable to enable ARAS (ADAS¹ for motorcycles) with the potential to avoid crashes. This is an important step towards making real preventive safety technologies in tilting vehicles. In addition, the feasibility study of the remote sensor for the triggering of the Motorcycle Autonomous Braking System (M-AEB) showed satisfactory results for the two cases analyzed: an intersection of streets, and the U-turn. The promising results, achieved so far and presented in this dissertation, ask for the validation of the remote sensor in a wider variety of conditions to foresee its application in motorcycle safety systems. For example: assessing the sensor and its algorithms in real crash emulation when cornering, under different levels of vibrations, and in tilting vehicles of different characteristics, in order to implement industrial prototypes of safety systems.

To conclude, this dissertation addresses a problem with a significant impact in terms of the future personal transportation in urban areas. The concepts and methods studied in this work represents a solid step towards the development of advanced safety systems with the potential to make motorcycles and tilting vehicles a safer means of personal transport.

¹ In the automotive safety context ADAS stands for Advanced Driver Assistance Systems

Appendix A

This doctoral research was part of an the Innovative Training Networks (ITN), called Marie Skłodowska-Curie Actions, which pursuits to train a new generation of creative and innovative early-stage researchers, able to face current and future challenges for economic and social benefit. In this context, the European project MOTORIST was created.

The research project consist in a multidisciplinary and holistic approach in powered-two wheelers safety. This integral approach was supported for three main pillars or research axes termed Work Packages (WPs) as Figure 116 depicts.

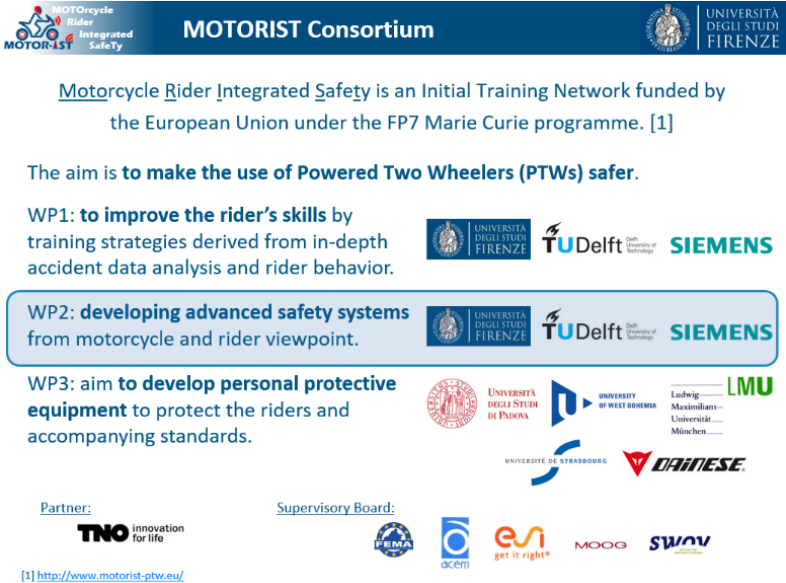


Figure 116. Descriptions of the Work Packages of MOTORIST project and the organizations involved. This research belongs to WP2 which is highlighted in light blue

The logo of the organizations involved in each part of the project is shown on the left side of a brief description of the goal of the WP. The three axis of research: 1) enhancing rider's skills; 2) developing advanced safety systems; and 3) enhancing protective equipment; helped to mix different disciplines and different type of professionals to works towards a common goal. Each researcher contributed with their expertise and different perspective and way of thinking about the problems to face. This allowed to find very creative solutions.

In addition, the more the field is under innovation, the more research tools and test reliable test assessment protocols are needed. This can be seen on the outcomes provide for each partner. I will focus only in WP2 that involved UNIFI, SIEMENS, and TU Delft, because are the related with the development of safety systems for motorcycles.

On the side of UNIFI, in addition of the enablement of a remote sensor for Advanced Rider Assistance Systems (ARAS or ADAS for motorcycles), the research conducted for other researchers outcome an innovative research approach which involves rider muscle activations for the assessment of rider behavior and rider profiting. UNIFI also developed and implement a test protocol for rider skills assessment and training. This protocol is also used in real instrumented motorcycles but also in advanced motorcycle simulators.

SIEMENS participates in the development of an advanced motorcycle simulator able to reproduce with high fidelity the behavior of a real scooter. This provides to the volunteer motorcyclist under study more realistic feedback of the riding situation, which is particularly difficult to achieve in a tilting vehicle due to its tilting dynamics.

TU Delft contribute with two stat-of-the-art bicycle simulators and the development of the first steer-by-wire bicycle. These unique research tools are very important to study the complex behavior of human riders which presents infinite degrees of freedom and this level of complexity must to be baking-it-down for a better understanding of rider behavior.

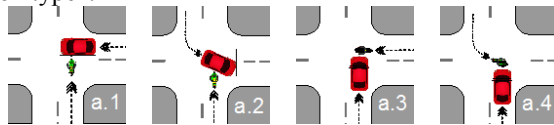
Appendix B

Pictograms (KBMS)

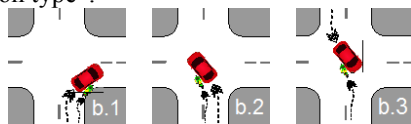
The following rows of pictograms represent the general crash scenarios to assess (named from A to D). The cases represent the same kind of a crash scenario but with more resolution or definition (i.e. labeled from a.1 to a.4). The present organization corresponds to the nine general scenarios of PTW crashes defined by the queries performed in the ISTAT road accident database. A different set of queries will rearrange each single pictogram in other organization.

Note: each pictogram (created in vector graphic format) may be downloaded and edited. The free graphical repository is: <https://openclipart.org/user-cliparts/Gusta>

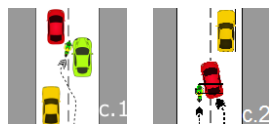
Scenario A: PTW crashes that happened in “intersection of streets” AND “angle collision type”.



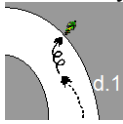
Scenario B: PTW crashes that happened in “intersection of streets” AND “sideswipe collision type”.



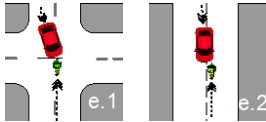
Scenario C: PTW crashes that happened in “straight street” AND “sideswipe collision type”.



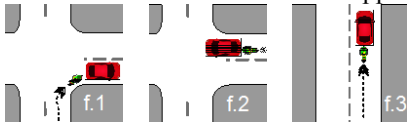
Scenario D: PTW crashes that happened in “rural road” OR “urban road” AND “single vehicle accident type” OR “run-off-the-road accident type” AND “curve layout”.



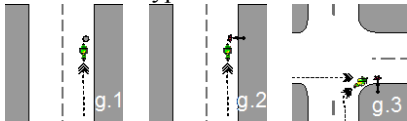
Scenario E: PTW crashes that happened in “head-on collision type”.



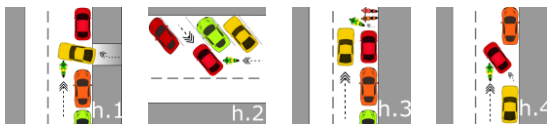
Scenario F: PTW crashes that happened in “rear-end collision type”.



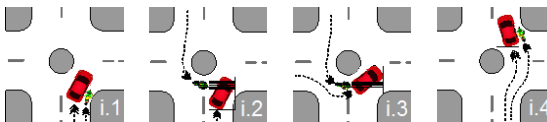
Scenario G: PTW crashes that happened in “hit-obstacle collision type” OR “hit pedestrian collision type”.



Scenario H: PTW crashes that happened in “straight street” AND “angle collision type”.



Scenario I: PTW crashes that happened in a “roundabout”.



Note: “roundabout” is a very particular case of “intersection” well studied in literature (Gross et al., 2013; Montella, 2011). For this reason, in the present methodology the crashes that happened in a roundabout are separated of the intersection crashes.

Appendix C

List of Queries

In the default framework, the above nine groups of scenarios were established performing the following queries on the traffic accident database.

PTW crashes that happened in:

- 1) Scenario A: “intersection of streets” AND “angle collision type”.
- 2) Scenario B: “intersection of streets” AND “sideswipe collision type”.
- 3) Scenario C: “straight street” AND “sideswipe collision type”.
- 4) Scenario D: [“rural road” OR “urban road”] AND [“single vehicle accident type” OR “run-off-the-road accident type”] AND “curve layout”.
- 5) Scenario E: “head-on collision type”.
- 6) Scenario F: “rear-end collision type”.
- 7) Scenario G: “hit-obstacle collision type” OR “hit pedestrian collision type”.
- 8) Scenario H: “straight street” AND “angle collision type”.
- 9) Scenario I: “roundabout”.

Appendix D

List of Safety Function for the KBMS

The list of Safety Functions (SFs) was conceived for the analysis that the experts in the field will perform for each road crash scenario. It is divided in seven main functionalities as: Crash avoidance or mitigation, PTW Stability managing, etc. aiming to simplify the process of classification and elaboration of these functionalities.

Acronyms used: OV (Other Vehicle) and PTW (Powered-Two Wheeler)

Crash avoidance or mitigation

1. Distribute more properly the braking action on the two wheels even if one brake is actioned
2. Assist the rider to perform a hard braking without falling from the PTW
3. Anti-stoppie (avoidance of the rear wheel lifting off the ground)
4. PTW Manoeuver advisor: Brake vs. Swerve (1)
During risky situations, indicates to the rider the best maneuver to perform: a hard straight line braking or evading the obstacle with a soft braking.
5. OV Manoeuver advisor: Brake vs. Swerve (1)
During risky situations, indicates to the driver the best maneuver to perform: a hard straight line braking or evading the obstacle with a soft braking.
6. PTW send a signal to Slow/Stop other vehicle (autonomous braking for collision avoidance) (2)
7. OV send a signal to Slow/Stop other vehicle (autonomous braking for collision avoidance) (2)

Remarks:

- (1) *requires precise obstacle distance detection and dynamic state of the vehicle*
- (2) *requires vehicular communication network*

PTW Stability managing

8. Enhance stability in straight paths
9. Enhance stability in curved paths
10. Avoidance of oversteer at high speed. Steering bar with additional and adaptive angular stiffness as a function of the velocity

Rider protection (injury reduction in a crash)

11. Head: kinetic energy dissipation element (3)
12. Neck: kinetic energy dissipation element
13. Thorax: kinetic energy dissipation element
14. Abdomen: kinetic energy dissipation element
15. Limbs: kinetic energy dissipation element
16. Anti-abrasion
17. Energy dissipation element placed in the PTW to dissipate vehicle kinetic energy during a crash. Case: frontal collision of the PTW
18. Energy dissipation element placed in the PTW to dissipate rider kinetic energy during a crash. Case: frontal collision of the PTW
19. Energy dissipation element placed in the OV to dissipate vehicle kinetic energy during a crash. Case: frontal collision of the PTW
20. Energy dissipation element placed in the OV to dissipate rider kinetic energy during a crash. Case: frontal collision of the PTW
21. Energy dissipation element placed in the PTW to dissipate vehicle kinetic energy during a crash. Case: rear collision of the PTW
22. Energy dissipation element placed in the PTW to dissipate rider kinetic energy during a crash. Case: rear collision of the PTW
23. Energy dissipation element placed in the OV to dissipate vehicle kinetic energy during a crash. Case: rear collision of the PTW
24. Energy dissipation element placed in the OV to dissipate rider kinetic energy during a crash. Case: rear collision of the PTW
25. Energy dissipation element placed in the PTW to dissipate vehicle kinetic energy during a crash. Case: lateral collision of the PTW
26. Energy dissipation element placed in the PTW to dissipate rider kinetic energy during a crash. Case: lateral collision of the PTW
27. Energy dissipation element placed in the OV to dissipate vehicle kinetic energy during a crash. Case: lateral collision of the PTW
28. Energy dissipation element placed in the OV to dissipate rider kinetic energy during a crash. Case: lateral collision of the PTW
29. Human body confinement (4)

Remarks:

- (3) *It does this by converting the kinetic energy of the shock into another form of energy; typically plastic deformation, sound energy and heat which is then dissipated*
- (4) *i.e. Protection system of BMW C1 four-point seat-belt*

Accident prevention

30. OV - Alert of oncoming PTW (from front)
31. OV - Alert of oncoming PTW (from rear)
32. OV - Alert of oncoming PTW (from right side)
33. OV - Alert of oncoming PTW (from left side)
34. PTW - Alert of oncoming vehicle (from front)
35. PTW - Alert of oncoming vehicle (from rear)
36. PTW - Alert of oncoming vehicle (from right side)
37. PTW - Alert of oncoming vehicle (from left side)

38. PTW - Pedestrian/cyclist in the path (notification)
39. Notification of non-correct pressure in the tires
40. Notification of approaching hazard (i.e. steep decline)
41. Prevent the crossing of wild animals on the road by means of additional infrastructure (e.g. eco-ducts, wildlife corridors)

Perception augmented

42. PTW Enhanced vision at night
43. OV Enhanced vision at night
44. Improvement of PTW conspicuously (help to the PTW to be seen for others)

Rescue

45. Crash signalization. Beacon that help to find the PTW crashed (most useful in rural areas)
46. Emergency call. System uses the cell phone network (or other) to inform the coordinates of the accident (GPS position) to the local authorities

Safe riding/driving

47. Rider state detection (guarantees a minimum level of alert)
48. Driver state detection (guarantees a minimum level of alert)
49. PTW Alcohol interlock
50. OV Alcohol interlock
51. PTW - Adaptive to road adherence condition. Change the acceleration and braking response of the vehicle according with the level of adherence to the road.
52. OV - Adaptive to road adherence condition. Change the acceleration and braking response of the vehicle according with the level of adherence to the road.
53. PTW restricts its maximum speed to street top speed
54. OV restricts its maximum speed to street top speed
55. PTW Adaptive cruise control
56. OV Adaptive cruise control
57. PTW Adaptive speed to traffic speed
58. OV Adaptive speed to traffic speed
59. PTW Lane keeping
60. OV Lane keeping
61. PTW autonomous-braking
62. OV autonomous-braking
63. Elimination of blind spot in PTW (side of vehicle)
64. Elimination of blind spot in OV (side of vehicle)

Appendix E

Selection of experts for the assessment

The ‘expert’ is a person with a recognized knowledge on the topic of interest. For the KBMS the experts could come from a variety of disciplines (e.g. crash analysis reconstruction, crash test analysis, energy absorbers design, traction & braking control, traffic control, driver/rider training, injuries assessment, etc.). In order to manage the degree of heterogeneity of the sources of knowledge involved, a categorization of the technical background of the experts involved in the KBMS was defined (e.g. Biomechanics, Mechanical Engineers, etc.).

The process of recruitment of experts, for the KBMS research, can be summarized by fulfilling a set of requirements:

Main activity	Research in Vehicle Safety
Years of experience	≥ 5
Geographical region of expertise	Tuscany, Lazio, Italy
Background	Mechanical Engineer
Name of best three publications on the topic	Paper #, Tech. Report, Book chapter...
Patents related with the topic	Patent ...
Participation in projects	Project 1 (tasks performed), ...

Table 17 Expert legitimization table for KBMS assessment (it is filled as an example)

In this way, it is possible to consider if the applicant could be accepted as a recognizable expert for the purpose of the KBMS or not, allowing recognizing bough: academicals and industrial experts.

Appendix F

Guidelines for the expert assessment

Defining boundaries to the analysis is vital to help the experts during the process of evaluation. I defined the next five directives to this intent based on the statistical results of more than one million of motorcycle accidents (ISTAT: 2000-2012 year).

Five directives:

1. *Pessimism*, in case of doubts about the potential benefit of a particular safety function for a specific crash scenario, the evaluation must be directed towards the less effective case. For example, if the scale of this study (Table 2) is used to determine the quantity of water in a glass that seems to be half full of water, the queried participant must respond without hesitation the score value 2.
2. *Clear visibility conditions* during the moment of the crash are assumed. No fog, smoke, trees or other external elements of the scenario that can decrease the field of view of the rider/driver.
3. *Good weather conditions* during the moment of the crash are assumed. Non rain, wind-shear, or other less favorable weather conditions.
4. *Correct pavement adherence* during the moment of the crash is assumed. No slippery conditions or irregularities on the surface of the pavement.
5. *Speeding in urban scenarios* is assumed in at least 70%. Motorcyclist's fault (In-Safe database: near to 13 km/h more than the road top limit – 50 or 60km/h in Italian roads).

Note: pedestrians, cyclist and PTWs are not considered as Other Vehicle (OV) in the safety function description

Appendix G

Technical terminology

In order to retrieving comparatively information from the expert consultation process, it is necessary to define a common vocabulary to guide the experts during the traffic accident evaluation. Indeed, for some safety functionalities to analyze already exists a safety system that can fulfill the requirements, but for others is not the case. The following terms are defined as follows in order to offer a common vocabulary to the experts' ideas during communications and workshops:

- **Crash mitigation:** making the consequence of the crash less severe in terms of people injured level. Example: 20% crash mitigation means "in 20% of accidents, the crash severity can be reduced".
- **Crash avoidance:** preventing the crash from happening. Example: 30% crash avoidance means "30% of accidents can be reduced in number".
- **Technology:** technical aspects that have made possible the development of a specific system.
- **Safety system:** specific system in charge of a determinate safety function. Different safety systems may use the same technology for accomplishing different objectives. For example in cars, the ABS (anti-lock braking system) and the ESP (Electronic Stability Programme) are sharing technology.
- **Safety function:** unequivocally describes the desired outcome for a safety solution, emphasizing in goals regardless the constitutive mechanisms or sub-systems. For instance, the safety function of the ABS is to avoid the wheel locking on different pavement conditions in order to maximize the deceleration. For the system ESP (for cars), the safety function is to ensure that the vehicle follows a trajectory consistent with the steering wheel action.
- **Primary safety or Active safety:** its main objective is to improve the vehicle safety through technology with the aim of preventing or avoiding a vehicle crash (e.g. alcohol lock, ABS).

- Secondary safety or Passive safety: systems designed to protect and reduce the risk of injury to the rider/driver (e.g. seat belt).
- Tertiary safety: a concept referred to alerting to rescue services after an accident occurrence to provide them the exact location of this event.

Appendix H

Prioritized safety functionalities list (PISa study)

The following lists present the SFs from the most to the less important (43 safety solutions assessed). For simplification only the 15 more relevant are presented.

PISa outcome 1: General ranking of safety functionalities

- 1) Automatically stop other vehicle without input from driver
- 2) Warn other vehicle of PTW presence
- 3) Communicate and warn PTW that vehicle travelling from left, right or oncoming is crossing PTW's path
- 4) Automatically stop PTW without input from rider
- 5) Detect and warn PTW that vehicle travelling from left, right or oncoming is crossing PTW's path
- 6) Improve PTW conspicuity
- 7) Avoid locking of wheels
- 8) Amplify braking force
- 9) Balance front to rear braking force
- 10) Warn PTW of traffic signal/pedestrian crossing (status chance from green to red)
- 11) Reduce closing speed
- 12) Warn PTW leading vehicle slowing/stopping
- 13) Protect fallen/rolling rider's body
- 14) Restrict PTW to posted speed limit
- 15) Help PTW rider to remain upright post impact

PISa outcome 2: Coarse ranking (contain only the maximum scores) of safety functionalities

- 1) Warn other vehicle of PTW presence
- 2) Automatically stop other vehicle without input from driver
- 3) Communicate and warn PTW that vehicle travelling from left, right or oncoming is crossing PTW's path
- 4) Automatically stop PTW without input from rider
- 5) Avoid locking of wheels
- 6) Warn PTW of traffic signal/pedestrian crossing (status chance from green to red)

- 7) Reduce closing speed
- 8) Balance front to rear braking force
- 9) Warn PTW leading vehicle slowing/stopping
- 10) Help PTW rider to remain upright post impact
- 11) Detect and warn PTW that vehicle travelling from left, right or oncoming is crossing PTW's path
- 12) Improve PTW conspicuity
- 13) Warn PTW that oncoming vehicle is in the same lane as PTW
- 14) Warn PTW rider of diagnostic status of PTW (brake, tire pressure, etc.)
- 15) Restrict PTW to posted speed limit

Remark: only the first 4 safety functionalities are almost matching in type and priority order of the safety importance between the previous outcomes.

Acknowledgements

The present thesis work was carried out in the Department of Industrial Engineering of the University of Florence. Foremost, I would like to express my sincere gratitude to all the people working in this Department, starting from my Supervisors, Marco Pierini and Giovanni Savino. Also I thanked to the leaders of the work package in which I participate during my international research, Rinder Happee and Arend Schwab from the Technical University of Delft, in Nederland. I thanks my colleagues in UNIFI in no especial order: Ramses Sala, Lorenzo Berzi, Simone Piantini, Marilee Nugent, Simon Rosalie, Pedro Huertas, Alessandro Grassi, Daniele Barbani, Francesco Del Pero, Antonio Virga, Niccolo Baldanzini, Laura Zanchi, Caterina Dattilo, and Ilaria Giorgi. I thanks my colleagues of the European consortium MOTORIST in no especial order: Siamak Farajzadeh Khosroshahi, Mohammad Nasim, Sounak Mojumder, Raúl Aranda, Tomasz Bonkowski, Oliver Lee, George Dialynas, Natalia Kovacsova, María Antonietta Di Gesù, Francesco Celiberti, and Marco Grottoli. Finally, I want to thanks to the Europe Union for the Innovative Training Networks (ITN) - Marie Skłodowska-Curie Actions for which I was benefited with and invaluable international research experience.

Bibliography

- Abediasl, H., Hashemi, H., 2015. Monolithic optical phased-array transceiver in a standard SOI CMOS process. *Opt. Express* 23, 6509. <https://doi.org/10.1364/OE.23.006509>
- Alahi, A., Ortiz, R., Vandergheynst, P., 2012. Freak: Fast retina keypoint, in: *Computer Vision and Pattern Recognition (CVPR), 2012 IEEE Conference on.* Ieee, pp. 510–517.
- Anderson, R.W., Australia, S., Australia, T.C., 2011. Analysis of crash data to estimate the benefits of emerging vehicle technology. Centre for Automotive Safety Research, University of Adelaide.
- Andres, M., Feil, P., Menzel, W., 2012. 3D-scattering center detection of automotive targets using 77 GHz UWB radar sensors, in: *Antennas and Propagation (EUCAP), 2012 6th European Conference on.* IEEE, pp. 3690–3693.
- Aupetit, S., Espié, S., Bouaziz, S., 2015. Naturalistic study of riders' behaviour in lane-splitting situations. *Cogn. Technol. Work* 17, 301–313. <https://doi.org/10.1007/s10111-014-0293-z>
- Badino, H., Franke, U., Mester, R., 2007. Free space computation using stochastic occupancy grids and dynamic programming, in: *Workshop on Dynamical Vision, ICCV, Rio de Janeiro, Brazil.*
- Badino, H., Franke, U., Pfeiffer, D., 2009. The Stixel World-A Compact Medium Level Representation of the 3D-World., in: *DAGM-Symposium.* Springer, pp. 51–60.
- Badino, H., Franke, U., Rabe, C., Gehrig, S., 2006. Stereo-vision based detection of moving objects under strong camera motion, in: *International Conference on Computer Vision Theory and Applications.* pp. 253–260.
- Baker, H.H., Bolles, R.C., 1989. Generalizing epipolar-plane image analysis on the spatiotemporal surface. *Int. J. Comput. Vis.* 3, 33–49.
- Banks, J., Corke, P., 2001. Quantitative evaluation of matching methods and validity measures for stereo vision. *Int. J. Robot. Res.* 20, 512–532.
- Barth, A., Franke, U., 2008. Where will the oncoming vehicle be the next second?, in: *Intelligent Vehicles Symposium, 2008 IEEE.* IEEE, pp. 1068–1073.
- Barth, A., Pfeiffer, D., Franke, U., 2009. Vehicle tracking at urban intersections using dense stereo, in: *3rd Workshop on Behaviour Monitoring and Interpretation, BMI.* pp. 47–58.
- Baur, K., Mayer, M., Binzer, T., Walter, T., 2011. Beamforming concepts for angular measurements in azimuth and elevation with 77 GHz lens based radar sensors, in: *Microwave Symposium Digest (MTT), 2011 IEEE MTT-S International.* IEEE, pp. 1–4.

- Bay, H., Ess, A., Tuytelaars, T., Van Gool, L., 2008. Speeded-Up Robust Features (SURF). *Comput. Vis. Image Underst.* 110, 346–359. <https://doi.org/10.1016/j.cviu.2007.09.014>
- Bay, H., Tuytelaars, T., Van Gool, L., 2006. Surf: Speeded up robust features. *Comput. Vision–ECCV 2006* 404–417.
- Bayly, M., Regan, M., Hosking, S., 2006. Intelligent Transport Systems and Motorcycle Safety. *Prevention* 28, 325–332.
- Benenson, R., Timofte, R., Van Gool, L., 2011. Stixels estimation without depth map computation, in: *Computer Vision Workshops (ICCV Workshops), 2011 IEEE International Conference on.* IEEE, pp. 2010–2017.
- Bernini, N., Bertozzi, M., Castangia, L., Patander, M., Sabbatelli, M., 2014. Real-time obstacle detection using stereo vision for autonomous ground vehicles: A survey, in: *Intelligent Transportation Systems (ITSC), 2014 IEEE 17th International Conference on.* IEEE, pp. 873–878.
- Berzi, L., Delogu, M., Pierini, M., Romoli, F., 2016. Evaluation of the end-of-life performance of a hybrid scooter with the application of recyclability and recoverability assessment methods. *Resour. Conserv. Recycl.* 108, 140–155. <https://doi.org/10.1016/j.resconrec.2016.01.013>
- Bildik, S., Dieter, S., Fritzsche, C., Menzel, W., Jakoby, R., 2015. Reconfigurable Folded Reflectarray Antenna Based Upon Liquid Crystal Technology. *IEEE Trans. Antennas Propag.* 63, 122–132. <https://doi.org/10.1109/TAP.2014.2367491>
- Bishop, J.D.K., Doucette, R.T., Robinson, D., Mills, B., McCulloch, M.D., 2011. Investigating the technical, economic and environmental performance of electric vehicles in the real-world: A case study using electric scooters. *J. Power Sources* 196, 10094–10104. <https://doi.org/10.1016/j.jpowsour.2011.08.021>
- Blount, G.N., Kneebone, S., Kingston, M.R., 1995. Selection of Knowledge-based Engineering Design Applications. *J. Eng. Des.* 6, 31–38. <https://doi.org/10.1080/09544829508907900>
- Bouguet, J.-Y., n.d. “Camera Calibration Toolbox for Matlab.” *Computational Vision at the California Institute of Technology.*
- Bradski, G.R., Kaehler, A., 2011. *Learning OpenCV: computer vision with the OpenCV library*, 1. ed., [Nachdr.] ed, Software that sees. O’Reilly, Beijing.
- Broggi, A., Caraffi, C., Fedriga, R.I., Grisleri, P., 2005. Obstacle detection with stereo vision for off-road vehicle navigation, in: *Computer Vision and Pattern Recognition-Workshops, 2005. CVPR Workshops. IEEE Computer Society Conference on.* IEEE, pp. 65–65.
- Broggi, A., Caraffi, C., Porta, P.P., Zani, P., 2006. The single frame stereo vision system for reliable obstacle detection used during the 2005 DARPA grand challenge on TerraMax, in: *Intelligent Transportation Systems Conference, 2006. ITSC’06.* IEEE. IEEE, pp. 745–752.
- Broggi, A., Cardarelli, E., Cattani, S., Sabbatelli, M., 2013a. Terrain mapping for off-road Autonomous Ground Vehicles using rational B-Spline surfaces and stereo vision, in: *Intelligent Vehicles Symposium (IV), 2013 IEEE.* IEEE, pp. 648–653.
- Broggi, A., Cattani, S., Patander, M., Sabbatelli, M., Zani, P., 2013b. A full-3D voxel-based dynamic obstacle detection for urban scenario using stereo vision. *IEEE*, pp. 71–76. <https://doi.org/10.1109/ITSC.2013.6728213>

- Broughton, J., Brandstaetter, C., Yannis, G., Evgenikos, P., Papantoniou, P., Candappa, N., Christoph, M., van Duijvenvoorde, K., Vis, M., Pace, J.-F., others, 2013. Traffic Safety Basic Facts 2012: Main figures.
- Buchanan, B., Feigenbaum, E., 1978. Dendral and Meta-Dendral: Their Applications Dimension.
- Burton, D., Delaney, A., Newstead, S., Logan, D., Fildes, B., 2004. Evaluation of Anti-lock Braking Systems Effectiveness.
- Carletta, J., 1996. Assessing agreement on classification tasks: the kappa statistic. *Comput. Linguist.* 22, 249–254.
- Chapman, C.P., Pinfold, M., 1999. Design engineering—a need to rethink the solution using knowledge based engineering. *Knowledge-Based Systems.*
- Chowdhury, A.R., Chellappa, R., 2003. Statistical error propagation in 3d modeling from monocular video, in: *Computer Vision and Pattern Recognition Workshop, 2003. CVPRW'03. Conference on. IEEE*, pp. 89–89.
- Clark F. Olson, Larry H. Matthies, Marcel Schoppers, Mark W. Maimone, 2001. Stereo Ego-motion Improvements for Robust Rover Navigation, in: *Proceedings 2001 ICRA. IEEE International Conference on Robotics and Automation (Cat. No.01CH37164)*. Seoul, South Korea. <https://doi.org/10.1109/ROBOT.2001.932758>
- Colville, R.N., Hutchinson, E.J., Mindell, J.S., Warren, R.F., 2001. The transport sector as a source of air pollution. *Atmos. Environ.* 35, 1537–1565.
- Corke, P., Lobo, J., Dias, J., 2007. An Introduction to Inertial and Visual Sensing. *Int. J. Robot. Res.* 26, 519–535. <https://doi.org/10.1177/0278364907079279>
- Corno, M., Panzani, G., Savaresi, S.M., 2015. Single-Track Vehicle Dynamics Control: State of the Art and Perspective. *IEEEASME Trans. Mechatron.* 20, 1521–1532. <https://doi.org/10.1109/TMECH.2014.2382717>
- de Hartog, J.J., Boogaard, H., Nijland, H., Hoek, G., 2010. Do the Health Benefits of Cycling Outweigh the Risks? *Environ. Health Perspect.* 118, 1109–1116. <https://doi.org/10.1289/ehp.0901747>
- Deutermann, W., 2004. Motorcycle Helmet Effectiveness Revisited.
- Di Stefano, L., Mattocchia, S., 2002. Real-Time Stereo within the VIDET Project. *Real-Time Imaging* 8, 439–453. <https://doi.org/10.1006/rtim.2002.0299>
- Dieter, S., Feil, P., Menzel, W., 2011. Folded reflectarray antenna using a modified polarization grid for beam-steering, in: *Antennas and Propagation (EUCAP), Proceedings of the 5th European Conference on. IEEE*, pp. 1400–1403.
- Ender, J., Brüggewirth, S., 2015. Cognitive Radar - Enabling Techniques for Next Generation Radar Systems. Presented at the 16th International Radar Symposium IRS.
- Festini, A., Tonoli, A., Zenerino, E., 2011. Urban and Extra Urban Vehicles: Re-Thinking the Vehicle Design, in: Chiaberge, M. (Ed.), *New Trends and Developments in Automotive System Engineering*. InTech.
- Fildes, B., Keall, M., Bos, N., Lie, A., Page, Y., Pastor, C., Pennisi, L., Rizzi, M., Thomas, P., Tingvall, C., 2015. Effectiveness of low speed autonomous emergency braking in real-world rear-end crashes. *Accid. Anal. Prev.* 81, 24–29. <https://doi.org/10.1016/j.aap.2015.03.029>
- Fortuny-Guasch, J., Chareau, J.-M., European Commission, Joint Research Centre, Institute for the Protection and the Security of the Citizen, 2013. Radar cross section measurements of pedestrian dummies and humans in the 24 / establishment of a reference library of RCS signatures of pedestrian dummies in the automotive radar bands. Publications Office, Luxembourg.

- Franci, A., Piantini, S., Pierini, M., Peris, A., Mangini, M., 2015. In-depth study of road accidents in Florence: understanding the biomechanical effects in major trauma involving vulnerable road users. *Crit. Care* 19, P311. <https://doi.org/10.1186/cc14391>
- Franke, U., Kutzbach, I., 1996. Fast stereo based object detection for stop&go traffic, in: *Intelligent Vehicles Symposium, 1996., Proceedings of the 1996 IEEE*. IEEE, pp. 339–344.
- Franke, U., Rabe, C., Badino, H., Gehrig, S., 2005. 6d-vision: Fusion of stereo and motion for robust environment perception, in: *DAGM-Symposium*. Springer, pp. 216–223.
- Freundlich, C., Zavlanos, M., Mordohai, P., 2015. Exact bias correction and covariance estimation for stereo vision, in: *Proceedings of the IEEE Conference on Computer Vision and Pattern Recognition*. pp. 3296–3304.
- Fritsch, J., Kuhn, T., Geiger, A., 2013. A new performance measure and evaluation benchmark for road detection algorithms, in: *Intelligent Transportation Systems-(ITSC), 2013 16th International IEEE Conference on*. IEEE, pp. 1693–1700.
- Garcia, J., Haider, M., Boverie, S., 2013. State of the Art report concerning acoustic warning strategies.
- Gehrig, S., Reznitskii, M., Schneider, N., Franke, U., Weickert, J., 2013. Priors for Stereo Vision under Adverse Weather Conditions. *IEEE*, pp. 238–245. <https://doi.org/10.1109/ICCVW.2013.39>
- Gehrig, S.K., Eberli, F., Meyer, T., 2009. A real-time low-power stereo vision engine using semi-global matching, in: *International Conference on Computer Vision Systems*. Springer, pp. 134–143.
- Gehrig, S.K., Franke, U., 2007. Improving stereo sub-pixel accuracy for long range stereo, in: *Computer Vision, 2007. ICCV 2007. IEEE 11th International Conference on*. IEEE, pp. 1–7.
- Geiger, A., Lenz, P., Stiller, C., Urtasun, R., 2013. Vision meets robotics: The KITTI dataset. *Int. J. Robot. Res.* 32, 1231–1237.
- Geiger, A., Lenz, P., Urtasun, R., 2012a. Are we ready for autonomous driving? the kitti vision benchmark suite, in: *Computer Vision and Pattern Recognition (CVPR), 2012 IEEE Conference on*. IEEE, pp. 3354–3361.
- Geiger, A., Moosmann, F., Car, Ö., Schuster, B., 2012b. Automatic camera and range sensor calibration using a single shot, in: *Robotics and Automation (ICRA), 2012 IEEE International Conference on*. IEEE, pp. 3936–3943.
- Geng, J., 2011. DLP-based structured light 3D imaging technologies and applications, in: *Proc. SPIE*. p. 79320B.
- Gennari, J.H., Musen, M.A., Ferguson, R.W., Grosso, W.E., Crubézy, M., Eriksson, H., Noy, N.F., Tu, S.W., 2003. The evolution of Protégé: an environment for knowledge-based systems development. *Int. J. Hum.-Comput. Stud.* 58, 89–123. [https://doi.org/10.1016/S1071-5819\(02\)00127-1](https://doi.org/10.1016/S1071-5819(02)00127-1)
- Gerland, P., Raftery, A.E., Evikova, H., Li, N., Gu, D., Spoorenberg, T., Alkema, L., Fosdick, B.K., Chunn, J., Lalic, N., Bay, G., Buettner, T., Heilig, G.K., Wilmoth, J., 2014. World population stabilization unlikely this century. *Science* 346, 234–237. <https://doi.org/10.1126/science.1257469>
- Gil, G., Savino, G., Piantini, S., Pierini, M., 2018. Is stereo vision a suitable remote sensing approach for motorcycle safety? An analysis of LIDAR, RADAR, and machine vision technologies subjected to the dynamics of a tilting vehicle., in: *7th Transport Research Arena TRA*. Vienna, Austria.

- Giuffrè, O., Granà, A., Giuffrè, T., Marino, R., Campisi, T., 2015. An Italian experience on crash modeling for roundabouts.
- Glassbrenner, D., 2012. An analysis of recent improvements to vehicle safety.
- Götschi, T., Garrard, J., Giles-Corti, B., 2016. Cycling as a Part of Daily Life: A Review of Health Perspectives. *Transp. Rev.* 36, 45–71. <https://doi.org/10.1080/01441647.2015.1057877>
- Grant, R.M., 1996. Toward a knowledge-based theory of the firm. *Strateg. Manag. J.* 17, 109–122.
- Gross, F., Lyon, C., Persaud, B., Srinivasan, R., 2013. Safety effectiveness of converting signalized intersections to roundabouts. *Accid. Anal. Prev.* 50, 234–241. <https://doi.org/10.1016/j.aap.2012.04.012>
- G.S. Young, R. Chellappa, n.d. Statistical analysis of inherent ambiguities in recovering 3-d motion from a noisy flow field, in: *IEEE Transactions Pattern Analysis and Machine Intelligence*, 14(10):995–1013, 1992.
- Gupta, M., Yin, Q., Nayar, S.K., 2013. Structured light in sunlight, in: *Proceedings of the IEEE International Conference on Computer Vision*. pp. 545–552.
- Gupta, V.K., Cecil, K., 2014. An Analytical Study of SIFT and SURF in Image Registration. *Int. J. Eng. Innov. Technol. IJEIT* 3.
- Gwet, K.L., 2008. Computing inter-rater reliability and its variance in the presence of high agreement. *Br. J. Math. Stat. Psychol.* 61, 29–48. <https://doi.org/10.1348/000711006X126600>
- Haeusler, R., Nair, R., Kondermann, D., 2013. Ensemble Learning for Confidence Measures in Stereo Vision. *IEEE*, pp. 305–312. <https://doi.org/10.1109/CVPR.2013.46>
- Haller, I., Nedeveschi, S., 2012. Design of Interpolation Functions for Subpixel-Accuracy Stereo-Vision Systems. *IEEE Trans. Image Process.* 21, 889–898. <https://doi.org/10.1109/TIP.2011.2163163>
- Han, S., Liu, X., Mao, H., Pu, J., Pedram, A., Horowitz, M.A., Dally, W.J., 2016. EIE: efficient inference engine on compressed deep neural network, in: *Proceedings of the 43rd International Symposium on Computer Architecture*. IEEE Press, pp. 243–254.
- Han, S., Mao, H., Dally, W.J., 2015. Deep compression: Compressing deep neural networks with pruning, trained quantization and huffman coding. *ArXiv Prepr. ArXiv151000149*.
- Hansen, P., Alismail, H., Rander, P., Browning, B., 2012. Online continuous stereo extrinsic parameter estimation, in: *Computer Vision and Pattern Recognition (CVPR), 2012 IEEE Conference on*. IEEE, pp. 1059–1066.
- Harms, H., Rehder, E., Lauer, M., 2015. Grid Map based Free Space Estimation using Stereo Vision, in: *Proc. Workshop Environment Perception Automated On-Road Vehicles, IEEE Intelligent Vehicles Symposium*.
- Hartley, R., Zisserman, A., 2004. *Multiple view geometry in computer vision*. Cambridge University Press, Cambridge.
- Hartley, R.I., 1997. In defense of the eight-point algorithm. *IEEE Trans. Pattern Anal. Mach. Intell.* 19, 580–593.
- Harvey, R., DiCaprio, P., Heinemann, K., 1991. A Neural Network Architecture for General Image Recognition. *Linc. Lab. J.* 4.
- Hasch, J., Topak, E., Schnabel, R., Zwick, T., Weigel, R., Waldschmidt, C., 2012. Millimeter-Wave Technology for Automotive Radar Sensors in the 77 GHz Frequency Band. *IEEE Trans. Microw. Theory Tech.* 60, 845–860. <https://doi.org/10.1109/TMTT.2011.2178427>

- Hasch, J., Wostradowski, U., Hellinger, R., Mittelstrass, D., 2011. 77 GHz automotive radar sensor in low-cost PCB technology, in: Radar Conference (EuRAD), 2011 European. IEEE, pp. 101–104.
- Haworth, N., 2012. Powered two wheelers in a changing world—Challenges and opportunities. *Accid. Anal. Prev.* 44, 12–18.
- Hayes-Roth, F., 1985. Rule-based systems. *Commun. ACM* 28, 921–932.
- Haykin, S., 2014. Cognitive Dynamic Systems [Scanning the Issue]. *Proc. IEEE* 102, 414–416. <https://doi.org/10.1109/JPROC.2014.2306249>
- Haykin, S., 2006. Cognitive radar: a way of the future. *IEEE Signal Process. Mag.* 23, 30–40. <https://doi.org/10.1109/MSP.2006.1593335>
- Heck, M.J.R., 2017. Highly integrated optical phased arrays: photonic integrated circuits for optical beam shaping and beam steering. *Nanophotonics* 6. <https://doi.org/10.1515/nanoph-2015-0152>
- Heikkila, J., Silven, O., 1997. A four-step camera calibration procedure with implicit image correction, in: Computer Vision and Pattern Recognition, 1997. Proceedings., 1997 IEEE Computer Society Conference on. IEEE, pp. 1106–1112.
- Heise, M., 2001. Statutes of Limitations.
- Hirschmuller, H., 2005. Accurate and efficient stereo processing by semi-global matching and mutual information, in: Computer Vision and Pattern Recognition, 2005. CVPR 2005. IEEE Computer Society Conference on. IEEE, pp. 807–814.
- Hirschmuller, H., Gehrig, S., 2009. Stereo matching in the presence of sub-pixel calibration errors, in: Computer Vision and Pattern Recognition, 2009. CVPR 2009. IEEE Conference on. IEEE, pp. 437–444.
- Hirschmuller, H., Scharstein, D., 2009. Evaluation of Stereo Matching Costs on Images with Radiometric Differences. *IEEE Trans. Pattern Anal. Mach. Intell.* 31, 1582–1599. <https://doi.org/10.1109/TPAMI.2008.221>
- Hu, Z., Uchimura, K., 2005. UV-disparity: an efficient algorithm for stereovision based scene analysis, in: Intelligent Vehicles Symposium, 2005. Proceedings. IEEE. IEEE, pp. 48–54.
- Iqbal, M., Morel, M., Meriaudeau, F., 2009. A survey on outdoor water hazard detection. *Skripsi Program Studi Siste Inf.*
- Jamson, S., Chorlton, K., 2009. The changing nature of motorcycling: Patterns of use and rider characteristics. *Transp. Res. Part F Traffic Psychol. Behav.* 12, 335–346. <https://doi.org/10.1016/j.trf.2009.04.002>
- Jin, E., Phillips, J., Farnand, S., Belska, M., Tran, V., Chang, E., Wang, Y., Tseng, B., 2017. Towards the Development of the IEEE P1858 CPIQ Standard – A validation study. *Electron. Imaging* 2017, 88–94. <https://doi.org/10.2352/ISSN.2470-1173.2017.12.IQSP-249>
- Jung, I.-K., Lacroix, S., 2005. Simultaneous localization and mapping with stereovision. *Robot. Res.* 315–324.
- Kellner, D., Barjenbruch, M., Klappstein, J., Dickmann, J., Dietmayer, K., 2016. Tracking of Extended Objects with High-Resolution Doppler Radar. *IEEE Trans. Intell. Transp. Syst.* 17, 1341–1353. <https://doi.org/10.1109/TITS.2015.2501759>
- Kelly, J., Matthies, L.H., Sukhatme, G.S., 2011. Simultaneous mapping and stereo extrinsic parameter calibration using GPS measurements, in: Robotics and Automation (ICRA), 2011 IEEE International Conference on. IEEE, pp. 279–286.

- Keren, D., Peleg, S., Brada, R., 1988. Image sequence enhancement using sub-pixel displacements, in: *Computer Vision and Pattern Recognition, 1988. Proceedings CVPR'88.*, Computer Society Conference on. IEEE, pp. 742–746.
- Kim, J., Baek, J., Choi, H., Kim, E., 2016. Wet area and puddle detection for Advanced Driver Assistance Systems (ADAS) using a stereo camera. *Int. J. Control Autom. Syst.* 14, 263–271. <https://doi.org/10.1007/s12555-015-0024-0>
- Kobayashi, M., Onuki, Y., Kawabata, K., Sekine, H., Tsuboi, T., Matsuno, Y., Takahashi, H., Koizumi, T., Sakurai, K., Yuzurihara, H., 2017. 4.5 A 1.8 e rms- temporal noise over 110dB dynamic range 3.4 μm pixel pitch global shutter CMOS image sensor with dual-gain amplifiers, SS-ADC and multiple-accumulation shutter, in: *Solid-State Circuits Conference (ISSCC), 2017 IEEE International.* IEEE, pp. 74–75.
- Köhler, M., Hasch, J., Blöcher, H.L., Schmidt, L.-P., 2013. Feasibility of automotive radar at frequencies beyond 100 GHz. *Int. J. Microw. Wirel. Technol.* 5, 49–54. <https://doi.org/10.1017/S175907871200075X>
- Kondermann, D., Abraham, S., Brostow, G., Förstner, W., Gehrig, S., Imiya, A., Jähne, B., Klose, F., Magnor, M., Mayer, H., 2012. On performance analysis of optical flow algorithms, in: *Outdoor and Large-Scale Real-World Scene Analysis.* Springer, pp. 329–355.
- Kostas Daniilidis, Minas E. Spetsakis, n.d. Understanding noise sensitivity in structure from motion, in: Chapter 4, in Y. Aloimonos (Ed.), *Visual Navigation*, Lawrence Erlbaum Associates, Hillsdale, NJ, 1996, Pp. 61-88.
- Ku, B.-H., Schmalenberg, P., Inac, O., Gurbuz, O.D., Lee, J.S., Shiozaki, K., Rebeiz, G.M., 2014. A 77–81-GHz 16-Element Phased-Array Receiver With 50 Beam Scanning for Advanced Automotive Radars. *IEEE Trans. Microw. Theory Tech.* 62, 2823–2832. <https://doi.org/10.1109/TMTT.2014.2354134>
- Kubota, S., Nakano, T., Okamoto, Y., 2007. A global optimization algorithm for real-time on-board stereo obstacle detection systems, in: *Intelligent Vehicles Symposium, 2007 IEEE.* IEEE, pp. 7–12.
- Kwong, D., Hosseini, A., Covey, J., Zhang, Y., Xu, X., Subbaraman, H., Chen, R.T., 2014. On-chip silicon optical phased array for two-dimensional beam steering. *Opt. Lett.* 39, 941. <https://doi.org/10.1364/OL.39.000941>
- Langer, D., Rosenblatt, J.K., Hebert, M., 1994. A behavior-based system for off-road navigation. *IEEE Trans. Robot. Autom.* 10, 776–783.
- Law, R., Harvey, A., Reay, D., 2016. A knowledge-based system for low-grade waste heat recovery in the process industries. *Appl. Therm. Eng.* 94, 590–599. <https://doi.org/10.1016/j.applthermaleng.2015.10.103>
- Lee, J., Jun, D., Eem, C., Hong, H., 2016. Improved census transform for noise robust stereo matching. *Opt. Eng.* 55, 063107. <https://doi.org/10.1117/1.OE.55.6.063107>
- Leutenegger, S., Chli, M., Siegwart, R.Y., 2011. BRISK: Binary robust invariant scalable keypoints, in: *Computer Vision (ICCV), 2011 IEEE International Conference on.* IEEE, pp. 2548–2555.
- Lie, A., Tingvall, C., Krafft, M., Kullgren, A., 2004. The Effectiveness of ESP (Electronic Stability Program) in Reducing Real Life Accidents. *Traffic Inj. Prev.* 5, 37–41. <https://doi.org/10.1080/15389580490269164>
- Likert, R., 1932. A Technique for the Measurement of Attitudes.
- Ling, Y., Shen, S., 2016. High-precision online markerless stereo extrinsic calibration, in: *Intelligent Robots and Systems (IROS), 2016 IEEE/RSJ International Conference on.* IEEE, pp. 1771–1778.

- Luong, Q.-T., Faugeras, O.D., 1996. The Fundamental matrix: theory, algorithms, and stability analysis. *International Journal of Computer Vision*. <https://doi.org/10.1007/BF00127818>
- Machida, S., Shishido, S., Tokuhara, T., Yanagida, M., Yamada, T., Izuchi, M., Sato, Y., Miyake, Y., Nakata, M., Murakami, M., 2017. 4.7 A 2.1 Mpixel organic-film stacked RGB-IR image sensor with electrically controllable IR sensitivity, in: *Solid-State Circuits Conference (ISSCC), 2017 IEEE International*. IEEE, pp. 78–79.
- Maddern, W., Pascoe, G., Linegar, C., Newman, P., 2017. 1 year, 1000 km: The Oxford RobotCar dataset. *IJ Robot. Res* 36, 3–15.
- Matthies, L., Shafer, S., 1987. Error modeling in stereo navigation. *IEEE J. Robot. Autom.* 3, 239–248.
- Mayer, M., Baur, K., Walter, T., 2009. Packaging technologies for highly integrated 77 GHz automotive radar sensors, in: *Microwave Conference, 2009. EuMC 2009. European*. IEEE, pp. 1311–1314.
- Menze, M., Geiger, A., 2015. Object scene flow for autonomous vehicles, in: *Proceedings of the IEEE Conference on Computer Vision and Pattern Recognition*. pp. 3061–3070.
- Menzel, W., Kessler, D., 2009. A folded reflectarray antenna for 2D scanning, in: *Microwave Conference, 2009 German*. IEEE, pp. 1–4.
- Meso, P., Smith, R., 2000. A resource- based view of organizational knowledge management systems. *J. Knowl. Manag.* 4, 224–234. <https://doi.org/10.1108/13673270010350020>
- Mikolajczyk, K., Schmid, C., 2005. A performance evaluation of local descriptors. *IEEE Trans. Pattern Anal. Mach. Intell.* 27, 1615–1630.
- Miksik, O., Mikolajczyk, K., 2012. Evaluation of local detectors and descriptors for fast feature matching, in: *Pattern Recognition (ICPR), 2012 21st International Conference on*. IEEE, pp. 2681–2684.
- Minsky, M., 1974. *A Framework for Representing Knowledge*. Artif. Intell.
- Montanari, R., Borin, A., Spadoni, A., 2011. SAFERIDER: results from Yamaha test site on advanced rider assistance system, in: *Proceedings of the 9th ACM SIGCHI Italian Chapter International Conference on Computer-Human Interaction: Facing Complexity*. ACM, pp. 132–138.
- Montella, A., 2011. Identifying crash contributory factors at urban roundabouts and using association rules to explore their relationships to different crash types. *Accid. Anal. Prev.* 43, 1451–1463. <https://doi.org/10.1016/j.aap.2011.02.023>
- Morales, A., Gonzalez-Aguilera, D., Gutiérrez, M., López, A., 2015. Energy Analysis of Road Accidents Based on Close-Range Photogrammetry. *Remote Sens.* 7, 15161–15178. <https://doi.org/10.3390/rs71115161>
- Mostegel, C., Rumpfer, M., Fraundorfer, F., Bischof, H., 2016. Using self-contradiction to learn confidence measures in stereo vision, in: *Proceedings of the IEEE Conference on Computer Vision and Pattern Recognition*. pp. 4067–4076.
- Mukhtar, A., Xia, L., Tang, T.B., 2015. Vehicle Detection Techniques for Collision Avoidance Systems: A Review. *IEEE Trans. Intell. Transp. Syst.* 16, 2318–2338. <https://doi.org/10.1109/TITS.2015.2409109>
- Mur-Artal, R., Tardos, J.D., 2017. ORB-SLAM2: An Open-Source SLAM System for Monocular, Stereo, and RGB-D Cameras. *IEEE Trans. Robot.* 1–8. <https://doi.org/10.1109/TRO.2017.2705103>
- Nedevschi, Sergiu, Danescu, R., Frentiu, D., Marita, T., Oniga, F., Pocol, C., Graf, T., Schmidt, R., 2004. High accuracy stereovision approach for obstacle detection on non-planar roads. *Proc IEEE INES* 211–216.

- Nedevschi, S., Schmidt, R., Danescu, R., Frentiu, D., Marita, T., Graf, T., Oniga, F., Pocol, C., 2004. High accuracy stereo vision system for far distance obstacle detection. *IEEE*, pp. 292–297. <https://doi.org/10.1109/IVS.2004.1336397>
- Negre, E., Rosenthal-Sabroux, C., Gasco, M., 2015. A Knowledge-Based Conceptual Vision of the Smart City. *IEEE*, pp. 2317–2325. <https://doi.org/10.1109/HICSS.2015.279>
- NHTSA, 2014. Traffic safety facts.
- NHTSA USA, 2015. Traffic Safety Facts. National Highway Traffic Safety Administration.
- Nicol, D., Heuer, W., Chrysler, S., Bloschock, M., Degges, P., Garber, N., Kolb, J., McGrath, M., Moreland, E., Tan, C., 2012. Infrastructure Countermeasures to Mitigate Motorcyclist Crashes in Europe.
- Oja, P., Titze, S., Bauman, A., de Geus, B., Krenn, P., Reger-Nash, B., Kohlberger, T., 2011. Health benefits of cycling: a systematic review: Cycling and health. *Scand. J. Med. Sci. Sports* 21, 496–509. <https://doi.org/10.1111/j.1600-0838.2011.01299.x>
- Oniga, F., Nedevschi, S., 2010. Processing Dense Stereo Data Using Elevation Maps: Road Surface, Traffic Isle, and Obstacle Detection. *IEEE Trans. Veh. Technol.* 59, 1172–1182. <https://doi.org/10.1109/TVT.2009.2039718>
- Ordonez, M., 2016. Powered-two and powered-three wheeler registrations up by 3.3% in the EU.
- Orgiazzi, A., Panagos, P., Yigini, Y., Dunbar, M.B., Gardi, C., Montanarella, L., Ballabio, C., 2016. A knowledge-based approach to estimating the magnitude and spatial patterns of potential threats to soil biodiversity. *Sci. Total Environ.* 545–546, 11–20. <https://doi.org/10.1016/j.scitotenv.2015.12.092>
- Orsi, C., Bertuccio, P., Morandi, A., Levi, F., Bosetti, C., La Vecchia, C., 2012. Trends in motor vehicle crash mortality in Europe, 1980–2007. *Saf. Sci.* 50, 1009–1018. <https://doi.org/10.1016/j.ssci.2011.12.008>
- Otte, D., Jansch, M., Wiese, B., 2013. Injury Severity and Causation Factors of Motorcyclists in Traffic Accidents in comparing Drivers of Motorcycle and All Kinds of Motorized Two-wheelers.
- Panchal, P.M., Panchal, S.R., Shah, S.K., 2013. A comparison of SIFT and SURF. *Int. J. Innov. Res. Comput. Commun. Eng.* 1, 323–327.
- Pandey, G., McBride, J.R., Eustice, R.M., 2011. Ford Campus vision and lidar data set. *Int. J. Robot. Res.* 30, 1543–1552. <https://doi.org/10.1177/0278364911400640>
- Pantilie, C.D., Nedevschi, S., 2012. SORT-SGM: Subpixel Optimized Real-Time Semiglobal Matching for Intelligent Vehicles. *IEEE Trans. Veh. Technol.* 61, 1032–1042. <https://doi.org/10.1109/TVT.2012.2186836>
- Pavlovic-Veselinovic, S., Hedge, A., Veselinovic, M., 2016. An ergonomic expert system for risk assessment of work-related musculo-skeletal disorders. *Int. J. Ind. Ergon.* 53, 130–139. <https://doi.org/10.1016/j.ergon.2015.11.008>
- Pecchini, D., Mauro, R., Giuliani, F., 2014. Model of Potential Crash Rates of Rural Roundabouts with Geometrical Features. *J. Transp. Eng.* 140, 04014055. [https://doi.org/10.1061/\(ASCE\)TE.1943-5436.0000705](https://doi.org/10.1061/(ASCE)TE.1943-5436.0000705)
- Pfeiffer, D., Franke, U., 2011. Modeling Dynamic 3D Environments by Means of The Stixel World. *IEEE Intell. Transp. Syst. Mag.* 3, 24–36. <https://doi.org/10.1109/MITS.2011.942207>
- Pfeiffer, D., Franke, U., 2010. Efficient representation of traffic scenes by means of dynamic stixels, in: *Intelligent Vehicles Symposium (IV), 2010 IEEE*. *IEEE*, pp. 217–224.

- Pfeiffer, D., Gehrig, S., Schneider, N., 2013. Exploiting the power of stereo confidences, in: Proceedings of the IEEE Conference on Computer Vision and Pattern Recognition. pp. 297–304.
- Piantini, S., Grassi, D., Mangini, M., Pierini, M., Spina, R., Peris, A., 2012. A pilot study of an integrated accident research system based on a medical and engineering data in the metropolitan area of Florence, in: International IRCOBI Conference on the Biomechanics of Impact, IRC-12. pp. 10–21.
- Piantini, S., Grassi, D., Mangini, M., Pierini, M., Zagli, G., Spina, R., Peris, A., 2013. Advanced accident research system based on a medical and engineering data in the metropolitan area of Florence. *Bmc Emerg. Med.* 13, 3.
- Piantini, S., Pierini, M., Delogu, M., Baldanzini, N., Franci, A., Mangini, M., Peris, A., 2016. Injury Analysis of Powered Two-Wheeler versus Other-Vehicle Urban Accidents, in: IRCOBI Conference., Malaga, Spain.
- Poggi, M., Tosi, F., Mattoccia, S., 2017. Quantitative evaluation of confidence measures in a machine learning world, in: International Conference on Computer Vision (ICCV 2017).
- Prather Lanier, Nathan Short, Kevin Kochersberger, Lynn Abbott, 2011. Modal-based Camera Correction for Large Pitch Stereo Imaging, in: Structural Dynamics, Volume 3. Springer, pp. 1225–1238.
- Proesmans, M., Van Gool, L., Oosterlinck, A., 1996. One-shot active 3D shape acquisition, in: Pattern Recognition, 1996., Proceedings of the 13th International Conference on. IEEE, pp. 336–340.
- Qian, N., 1997. Binocular disparity and the perception of depth. *Neuron* 18, 359–368.
- Quintana-Amate, S., Bermell-Garcia, P., Tiwari, A., 2015. Transforming expertise into Knowledge-Based Engineering tools: A survey of knowledge sourcing in the context of engineering design. *Knowl.-Based Syst.* 84, 89–97. <https://doi.org/10.1016/j.knosys.2015.04.002>
- Radivojevic, S., Milbredt, O., 2016. A decision support tool for evaluating decision options for out-bound flight delays considering high-valuable passengers. *Eur. Transp. Res. Rev.* 8. <https://doi.org/10.1007/s12544-015-0189-x>
- Ramos, S., Gehrig, S., Pinggera, P., Franke, U., Rother, C., 2017. Detecting unexpected obstacles for self-driving cars: Fusing deep learning and geometric modeling, in: Intelligent Vehicles Symposium (IV), 2017 IEEE. IEEE, pp. 1025–1032.
- Rankin, A.L., Huertas, A., Matthies, L.H., 2009. Stereo vision based terrain mapping for off-road autonomous navigation.
- Rehder, E., Kinzig, C., Bender, P., Lauer, M., 2017. Online stereo camera calibration from scratch, in: Intelligent Vehicles Symposium (IV), 2017 IEEE. IEEE, pp. 1694–1699.
- Rogers, N., 2008. Trends in Motorcycles Fleet Worldwide. Presentation to Joint OECD/ITF Transport Research Committee Workshop on Motorcycling Safety.
- Roques, S., Jahan, L., Rougé, B., Thiebaut, C., 2004. Satellite attitude instability effects on stereo images, in: Acoustics, Speech, and Signal Processing, 2004. Proceedings.(ICASSP'04). IEEE International Conference on. IEEE, p. iii–477.
- Ruan, Y., Hang, C.C., Wang, Y.M., 2014. Government's role in disruptive innovation and industry emergence: The case of the electric bike in China. *Technovation* 34, 785–796. <https://doi.org/10.1016/j.technovation.2014.09.003>
- Rublee, E., Rabaud, V., Konolige, K., Bradski, G., 2011. ORB: An efficient alternative to SIFT or SURF, in: Computer Vision (ICCV), 2011 IEEE International Conference on. IEEE, pp. 2564–2571.

- Sacchi, E., Bassani, M., Persaud, B., 2011. Comparison of Safety Performance Models for Urban Roundabouts in Italy and Other Countries. *Transp. Res. Rec. J. Transp. Res. Board* 2265, 253–259. <https://doi.org/10.3141/2265-28>
- Sainter, P., Oldham, K., Larkin, A., 2000. Achieving benefits from knowledge-based engineering systems in the longer term as well as in the short term, in: *Proceedings of: 6th International Conference on Concurrent Enterprising*. Citeseer.
- Santucci, M., Pieve, M., Pierini, M., 2016. Electric L-category Vehicles for Smart Urban Mobility. *Transp. Res. Procedia, Transport Research Arena TRA2016* 14, 3651–3660. <https://doi.org/10.1016/j.trpro.2016.05.433>
- Savino, G., Giovannini, F., Baldanzini, N., Pierini, M., Rizzi, M., 2013. Assessing the Potential Benefits of the Motorcycle Autonomous Emergency Braking Using Detailed Crash Reconstructions. *Traffic Inj. Prev.* 14, S40–S49. <https://doi.org/10.1080/15389588.2013.803280>
- Savino, G., Giovannini, F., Fitzharris, M., Pierini, M., 2016. Inevitable Collision States for Motorcycle-to-Car Collision Scenarios. *IEEE Trans. Intell. Transp. Syst.* 17, 2563–2573. <https://doi.org/10.1109/TITS.2016.2520084>
- Savino, G., Penumaka, A., Pierini, M., Baldanzini, N., Roessler, B., 2009. Design of the decision logic for a PTW integrated safety system. pp. 1–12.
- Savino, G., Piantini, S., Gil, G., Pierini, M., 2017. Obstacle detection test in real-world traffic contexts for the purposes of motorcycle autonomous emergency braking (MAEB). Presented at the 25th International Technical Conference on the Enhanced Safety of Vehicles (2017), Detroit, USA. <https://doi.org/10.1109/ETC.2017.7993435>
- Savino, G., Pierini, M., Baldanzini, N., 2012a. Decision logic of an active braking system for powered two wheelers. *Proc. Inst. Mech. Eng. Part J. Automob. Eng.* 226, 1026–1036. <https://doi.org/10.1177/0954407011434445>
- Savino, G., Pierini, M., Rizzi, M., Frampton, R., 2012b. Evaluation of an Autonomous Braking System in Real-World PTW Crashes. *Traffic Inj. Prev.* 14, 532–543. <https://doi.org/10.1080/15389588.2012.725878>
- Savino, G., Rizzi, M., Brown, J., Piantini, S., Meredith, L., Albanese, B., Pierini, M., Fitzharris, M., 2014. Further Development of Motorcycle Autonomous Emergency Braking (MAEB), What Can In-Depth Studies Tell Us? A Multinational Study. *Traffic Inj. Prev.* 15, S165–S172. <https://doi.org/10.1080/15389588.2014.926009>
- Saygili, G., van der Maaten, L., Hendriks, E.A., 2015. Adaptive stereo similarity fusion using confidence measures. *Comput. Vis. Image Underst.* 135, 95–108. <https://doi.org/10.1016/j.cviu.2015.02.005>
- Saygili, G., van der Maaten, L., Hendriks, E.A., 2014. Stereo Similarity Metric Fusion Using Stereo Confidence, in: *Pattern Recognition (ICPR), 2014 22nd International Conference on*. IEEE, pp. 2161–2166.
- Schaeffer, C., 2013. A Comparison of Keypoint Descriptors in the Context of Pedestrian Detection: FREAK vs. SURF vs. BRISK. *Cité En* 12.
- Schaller, S., Perlot, A., 2016. ACEM 2015 Industry Report.
- Scharstein, D., Szeliski, R., 2002. A taxonomy and evaluation of dense two-frame stereo correspondence algorithms. *Int. J. Comput. Vis.* 47, 7–42.
- Scharwächter, T., 2013. Stixel-Based Target Existence Estimation under Adverse Conditions, in: *German Conference on Pattern Recognition*. Springer, pp. 225–230.
- Schepers, P., Fishman, E., Beelen, R., Heinen, E., Wijnen, W., Parkin, J., 2015. The mortality impact of bicycle paths and lanes related to physical activity, air pollution exposure

- and road safety. *J. Transp. Health* 2, 460–473. <https://doi.org/10.1016/j.jth.2015.09.004>
- Schneider, M., 2005. Automotive radar-status and trends, in: German Microwave Conference. pp. 144–147.
- Sekine, T., 2014. Utilization of probe powered two-wheeler vehicles to realize a safe mobile society. *IATSS Res.* 38, 58–70. <https://doi.org/10.1016/j.iatssr.2014.08.002>
- Shaw, M.L., Gaines, 1987. KITTEN: Knowledge initiation and transfer tools for experts and novices. *Int. J. Man-Machine Studies.*
- Shimizu, M., Okutomi, M., 2002. Precise subpixel estimation on area-based matching. *Syst. Comput. Jpn.* 33, 1–10.
- Shortliffe, E.H., 1976. Computer-based medical consultations, MYCIN. Elsevier, New York.
- Shuhaili, A., Fadzil, A., Ihsan, S.I., Faris, W.F., 2013. Air Pollution Study of Vehicles Emission In High Volume Traffic: Selangor, Malaysia As A Case Study. *WSEAS Trans. Syst.* 12, 67–84.
- Sibley, G., Matthies, L., Sukhatme, G., 2007. Bias reduction and filter convergence for long range stereo. *Robot. Res.* 285–294.
- Simha, P., 2016. Disruptive Innovation on Two Wheels: Chinese Urban Transportation and Electrification of the Humble Bike. *Period. Polytech. Transp. Eng.* 44, 222–227. <https://doi.org/10.3311/PPtr.8811>
- Sindha, J., Chakraborty, B., Chakravarty, D., 2017. Automatic stability control of three-wheeler vehicles – recent developments and concerns towards a sustainable technology. *Proc. Inst. Mech. Eng. Part J. Automob. Eng.* 0954407017701285. <https://doi.org/10.1177/0954407017701285>
- Soliman, F., Spooner, K., 2000. Strategies for implementing knowledge management: role of human resources management. *J. Knowl. Manag.* 4, 337–345. <https://doi.org/10.1108/13673270010379894>
- Spangenberg, R., Langner, T., Rojas, R., 2013. Weighted Semi-Global Matching and Center-Symmetric Census Transform for Robust Driver Assistance, in: Wilson, R., Hancock, E., Bors, A., Smith, W. (Eds.), *Computer Analysis of Images and Patterns: 15th International Conference, CAIP 2013, York, UK, August 27-29, 2013, Proceedings, Part II*. Springer Berlin Heidelberg, Berlin, Heidelberg, pp. 34–41. https://doi.org/10.1007/978-3-642-40246-3_5
- Suganuma, N., Fujiwara, N., 2007a. An obstacle extraction method using virtual disparity image, in: *Intelligent Vehicles Symposium, 2007 IEEE*. IEEE, pp. 456–461.
- Suganuma, N., Fujiwara, N., 2007b. An obstacle extraction method using virtual disparity image, in: *Intelligent Vehicles Symposium, 2007 IEEE*. IEEE, pp. 456–461.
- Suganuma, N., Shimoyama, M., Fujiwara, N., 2008. Obstacle detection using virtual disparity image for non-flat road, in: *Intelligent Vehicles Symposium, 2008 IEEE*. IEEE, pp. 596–601.
- Szeliski, R., Scharstein, D., 2004. Sampling the disparity space image. *IEEE Trans. Pattern Anal. Mach. Intell.* 26, 419–425.
- Thorn, C.F., Klein, T.E., Altman, R.B., 2013. PharmGKB: The Pharmacogenomics Knowledge Base, in: Innocenti, F., van Schaik, R.H.N. (Eds.), *Pharmacogenomics*. Humana Press, Totowa, NJ, pp. 311–320.
- Thrun, S., Montemerlo, M., Dahlkamp, H., Stavens, D., Aron, A., Diebel, J., Fong, P., Gale, J., Halpenny, M., Hoffmann, G., Lau, K., Oakley, C., Palatucci, M., Pratt, V., Stang, P., Strohband, S., Dupont, C., Jendrossek, L.-E., Koelen, C., Markey, C., Rummel, C., van Niekirk, J., Jensen, E., Alessandrini, P., Bradski, G., Davies, B., Ettinger, S.,

- Kaehler, A., Nefian, A., Mahoney, P., 2006. Stanley: The robot that won the DARPA Grand Challenge. *J. Field Robot.* 23, 661–692. <https://doi.org/10.1002/rob.20147>
- Tosi, F., Poggi, M., Tonioni, A., Di Stefano, L., Mattoccia, S., 2017. Learning confidence measures in the wild, in: 28th British Machine Vision Conference (BMVC 2017).
- UN, 2017. World Population Prospects: The 2017 Revision, Key Findings and Advance Tables. United Nations, Department of Economic and Social Affairs, Population Division. Working Paper No. ESA/P/WP/248.
- Unger, C., Wahl, E., Ilic, S., 2011. Efficient stereo matching for moving cameras and decalibrated rigs, in: Intelligent Vehicles Symposium (IV), 2011 IEEE. IEEE, pp. 417–422.
- Van Elslande, P., Hermitte, T., Jaffard, M., Fournier, J.Y., Silvestrelli, A., Perrin, C., 2012. Deliverable 5.5 Drivers needs and validation of technologies.
- Vavryn, K., Winkelbauer, M., 2004. Braking performance of experienced and novice motorcycle riders—results of a field study, in: International Conference on Transport and Traffic Psychology. Nottingham, United Kingdom.
- Verhagen, W.J.C., Bermell-Garcia, P., van Dijk, R.E.C., Curran, R., 2012. A critical review of Knowledge-Based Engineering: An identification of research challenges. *Adv. Eng. Inform.* 26, 5–15. <https://doi.org/10.1016/j.aei.2011.06.004>
- Verheugen, G., 2005. COMMISSION DIRECTIVE 2005/49/EC. Off. J. Eur. Union.
- Warner, H.R., 1968. Experiences with Computer-Based Patient Monitoring: Third Becton, Dickinson and Company Oscar Schwidetzky Memorial Lecture. *Anesth. Analg.* 47, 453–462.
- Warren, M., McKinnon, D., Upcroft, B., 2013. Online calibration of stereo rigs for long-term autonomy. IEEE, pp. 3692–3698. <https://doi.org/10.1109/ICRA.2013.6631096>
- Waterman, D.A., 1986. How do expert systems differ from conventional programs?*. *Expert Syst.* 3, 16–19.
- Waterman, D.A., 1978. A rule-based approach to knowledge acquisition for man-machine interface programs.
- Waterman, D.A., 1976. An introduction to production systems. DTIC Document.
- Waterman, D.A., Jenkins, B., 1976. Heuristic modeling using rule-based computer systems.
- Wedel, A., Franke, U., 2007. Monocular video serves radar-based emergency braking, in: Intelligent Vehicles Symposium, 2007 IEEE. IEEE, pp. 93–98.
- Weihua Guo, Binetti, P.R.A., Althouse, C., Masanovic, M.L., Ambrosius, H.P.M.M., Johansson, L.A., Coldren, L.A., 2013. Two-Dimensional Optical Beam Steering With InP-Based Photonic Integrated Circuits. *IEEE J. Sel. Top. Quantum Electron.* 19, 6100212–6100212. <https://doi.org/10.1109/JSTQE.2013.2238218>
- Weiss, M., Dekker, P., Moro, A., Scholz, H., Patel, M.K., 2015. On the electrification of road transportation – A review of the environmental, economic, and social performance of electric two-wheelers. *Transp. Res. Part Transp. Environ.* 41, 348–366. <https://doi.org/10.1016/j.trd.2015.09.007>
- Wigan, M., 2000. Motorcycle Transport: Powered Two Wheelers in Victoria. A report for Vic Roads on behalf of the Victorian Motorcycle Advisory Council by Oxford Systematics, Melbourne.
- Will, F., Davdison, J.N., Couchman, P., Bednall, D., 2011. Tomorrow's Car - For Today's People: Can Tilting Three Wheeled Vehicles be a Solution for the Problems of Today and the Future? (SAE Technical Paper No. 2011-28-0001). SAE International, Warrendale, PA.

- Williamson, T.A., 1998. A high-performance stereo vision system for obstacle detection. Carnegie Mellon University.
- World Health Organization, 2015. Global Status Report on Road Safety 2015. [WWW Document]. URL http://www.who.int/violence_injury_prevention/road_safety_status/2015/GSRRS2015_Summary_EN_final2.pdf?ua=1
- Xia, L., Chung, T.D., Kassim, K.A.A., 2014. An Automobile Detection Algorithm Development for Automated Emergency Braking System. ACM Press, pp. 1–6. <https://doi.org/10.1145/2593069.2593083>
- Xu, Q., Wehrle, E., Baier, H., 2012. Adaptive and Engineering Knowledge based Metamodeling in Multidisciplinary Design Optimization of Aircraft Wing Structures. American Institute of Aeronautics and Astronautics. <https://doi.org/10.2514/6.2012-5448>
- Zabih, R., Woodfill, J., 1994. Non-parametric local transforms for computing visual correspondence, in: European Conference on Computer Vision. Springer, pp. 151–158.
- Zaiontz, C., 2015. Real Statistics Using Excel.
- Zbontar, J., LeCun, Y., 2015. Computing the stereo matching cost with a convolutional neural network, in: Proceedings of the IEEE Conference on Computer Vision and Pattern Recognition. pp. 1592–1599.
- Zhang, Z., 2000a. A flexible new technique for camera calibration. *IEEE Trans. Pattern Anal. Mach. Intell.* 22, 1330–1334.
- Zhang, Z., 2000b. A flexible new technique for camera calibration. *IEEE Trans. Pattern Anal. Mach. Intell.* 22, 1330–1334.
- Zhang, Z., Weiss, R., Hanson, A.R., 1997. Obstacle detection based on qualitative and quantitative 3D reconstruction. *IEEE Trans. Pattern Anal. Mach. Intell.* 19, 15–26.
- Zhu, Z., Van Tooren, M., La Rocca, G., 2012. A KBE Application for Automatic Aircraft Wire Harness Routing. American Institute of Aeronautics and Astronautics. <https://doi.org/10.2514/6.2012-1843>